Removal of dissolved metals from storm water runoff by zero-valent iron

vorgelegt von

Ropru Rangsivek, M.Sc.
aus Pattani, Thailand

von der Fakultät III
– Prozeßwissenschaften –
der Technischen Universität Berlin
zur Erlangung des akademischen Grades

Doktor der Ingenieurwissenschaften
- Dr.-Ing.-

genehmigte Dissertation

Promotionsausschuß:

Vorsitzender: Prof. Dr.-Ing. Sven-Uwe Geißen
Gutachter: Prof. Dr.-Ing. Martin Jekel
Gutachter: Prof. Dr.-Ing. Matthias Barjenbruch
Gutachter: Prof. Dr.-Ing. Heiko Diestel

Tag der wissenschaftlichen Aussprache: 23 April 2010

Berlin 2010
D 83

Acknowledgements

This PhD thesis was written based on my research work carried out at the department of water quality control at the Technical University of Berlin (TU-Berlin) from June 2003 to December 2006 under the supervision of Prof. Dr.-Ing. Martin Jekel. I would like to express sincere thanks to him for giving me this opportunity and also for providing me all the support over these years. I would also like to express gratitude to Prof. Dr.-Ing. Heiko Diestel and Prof. Dr.-Ing. Horst Borgmann without their help I would never had such a chance. Prof. Dr. Gary Amy has given me valuable guidance, expertise in research and continuous support during a sabbatical year in Berlin. Prof. Dr.-Ing. Matthias Barjenbruch and Prof. Dr.-Ing. Sven-Uwe Geißen for his suggestions, review and taking up the examination job. They all have paved the way for my life today.

I would like to acknowledge Dr.-Ing. Mathias Ernst, Dipl.-Ing. Marco Schmidt, Dipl.-Geogr. Katharina Teschner, Dr.-Ing. Kyung-Ho Kwon, M.Sc. Agueda Sollis Tellez, Dipl.-Ing. Carsten Bahr, M.Sc. Xing Zheng and other colleagues at the department for having great discussions both on the research and other out-of-the-room topics throughout my stay in Berlin. A thousand thanks must be devoted to Dr.-Ing. Thomas Ludwig who has helped me in several aspects of the research works. Dr. Anke Putschew, Gisela Sosna, Ulrike Förster, Angelika Kersten as well as others have enlightened me in laboratory equipments and methods. Special thanks to Werner Däumler and Thomas Thele for technical-assistance. Their works are really amazing. Wolfgang Wichmann, Michael Markmann and Bärbel Bleicke are also acknowledged. Thank you to Karin von Nordheim for helping in documentation over the years.

Parts of my work have been reviewed by Priv.-Doz. Dr.-Ing. Thorsten Reemtsma, Dr.-Ing. Arne Genz, Dipl.-Chem. Dirk Bloem, M.Sc. Amnuay Wattanakornsiri. Several journal reviewers have greatly helped in improving the works. This includes Dr. Chicgoua Noubactep and his profound knowledge of Fe^0 and the constructive email discussions. Special thanks are extended to Rebeca, Shawn, Babara, Phra William (William Leslie), Mai-Lan Ha and Katja for editorial work.

The SEM and EDX analyses were carried out at Zentraleinrichtung Elektronenmikroskopie (ZELMI), TU Berlin. The author wishes to thank Dr. Burkhard Peplinski at Federal Institute for Materials Research and Testing (BAM) and Dr. Andreas Hösch, Institute of Applied Geosciences, TU-Berlin, for kindly helping in XRD analysis. Further AES and XRD were performed by Dipl.-Ing. Bettina Camin and Dipl.-Ing. Eric Wild, Metallische Werkstoff at the TU Berlin (Prof. Dr. Walter Reimers). Thank to Frau Maike Mai from the department of waste management, TU-Berlin for providing the XAD Resin apparatus.

There are many more people who should be acknowledged for this project both directly and indirectly, e.g., a small party at the small corner of the lab in the late evening playing loud German country songs has always been in my memory. Heartfelt thanks to my Thai friends who are always together: P' Gai U, P' Orn, P' Ja, P'Baan, P' Tum, A U, P' Tay, Luang A

Payom, Luang A Boonma, I Den, E Tud Net; N. Cap and several others. Phra A. Tony, Phra Maha Sorasak, Laung P' Tep, Mae Rabaeb, P'Aew, P' Buay for being dhamma friends.

I would like to thank to my parents, Papa and Mama, for persistent and endless support through these long years. Thanks also to Irene and Ingo Lindner. Without them and their daughter, Katja, this work would not have been possible. Living for a period in Germany was so great with Katja's (also my German) family. Thank you also to Oleang for being a good friend during a cold winter in Chiangmai and now. Last but not least, Donmei, my son even though he is the smallest person here, he has been the greatest driving force that pushes me through this work at this late period while he is in Denmark with his mother.

Abstract

This study investigates the novel treatment method for heavy metals from contaminated runoff by employing Fe^0. Batch kinetic, equilibrium and flow-through configurations were thoroughly studied. Based on the investigation, it was found that Fe^0 achieves a comparable capacity to a commercial adsorbent like granular ferric hydroxide (GFH). The removal of Cu^{2+} and Zn^{2+} by Fe^0 takes place through an array of rate-limiting steps including iron oxidation, iron (oxy)hydroxide precipitation and metal adsorption/co-precipitation. Cu^{2+} is directly or indirectly reduced by Fe^0 and/or dissolved, structured Fe^{2+}, and forms Cu^0 and Cu_2O as reduction products. The removal of Zn^{2+} is mainly due to the adsorption and co-precipitation processes. Results of batch kinetic tests using showed that when the solution is low in DO, T, pH, IS or reactions take place under high metal and DOC concentrations, the removal rate of Zn^{2+} dramatically decreases.

The breakthrough column tests showed that the exhaustion of zinc occurred more rapidly than copper; yielding a metal loading capacity of an average 76 mg g^{-1} Fe^0 for copper (with min: 55 and max: 96 mg g^{-1}) and 55 mg g^{-1} Fe^0 for zinc (min: 22, max: 69 mg g^{-1}). Increased pH and temperature generally favor faster retention rates of copper and zinc, whereas increases in DO and conductivity of the solution hinder the removal of copper in the column system. Among parameters studied, NOM shows to be the most influent compound that results in a dramatically decreased metal uptake rate. Inhibition of NOM on the removal of metals by Fe^0 was due to competitive adsorption, metal-ligand complexes and the inhibition that was caused by surface coverage of iron corrosion products. The NOM fraction that mainly interacts with metals is a larger size hydrophobic fraction with high aromaticity.

With aims to upscale the treatment process and to be able to simulate the breakthrough curves at various scenarios, a pore-surface diffusion model (PSDM) was attempted. Generally, the PSDM can adequately capture most of the determined curves but at increased NOM concentration, an over prediction of the curve was observed.

Following the test and modeling at various scenarios, optimization of the processes was carried out by incorporating Fe^0 with calcite, dolomite and magnesite media. The recommended system for on-site treatment of metal-contaminated runoffs consisted of columns filled with spiral shaped irons followed by an aeration unit and post filtration of pumice/dolomite. According to the test, about 60-100 and 30-80 % of metal concentrations could be removed at an EBCT of 5 and 1 min EBCT, respectively. A longer EBCT will yield a better performance. For practical operations, carbonate materials tend to be passivated by various minerals and biofilms. An occasional backwash in order to reactivate the surface of materials inside and to maintain the hydraulic conductivity of the system is required.

Finally, cost analysis showed that Fe^0 is a suitable medium for stormwater runoff treatment.

Zusammenfassung

In dieser Studie wurde eine neuartige Methode zur Aufbereitung von schwermetallbelasteten Oberflächenabflüssen untersucht. Dabei kam nullwertiges Eisen (Fe^0) als Barrieresystem zum Einsatz. In Batch- und Säulenversuchen wurden die Mechanismen und der Einfluss der Wasserqualität auf die Schwermetallentfernung in dem Fe^0-Barrierensystem untersucht. Die Untersuchungen haben gezeigt, dass mit Fe^0 eine vergleichbare Beladungskapazität erzielt wird wie mit granuliertem Eisenhydroxid (GEH). Die Entfernung von gelöstem Kupfer und Zink durch Fe^0 ist auf mehrere geschwindigkeitsbestimmende Schritte zurückzuführen, wobei die Eisenoxidation, die Eisenhydroxidbildung, die Metalladsorption und die Mitfällung von Bedeutung sind. Das gelöste Kupfer wird direkt oder indirekt durch Fe^0 reduziert. Als Reaktionsprodukte wurden Cu^0 und Cu_2O festgestellt. Die Zinkentfernung ist hauptsächlich auf die Adsorption und auf die Mitfällung zurückzuführen. Die kinetischen Batchversuche haben gezeigt, dass die Zinkentfernung durch geringe Sauerstoffgehalte, niedrige Temperaturen und niedrige pH-Werte sowie hohe DOC- und Metallgehalte verringert wird.

Die Säulenversuche mit Fe^0 zeigten, dass das gelöste Kupfer besser zurückgehalten wird als das gelöste Zink. Dabei wurde eine mittlere Beladung des Fe^0 in Höhe von 76 mg g^{-1} (mit min.: 55 und max.: 96 mg g^{-1}) für Kupfer und von 55 mg g^{-1} (mit min.: 22 und max.: 69 mg g^{-1}) für Zink ermittelt. Es zeigte sich ein besserer Rückhalt bei erhöhten pH-Werten sowie bei einer erhöhten Wassertemperatur. Demgegenüber verringerte sich der Kupfer- und Zinkrückhalt bei einer Zunahme der Gelöstsauerstoffkonzentration bzw. der Leitfähigkeit. Von den untersuchten Einflussgrößen auf den Metallrückhalt wurde der NOM-Gehalt im Oberflächenabfluss als wichtigster Einflussparameter identifiziert, der zu einer drastischen Verringerung der Metallrückhaltes. Die festgestellte Inhibierung des Metallrückhaltes in Gegenwart von NOM kann auf die konkurrierende Adsorption, auf die Bildung von metallorganischen Komplexen sowie auf die Hemmung der Eisenkorrosion zurückgeführt werden. Die im Rahmen der Versuche ergab sich, dass vorzugsweise die höhermolekularen, hydrophoben NOM-Fraktionen mit der Eisenoberfläche reagieren.

Zur Simulation der Durchbruchskurven unter verschiedenen Randbedingungen wurden Modellrechnungen mit einem Poren-Diffusionsmodell durchgeführt. Dabei konnten die experimentell ermittelten Durchbruchskurven durch geeignete Wahl der Modellparameter hinreichend abgebildet werden. Im Falle erhöhter NOM-Gehalte im Oberflächenabfluss war zur Modellierung der Durchbruchskurven allerdings eine weitere Anpassung der Modellparameter erforderlich.

Mit dem Ziel der Verbesserung der Ausfällung und der Metalladsorption an der Eisenoxidoberfläche wurden Untersuchungen mit karbonatischen Materialien (Calcit, Dolomit, Magnesit) durchgeführt. Die Versuche haben gezeigt, dass bei mittleren Verweilzeiten von 1 bzw. 5 Minuten ca. 30 bis 80 % bzw. ca. 60 bis 100 % der Metallkonzentrationen entfernt werden können. Mit einer Erhöhung der Verweilzeit kann dabei ein verbesserter Rückhalt erzielt werden. Das zur on-site Behandlung von schwermetallhaltigen Oberflächenabflüssen empfohlene Reinigungssystem besteht aus einer mit spiralförmigen Eisenspänen gefüllten Säule gefolgt von einer Belüftungseinheit und einer nachgeschalteten Filtereinheit aus Bimsstein / Dolomitstein. Für die praktische Anwendung ist zu beachten, dass die karbonatischen Materialien durch Ausbildung von Biofilmen und Deckschichten passiviert werden. Zum Erhalt der hydraulischen Leitfähigkeit sowie zur Reaktivierung der Oberflächen ist deshalb eine gelegentliche Rückspülung des Systems erforderlich.

Die Kostenanalyse ergab, dass Fe^0 ein geeignetes Medium für Aufbereitung von schwermetallbelasteten Oberflächenabflüssen ist.

Publication lists

Conference paper

Rangsivek, R., Amy, G.L. and Jekel, M.R. (2005), Removal of dissolved metals by zero-valent iron (ZVI) under storm water conditions, *presented for 1st International conference on environmental science and technology(EST),* 23-26 January, New Orleans, Louisiana, USA.

Rangsivek, R. and Jekel, M.R. (2005), Removal of dissolved metals by zero-valent iron (ZVI): Kinetics, equilibria, processes and implications for storm water runoff treatment, *presented at 10st International conference on urban drainage,* 21-26 August, Copenhagen, Denmark.

Rangsivek, R. and Jekel, M.R. (2007), A column investigation of Fe^0 for treatment of copper and zinc under varying quality of runoff, *presented at the 6th International conference on sustainable techniques and strategies in urban water management (NOVATECH),* 25-28 June, Lyon, France.

Poster presentation

Rangsivek, R. and Jekel, M.R. (2007), Interaction of natural organic matter (NOM) on Fe^0 treatment processes of metal contaminated-runoff, *presented at the 6th NOVATECH,* 25-28 June, Lyon, France.

Publication in Journals

Rangsivek, R. and Jekel, M.R. (2005), Removal of dissolved metals by zero-valent iron (ZVI): Kinetics, equilibria, processes and implications for storm water runoff treatment, Wat. Res., 39, 17, p. 4153-4163 (*at the 20th hottest article on Science Direct*)

Rangsivek, R. and Jekel, M.R. (2008), Natural organic matter in roof runoff and its impact on the Fe^0 treatment system of dissolved metals, *Chemosphere, 71, 18-29.*

Rangsivek, R. and Jekel, M.R. (2007), Development of an on-site Fe^0 system for treatment of copper- and zinc- contaminated roof runoff, *international journal of environmental and waste management* (IJEWM)*: Metal ions removal from liquid effluents*, *accepted*

Rangsivek, R., and Jekel, M.R. (2010), Removal of dissolved metals from roof runoff in Fe^0 columns: water quality impacts, processes, modeling and optimization, *submited.*

Content

Content of Figures

Content of Tables

Nomanclarture

AES	Auger Electron Spectroscopy
BET	Brunauer Emmett Teller
BV	Bed volume
BVT	Bed volume treated
CPHSDM	constant pattern homogeneous surface diffusion model
Cu-R	Copper roof runoff
DMS	Dolomite – Magno Fielt
DML	Dolomite – Magno Dol
DI	Deionised water
DO	Dissolved oxygen
DOC	Dissolved organic carbon
EBCT	Empty bed contact time
EDX	Energy dispersive X-ray analyzer
GFH	Granular ferric hydroxide
HA	Humic Acid
HPO	Hydrophobic fraction of NOM
HPI	Hydrophillic fraction of NOM
HSDM	Homogeneous surface diffusion model
IHSS	International humic substance society
IS	Ionic strenght
LC-OCD	Liquid chormatography and online carbon detection
$MINEQL^{+}$	Chemical equilibrium software
NOM	Natural organic matter
ORP	Oxidation-reduction potential
pH_{PZC}	pH at point of zero charge
PSDM	Pore and surface diffusion model
SEM	Scanning electron microscopy
SRFA	Suwannee river fulvic acid
SR-NOM	Suwannee river NOM
SSWR	Simulated storm water runoff (1:5 of tab water and DI)
T	Temperature
TPI	Transphillic fraction of NOM
TU-FF	First flush of TU roof runoff
TU-SW	Runoff from TU roof
UDK	University of art, Berlin
UVD	UV detection
XRD	X-Ray Diffractograms
ZVI, Fe^{0}	Zero valent iron
ZVIB	Zero valent iron barrier
ZVICB	Zero valent iron incorperated carbonatic materials

Symbol

K_F	Freundlich constant
k_f	Film diffusion coefficient
D_S	Surface/pore diffusion coefficient
K_{s0}	Solubility constant
Eh^0	Standard electrode potentials
K_a^s	equilibrium constants
Cu^{2+}/Cu^0	Redox couple of Cu^{2+} and Cu^0
pH_i	Inlet pH
pH_f	Effluent or outlet pH
q(c)	The solid-phase concentration
ρ	Bulk density
Θ	Water content
R_f	Retardation factor
n	Number of bed required
$C_{in}\ (Zn)$	Inlet concentration of zinc
$Cu_{out}(Zn)$	Outlet concentration of zinc
q_M	Load of metal uptake
$C_{in}\ (DO)$	Inlet concentraion of dissolved oxygen
$Cu_{out}(DO)$	Outlet concentraiton of dissolved oxygen
v_F	Flow velocity
$r(DO)$	Iron corrosion rate
a_v	Volumetric surface area of Fe^0
η_Σ	Total removal rate
$m_\Sigma(Fe)$	Total iron mass
t_{50}	Time to reach 50% usage of iron
$Fe(Ox)$	Concentration of oxidized iron
c_S	Mass of sludge
$M_{Fe(OH)_2}$	Mass of iron hydroxides
M_{Fe}	Iron mass

1 Introduction

1.1 New concepts of urban water management

The rapid and improper development of an urban catchment contributes to a significant increase in sealed surface area, i.e., concrete and asphalt on building, pavement, street and highway structures. As compared with a natural surface, impermeable surfaces destructively impact the water balance in the cities. This results in an array of problems including an increased volume of stormwater runoff and higher peak flow rates, which are regarded as the main causes of flooding. Furthermore, the concept of transporting rainwater out of the catchments through modern sewer systems as rapidly as possible also led to a great decline of urban soil moisture and natural recharge of the groundwater.

The infiltration of roof, street and highway runoffs is a recent idea of urban water management of increased interest. Infiltration of stormwater may be performed through different strategies using swale, pit, and trench or through infiltration ponds and porous pavement systems. Wherever possible, stormwater runoff shall be infiltrated onsite in order to decrease the flooding potential, while the filtrate also sustains the declining groundwater resource (Boller, 1997). Despite this positive fact, application of stormwater runoff percolation remains questionable in many cases, primarily due to the occurrence and increased load of dissolved and particulate contaminants in stormwater runoff.

1.2 Contaminants in urban stormwater runoff

The relevant contaminants present in urban runoffs are mostly associated with surface materials that the runoff passes through. Major sources of contaminants for street and highway runoffs are fuel combustion products, lubrication system losses, degradation of automobile tires, loss of transported load, as well as paint and corrosion products. Airborne, soil erosion, industry, litter, animals, vegetation are some of the other sources of stormwater pollution that may be transported by rainfall and wind from other sites and deposited in the highway catchment (Barbosa, 1999). The pollution load in highway runoff depends on the average daily traffic, air quality and rainfall intensity and duration (Hvitved-Jacobsen et al., 1994). Of the various kinds of pollutants, heavy metals generated by vehicle wear and emissions are considered priority pollutants because of their toxicity (FHWA, 1996). These heavy metal species, unlike organic pollutants, do not degrade in the environment (Barbosa, 1999). The most commonly detected heavy metals in street and highway runoffs are copper (Cu), lead (Pb) and zinc (Zn).

In contrast to street and highway runoffs, roof runoff has been traditionally considered as a clean water resource suitable for groundwater recharge. Roof runoff generally contains less organic and inorganic particulates. However, when runoffs originated from large surfaces have to be discharged into small- and middle-sized streams, they can be contaminated with

concentrations of organic and inorganic pollutants, particularly dissolved heavy metals from the roof surface. These may exceed the legal dissolved concentration level (Fig. 1.1).

When addressing groundwater-associated runoff problems, heavy metals including cadmium (Cd), copper, chromium (Cr), lead and zinc should be ranked in priority because of their toxicity and persistent characteristics. In urban runoff samples, Cu, Pb and Zn are detected in over 90% of the samples, cadmium and chromium are found to a lesser extent (Pitt, 1996). Due to fuel regulations, lead usage is generally declining. Simultaneously, significant emissions of copper and zinc have been reported in runoff originating from copper and zinc roofs, typical metallic components found in urban areas. For subsequent groundwater recharge, metals which are bound to particles can be readily removed by surface filtration and sedimentation (Pitt, 1996). Due to the accumulation of heavy metals, the upper soil layers are considered as hazardous materials. Additionally, dissolved heavy metals require particular consideration as they are highly mobile. As a consequence, percolation of the contaminated runoff waters may not only lead to a diffuse accumulation of pollutants in the soil or subsoil layers but they may also be considered as a potential cause of long-term deterioration of groundwater quality. This especially concerns the recharge sites that contain mainly sandy and loamy soils or sites that have been subjected to acidic conditions (Pitt, 1996). To assure the quality of filtrate water, a pretreatment system for contaminated runoff is required.

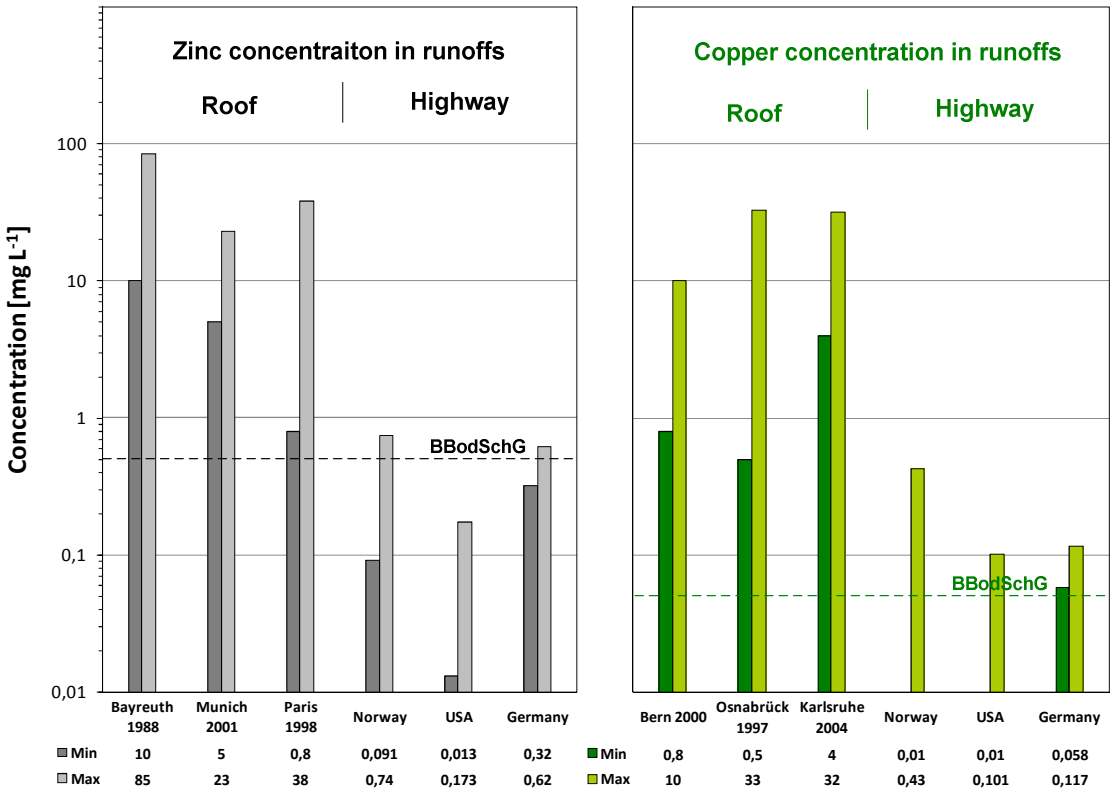

Fig. 1.1 Concentration of copper and zinc in roof and highway runoffs (c.f., Table A2 and A3)

1.3 Objectives of the study

The goal of this research work was to develop a novel treatment system of stormwater runoff contaminated with heavy metals. A simple and cost effective system was targeted. Therefore, a fixed-bed system containing reactive materials was primarily considered. The system can be placed downstream of the contaminated-flow and requires no consumption of energy, making it economically feasible.

In this study, zero-valent iron (ZVI, Fe^0) was chosen as a promising treatment medium. Fe^0 has advantages over other media, e.g., granular ferric hydroxide (GFH) (Driehaus et al., 1998; Boller and Steiner, 2002; Steiner, 2003), due to its low cost as well as environmental benefits in terms of reuse of solid wastes. Furthermore, ZVI has been successfully implemented as a fixed-bed barrier for an on-site remediation system (e.g., Morrison et al., 2002). The reactive materials have been shown to be environmentally safe, possess stability and sufficient permeability. Nevertheless, when Fe^0 has to be applied under runoff conditions, issues governing mechanisms of metal removal, source variations of runoff that may affect the performance of treatment barrier, quality of the treated-water and a potential clogging of the Fe^0 barrier need to be assessed. The design of a Fe^0 barrier requires the knowledge of site characteristics such as geotechnical data, nature of the contaminants and the investigation of critical parameters such as the required contaminant/reactant residence time and the stability of possible transformation products. Major issues that must be resolved before the installation of a system are the long term performance when operating under high oxygenated and high flow conditions.

For a complete study of processes and development of a final engineering design of stormwater runoff treatment systems, this PhD research had the following objectives:

(1) to understand the processes, kinetics as well as the equilibrium and maximum uptake loads of metal removal in Fe^0 system,

(2) to investigate the behaviour of metal removal by Fe^0 under flow-through conditions and changing runoff qualities,

(3) to understand the nature of natural organic matter (NOM) in roof runoffs and its impact on the treatment processes,

(4) to model the breakthrough of Fe^0 column allowing the prediction of the results and further up-scaling of the process, and

(5) finally to further optimize the treatment barrier using carbonate bearing materials.

Based on the understanding of these processes involved, the final engineering design of stormwater runoff treatment systems can be established.

1.4 Structure and outline of the thesis

At the beginning of the study, the processes and mechanisms for copper and zinc removal from stormwater runoff employing Fe^0 were investigated employing batch kinetic and equilibrium tests (Section 4.1). The study employed stormwater runoffs taken from roof, street and highway. The impact of stormwater characteristics, e.g., dissolved oxygen (DO), pH, temperature (T), dissolved organic carbon (DOC), ionic strength (IS) and metal concentration on metal removal were thoroughly studied. Following the batch test, Fe^0 was further assessed using a flow-through system offering a closer condition to actual implication of the iron barrier. The breakthrough, kinetics and mass flow analyses were performed using Fe^0 particle supported with pumice columns. They were tested using runoff collected from a roof with varying water quality parameters (Section 4.2).

A model capable of simulating the dynamic processes of copper and zinc removal by Fe^0 at varying runoff conditions is important for the engineering design of the treatment barrier. Generally, a modeling approach for metal removal in Fe^0 system is complex and requires several parameters that need extensive studies. Section 4.2.3 demonstrates a simple approach for modeling the metal breakthrough curves in a Fe^0 system. The model was based on a pore-surface-diffusion model (PSDM) using the AdsorbDesign software. It was shown that the model is able to predict breakthrough curves obtained from column tests adequately and allows the prediction of breakthroughs of metals at various scenarios.

In the course of the study, it was found that removal of metals dramatically decreases in the presence of natural organic matter (NOM). Currently, there are only a limited number of investigations that lead to the understanding of NOM impacts on the removal of contaminants using Fe^0 in literature. Therefore, one of crucial aims of this study was to assess the impacts and mechanisms associated with NOM in the Fe^0 treatment system of Cu^{2+} and Zn^{2+}. In section 4.3, the runoff samples from two roofs taken at various periods of time were characterized exclusively using XAD-4/8 adsorption resins, copper complexation, acidic capacity and liquid chromatography with online carbon detection. Batch kinetic experiments and flow-through configurations were performed and the results of metal removal were elucidated taking into account the characteristics of NOM.

Following the laboratory test and modeling, the iron system was optimized in order to ensure the required removal of pollutants within an appropriate time frame. To enhance the removal of metals of Fe^0 columns, carbonatic materials were added to the iron system and tested at various configurations. The result showed that a higher efficiency in terms of metal immobilization could be achieved. Nevertheless, this also brings about a high clogging potential of the treatment barrier by extensive accumulation of precipitated products. The most promising configuration consisted of a spiral shape of Fe^0 followed by aeration and a fixed-bed pumice/dolomite filter installed on-site for treatment of copper and zinc roof runoff (Section 4.4).

In the last chapter (Chapter 5), a summary of the results of this work and a recommendation for further up-scale of the treatment system is discussed.

2 Theory and background of zero-valent iron barrier

2.1 Zero-valent iron barrier (ZVIB) for water treatment

A permeable reactive barrier (PRB) is an engineered zone of reactive materials placed downstream of contaminated water (Fig. 2.1). The PRBs have been successfully employed for remediation of a variety of compounds such as chlorinated hydrocarbons (Gillham and O'Hannesin, 1992; 1994), nitrate (Robertson and Cherry, 1995; Huang and Zhang, 2005), metals (Shokes and Möller, 1999) and radionuclides (Cantrell et al., 1995). Depending on the targeted compounds, PRBs may be named in different terminologies such as a de-nitrification barrier for the removal of NO_3^-, permeable reactive walls and biological reactive barriers (Robertson and Cherry, 1995; Tombre et al., 1997). In groundwater contaminated with acid mine drainage, the reactive barriers may be constructed primarily of limestone, which is referred to as a limestone drain (Hedin et al., 1994).

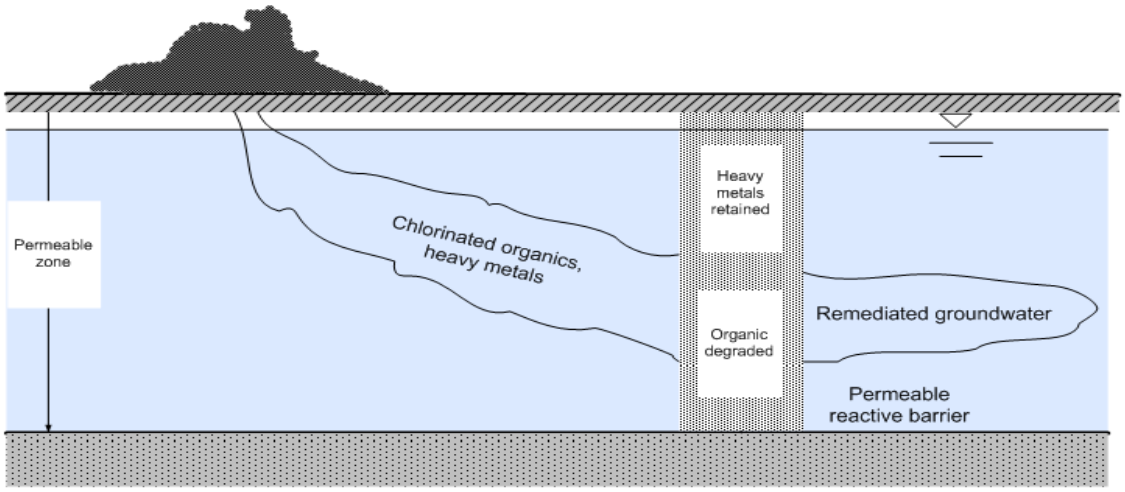

Fig. 2.1 Permeable reactive barriers for treatment of contaminanted groundwater

The so called "Zero-valent iron barrier" is the most common type of a permeable reactive barrier. In this barrier system, Fe^0 is the medium primarily used for the treatment of contaminants. The environmental usage of a Fe^0 barrier derived from a discovery by researchers at the University of Waterloo in 1992 (Gillham and O'Hannesin, 1992). The application of the technology was attributed earlier to halogenated aliphatics such as trichloroethylene (TCE), cis- and trans-dichloroethylene (DCE) and vinyl chloride (VC) (Gillham and O'Hannesin, 1992). Later, this was expanded to the treatment of acid mine drainage (Wilkin and McNeil, 2003), inorganic contaminant chromate (CrO_4^{2-}) and redionuclides such as Uranite and a range of inorganic heavy metals such as Cd^{2+}, Co^{2+}, Zn^{2+}, Pb^{2+}, Mn^{2+}, Ni^{2+} and complex ions such as UO_2^{2+} as well as SO_4^{2-}, NO_3^-, SeO_4^{2-}, TcO_4^{2-}, and CrO_4^{2-} (Cantrell et al., 1995; Blowes and Ptacek, 1992). Most recently, Fe^0 was investigated

and applied to the treatment of Arsenate contaminated drinking water resources (Bang et al., 2005; Karchunker and Jekel, 2002) and stormwater runoff treatment (Rangsivek and Jekel, 2005; 2007; 2008; Ludwig and Jekel, 2007).

2.2 Iron corrosion

The fundamental knowledge on the corrosion processes of iron, corrosion products and their behaviors on metal removals is crucial to the understanding of the remediation processes for inorganic contaminants in the Fe^0 barrier system as presented in the following;

2.2.1 Corrosion processes and mechanisms

When Fe^0 is immersed in an aqueous solution, an electrochemical corrosion will take place. The corrosion of iron can be described as the oxidation of iron and its corresponding reduction reaction: electrons are released from the anodic region of iron thus forming a soluble ferrous iron (Fe^{2+}) that dissipates out. In concomitant with the oxidation, the reduction of oxygen takes place at the cathodic site and in the bulk water phase this also yields an aqueous OH^- that leads to an increase in pH (Eq. 2.1).

The fate of Fe^{2+} depends on the solution chemistry. In the presence of sufficient DO and other related oxidants, Fe^{2+} will be oxidized and form Fe^{3+}, which is subsequently precipitated into amorphous ferric hydroxides ($Fe(OH)_{3(s)}$ or ferrihydrite) according to equation 2.2 and 2.3. The precipitates of these insoluble ferric hydroxides and oxyhydroxides may either localize close to the metallic iron surface or dissipate out into the bulk solution (Smith, 1998; Farrell et al., 2000). In the Fe^0 barrier, the pH of the system generally fluctuates; there is a consumption of proton as corrosion progresses in contrast to the formation of $Fe(OH)_3$ that leads to a decrease in pH.

Aerobic Corrosion

$$2Fe^0 + O_2 + 2H_2O \Rightarrow 2Fe^{2+} + 4OH^- \quad (2.1)$$

$$4Fe^{2+} + O_2 + 2H^+ \Rightarrow 4Fe^{3+} + 2OH^- \quad (2.2)$$

$$Fe^{3+} + 2OH^- \Rightarrow Fe(OH)_{3(s)} \quad (2.3)$$

Anaerobic Corrosion

$$Fe^0 + 2H_2O \Rightarrow Fe^{2+} + H_2 + 2OH^- \quad (2.4)$$

$$Fe^{2+} + 2OH^- \Rightarrow Fe(OH)_{2(s)} \quad (2.5)$$

$$3Fe(OH)_2 \Rightarrow Fe_3O_4 + H_2 + 2H_2O \quad (2.6)$$

In the absence of DO, the corrosion of iron takes place through different pathways which results in the formation of hydrous ferrous oxide ($FeO.nH_2O$) or ferrous hydroxide ($Fe(OH)_2$) and H_2 (2.4-2.6). The rate of hydrogen reduction is much slower than as compared to a high

DO condition. In the Fe^0 barrier, it can be anticipated that an anoxic or anaerobic corrosion can occur at the flow's downstream as dissolved oxygen is depleted during the transport through the Fe^0 barrier. Moreover, this type of iron corrosion can take place on the inner rust layer that has been previously formed following the complete exhaustion of dissolved oxygen at the outer layer of oxides.

2.2.2 Corrosion products

Although the mechanism of iron corrosion has been intensively studied, there is no general agreement on the conditions where a single corrosion product can be formed and stabilized. This is partly because the composition of rust depends on the condition where corrosion occurs and the resulting corrosion products usually change with time.

Table 2.1 Species of iron oxides detected in the Fe^0 corrosion system*

Sources	Metrix	Condition	Detected iron oxide species
Phillips et al. (2000)	G	Aerobic/anaerobic	Iron oxyhydroxides, akaganeit (β-FeOOH), goethite (α-FeOOH), aragonite ($CaCO_3$), siderite ($FeCO_3$), iron sulfide (FeS)
Roh et al. (2000)	G	Aerobic/anaerobic	Green rust, lepidocrocite, goethite, akaganeite, siderite, amorphous iron hydroxides, magnetite, akageneite etc.
Furukawa et al. (2002)	G	Anerobicic	Ferrihydrite, magnetite, green rust 1, aragonite, calcite, mackinawite, greigite and lepidocrocite
Odziemkowski (1998)	sG	Anaerobic	Ferrous hydroxide, magnetite
Farrel et al (2000)	sG	Anaerobic	Magnetite, maghemite
Manning et al. (2002)	sG	Anaerobic	Lepidrocrocite, magnetite and maghemite
Liang et al. (2003)	G	Anaerobic	Iron oxides, -carbonate, -sulfides
Su et al. (2004)	sG	-	Magnetite, hematite and lepidrocrocite
Kohn et al. (2005)	G	Anaerobic	Wüstite (FeO), magnetite (Fe_3O_4), maghemit (γ-Fe_2O^3), fayalite (Fe_2SiO_4)
Wilkin and McNeil (2005)	sG	Anaerobic	Green rust 1 and 2, mixed valent of iron hydroxides
Rangsivek and Jekel (2005)	R	Aerobic	Lepidocrocite, goethite and hematite

* data complied by Ludwig (2007) with additional references, G: groundwater; sG: simulated groundwater, R: runoff water

Many factors may influence the speciation and morphology of the iron corrosion products (Table 2.1). Compounds which are often reported as iron corrosion phases in the Fe^0 barrier usually include goethite (α-FeOOH), lepidocrocite (γ-FeOOH), magnetite (Fe_3O_4), siderite ($FeCO_3$), ferrous hydroxide ($Fe(OH)_2$), ferric hydroxide ($Fe(OH)_3$), ferrihydrite ($5Fe_2O_3$ $9H_2O$), and green rusts (Roh et al., 2000; Phillips et al., 2000; Furukawa et al., 2002; Wilkin and McNeil, 2005). Under anaerobic conditions, amorphous ferrous hydroxide, $Fe(OH)_2$, is the first corrosion product that forms which can be oxidized to form magnetite (Fe_3O_4) (Cornell and Schwertmann, 1996; Odziemkowski, 1998). Green rusts are often found in water containing carbonate, chloride and sulfate and is stable only at low redox potentials. Their oxidation commonly leads to the formation of maghemite (γ-Fe_2O_3) and lepidocrocite (Cornell and Schwertmann, 1996). In contrast, the oxidation of the Fe^{2+} ions in well-aerated

systems at neutral pH leads to the formation of ferrihydrite $Fe(OH)_3(s)$ (Cornell and Schwertmann, 1996). As $Fe(OH)_3$ is dehydrated over time it loses water molecules and slowly changes into other trivalent irons such as lepidocrocite, goethite and most of the hydrous ferric oxides as ordinary rust and oxide scales (Cornell and Schwertmann, 1996). Both rust and oxide scales are usually comprised of a mixture of iron oxides together with other Fe (e.g., siderite ($FeCO_3$)) and non-Fe compounds ($CaCO_3$) which are often found in the processes of steel pipe corrosion (Stumm, 1957; 1959; Smith et al., 1997). On pure iron, γ-FeOOH transforms to become the more stable α-FeOOH. With increasing time, goethite converts to either maghemite or hematite, the later usually requires higher temperatures. It can exist as the non-magnetic FeOOH, α-Fe_2O_3 or magnetic γ-Fe_2O_3 (Cornell and Schwertmann, 1996).

2.2.3 Corrosion rate

A high corrosion rate of iron is an important factor in controlling the removal of contaminants in natural water. The rate of iron dissolution depends on various physical and chemical parameters; it increased with temperature and flow velocity as a result of a higher mass transport through reactive surfaces. The high flow velocity transports Fe^{2+} ions away from the Fe^0 surface thus lowers the supersaturation of precipitation production (Noubactep, 2008). The increase of flow rate may also breakdown the previously formed iron oxides layer on the Fe^0 surface. Since iron solubility is very low at natural pH, a higher corrosion rate of iron can also lead to a formation of passivating layer that may subsequently retard the rate of oxygen transport and iron corrosion in the long-term. Besides these factors, the increase of ionic strength was also found to increase corrosion rate of iron by inducing precipitation of iron oxides away from the iron surface (Furukawa et al., 2002; Rangsivek and Jekel, 2005).

Iron corrosion rate may be indirectly determined with the balance of dissolved oxygen consumption before and after passing the iron surface as illustrated by Kuch (1984), Merkel (2002), Karschunke (2005) and Ludwig (2007). The application of balance of oxygen depends on the assumption of known final corrosion products and iron surface area. In a drinking water pipeline, the corrosion rate was reported to be approx. 20 g m^{-2} d^{-1} (T = 12 °C, v = 0.5 m s^{-1}) at the beginning, which significantly dropped to 4 g m^{-2} d^{-1} after one week of operation. With approx. 2 years operation, the final stable corrosion rate of approx. 0.1 g m^{-2} d^{-1} was found (Sontheimer et al., 1981). In the study of metal removal in cast iron barrier, Karschunke (2005) and Ludwig (2007) assumed the final products for Fe^{2+}, Fe_3O_4 and Fe^{3+}, which results in corrosion rates between 0.5-2.4 g m^{-2} d^{-1} with oxygen consumption rate of 0.06-0.02 L m^{-2} min^{-1}. A significantly lower iron corrison rate was found in the batch investigation by Rangsivek and Jekel (2005) which were 0.005-0.034 g m^{-2} d^{-1}. This was likely due to a larger surface area of iron determined by BET method as compared to calculated values from physical data in other works. Although, the BET method, involving adsorption isotherm of inert gas onto solid pore, give reproducible results, it is known that validity of the method depends on the assumption underlying the data analysis of the method (Dzombak and Morel, 1990).

2.3 Removal processes in a ZVI system

2.3.1 Removal mechanisms

Four most possible and important physico-chemical processes involving immobilization of inorganic compounds in the iron barrier are reductive transformation, adsorption/co-precipitation, and precipitation (Fig. 2.2 and 2.4).

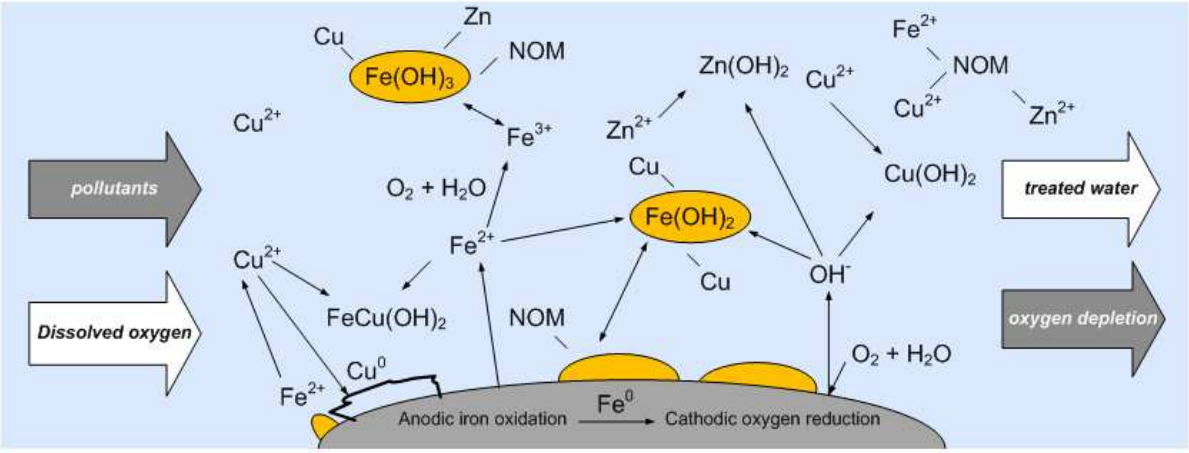

Fig. 2.2 Schematic of possible reactions relevant to inorganic (i.e., copper and zinc) removal in Fe^0 barrier (c.f., text)

Reductive transformation process

Reductive transformation consists of two partial redox-reactions, i.e., the oxidation of one species and the reduction of another that can be characterized by oxygen or electron transfer. Accordingly, several inorganic contaminants may be reduced into their insoluble forms. The reductive transformation process is the so-called "cementation" process in hydrometallurgical processes for recovery of metal from the waste solution (Lung, 1986). It is well-known that the cementation apparently takes place under acidic conditions in the absence of dissolved oxygen at condition where iron is relatively soluble. The general accepted stoichiometry of the cementation process can be described according to the following equation (2.7).

$$nMe^{m+} + mN \Rightarrow nM + mN^{n+} \quad (2.7)$$

The schematic for the recovery of metallic copper is shown in the following equation; (Nadkarni et al., 1967; Nadkarni and Wadsworth, 1967; Annamalai and Murr, 1979; Strickland and Lawson, 1971; Biswas and Reid, 1972; Ku and Chen, 1992);

$$Cu^{2+} + Fe^0 \Rightarrow Cu^0 + Fe^{2+} \quad (2.8)$$

$$Eh^0_{\left(\frac{Cu^{2+}}{Cu_0}\right)} = +0.34\,V$$

Table 2.2 Standard electrode potentials (E^0) of contaminants relevant for Fe^0 barrier

Reaction						Eh°(V)
$2H_2O$		$+2e^-$	$\Leftrightarrow$	$2H_2O$	$+2OH^-$	-0.83
$Fe^{2+}(aq)$		$+2e^-$	$\Leftrightarrow$	Fe^0		-0.44
$Cd^{2+}(aq)$		$+2e^-$	$\Leftrightarrow$	Cd^0		-0.40
H^+		$+e^-$	$\Leftrightarrow$	$1/2\,H_2(g)$		-0.00
$Cu^{2+}(aq)$		$+2e^-$	$\Leftrightarrow$	Cu^0		+0.34
$Zn^{2+}(aq)$		$+2e^-$	$\Leftrightarrow$	Zn^0		+0.76
$Fe^{3+}(aq)$		$+e^-$	$\Leftrightarrow$	$Fe^{2+}(aq)$		+0.77
O_2	$+2H_2O$	$+4e^-$	$\Leftrightarrow$	$4OH^-$		-0.81
$2Hg^{2+}(aq)$		$+2e^-$	$\Leftrightarrow$	Hg^{2+}		+0.92
$Fe(OH)_{3(S)}$	$+3H^+$	$+e^-$	$\Leftrightarrow$	$Fe^{2+}(aq)$	$+3H_2O$	+0.93
$Pd^{2+}(aq)$		$+2e^-$	$\Leftrightarrow$	Pd^0		+0.99
$Fe^{2+}(aq)$	$+3H_2O$		$\Leftrightarrow$	$4OH^-$		+0.81
$Cr_2O_7^{2-}$	$+14H^+$	$+6e^-$	$\Leftrightarrow$	$2Cr^{3+}$	$+7H_2O$	+1.33

Ref. Benjamin (2002); Karschunker (2005); Hamann (1975) ; chemiemaster.de; Farrel et al. (2001)

With a stoichiometry factor *(m/n)* equal to 1, hence, about 0.88 g of iron is required for 1 g of copper removal. The cementation of copper takes place due to a strong driving force for Cu^{2+} reduction [+0.34 V for Cu^{2+}/Cu^0; -0.44 V for Fe^{2+}/Fe^0]. Table 2.2 depicts the standard electrode potential for various compounds relevant for Fe^0 barrier in water treatment processes.

In natural aerated water, the electrochemical reduction of redox-sensitive compounds takes place through other redox couples than Fe^0. Ongoing researches have shown that the reduction of copper in natural water conditions likely takes palce via the reduction of aqueous Fe^{2+} or by the adsorbed or structural Fe^{2+} [-0.35 to -0.56 V for Fe^{3+}/Fe^{2+}] (Noubactep, 2009). This is the case since it was found that dissolved oxygen is mostly consumed by Fe^{2+} rather than by the surface of metallic irons (Fe^0) (Huang and Zhang, 2005). The reaction follows;

$$Cu^{2+} + 2Fe^{2+} \Rightarrow Cu^0 + 2Fe^{3+} \qquad (2.9)$$

Adsorption process

Adsorption implies a process where chemical contaminants partition from an aqueous solution onto a solid surface, resulting in an immobilization of contaminants. Among the variable surfaces, iron (oxy)hydroxides produced by the corrosion of iron is the dominant adsorptive sites in the iron barriers. Iron corrosion products are very effective adsorbents for both organic and inorganic contaminants; e.g., the cation can be bounded on the solid surface by an exchange of the protons as described in equation 2.10 (Smith, 1998; Benjamin, 2002).

$$\equiv Fe - OH + Me^{2+} \Rightarrow (FeO) - Me^+ + H^+ \qquad (2.10)$$

The charge on the iron oxides develops due to the dissociation of the surface hydroxyl groups,

which arises from the protonation and deprotonation of the functional group of the surface (OH-group). The reactions can be expressed as acids/bases equilibrium by the following dissociation reactions,

$$\equiv FeOH_2^+ \quad \Leftrightarrow \equiv FeOH \; + H^+ \qquad K_{a,1}^S \qquad (2.11)$$

$$\equiv FeOH \quad \Leftrightarrow \equiv FeO^- \; + H^+ \qquad K_{a,2}^S \qquad (2.12)$$

The equilibrium constants for these reactions are termed acidity constants, $K_{a,1}^S$, $K_{a,2}^S$, with the surface (≡Fe) and can be derived by the law of mass reaction:

$$K_{a,1}^S = \frac{\{\equiv FeOH\}\{H^+\}}{\{\equiv FeOH_2^+\}} \qquad (2.13)$$

$$K_{a,2}^S = \frac{\{\equiv FeO^-\}\{H^+\}}{\{\equiv FeOH\}} \qquad (2.14)$$

The affinity of adsorption is generally determined by pH_{PZC}. The pH_{pzc} is the pH at which a positive charge by protonation exists in approximately equal numbers with negative charges caused by the development of deprotonation on the iron surface (equations 2.15 and 2.16);

$$\{\equiv FeOH^{2+}\} \Leftrightarrow \{\equiv FeO^-\} \qquad (2.15)$$

$$pH_{pzc} = 0.5\,(pK_{a,1}^S + pK_{a,2}^S) \qquad (2.16)$$

Under an acidic condition or pH below pH_{pzc}, protons are sorbed on the functional group that causes the iron surface to have a net positive charge and, thus, inhibit cation adsorption. At

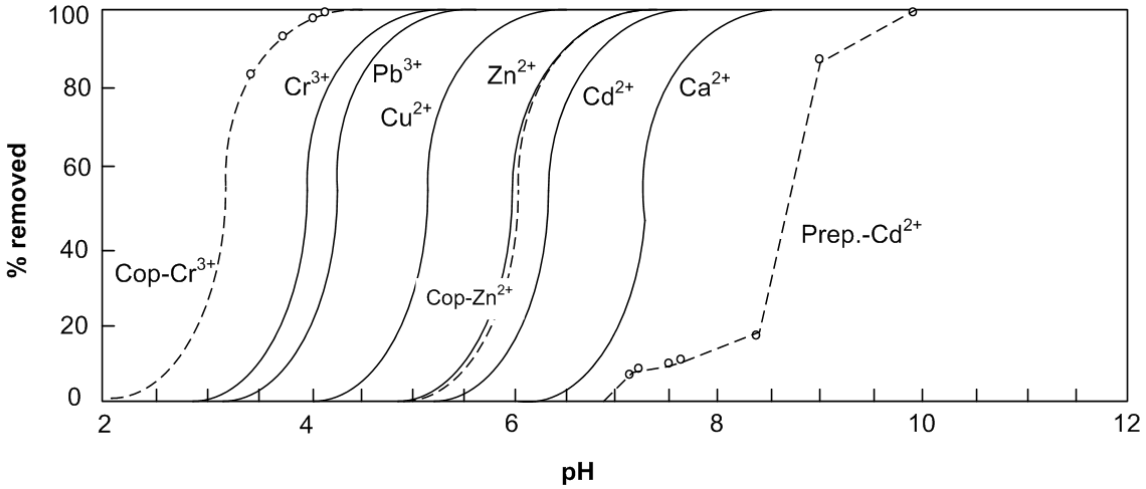

Fig. 2.3 pH dependent sorption of metal cations on iron hydroxide (adapted from Denver, 1997). The co-precipitation results of Cr^{3+} and Zn^{2+} and precipitation of Cd^{2+} were obtained from Crawford et al. (1993) and Smith (1996), respectively.

above $pH_{pzc,}$ the oxygenatom stays deprotonized and the surface prevails to have a net negative charge, thus, enhancing cation adsorption (Benjamin, 2002; Merkel and Planer-Friedrich, 2005). Other than pH, the adsorption is dependent on the media properties such as surface area of oxides and other water quality parameters such as ionic strength, temperature, and concentration of compounds in the water solution. General properties of iron oxides are demonstrated in Table 2.3.The pH dependent sorption of metals on iron hydroxide is illustrated in Fig. 2.3.

Most adsorption reactions are reversible and occur at relatively rapid rates. Some adsorption reactions are specific with the attachment occurring preferentially at particular sites. Other adsorption reactions are less specific and have more of a tendency to compete with other ions for attachment sites. In addition, the adsorption can result from either inner-sphere or outer-sphere complexation adsorption resulting from ion-pair bonding due to electrostatic forces and hydration water that separates the solvated ion from the surface. Surface complexation models have been used effectively to predict the reaction chemistry of adsorption processes (Dzombak and Morel, 1990).

Co-precipitation process

Another fundamental mechanism that is involved in the uptake of contaminants in the Fe^0 barrier is known as co-precipitation. Co-precipitation occurs whenever species (e.g., iron) precipitate (e.g., as hydroxide) co-exists with a trace amounts of foreign species. In this process, the foreign species are simply entrapped in the mass of precipitates (co-precipitation). Co-precipitation is a well-known unspecific removal mechanism of species from the aqueous solution (Noubactep, 2008a) and independently takes place. There is no general clear cut distinction between adsorption and co-precipitation (Crawford et al., 1993). In the case of adsorption, the adsorptive surface is initially present prior to the addition of the metal ion whereas the co-precipitation of metals takes place is in a way that the precipitating surface is formed in the presence of the metal iron to be removed. Crawford et al. (1993) showed that there is a large enhancement of Ni^{2+} and Cr^{2+} removal and smaller for Zn^{2+} taking place by the co-precipitation processes, where metal removal occurs at a lower pH than the

Table 2.3 General properties of iron and iron oxides

Substance	Formula[b]	Color[b]	Density[b] [g m^{-3}]	pH_{PZC} [-]	Surface area[b] [m^2 g^{-1}]
Zero-valent iron[a]	Fe^0	-	7.86[c]	-	0.385[a]
Wüstite	FeO	black	5.9-5.99		
Ferrihydrite	$5Fe_2O_39H_2O$	red-brown	3.96		159-600[d]
Magnetite	Fe_3O_4	black	5.18	8.0	4-100
Maghemite	Fe_2O_3	reddish-brown	4.87		
Goethite	α-FeOOH	red-brown	4.26	7.5	52
Akaganeit	β-FeOOH	yellow-brown	3.56	7.9	178
Lepidocrocite	γ-FeOOH	orange	4.09		15-260
Haemetite	Fe_2O_3	red	5.26	8.6	43.5
Rust[a]	α-FeOOH, γ-FeOOH, Fe_2O_3	red-brown	-	7.2	42

Ref: (a) This work; (b) Cornell and Schwertmann (1996); (c) Noubactep (2008); (d) Dzombak and Morel (1990)

adsorption and precipitation (Fig.2.3). It is evident from several investigations that co-precipitation is one of the main removal mechanisms of organic and inorganic contaminants in the Fe^0 barrier (Noubactep, 2008a; Wilkin and McNeil, 2003).

Chemical precipitation process

Precipitation of heavy metals is a commonly used process in wastewater treatment plants. The precipitation of metals takes place when the solubility product of the solid is reached and, as a result, the dissolved form of contaminants will be converted into its various insoluble species such as hydroxides, sulfides and carbonates. Solubility of minerals can be expressed by dissolution of metal hydroxides and the corresponding equilibrium constants as demonstrated in the following;

$$Me(OH)_2(s) \Leftrightarrow Me^{2+} + 2(OH)^- \quad (2.16)$$

$$K_{s0} = \frac{\{Me^{2+}\}\{OH^-\}^2}{\{Me(OH)_2\}}$$

$$Me(CO)_3(s) + H^+ \Leftrightarrow Me^{2+} + HCO^{3-} \quad (2.17)$$

$$K_{s0} = \frac{\{Me^{2+}\}\{HCO^{3-}\}}{\{MeCO_3\}\{H^+\}}$$

Table 2.4 shows the solubility of calcium, copper, zinc and iron minerals relevant to the Fe^0 barrier. The precipitation of metals typically results in a sharp sigmoidal removal profile occurring at a higher pH than adsorption/co-precipitation processes (Fig. 2.3). In contrast to

Table 2.4 The solubility and K_{s0} values of some minerals relevant to Fe^0 barrier*

Mineral	Reaction			Log L
Calcite	$CaCO_3(s)$	⇔	$Ca^{2+} + CO_3^{2-}$	-8.35
Dolomite	$CaCO_3MgCO_3(s)$	⇔	$Ca^{2+} + Mg^{2+} + 2CO_3^{2-}$	-1.70
Siderite	$FeCO_3$	⇔	$Fe^{2+} + CO_3^{2-}$	-10.7
Smithsonite	$ZnCO_3$ (s)	⇔	$Zn^{2+} + CO_3^{2-}$	-10.78
Malachite	$Cu_2(OH)_2CO_3(s) + 2H^+$	⇔	$2Cu^{2+} + CO_3^{2-} + 2H_2O$	-5.80
Azurite	$Cu3(OH)_2(CO_3)_2(s) + 2H^+$	⇔	$3Cu^{2+} + 2CO_3^{2-} + 2H_2O$	-18.0
Portlandite	$Ca(OH)_2(s)$	⇔	$Ca^{2+} + 2OH^-$	-5.19
	$Fe(OH)_2(s)$	⇔	$Fe^{2+} + 2OH^-$	-15.10
Goethite	α-$FeOOH(s) + H_2O$	⇔	$Fe^{3+} + 3OH^-$	-40.4
Haematite	$0.5Fe_2O_3(s) + 1.5H_2O$	⇔	$Fe^{3+} + 3OH^-$	-42.7
Tenorite	$CuO(s) + 2H^+$	⇔	$Cu^{2+} + H_2O$	-7.65
	$Cu(OH)_2$	⇔	$Cu^{2+} + 2OH^-$	-19.4
Zinckite	$ZnO(s) + 2H^+$	⇔	$Zn^{2+} + H_2O$	-11.33
	$ZnO(s) + H_2O$	⇔	$Zn^{2+} + 2OH^-$	-16.89
	$Zn(OH)_2(s)$	⇔	$Zn^{2+} + 2OH^-$	-1.6.4

References: * Data complied by Ludwig (2007) with modification of K_{s0} in according with; Morel et al. (1993); Mann (1980); Sigg and Stumn (1996); Schecher et al. (2001); Feiknecht (1963); Benjamin (2002); Schecher and McAvoy (2001)

reductive transformation and adsorption/co-precipitation processes, the precipitation of metal hydroxide is a fast reaction and can proceed within a magnitude of a second under an alkaline pH (Merkel and Planer-Friedrich, 2005). However, such a process implies that Fe^0 barriers will sooner or later encounter different degrees of permeability losses, amour of reactive surface and clogging by precipitated products (Simon et al., 2001; Cravotta and Watzlaf, 2002).

2.3.2 Removal of inorganic pollutants

A number of studies have been devoted to identifying the mechanisms involved in the removal of inorganic compounds during transport through the reactive iron barrier. Nevertheless, there has been greatly inconsistency among these works (c.f., Table A4 in appendix). These inconsistencies can be attributed mainly due to the complexity of the iron barrier itself, in which multiple reactions are possible, as well as the differences in the employed experimental conditions.

Gu et al. (1998) conducted two batch experiments to compare the removal rate of iron and iron oxides. In their experiments, a very high concentration of U^{6+} per iron or iron oxides mass ratio was tested under well mixed conditions. They observed the precipitation of insoluble U^{4+} on the iron surface and concluded that the uptake of U^{6+} was primarily due to the reductive transformation processes. Contrary to the shaking batch test, Noubactep et al. (2003) performed the test using un-shook vials presumably closer to actual groundwater conditions. The experiment was maintained undisturbed for over 50 days in darkness and water quality parameters were measured at interval periods. Based on the observation; the removal of U^{6+} increased considerably from a mild pH range, i.e., from 18% at pH 3.9 to 94% at pH 4.4 indicating the role of adsorption/co-precipitation processes because if the reductive transformation was the main removal mechanism, there should have been a higher removal of U^{6+} at a mildly acidic pH (pH 3.9) compared to a higher pH. In addition to this work, Fiedor et al. (1998) compared the reaction of U^{6+} with Fe^0 under two distinguished conditions; deoxygenated and oxygenated conditions and found that the adsorption is the dominant removal mechanism. Qui et al. (2000) observed no transformation or only partial reduction of metals (U^{6+}, Cr^{6+} and Se^{6+}) on the Fe^0 surface.

The batch investigation of Fe^0 treatment of heavy metals under an acid mine drainage condition shows that most of the metals including Cu^{2+} and Zn^{2+} were removed via adsorption and precipitation processes. The Hg^{2+} was, however, removed by reductive transformation because of its high driving force (Wilkin and McNeil, 2003). Gibert et al. (2003) reported a formation of nodular shaped copper metals on the iron surface during passage through a Fe^0/organic-composed barrier and concluded that Cu^{2+} was removed mainly through cementation processes whereas Zn^{2+} was removed via a metal sulfide-complex and the adsorption onto iron (oxy)hydroxide and organic matter. Tranyek et al. (2005) reported the rates of copper reductive transformation based on a range of batch tests. Lopez et al. (2003) found that reductive transformation of copper prevailed only at a relatively high temperature and at a high Cu^{2+} per iron ratio. In their study, the reactive iron originated from short-blast

iron materials that contained only 7% metallic iron per its total unit mass. The reduction process of Cu^{2+} by Fe^0 has long been well established but generally limited in hydrometallurgical processes under which growth of metallic copper on iron surfaces and a sponge-like amorphous structure were often observed (Ku and Chen, 1992).

Based on these existing literatures, it is difficult to anticipate which reaction is prevalent at a specific remediation site during Fe^0 treatment of heavy metals in the iron barrier. The variability in physical and chemical characteristics as well as the strong ability of Fe^0 and related corrosion products in regulating the redox chemistry of the solution makes the processes extremely complex. Nevertheless, mechanisms that are most important in the removal of inorganic pollutants in an Fe^0 barrier system can be named; (1) reductive transformation, (2) adsorption/co-precipitation and (3) chemical precipitation (Cantrell et al., 1995; Smith, 1996; Fiedor et al., 1998; Gu et al., 1998; Shokes and Moller, 1999; Blowes et al., 2000; Naftz et al., 2002; Noubactep et al., 2003; Wilkin and McNeil, 2003). Generally, the latter two processes are favored at higher pH in accordance with the corrosion processes in the presence of dissolved oxygen. The "reductive transformation" or ''cementation'' process, imply that redox-sensitive compounds are reduced into insoluble forms, has been generally shown to be highly effective under acidic conditions in the absence of DO (Nadkarni et al., 1967; Nadkarni and Wadsworth, 1967; Annamalai and Murr, 1979; Strickland and Lawson, 1971; Biswas and Reid, 1972; Ku and Chen, 1992).

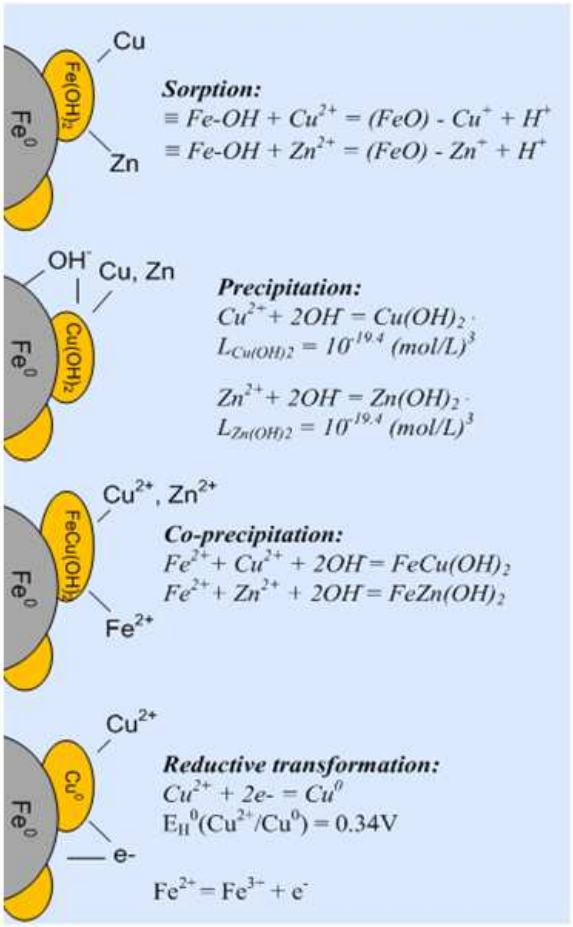

Fig. 2.4 Schematic of copper and zinc removal in Fe^0 system

2.4 Fe^0 treatment of metal contaminated runoff

2.4.1 Process of metal removal

The schematic of reaction pathways possibly involved in the Fe^0 treatment barrier of Cu^{2+}- and Zn^{2+}- contaminated roof runoff are demonstrated in Fig. 2.4. The "cementation" process implies that redox-sensitive compounds such as copper are reduced into insoluble forms. Although, it is well-known that the cementation reaction apparently takes place under acidic conditions in the absence of dissolved oxygen (Nadkarni et al., 1967; Nadkarni and Wadsworth, 1967; Annamalai and Murr, 1979; Strickland and Lawson, 1971; Biswas and Reid, 1972; Ku and Chen, 1992), this process may not play significant role in an oxygenated runoff. The reductive precipitation has been believed taking place via reaction with Fe^0 surfaces [0.34 V for Cu^{2+}/Cu^0; 0.76 V for Zn^{2+}/Zn^0, -0.44 V for Fe^{2+}/Fe^0], however, more insight research has demonstrated that the indirect reduction with dissolved and structured Fe^{2+} in the vicinity of Fe^0 surface plays a major role in the process (Noubactep, 2008; Ghauch et al., accepted).

When Fe^0 is placed in a flowing oxygenated runoff solution, Fe^{2+} dissolutes out into the bulk water phase and forms Fe^{3+} which is subsequently precipitated into amorphous ferric hydroxides ($Fe(OH)_{3(s)}$ or ferrihydrite) at an alkaline pH. The precipitates of ferric oxides are either localized close to a metallic iron surface or dissipate out into the bulk solution (Smith, 1998; Farrell et al., 2000). The latter is more likely under stormwater runoff conditions due to the low ionic strength of the runoff solution (Rangsivek and Jekel, 2005). The produced iron oxides behave as a very effective adsorbent for several inorganic compounds, and thus, both Cu^{2+} and Zn^{2+} can be removed via the adsorption reactions. Under the considered system, it is also anticipated that the adsorbed heavy metals are slowly incorporated into the structure of iron corrosion products while precipitating and transforming into other stable states such as Goethite, Lepidocrocite and Hematite (α-, γ-FeOOH and Fe_2O_3, respectively).

As a result of a production of OH^- during iron corrosion, the runoff water can be naturalized and if the increase of pH is high enough this may also lead to precipitation of various hydroxides and carbonates of copper and zinc, e.g., $CuOH^+$, $CuCO_3$, $ZnCO_3$ and $Zn(OH)_2$. The solubility for copper and zinc equilibrium in a hydroxide-carbonate system are about 15-50 µg L^{-1} in the pH range of 8-9 and 0.5-3.0 mg L^{-1} at pH 9-11, respectively (Ludwig, 2007). The lowest solubility of iron hydroxides is about 0.03 µg L^{-1} at pH 8-9. At concentrations up to 0.5-2 mg L^{-1} DOC, the solubility of copper may increase up to 0.92-1 mg L^{-1} in the equilibrium with malachite (Merkel, 2002). The copper solubility increases significantly from approx. 0.14 mg L^{-1} up to approx. 1 mg L^{-1} in the presence of small quantities of DOC (0.5 to 2 mg L^{-1}).

2.4.2 Practical issues of Fe^0 barrier

For simplicity and the desirable low cost of a runoff treatment system, a Fe^0 fixed bed is considered feasible. However, the successful application of the system is usually limited by two factors. The first is the system's efficiency in coping with the effluent's quality at variable runoff characteristics. Rangsivek and Jekel (2005) reported about twofold lower rates of metal removal in the presence of a fraction of NOM. Also, the corrosion rates, phases and morphology of the iron corrosion products can be strongly affected by water qualities and operational parameters (Rangsivek and Jekel, 2005; 2008; Noubactep, 2008) and, thus, influence the removal rate of metals. The second limitations for the actual implementation of a Fe^0 system in especially oxygenated-water at high flow conditions of storm water runoff conditions arise due to a loss of porosity and a decrease of the mass transport rate of contaminants by generations of secondary minerals (Roh et al., 2000; Furukawa et al., 2002; Kamolpornwijit et al., 2003). These problems are alleviated generally by mixing the Fe^0 media with sand.

2.5 Natural organic matter

2.5.1 Significance of NOM

Natural organic matter (NOM) is a complex mixture of a variety of polyfunctional organic ligands, ranging from simple to more complex compounds of humic and fulvic acids. NOM is highly heterogeneous, having a mixture of two major types of functional groups, carboxylic and phenolic compounds, in which the pK_a values are estimated to be 4.5 and 10, respectively (Perdue, 1985). Based on these charateristics, NOM plays a crucial role in the transport and fate of metals in aquatic environments (Aiken et al., 1985).

NOM is originated by different sources and can be classified into terrestrial zone, aquatic zone, e.g., stream water, groundwater and seawater which are subsequently transported into subsurface aquifers. NOM produced during sewage treatment processes is commonly referred to as "effluent organic matter (EfOM)". Surface water NOM are believed to be the degradation products of soil organic matter. In general, NOM are a mixture of by-products of plants and microorganisms. It can exist in an aquatic environment as dissolved and particulate compounds. NOM from different origins possesses independent characteristics and properties. As compared with NOM in groundwater, the surface water is higher in hydrophobic compounds and aromaticity (Table 2.5). The groundwater NOM is usually a residual of surface water NOM, which has been adsorbed and degraded during transport to underground. As a focal aim of this work, when rainwater falls into various surfaces, the generated runoff may be enriched with natural organic matter and because of a wide variety of original material on the catchment area, origin, age, chemical characteristics of the substances, can lead to a variety of ways for its degradation and transformation. Thus, a complex structure and mixture of the resulting substances may be produced.

Generally, NOM samples in the aquatic environment contain approximately 50% hydrophobic and 30% hydrophilic fractions and the remaining 20% of total NOM concentration are comprised of carbohydrates, amino acids, and other simple molecules (Table 2.5). Among all fractions, the hydrophobic humic and fulvic acids are the most reactive compounds which exhibit strong ligands. DOC may also include xenobiotic ligands, like EDTA, NTA, or phosphonates in anthropogenically contaminated waters.

NOM are generally not toxic but direct problems arise with the presence of NOM with regard to the drinkability resulting from aesthetic reasons such as undesirable smell, taste impairments and color. A yellowish color is a result of humic acid in the drinking water. However, the presence of NOM can also cause many problems in the drinking water treatment process. During coagulation and flocculation reactions, NOM stabilizes dispersed and colloidal particles in the water. NOM are known as an important precursor for potentially hazardous Trihalomethanes (THM) or Halogenic acid (HAA) during the chlorination processes. NOM is also considered a major cause of membrane fouling that is still a subject of extensive studies. It is well known that NOM plays a crucial role in the transport of metals in an aquatic environment. During the conventional treatment processes, NOM may compete for adsorption sites with metals resulting in a decreasing capacity. It can significantly change electrochemistry of the underlying layer of an adsorbent. For these reasons, it is anticipated that NOM can strongly impact the removal of heavy metals in the Fe^0 treatment barrier.

2.5.2 Characterization of NOM

Due to the complexity of NOM, several techniques are required to completely characterize all the essential information of NOM chemistry. Important characteristics of NOM include composition, molecular size, molecular weight, structure and functionality. A brief review of fractionation and characterization methods, which are employed in the present thesis, is described in this section. The fractionation of NOM followed the XAD adsorption method described by Aiken et al. (1985). The determination of molecular size/weight and acidity are discussed according to gel permeation chromatography and potentiometric titration methods, respectively. The copper complexation capacity is employed in order to gain the basic knowledge of metal complexation capacity of NOM.

Natural organic matter exists in the environment both in dissolved and particulate forms. However, when addressing NOM in the aquatic environment, the dissolved compound is often the main interest to the study of aquatic chemistry. An effective means of isolation of dissolved compounds from the total NOM samples can be performed by means of a membrane procedure, a separation can be based on molecule size cutoff through 0.22 um. However, in several cases this pore size of membrane pore size is too small and often results in fouling and high operational cost. For general cases, filtration of NOM solution through 0.45 um membrane is suitable.

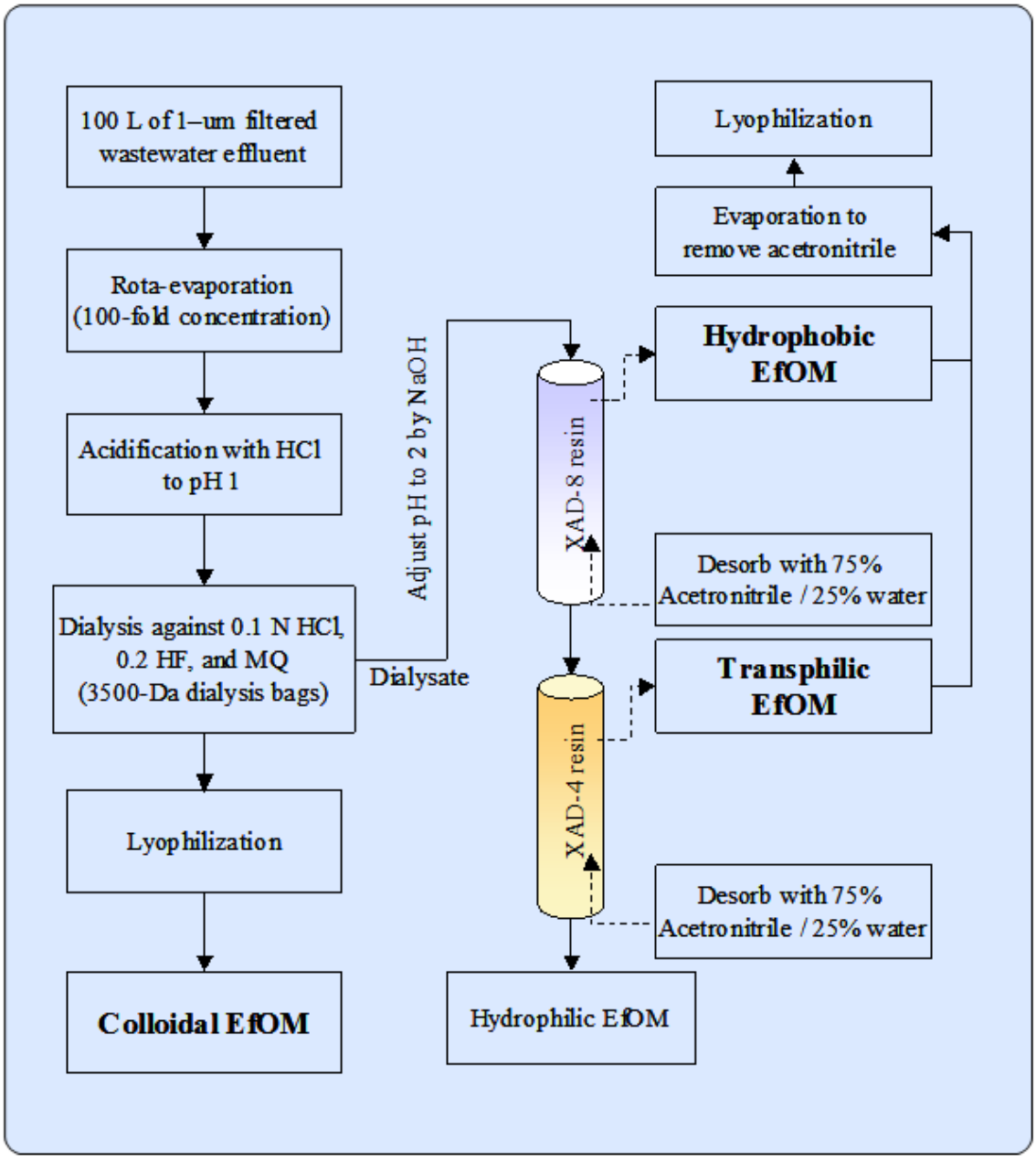

Fig. 2.5 NOM fractionation methods (Jarusuttirak, 2002)

In order to fractionate NOM, the state-of-art method or so called "XAD-adsorption method" described by the international humic society is generally employed, which can be illustrated in Fig. 2.5. The method is used to isolate humic substances from natural water. During the procedure, the dissolved organic matter (DOM) was passed through XAD-4 and XAD-8 or a combination of both columns. XAD resins are nonionic macropodous copolymers with large surface areas. The "hydrophobic effect" is the principle driving force for organic sorption on these resins. Sorption of organic acids such as humic substances is determined by the solute's solubility and solution pH. Fundamentally, the hydrophobic fraction refers to the fraction that

is adsorbed onto the XAD-8 resin, which can be obtained by extracting the adsorbed compounds using an alkaline extraction, i.e., NaOH. The same procedures were employed in order to fractionate the hydrophobic and transphilic fractions. In the later cases, filtration was made to XAD-4 and a combination of both columns, respectively. The fraction that can neither be adsorbed on XAD-8 nor XAD-4 is designated as a hydrophilic, consisting of small molecular polar materials as well as carbon- and amino acids and places 17 to 45% on the DOC (Aiken et al. 1993). Before the XAD-fractionation, dialysis can lead to a separation of colloids of existing NOM (Leenheer, 2004). To obtain fulvic acid out of humic substances, the total fraction is precipitated at a low pH and passed through a desalting step using a cation exchange. The humic acid and fulvic acid that are isolated from aqueous samples thus contain only hydrophobic organic acids, but samples extracted from solid-phase materials include both hydrophobic and hydrophilic acids (IHSS).

In a subsequent test for carbon-determination and UV-determination, the method is called liquid chromatography (LC-OCD). The method divids total dissolved NOM into polysaccharide, humic substances, building blocks, low molecular weight and amphilic compounds (Huber and Frimmel, 1996). The measurement of the molecular size employed in this work was based on gel permeation chromatography techniques (Huber and Frimmel, 1996). The principle of this technique is that the gel structure is perfused by a system of pores, and the size of these is determined by the degree of cross-linking in the polymer. These pores enable the gel to act as a chromatographic medium giving separations based on differences in molecular size. When a solution, containing a mixture of molecules of varying sizes, is applied to the top of a gel column and eluted with solvent, those molecules which cannot enter the pores in the beads will pass between the beads and will be eluted first from the column. Molecules smaller than the pore sizes of the gel will enter the pores and their passage through the column will be retarded.

The most commonly encountered acidic functional groups in organic compounds include carboxylic acids, phenols, ammonium ions, alcohols, and thiols. The most active organic groups of NOM are carboxylic and phenolic compounds. In order to properly describe the acid-base properties of a particular humic substance, it is essential that the identification and quantification of acidic functional groups is accomplished. In this study, a direct titration

Table 2.5 Characteristics of NOM containing water from different sources

Source*	pH	Condc.	DOC	UVA_{254}	SUVA	HPO	HPI	TPI
		($\mu S\ cm^{-1}$)	($mg\ L^{-1}$)	(m^{-1})	($m^{-1}\ mg^{-1}\ L$)	%	%	%
Natural water[a]	7.1-8.5	183-384	2.7-8.4	5.7-29.5	1.4-3.5	39-50	24-35	22-28
Ground water[b]			0.94	2.1	2.2		42	
SRHA[b]	6.8	300	10	74	7.4	94	1	5
AOM (Algal OM)[b]	6.8	300	10	42	4.2	26	57	17
Influents to WWTP[c]	6.5-7.4			4-4.9		43-53	37-40	
EfOM[d]	7.56-8.08	558-1195	5.9-14.3	16-26	1.82-2.71	32-40	40-45	20-23
Natural water[e]	6.6-8.0	5.6-50.3	3.1-6.8	9-38	2.9-5.6	38-79	9-31	11-31

References: (a) Lee et al. (2004); (b) Amy 2004 (c) Korshin et al. (1997) (d) Jarusutthirak (e) Yoon et al. (2005)

technique is employed because it is a relatively simple, fast and commonly employed method that will allow for comparison of the results. The potentiometric titration is operationally defined by the carboxyl content as the concentration of functional groups that are neutralized at a specified pH. The carboxylic group was determined in order to estimate carboxyl content at the equivalence point for titration of pH around 7. The phenolic group was estimated at about the double consumption of the base required for the carboxylic group (Oden et al., 1993).

DOC was determined by means of thermal-catalytic oxidation using a high-TOC analyser. In combination with spectroscopic methods, the aromaticity and the humic characteristic of the water samples can be identified through the determination of spectral absorption at 254 nm (UVA_{254}), as well as the UVA/DOC ratio. The UV adsorption, conceptually linked to the amount of aromatic carboxyl and phenolic groups. At the same time it is generally perceived that specific UV radiation (UVA_{254}/DOC) is an important proxy of aromaticity, total C-content and molecular weight. By means of fluorescence and infrared-spectroscopic, single structure features and functional groups can be identified (Senesi, 1990). The C13-NMR (Nuclear magnetic resonance) represents a method to obtain information about the functionality of the carbon atoms in the NOM-connections (Wong et al., 2002). A non-destruction free method is the Pyrolyse-GC/MS; by using high temperatures to disaggregate NOM into fleeting fragments, that can be identified by GC/MS-Analysis. Based on the fragments, conclusions can be made on single material groups (protein, polysaccharide etc.) (Abbt-brown et al. 1990; Croué, 2002). Other important characteristics of NOM involves the determination of elemental content of the redissolved samples (DOC, Na, Ca, Cu, Fe, and Mn), proton capacity and content of hydrolysable amino acids and carbohydrates.

2.5.3 Impacts of NOM on iron corrosion processes

Limited investigations are reported in the literatures that deal directly with NOM impacts on the removal of contaminants using Fe^0 (Tratnyek et al. 2001; Dries et al., 2005). Nevertheless, many previous studies that help in the understanding of the transport, fate and impact of NOM were extensive. These works studied iron oxides or corrosion products, e.g., Davis and Leckie (1978), Laxen (1985), Liang et al. (1993), Stevenson (1994), Gu et al. (2000), and Kieber et al. (2005). Tratnyek et al. (2001) carried out the batch test to determine the impact of NOM on Fe^0 reduction of several model organic compounds. In their study, NOM was found to contribute to the inhibition effect on carbon tetrachloride and trichloroethylene (TCE), presumably due to the adsorptive competition of the compounds for surface sites. The increase in the reductive transformation rate of organic compounds was also observed in the system containing juglone, lawsone, and anthraquinone disulfonate (modeled NOM compounds), which was attributed to an electron mediation mechanism.

Dries et al. (2005) investigated the impact of Aldrich humic acid (HA) on the removal of zinc, nickel and chromium in a Fe^0 system. In the batch test, the removal rate of Zn and Ni (5 mg l^{-1}) was lower in the presence of HA (20 mg l^{-1}) than in the absence of HA. The column system

shows similar results, as a significant breakthrough of Ni and Zn occurred in the column system fed with HA. The decrease removal of zinc and nickel was presumably due to the formation of metal-humate complexes and binding of the adsorptive surface site. In both systems, chromate was not affected significantly.

Laxen (1985) found that the adsorption of humic substances reduces the complexation of Cd^{2+}, Cu^{2+} and Ni^{2+} onto the ferric hydroxide surface. A ligand exchange has often been described as an important mechanism between NOM removal in the presence of iron oxides (Gu et al., 1998). The general reaction scheme can be expressed by the equations (Chi and Amy, 2004);

$$\equiv FeOH_2^+ + S - COO^- \Leftrightarrow \equiv FeOOC - S + H_2O \quad (2.18)$$

$$\equiv FeOH + S - COO \Leftrightarrow \equiv FeOOC - S + OH^- \quad (2.19)$$

where ≡FeOH and $\equiv FeOH_2^+$ represent 1 mole of reactive hydroxyls and water, respectively, bound to a surface of Fe mineral, and S–COO− represents 1 mol of carboxylate groups on NOM. On the contrary, Davis and Bhatnagar (1995) observed that HA accelerates the Cd^{2+} adsorption onto Hematite. Davis and Leckie (1978) demonstrated that organic substances could either enhance or diminish Cu^{2+} adsorption on amorphous iron oxide by neutralizing the surface charge of the adsorption sites. According to a number of studies, the oxidation of ferrous to ferric iron can be affected by NOM. The oxidation rate is typically inhibited in the presence of organic compounds at high DO, ranging from mild to strong effects. Humic substance generally inhibits the oxidation rate hypothesized because of Fe^{2+} ligand-complexes (Kieber et al., 2005; Liang et al., 1993). However in the case of Fe^{2+} oxidation under low DO partial pressures, Liang et al. (1993) showed the oxidation rate is enhanced. They also found that the iron hydroxides formed in a NOM containing solution have a predominantly negative surface charge at natural pH. Besides these effects, NOM is known for having a reductive property toward several inorganic contaminants (Stevenson, 1994). Gu et al. (2000) observed that ferric iron hydroxide and CrO_4^{2-} were reduced by different fractions of NOM. Davis and Leckie (1978) gave a short summary stating that three mechanisms may be involved in the adsorption of organic and metal on iron oxides: (i) binding of NOM to the oxide surface can block the binding site and can also compete with metal removal (ii) NOM complexes with metal remaining in the solution prevent the metals from being adsorbed at the oxide surface, and (iii) the removal of metals is enhanced by the adsorbed NOM at the iron oxide surface. Taken this into account and the fact that natural roof runoff NOM can vary greatly in molecular weight, molecular size, organic functional group and other properties due to its variable composition, it is likely that the impacts of NOM on the iron system are complex and are governed by several reactions**.** Yet, a thorough understanding of the processes involved has not been developed.

2.6 Modeling of the F^0 system

A model capable of simulating the dynamic processes of copper and zinc removal by Fe^0 at varying runoff conditions is important for the engineering design of the treatment barrier. In most of the reported works, the surface complexation model coupled with the mass transfer kinetics has been employed (Table 2.3). Smith (1996; 1998) successfully describes the removal of Cd^{2+}, Pb^{2+} and Zn^{2+} by short blast iron using a dual mass transport incorporating a triple layer model. Steiner et al. (2006) simulated copper removal by granular ferric hydroxide using a Two Region Model, which considered film and pore diffusions as removal mechanisms. Nikolaidis et al. (2003) and Tyrovola et al. (2007) employed a one dimension advection-reaction-dispersion equation and considered the surface adsorption/co-precipitation and the reductive transformation as removal pathways of Arsenic in Fe^0 column. In a more complex modeling approaches, Wang and Salvage (2005) and Kouznetsova et al. (2007) added terms describing the dynamic aging of iron which allow the simulation of treatment processes of U(VI) and chlorinated ethenes, respectively, at a non-equilibrium condition. Sperlich et al (2005; 2008) employed a constant pattern homogeneous surface diffusion model (CPHSDM) to model the adsorption of arsenic by granular ferric hydroxide (GFH). In most of the modeling approaches presented, both the kinetic and isotherm parameters required are generally described in lump sum form of parameters (Sperlich, 2005) as these may have been very difficult to determine at each experimental conditions (Smith, 1996; 1998; Sperlich, 2005; 2008). The following text discussed the adsorption equilibrium and adsorption dynamic relevant to adsorption of metals in aqueous phase. It is aimed to apply these mathematical models for describing the removal of metals in Fe^0 system. Further detailed discussions of the model can be found in Sperlich et al (2005; 2008).

Adsorption Equilibrium

The adsorption equilibrium is defined as the amount of adsorbate which can be removed in the treatment processes. It is the main parameter that is used for adsorption design, which is described by the steady state conditions which exist between the aqueous-phase concentration of the adsorbate and its solid-phase concentration. The equilibrium solid-phase concentration depends on the properties of the adsorbent and the adsorbate, the solvent, temperature, and the equilibrium aqueous-phase concentration.

The most common mathematical model used for describing the adsorption equilibrium are the Freundlich (1906) and the Langmuir models (1918). The Langmuir model assumes a homogeneous structure of an adsorption surface with a limited number of sorption, thus, its application to a heterogeneous nature of adsorbents is limited. The Freundlich isotherm describes adsorption equilibrium in terms of an exponential relation between the sorbed and dissolved molecules. The shape of the Langmuir isotherm is a gradual positive curve that flattens to a constant value whereas the Freundlich isotherm has a curved shape representing in an exponential form. In contrast to the Langmuir isotherm which is derived from a theoretical basis, the Freundlich isotherm has been developed empirically by fitting the curve with experimental data. The Freundlich isotherm can be suggested as the following;

$$q(c) = K_F \cdot c^n \quad (2.19)$$

where q(c) is the solid-phase concentration, K_F is the Freundlich constant, c is the concentration in the bulk water phase, and n is the Freundlich exponent. The parameters K_F and n can be determined from an empirical correlation of batch adsorption experiments by plotting logarithmic regression of the data and the linearized. The Freundlich components can be calculated according to the following equation;

$$\log q = log\ K_F + n \log c \quad (2.20)$$

The index n indicates whether the adsorption is favorable $(n < 1)$ or unfavorable $(n > 1)$. For a given n, the value of K_F directly reflects the adsorption capacity.

It is also possible to describe the transport of metals in the reactive barrier in terms of a retardation factor, R_f , of contaminants which is referred to the ratio between the rate of water movement and rate of contaminant movement. This can be calculated by the equation;

$$R_f = 1 + \frac{\rho}{\theta} \cdot n \cdot K_F \cdot C^{n-1} \quad (2.21)$$

Where ρ is bulk density and θ is the water content

Adsorption dynamic

In order to describe the adsorption processes and effectively design the dynamic processes of an adsorber, it is essential to know adsorption kinetics. The adsorption kinetics is expressed in the breakthrough curves. The breakthrough of the column depends on the properties of the adsorbate and adsorbent as well as the hydrodynamics of the system involving three steps of transport, namely:

a) Film diffusion

Film diffusion describes mass transport of adsorbate molecules from the bulk to the outer surface of the adsorbent. A linear concentration gradient is generally used to describe the mass transfer resistance since the thickness of the boundary layer is not known. The film diffusion coefficient can be determined by a slope of the plot of the metal concentration against time and the linear curves in a semi-logarithmic concentration-time curve can be obtained. The following equation describes the mechanism (Mertz et al., 1999):

$$\dot{n}_{F,i} = D_{F,i}(c_i - c_i^*) \quad (2.22)$$

in which $\dot{n}_{F,i}$ is the mass transfer rate per unit of surface area, $D_{F,i}$ is a film diffusion coefficient, c_i is the adsorbate concentration in the bulk and c_i^* is the adsorbate concentration on the external surface of the adsorbent.

The film diffusion coefficient can also be estimated using the Gnielinski correlation as following (Sontheimer et al., 1988);

$$k_f = \frac{[1+1.5(1-\varepsilon)]D}{d_p}\left[2 + 0.644Re^{1/2}Sc^{1/3}\right] \quad (2.23)$$

in which $d_p$is the adsorbent particle diameter (m), D is the adsorbate gas or liquid phase diffusivity ($m^2\ s^{-1}$) and ε is the bed void fraction. Re and Sc refer to the Reynolds and Schmidt number.

b) Intraparticle diffusion

The next step for the mass transfer interior of the adsorbent particles is the intraparticle diffusion steps involving two kinetic mechanism; surface diffusion and pore diffusion. The former describes the transport of adsorbate along the surface wall where the travel within the liquid-filled pores in the particles is described as pore diffusion. The surface diffusion model presumes a spherical particle of homogenous structure, although the adsorbent grains in reality are very heterogeneous in structure. The mass transfer of surface diffusion can be described by Fick's first law as follows;

$$\dot{n}_{S,i} = \rho_P D_{S,i} \frac{\partial q_i}{\partial r} \quad (2.24)$$

where $\dot{n}_{S,i}$ is the pore diffusion flux; $\rho_P$is the particle density of adsorbent grain; q_i is the solid-phase concentration in the pores; $D_{S,i}$ is the pore diffusion coefficient. Analogous to surface diffusion, the following equation describes the pore diffusion flux

$$\dot{n}_{P,i} = \varepsilon_P D_{P,i} \frac{\partial C_{P,i}}{\partial r} \quad (2.25)$$

in which $\dot{n}_{P,i}$ is the pore diffusion flux; $C_{P,i}$ is the adsorbate concentration in the pores; $D_{P,i}$ is the pore diffusion coefficient; for the pore diffusion model, it is assumed that the pore fluid concentration, $C_{P,i}$, is in equilibrium with the local solid-phase concentration.

The determination of the mass transfer coefficient can be done both by means of a batch experiment and using empirical equations. The pore diffusion coefficient is related to the adsorbate diffusitiy and the intraparicle physical properties as shown in the following equation (Sontheimer et al. 1988);

$$D_p = \frac{D}{\tau_p} \quad (2.26)$$

in which D is the adsorbate gas or liquid phase diffusivity; τ_p is the adsorbent tortuosity (-); D_p is the pore diffusion coefficient.

Generally, it is assumed that surface diffusion dominated over pore diffusion especially in lower concentration range. The surface diffusion flux is also usually many times greater than pore diffusion flux for the strongly adsorbed species. For natural waters, where both weak and strong species exist, modeling that takes pore and surface mechanisms into account may better describe the adsorption processes. Which transport mechanism controls the adsorption

processes can be determined using the surface to pore diffusion flux ratio (SPDRF) as described by Sontheimer et al. (1988).

$$D_s = \frac{D\varepsilon_p C_0}{\tau_p \rho_a q_0} SPDFR \tag{2.27}$$

in which C_0 is the initial inlet concentration; D is the adsorbate gas or liquid phase diffusivity; D_S is the surface diffusion coefficient; q_0 is the solid phase concentration in equilibrium with C_0 for a sigle-solute equilibrium; ε_p is the void fraction (porosity) of the adsorbent (-); ρ_A is the apparent adsorbent density; τ_p is the adsorbent tortuosity (-).

Table 2.6 Experimental and modeling approaches of inorganic removal by Fe^0 and iron oxides

Source	Substance	Conc. [mg L^{-1}]	NOM [mg L^{-1}]	pH [-]	Flow or EBCT	KF [L^n mg mg^{-n} g^{-1}]	1/n [-]	Film diffusion Coefficient k_f [cm s^{-1}]	Surface diffusivity, DS (cm^2 s^{-1})	Modeling
Smith (1998)	Pb^{2+}, Cd^{2+}, Zn^{2+}	5.0	-	4.0-5.5	70 h	18.5-28.9	0.66-0.71	1.5-5.0	1.0×10^{12}	TLM
Smith (2000)	Pb^{2+}	10	-	4.0	0.35 cm s^{-1}			1.5×10^{-3}	1.5×10^{-10}	TLM
Nikolaidis et al. (2003)	AsO_4^{3+}	0.35	8-11	6-6.3	6.4 cm min^{-1}	K_d 4,300 l kg^{-1}				ADT
Steiner (2006)	Cu^{2+}									TRM
Sperlich (2005)	AsO_4^{3+}	4.0-4.8	-	7.0	0.9-23 ml h^{-1}	63.2	0.17	1.11×10^{-3}	2.64×10^{-9}	HSDM
Tyrovola et al. (2007)	AsO_4^{3+}	2.0	-	7-8	10 min	K_d 160-210 l kd^{-1}	-	4.5×10^{-4}-3.3×10^{-3}		HM1D, TLM
Wang and Salvage (2005)	UO_2^{2+}	6-1134	-	5-6	1-72 h					EQM*
Kouznetsova et al. (2007)	TCE	0.9-245	-		0.5 m d^{-1}	111	0,59	3.57×10^{-3}	1.3×10^{-10}	RSNM
Genz et al. (2008)	NOM		4.2-8.7	7.8	1.4-3.0 m h^{-1}	8-12	0.6-0.9	1.8-3.7	1.5×10^{-10} m^2	HSDM
Yu et al. (2007)	BTA	10	-	6-7	18-20 mL h^{-1}	0.79-2.0	0.67	-	-	ADT
Rangsivek and Jekel (prep.)	Cu^{2+}	5	0-70	5-6	5 min	20-100	0.4-0.6	9.0	1.0×10^{12}	PSDM
	Zn^{2+}	5-7	0-70	5-6	5 min	10	1.0	9.0	3.5×10^{12}	PSDM

TLM:Triple layer model; TRM: Two region model; HSDM: Homogenous surface diffusion model; ADT: Advection-Dispersion Transport; PSDM: Pore and surface diffusion model; BTA: Benzotriazole; RSNM: Reactor-specific numerical models; EQM: based on equilibrium modeling that considers corrosion of iron, reductive precipitation, adsorption, speciation using PHREEQC program;

3 Materials and methods

3.1 Batch experiments

3.1.1 Materials

Reagent and preparation

All chemicals are reagent grade (Merck, Germany). Metal stock solutions were prepared using $Cu(NO_3)_2 \cdot 3H_2O$, $Pb(NO_3)_2 \cdot 3H_2O$ and $Zn(NO_3)_2 \cdot 6H_2O$ in deionised water (DI).

Stormwater runoff

Model runoff solutions were either prepared in the laboratory using DI with/without Suwannee river fulvic acid (SRFA, IHSS, USA, for DOC study) and simulated stormwater runoff (SSWR) or collected *in-situ* from roof, street and highway catchments. Detailed characterizations of model waters are shown in table 3.1.

Table 3.1 Characteristics of source waters for batch investigation

Source*	pH	Condc.	Alk.	Hardness	Cl^-	NO_3^-	SO_4^{2-}	DOC	UVA_{254}	SUVA	Color
		($\mu S\ cm^{-1}$)	($mg\ L^{-1}\ CaCO_3$)			($mg\ L^{-1}$)		($mg\ L^{-1}$)	(m^{-1})	($m^{-1}\ mg^{-1}\ L$)	(m^{-1})
SSWR[1]	7.40	200	40.0	70	9.76	0.18	17.99	0.99	3.24	3.27	0.20
Lankwitz[2]	6.88	82	23.8	45	5.39	11.83	5.30	1.29	3.65	2.83	0.12
TU-SW[3]	5.35	80	1.90	15	2.41	3.33	5.50	3.49	11.73	3.36	0.42
SRFA[4]	5.01	200	2.50	50	1.41	53.1	0.65	4.66	19.59	4.20	1.01
UFA[5]	7.53	128	48.8	65	5.70	0.96	11.94	7.29	29.24	4.01	1.62
Halensee[6]	7.42	1400	11.6	250	165	25.6	26.5	33.59	28.4	0.845	1.27

* Pre-filtrated using 1 µm glass filter ** samples for Cl^-, NO_3^-, SO_4^{2-}, DOC, UV were separated by 0.45 µm membrane filter

1. SSWR: Simulated Stormwater Runoff prepared by dilution of 1:5 of Berlin tap water and DI;
2. Lankwitz: Roof and Street runoff from residential area in Berlin-Lankwitz;
3. TU-SW: Bitumen roof nearby the city center area of Berlin-Zoologischer Garten;
4. SRFA: prepared using Suwannee River Fulvic Acid (Cat. no. 1S101F) in DI;
5. UFA: Roof (with extensive greened roofing) and street runoff from residential area in Berlin-Tempelhof
6. Halensee: Runoff from separated stormwater sewer discharging highway runoff to the Halensee lake in Berlin Charlottenburg-Wilmersdorf

Characterization of Fe^0

Fe^0 was prepared as scrap iron from a steel cylinder (ASTM A284 Steel grade C) using a sawing machine. The iron contains approximately 98% Fe^0, 0.24-0.36% C, <0.9% Mn, <0.04% P, <0.05% S and <0.28% Si (Wt.%). The compositions of ZVI were obtained from an available online-database (www.matweb.com) which corresponded to EDX examination. Its particle size ranges between 0.4 and 1.25 mm with a surface area of 0.384 $m^2\ g^{-1}$ using a Brunauer Emmett Teller (BET) method (Gemini Analyser, Micromeritics) with argon gas. It was pre-washed with acetone, dried and kept in an oxygen free environment until used. Visual inspection, SEM and EDX analysis showed no oxides present on the iron particles (Fig. 3.1).

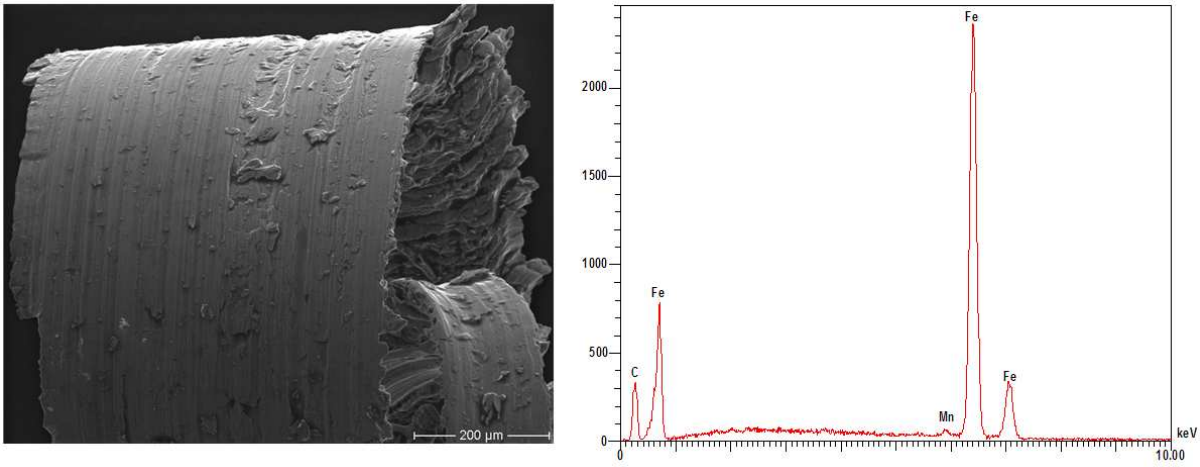

Fig. 3.1 SEM and EDX mapping of Fe^0 used in this study

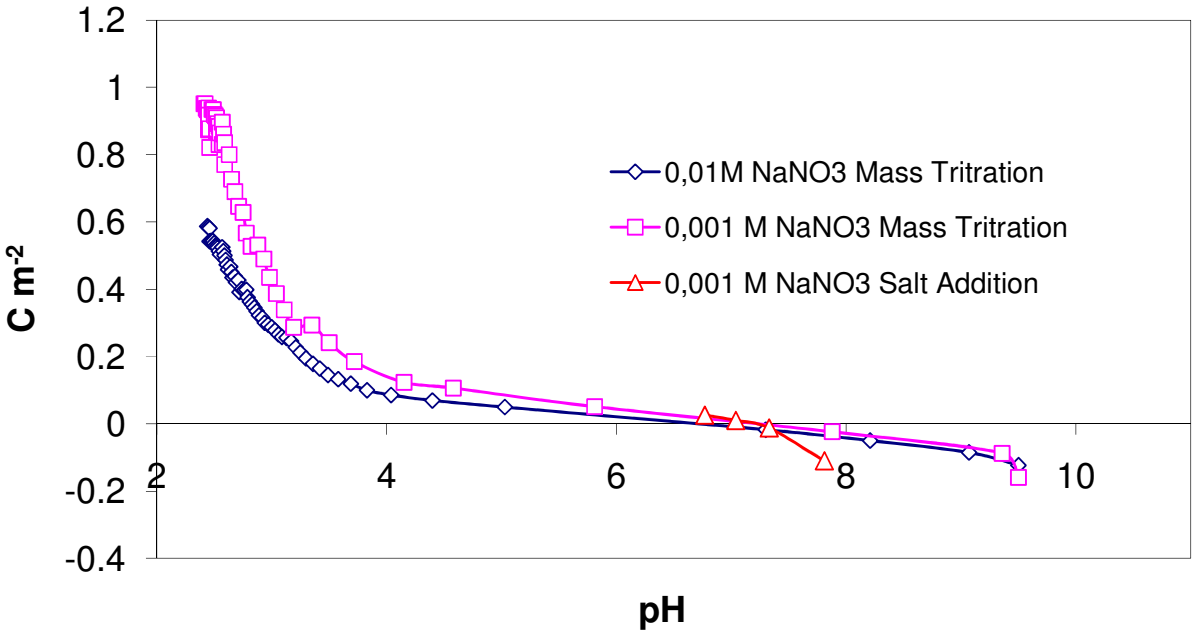

Fig. 3.2 pH_{PZC} of iron oxides produced by corrosion of iron

Beside Fe^0, iron oxides or rust and corrode iron produced by oxygen-corrosion of iron in deionised water and air dried were also used in some experiments for this work. The pH_{PZC} of iron oxides was determined employing two methods, salt addition and acid-based titration, according to Mullet *et al*. (1999) and Mustafa *et al.* (2002), respectively. Identical results were obtained for both methods (Fig. 3.2). Table 3.2 shows the characteristic of the materials employed in this work. In a comparasion study, Granular Ferric Hydroxide (GFH) obtained from the same source studied by Genz *et al*. (2004) was used.

3.1.2 Kinetic batch tests

In order to determine the rates and capacities of metal removal by Fe^0, both kinetic and equilibrium studies were performed. The kinetic investigation was carried out using a double wall, gas-tight and thermostat controlled reactor with total volume of 3.4 L (Fig. 3.3). The metal containing solution (3.0 L) was pre-equilibrated to achieve saturation using humidified N_2 or air at a constant mixing rate (r), pH and temperature (T). The gas was then turned off. Unless stated, the equilibrated solution contains 1 mg Cu^{2+} L^{-1}, 5 mg Zn^{2+} L^{-1}, pH_i (initial) 5.0 ± 0.1, ~50-200 µS cm^{-1}, 20°C at 150 rpm. The Cu^{2+}/Zn^{2+} ratio was chosen as a general concentration range detected in urban runoff. At the beginning of the experiment, an initial control sample was taken, after which ZVI (0.5 g L^{-1}) was introduced. Periodically, samples were acquired from the reactor through an auto-sampler. They were filtered using a cellulose nitrate membrane filter (0.45 µm) for analysis of Cu^{2+}, Zn^{2+} and Fe^{2+}. The pH was either maintained constant using HNO_3 and NaOH or otherwise uncontrolled. The pH, DO and redox potential (Eh) were measured and recorded by a computer throughout the run. The usage of NO_3^- background contributes insignificant interferences due to its much slower reaction rate compared to that of Cu^{2+}(Meihr et al. 2004). Under various experimental conditions in this study, the measured conductivity was relatively unchanged.

In the separate comparative experiments for determination of the removal rate of Cu^{2+} and Zn^{2+} by ZVI, corroded ZVI and GFH, methods of pulse doses of metals were employed. This method involved the addition of both metals to the reactor at interval times throughout the run rather than only at the beginning (e.g., Fig. B1-B3, Appendix B). In this ways, both the kinetic and total metal uptake load can be determined. The pulsed doses were at 5 mg L^{-1} with 4

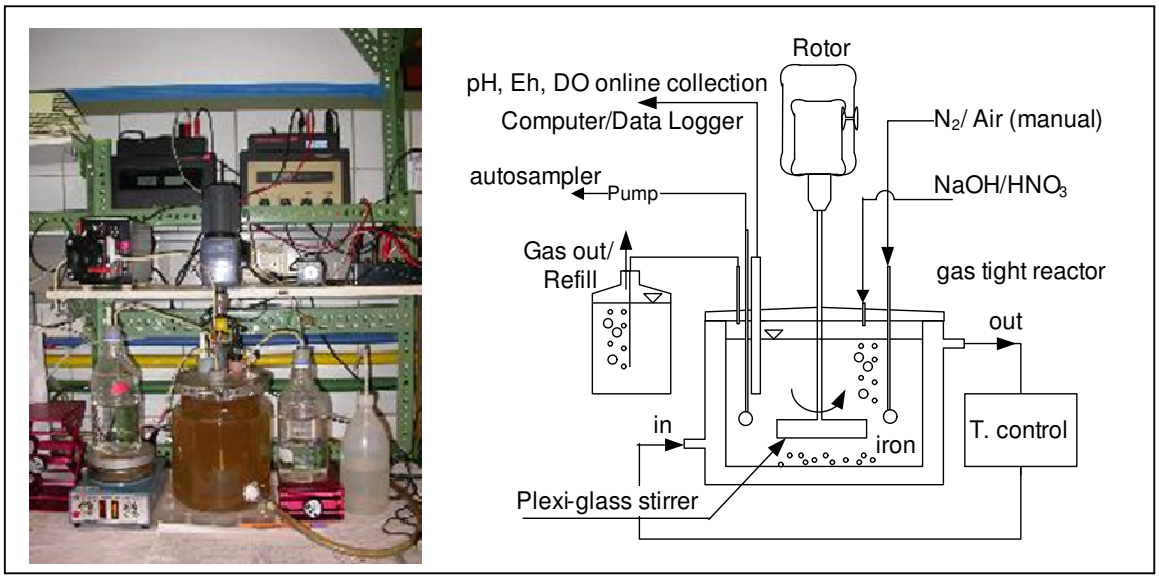

Fig. 3.3 Kinetic batch reactor

pulsed and, thus, total concentration of metal added was 20 mg L^{-1}. In some of the experiments, Pb^{2+} was also employed for comparison with Cu^{2+} and Zn^{2+} (Fig. 4.2).

3.1.3 Equilibrium tests

The equilibrium tests were performed by means of varying ZVI doses (0-1.5 g L^{-1}) in a set of model runoff volumes (50mL). They either contained no initial metal concentration or 2-7 mg L^{-1} of Cu^{2+} or Zn^{2+} alone, or in combination. pH and conductivity was adjusted initially to 5.0 ± 0.1 and 200 µS cm^{-1} (except the Halensee sample which has 1400 µS cm^{-1}) using HNO_3 and NaOH, respectively. The sets of vials were rotated at ~20°C in darkness for 48 h (a pre-determined time that sufficiently describes the equilibrium condition for stormwater runoff treatment). Subsequently, samples were filtrated and analyzed for metals, DOC, UV_{254}, color (UV_{436}) and pH.

3.2 Column experiments

3.2.1 Materials

Stormwater runoff
The model runoff (TU-SW) used in this work originated from a Bitumen roof with zinc gutter at Technical University of Berlin (TU-Berlin).

Fe^0
Fe^0 was prepared as scrape iron particles (0.70-1.25 mm) having an average surface area of 0.348 m^2 BET g^{-1} (Rangsivek and Jekel, 2005). This Fe^0 particle was mixed with granulated pumice (PM) and particularly used in the investigation of laboratory column. Under field investigation, the iron was also prepared in a spiral shape. According to the column experiment using the same iron mass, both particle and spiral iron exhibited more or less the same removal rates of metals (Fig. B8, appendix B).

Pumice
Pumice obtained from the Raab group (Germany) was mixed with Fe^0 to enhance the hydraulic conductivity. It is characterized by a high porosity and has original compositions consisting of non-fibrous, amorphous sodium-aluminium-silicate without considerable crystalline silicic acid. As compared with Fe^0, pumice is considered not reactive toward metals. According to the provider, major compositions of pumices are 55% SiO_2 and 22% Al_2O_3 (Table 3.2, p. 40). Pumice was sieved to 0.40-1.25 mm and, subsequently, washed in a flowing DI several times. The pumice was dried at 105°C and kept at room conditions.

Carbonatic, activated carbon and GFH materials (see method in section 3.4)
For optimization of the Fe^0 barrier, i.e., to enhance the precipitation of metals, a pure calcium carbonate ($CaCO_3$) (hydro-calcit, Akdolit, Germany), a mixed mineral of Ca and Mg carbonate ($CaMg(CO_3)_2$) (Magdo-Dol, Akdolit, Germany) and a Mg carbonate ($MgCO_3$) (Magnesia 314, Magnesia, Germany) were employed. The characteristics of these materials are shown in Table 3.2. In addition, granular activated carbon (Chemron, Germay) and GFH as employed in the study by Genz *et al.* (2004) were also trialed for this purpose. The media were sieved to have a similar size to Fe^0 and used with no further treatment.

3.2.2 Laboratory experiments

Table 3.3 (p. 40) summarizes the breakthrough experiments both carried out in the laboratory and at field conditions and the results of the tests are illustrated and discussed in section 4.2. The laboratory breakthrough columns tests were conducted as a set of comparative tests, usually consisting of 4-6 columns in each run. Unless otherwise stated, a column (2.5 cm diameter, 25 cm length) containing Fe^0 particles (15 g) homogeneously mixed with PM (20 g) (~10% Fe^0 v/v) was employed as a standard criteria (Col. 2 in Table 3.3). There were two sampling ports with Teflon sieves at the inlet and the outlet ends of the column. The media were supported by glass beads (diameter 2 mm) at both ends. To begin a set of breakthrough experiments (Col.1 in Table 3.3), a pump (Ismatec, Ecoline, Switzerland) drove the runoff up into the columns with a Tygon tube (diameter 2.79 mm) in an up-flow mode, while the other

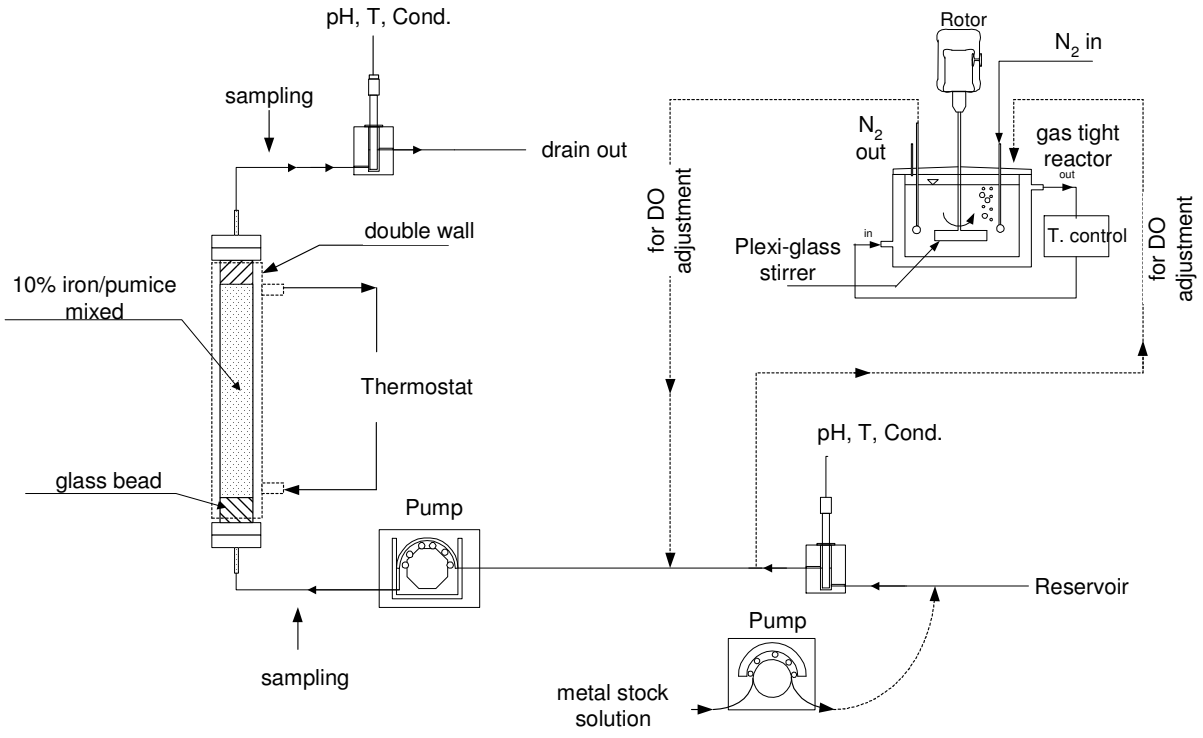

Fig. 3.4 Laboratory column experiment (c.f., text)

pump incrementally injected the prepared-metal stock solution into the flowing stream (Fig. 3.4) giving a distinctly different characteristic of water quality parameters. In a typical run, concentrations of copper and zinc in the runoff solution were each set at 5.0 mg L^{-1} of Cu^{2+} and 5.0-6.5 mg L^{-1} of Zn^{2+}, which was done by spiking a concentrated stock solution into the runoff (Merck, Germany). The differences in concentration of copper and zinc were due to variations in the natural occurrence of the zinc in the source runoff (i.e., 1-2 mg L^{-1}) (Rangsivek and Jekel, 2008). Temperature was controlled at 20°C using a Haake thermostat (Germany).

In the investigation, various water quality parameters were varied as follows: pH 4.2, 5.8 and 6.5; conductivity 80 and 200 µS cm^{-1}; dissolved oxygen (DO) <1.3 and 8 mg L^{-1}; water temperature 15, 20, 30°C; natural organic matter (NOM) 0-61 mg L^{-1} and empty bed contact time (EBCT) of 5 and 20 min. These investigated water quality parameters are within the range found for typical roof runoffs. In every set of the runs, a controlled column was integrated. The runoff solutions were filled up daily and thus source variation of stormwater could not be prevented. The obtained results from the comparative columns are attributed to differences in the investigating water quality parameter.

To investigate the possibility of up-scaling of the iron barriers and to assess prediction of the model (c.f., Table 3.2.4 and section 4.2.3), another breakthrough test was carried out. This employed Plexiglas columns measuring 3.5 cm in diameter and 56 cm in length. The column had 7 ports along the side wall separated at an eqal distance of 7 cm, allowing the determination of the removal rate of metals after an elapsed distance along the flow. The experiment was operated using 10%, 20% and 30% Fe^0 (v/v) columns mixed with pumice at empty bed contact times (EBCT) of 2.25 min. After an extended period of time, clogging prevailed and it was necessary to adjust the flow to a lower rate and, thus, only data from the first two ports of 20%Fe^0 column has been obtained for comparison.

3.2.3 Model prediction

The equilibrium software MINEQL$^+$ was employed for the evaluation of the mechanisms that involved the removal of copper and zinc within the column test (Schecher and McAvoy, 2001). To predict the breakthrough curves of the Fe^0 system, a pore surface diffusion model (PSDM) was employed. This was modeled using a commercial software - AdDesign (MichiganTech, USA) (Mertz et al., 1999) incorporating the following assumptions: plug-flow condition in the bed, linear liquid-phase mass transfer, solid phase mass transfer by pore and surface diffusion, constant hydraulic loading rate and diffusion coefficients, spherical adsorbent grains and the Freundlich isotherm to describe the adsorption equilibrium. Furthermore, the model assumes the transport of contaminants to the reactive surface governed by film diffusion, intra-particle or pore and surface diffusion and internal surface diffusion. Detailed derivation of the equations can be found in Friedman (1984), Crittenden (1985a; 1985b) and Sontheimer et al. (1988) and is described in part in Appendix D.

In the modeling procedures, the adsorption equilibrium parameters (K_F and n) were acquired from batch investigations previously described in equilibrium batch test. In short, a varying concentration of Cu^{2+} and Zn^{2+} (0-7 mg L^{-1}) was equilibrated with doses of 0-1.5 g Fe^0 L^{-1} using roof, street and highway runoffs. It was rotated in darkness for 48 h while the initial pH 5.0 was allowed to vary over the run. In this way, the resulting isotherm coefficients are derived from the conditions under a wider range than roof runoff conditions, which can better describe the breakthrough curves (i.e., cover the variability of the runoff qualities). The remaining parameters, i.e., the film transfer coefficient k_F, the surface diffusion coefficient D_S, and the pore diffusion coefficients D_P, were obtained during the calibration process of the model applying breakthrough results of the column tests. The modeling attempt was to reasonably capture the curves. Empirically calculated values using, e.g., Gnielinski's equation and previously reported values from other related works, e.g., from Smith (1998), Sperlich et al. (2005; 2008) were used as a first approximation. The uptake of NOM in the Fe^0 system was modeled employing kinetic and adsorption equilibrium parameters databases that was provided with the AdDesign Software.

Subsequently to the calibration of the model, the model was further validated utilizing results obtained from the large column tests. Thereafter, the model was used to predict the breakthroughs of copper and zinc at various scenarios, e.g., to test if the increase of EBCT or iron ratio of 50% Fe^0 (v/v) is sufficient to improve the performance of the system.

3.3 NOM experiments

3.3.1Materials and characterizations

Stormwater runoffs

The runoff solutions originated from two roof types, a copper roof (UDK) and a bitumen roof with a zinc gutter (TU) (Rangsivek and Jekel, 2005; 2008). The roof areas are located in the same catchment (approx. 100 m distance), near the city centre of Berlin-Zoologischer Garten. The runoff samples were collected from the reservoirs installed onsite. TU-FF and TU-SW are representatives of the TU roof and considered as a first flush volume from the beginning of Summer and the late Summer of the year 2005, respectively. The Cu-R sample was collected from the copper roof in Autumn, operationally defined as an event mean volume. After collection, the runoff samples were pre-filtrated using 0.45 µm cellulose nitrate membrane filters (Sartorius, Germany) and kept at 4°C. In addition to that, Suwannee River natural organic matter (SR-NOM, IHSS, USA) was also employed as a reference standard. It was diluted in deionised water and then adjusted to have a similar characteristic to the realistic runoff solutions. The detailed characterization of the source waters employed in this study is described in Table 4.3.

XAD-Resin fractionations

Isolation of NOM was performed according to the method described by Aiken et al. (1992). In the fractionation procedures, Amberlite XAD-8 and XAD-4 resin adsorption chromatography were employed, for which three fractions including hydrophobic, hydrophilic and transphilic fractions were obtained from the procedures. Because a smaller amount of isolated fraction was obtained at each step of fractionation, only bulk runoffs and their corresponding hydrophobic fractions were further characterized for copper complexation and acidity.

Copper complexation

The complexation of copper was carried out by measuring the free copper against the ion selective electrode (ISE, Neolab, Germany) in an equilibrated solution, of which the Cu^{2+} concentration was increased with the stepwise addition of a Cu^{2+} stock solution. In the titration experiment, a 100 mL of NOM solution in 0.015 M KNO_3 background was initially purged with N_2 for 15 min. A Cu^{2+} stock solution was introduced into equilibrating volume using pipettes. The titrant was added every 5-20 min, which resulted in stable potential readings (<0.5mV/5min). The pH was kept constant (±0.02pH) by additions of 0.1 M HNO_3 and NaOH as necessary using a titrator with a syrine tip (T 80/50 Schott, Germany). The added volume of titrant and solution for controlling pH was less than 10% of total NOM volume.

Acidic density of NOM

The carboxylic and phenolic acid density of runoff NOM was performed by a potentiometric titration. The titration experiment was performed using a 100 mL solution, previously adjusted to obtain a constant ionic strength of 0.015 M NaCl. It was acidified to pH 2.8 and purged with N_2 for 30 minutes. Subsequently, a calcium free 0.01 M NaOH solution was added drop-wise into the solution under a N_2 atmosphere using a titrator with a syrine tip (T 80/50 Schott, Germany) whereas the pH was noted at an exact amount of base. The carboxylic acidic group is defined by the consumption of NaOH from pH 3 to 8 whereas the phenolic group required twice the amount of titrant as an estimation (Oden et al., 1993). For most titrations about 60-70 additions were made in 2-5 min windows between additions to allow for reactions. The pH usually became stable (<0.05 pH unit) in less than 2 min.

3.3.2 Kinetic batch and column experiments

All runoff solutions were adjusted to have a constant pH and conductivity of 300 µS cm^{-1} using NaOH and HNO_3. The concentrations of Cu^{2+} and Zn^{2+} were brought to 5 mg L^{-1} at two initial pHs, e.g, 2.5 and 5.0. The batch tests were carried out by equilibrating 50 mL of the runoff solutions with a Fe^0 concentration of 0.5 g L^{-1} (0.186 m^2 L^{-1} Fe^0 by method of BET adsorption) for 200 h. This Fe^0 has been characterized and used in previous investigations (Rangsivek and Jekel, 2005). The pH was allowed to vary over the course of the run. The experiment at pH_i 2.5 was not typical for roof runoff conditions; however, at this acidic pH, evaluation of the mechanisms of NOM impact on the Fe^0 system could be observed in a clearer manner. In addition, the final pH (pH_f) of the solution ranged in a typical runoff condition.

In order to determine the removal rate of metals, water samples of 1 or 2 ml were taken at regular intervals. The samples were subsequently filtrated using a glass filter. Their volumes were made up to 10 mL with a 5% HNO_3 solution and kept cool at 4°C before analysis of Cu^{2+}, Zn^{2+} and Fe^{2+}. pH, UV_{254}, UV_{436} and LC-OCD sample analysis were taken at the beginning and at the end of experiments. A comparison of samples filtrated using either 0.45 µm cellulose or grass filter reveals similar result; therefore, the analyzed metal concentrations were defined as dissolved substances.

The results of the column investigations to determine of the impact of NOM on the removal of metals in Fe^0 system were evaluated (results from section 3.2.2). The experimental works are described briefly; TU roof runoff spiked with heavy metals was fed into the column containing Fe^0 and pumice. The columns were run in an up-flow mode at either 5 or 20 min empty bed contact times (EBCT). The concentrations of NOM in the feeding solutions were varied in order to examine the impact of EBCT and NOM concentrations on the treatment process, respectively. Water samples were taken before and after passing through the columns. They were analyzed for the total concentrations of copper, zinc and iron. The differences in measured concentrations were attributed to the removal performance as a result of a reaction with Fe^0. A preliminary study showed that total metals (Cu_T, Zn_T and Fe_T) remain relatively dissolved in the runoff solution. Hence, bulk concentrations were defined as the dissolved compounds.

3.4 Optimization and Field experiments

To optimize the Fe^0 columns, carbonate bearing materials were employed into the column tests both as composited and sequential configurations (experiment Col. 2 and Col. 3 in Table 3.3). In the composited column, the carbonatic media was introduced into the Fe^0 and PM columns at 10% (v/v) whereas the sequential columns integrate the carbonatic materials in a separate column (10% media v/v) which was installed prior or after passing the Fe^0 column. Unless otherwise stated, procedures of laboratory and field optimization experiments followed those of breakthrough column tests previously described in section 3.2.2.

The onsite optimization studies were carried out both at the UDK and TU roof sites. The Fe^0 treatment barrier received copper and zinc roof runoff at realistic conditions. The large columns sizes (3.5 cm diameter, 56 cm length) were employed. After successful optimization of the column test established in the laboratory, it was found that spiral shaped iron showed the most promising results. Thereafter, the on-site columns (Col. 4) were filled only with

Table 3.2 Chemical and physical paramters of media used in this study

Parameters	Unit	Fe^0	spiral Fe^0	Pumice	Calcite	Dolomite	Magnesite
Source of materials	-	TU-Berlin	TU-Berlin	Raab group, DE	Rheinkalk Akdolit, DE	Rheinkalk Akdolit, DE	Magnesia, DE
Name	-	ASTM grade C	ASTM grade C	-	Hydro-calcit	Magno Dol, Magno Filt	Magnesia 314
Name in experiment	-	ZVI, Fe^0	spiral Fe^0	PM	$CaCO_3$	DML and DMS	MAG
Shape	-	particle	spiral	particle	grain	particle	particle
Size	mm	0.4-1.25		0.4-1.25	0.4-1.25	0.4-1.25	0.4-1.25
BET surface area	$m^2\ g^{-1}$	0.384	~0.38*	-	-	-	-
Filled in column density	$kg\ m^{-3}$	2037	204	272	1020	1020	1020
Chemcial data	-	98% Fe^0	98% Fe^0	55% SiO_2	97% $CaCO_3$	46% $MgCO_3$	48%MgO_3
		0.24-0.36% C	0.24-0.36% C	Al_2O_3 22%	2.0% CaO	54%$CaCO_3$	52.2%CO_2
		0.04% Mn,	0.04% Mn	12%K2O+Na_2O	0.6% $MgCO_3$		
		0.05% P	0,05% P	Fe_2O_3, CaO,	0.2% Fe_2O_3		
		0.28% S	0,28% S	MgO, TiO_2	0,3% Al_2O_3 and SiO_2		

*based on the kinetic column test of two iron (Fig. B8 in Appendix B)

Table 3.3 Experimetal setting and eperational parameters of the column tests

Pameters	Unit	Standard columns	Composite columns	Sequential Columns	Sequential Columns
Experiment	-	Col. 1	Col. 2	Col. 3	Col. 4
Matrix	-	TU-SW	TU-SW and UDK	TU-SW	TU-SW with addition of Cu and DOC
Components	-	Cu+Zn	Cu + Zn	Cu/Zn/Cu+Zn	Cu/Zn/Cu+Zn
Flow characteristic	-	manual	natural drain/manual/down flow	manual	natural/manual
Cu	$mg\ L^{-1}$	5.0	4.9-9.1	5.0	2.0
Zn	$mg\ L^{-1}$	5.0-7.0	5.0-7.0	5.0-7.0	2 – 5.0
NOM	$mg\ L^{-1}$	5 - 61	5 - 61	5-61	2.9 - 20
pH	-	4.8 - 6.2	4.8 - 6.2	4.8 - 6.2	4.8 - 6.2
Conductivity	$\mu S\ cm^{-1}$	30-600	30 - 65	30-600	30 - 65
Column configuration	-	Fe^0	Calcite/Fe^0, DML/Fe^0, Mag/Fe^0	$CaCO_3$-Fe^0, DML-Fe^0, DMS-Fe^0, Mag-Fe^0	Spiral Fe^0/aeration/filtration of DML/PM
Column's diameter	cm	2.5	2.5 or 3.5	2.5	3.5
Column's length	cm	15	15 or 56	15	56
Characteristic of iron	-	particle	particle	particle	spiral
Mass of media					
1st column:	-	10% Fe^0/PM (v/v) and 50%	10%, 20%, 30% Fe^0/PM (v/v)	10% Fe^0/PM (v/v)	2 x 10% Fe^0/PM (v/v) ~ 100 g each
2nd column:	-	-	-	10% carbonate media/PM (v/v)	-
Post treatment system	g	-	-	-	800 g DML/800 g PM
Porosity	-	80%	70%	80%	90%
Flow rate	$mL\ min^{-1}$	15	15 and 108	15	540 and 108
EBCT (in Fe^0 bed)	min	5 and some exp. 20	1 and 5	5	1 and 5

Col. 1: Breakthrough experiment, Col. 2: Laboratory and field condition, Col. 3: Sequential column test in the laboratory and Col. 4: Final design of breakthrough column tests

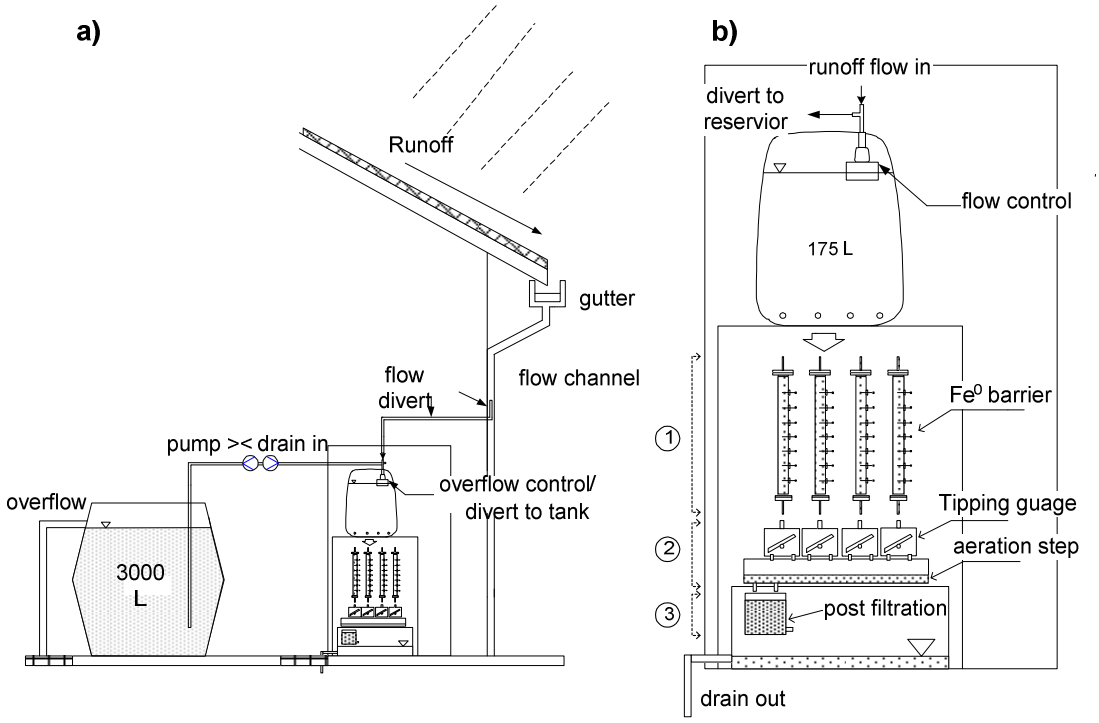

Fig. 3.5 a) The overall view and b) the detailed onsite experiments of Fe^0 system for treatment of copper and zinc roof runoff. The systems include 3 treatment steps; 1) Fe^0 treatment columns, 2) aeration step using tipping counter and aeration basin, and 3) post-filtration of pumice and dolomite

spiral shaped iron without any other media, followed by an aeration step and post-filtration system of pumice and dolomite, homogenously mixed within the same fixed-bed filtration. A detailed schematic of the onsite-treatment is illustrated in Fig. 3.5. The samples taken before and after the were analyzed for copper, zinc and iron. A total concentration was measured. pH and conductivity were measured following the description in section 3.5, respectively. The flow of the water was measured by means of a tipping counter which transmits signal data to a data logger (Amonit, Germany). To elucidate the mechanism involved in the treatment processes, the solids precipitated after the columns test were analyzed employing SEM and EDX together with an equilibrium calculation using MINEQL$^+$ software.

3.5 Analysis

3.5.1 Iron, copper, zinc

The samples were analyzed for copper, zinc and iron using a VARIAN (SpectrAA-300/400, Australia) or a GBC atomic adsorption spectrophotometer (GBC 906AA, Australia). In the batch test, the samples were filtered using a cellulose nitrate membrane filter (0.45 µm) before analysis of Cu^{2+}, Zn^{2+} and Fe^{2+}. For the column test, the total samples were collected andanalysed. A comparison of un-filtrated and filtrated samples (0.45 µm, cellulose nitrate

filter, Sartorius, Germany) revealed that the total concentration of copper and zinc results were similar in both cases and they can be defined as dissolved concentrations.

3.5.2 DOC, NOM

DOC was determined by means of thermal-catalytic oxidation using a high-TOC analyser (Elementar, Germany). UV_{254} and colour were measured using a Lambda 12UV/VIS spectrophotometer (Perkin-Elmer, Germany). SUVA (UV_{254}/DOC) is an index of relative aromaticity. For advanced DOC fractionation, liquid chromatography-organic carbon detection (LC-OCD) was employed according to the method described by Huber and Frimmel (1996). The method divided up DOC fractions into polysaccharides, humic substances, hydrolysates (building blocks), low molecular acids and amphiphylics.

3.5.3 Others

pH and conductivity were measured using pH and conductivity electrodes (WTW, Germany), respectively. Phosphate was measured using the FIA-Star 5000 Analyser (FOSS, Denmark).

3.5.4 Solid precipitates

At the end of selected experiments, iron samples were carefully transferred, and dried in an inert nitrogen-purged glove box for further characterizations employing Scanning Electron Microscopy (SEM), Energy Dispersive X-Ray analyzer (EDX) and X-Ray Diffraction (XRD). For some particular cases, an Auger Electron Spectroscopy (AES) was also employed. The scanning electron microscopy was carried out at 20 kV using a Hitachi S-2700 scanning electron microscope, equipped with a LaB6 filament and a thin window X-ray PGT detector for elemental analysis. All the powder samples were coated with a conductive layer of gold prior to analysis. An X-ray diffractometer was used at 40 kV, 20 mA (CuKa radiation) with a graphite monochromator in the diffracted beam path. Data were collected using a step width of 0.02° with a count time of 5 sec per step. The XRD measurements were performed on a Siemens D5000 (Bruker-AXS, Siemens) in Bragg-Brentano geometry using copper radiation Kalpha (40 kV, 40 mA). The diffractogram was between 5 and 120 degrees with a step size of 0.02°. The sample was used without sample spinning and with the V6 automatic aperture through a diffraction angle of 6 mm. The AES were carried out under vacuum conditions at a pressure of $5x10^{-9}$ employing PHI660 (Physical electronics). The energy of the excited electrons was 3keV.

For the purpose of analysis and to improve the detection in the batch test, solids were either crushed or another preparation method was used to increase the metal load to iron surface area. In this case, ZVI was prepared to have a certain geometry, i.e., 2.1x1.05x0.5 cm^3 was used in the treatment process. The solid precipitates from column tests were powderized before analysis.

4 Results and discussion

4.1. Batch experiments

4.1.1 Kinetics and Stoichiometry of metal uptake

An example plot of normalized Cu^{2+} and Zn^{2+} concentration as a function of elapsed time obtained from duplicate kinetic tests in SSWR under uncontrolled pH is depicted in Figure 4.1a). The experimental data follows a pseudo-first-order rate law, $C_t = C_0 e^{-k_{obs}t}$, where C_0 and C_t are metal ion concentrations at initial and at time t, respectively. By fitting to the rate equation ($6<n_c<16$, where n_c is the number of correlated data), observed kinetic rate constants (k_{obs}) were calculated and used to interpret the experimental results. Accordingly, the results in the Figure 4.1a) show that Cu^{2+} uptake exhibited approximately twofold higher rates than uptake of Zn^{2+}, in which k_{obs} of 0.275 ± 0.019 h^{-1} ($t_{1/2}$ 2.52 ± 0.17 h) and 0.123 ± 0.001 h^{-1} ($t_{1/2}$ 5.62 ± 0.05 h) were obtained, respectively.

Kinetically-determined parameters among the samples obtained in this study, cf. Table 4.2, yielded comparable results to the findings in acid rock and acid mine drainage matrixes by Shokes and Möller (1999) and Wilkin and McNeil (2003), owing to high variability of ZVI reactivity (Meihr *et al.*, 2004). In their studies, $t_{1/2}$ values of Cu^{2+} uptake were reported of one to two orders of magnitude smaller than Zn^{2+}, varying in the range of 0.6 min - 2.0 h and 121 min - 8.2 h, respectively. Furthermore, it is generally agreed that the uptake of Zn^{2+} essentially requires precipitation of iron oxides as sorption sites, whereas, reduction of Cu^{2+} by Fe^0 is thermodynamically favoured. In hydrometallurgical processes the cementation of Cu^{2+} is suggested to follow as $Cu^{2+} + Fe^0 \rightarrow Cu^0 + Fe^{2+}$ with $k = 1.9 \times 10^{26}$ (Nadkarni *et al.*, 1967; Nadkarni and Wadsworth, 1967; Annamalai and Murr, 1979; Ku and Chen, 1992;

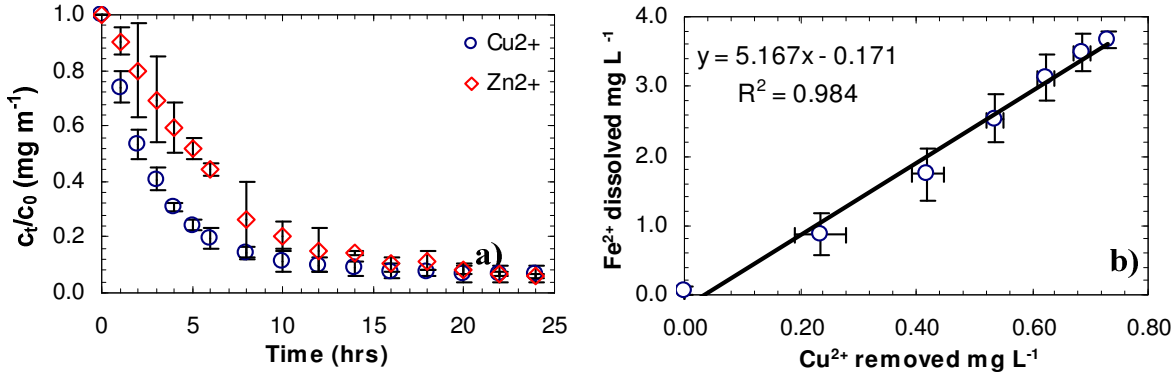

Fig. 4.1 Plots of a) normalized Cu^{2+} and Zn^{2+} concentration as a function of time, b) stoichiometry determination of Cu^{2+} cementation process [Cu_i^{2+} 1 mg L^{-1}, Zn_i^{2+} 5 mg L^{-1}, 0.5 g L^{-1} ZVI, pH_i 5.0 ± 0.1, pH_f 5.83, DO_i 8.0 mg L^{-1}, T 20 ± 1.0 °C, 150 rpm in SSWR]. Error bars represent 95% confidence intervals from duplicate experiments

Lopéz *et al.* 2003; Wilkin and McNeil, 2003). However, previous findings may not allow sufficient interpretation of the results under stormwater runoff conditions. It is anticipated that DO, pH, T, IS, DOC as well as other constituents in runoff conditions may exert a significant influence on the stoichiometry and the role of each treatment process: cementation and adsorption.

The stoichiometry for the Cu^{2+}/Fe^{0} redox-couple under stormwater runoff conditions was experimentally evaluated in the present study. Depicted in Figure 4.1b) are the iron concentrations that are dissolved into the solution plotted against copper ion that was removed during the first 6 h run. Determination of stoichiometry factors ($\Delta Fe^{2+}/\Delta Cu^{2+}$) was obtained from the regression, which demonstrated that about 5.0 mg of iron is required to remove 1 mg of Cu^{2+} (R^2=0.984). This value was significantly greater than the typically reported one of 0.88 mg mg^{-1} (Nadkarni and Wadsworth, 1967) under acidic pH and in the absence of DO, which is presumably attributable to an excessive iron consumption by DO and accumulated intermediate products, e.g., Fe^{3+} (Nadkarni and Wadsworth, 1967; Bisward and Reid, 1972). Generally, the factors observed for $\Delta Fe^{2+}/\Delta Cu^{2+}$ are in a significantly higher range of 0.3-12.0, depending highly on the water qualities and experimental conditions, cf. Table 4.2. It is noteworthy, however, that the stoichiometry factors determined under the present conditions

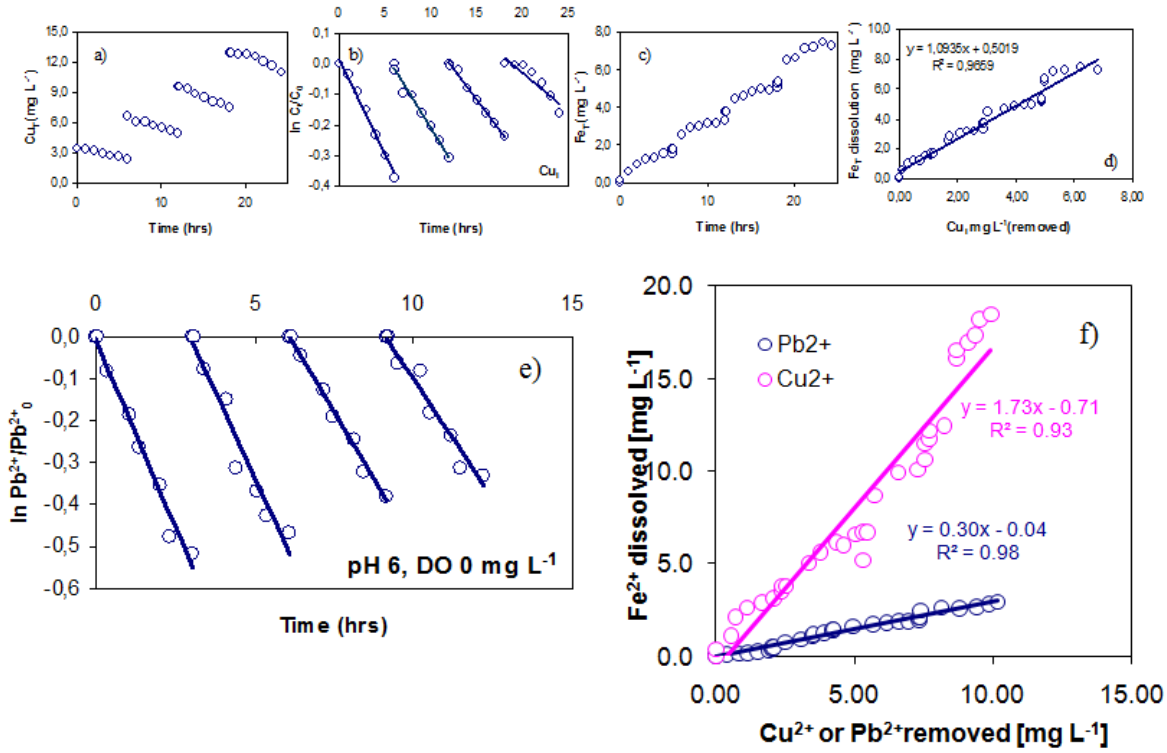

Fig. 4.2 Results from batch experiments with pulsed dosing – Plots of a) Total Cu vs. time, b) $\ln(C_t/C_0)$ vs time, c) Total Fe vs. time, and d) Total Fe dissoluted vs. Total Cu removed at Cu_0 5 mg L^{-1} (pulse dosing with 5 mg L^{-1}), ZVI 0.5 g L^{-1} (0.192 m^2 L^{-1}), pH 7, DO 0 mg L^{-1}, T 20°C and 150 rpm. The below figures e) and f) were the results from identical experiment with Pb^{2+} and Cu^{2+} dosing, respectively.

may not be solely caused by the cementation process but rather have been influenced by other processes, i.e., iron hydroxide precipitation and reoxidation by accumulated products. To verify this, experiments with pulse dosing of Cu^{2+} and Pb^{2+} were performed under deoxygenated condition. It was found that the $\Delta Fe^{2+}/\Delta Cu^{2+}$ factor of 1.1-1.7 (R^2=0.93-0.966) and 0.3 for Pb^{2+} (R^2=0.98) were obtained. These values followed (or are close to) the stoichiometry of 0.88 and 0.27 mg mg^{-1} although they were obtained from the regression of a 24 h run. Thus, to minimize the effects, the stoichiometry factors under stormwater runoff conditions were calculated, based on the data obtained during an initial period.

4.1.2 Impact of the quality of stormwater runoff

Effect of DO and pH (Fig. 4.3)

Under oxygen limiting conditions (DO<0.5 mg L^{-1}) in DI, regardless of pH, Cu^{2+} concentrations gradually decreased from its initial values to nearly complete removal at 24 h

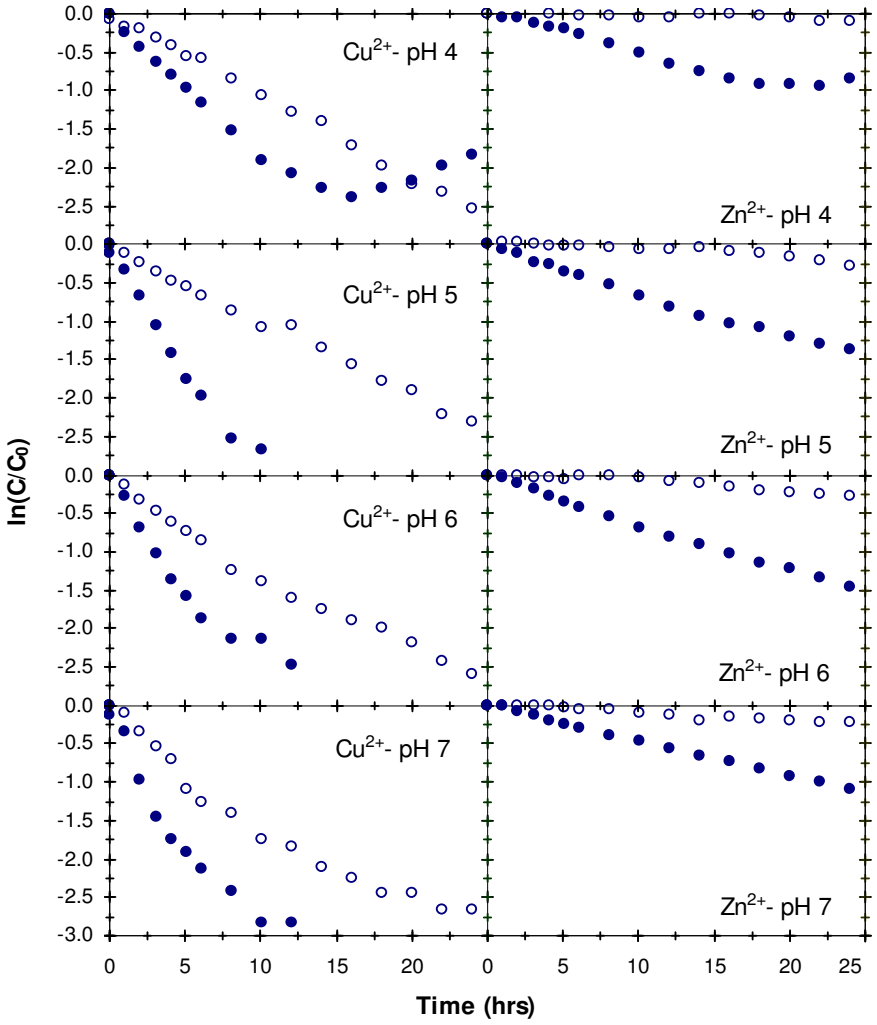

Fig. 4.3 Comparison of experimental results carried out in (○) limiting and (●) un-limiting DO concentration at varying pH 4.0-7.0 (controlled). [Cu_i^{2+} 1 mg L^{-1}, Zn_i^{2+} 5 mg L^{-1}, 0.5 g L^{-1} ZVI, T 20 ± 1.0 °C, 150 rpm in DI]

Table 4.1 Experimental conditions and kinetic parameters on the effects of DOC and IS

						Cu^{2+}			Zn^{2+}			$\Delta Fe^{2+}/\Delta Cu^{2+}$	
Parameters	Cu_i^{2+}	Zn_i^{2+}	pH_f	Eh_f	**OUR**	k_{obs}	$t_{1/2}$	R^2	k_{obs}	$t_{1/2}$	R^2	*m/n*	R^2
Solution/Unit	mg/l	mg/l	-	mV	mg/l h	h^{-1}	*h*	-	h^{-1}	*h*	-	*g/g*	-
Effect of DOC													
DI (DOC 0 mg L^{-1})	5.0	5.0	5.42	246	0.04	0.206	3.36	0.93	0.021	33.8	0.86	0.73	0.95
SSWR	1.0	5.0	5.83	118	0.12	0.275	2.52	0.99	0.123	5.64	0.97	5.00	0.98
Lankwitz	1.0	5.0	5.65	175	0.06	0.169	4.10	0.99	0.072	9.63	0.99	2.68	0.91
TU-SW	1.0	5.0	5.77	182	0.06	0.208	3.33	0.98	0.055	12.6	0.98	2.89	0.97
SRFA	5.0	5.0	5.52	248	0.07	0.209	3.32	0.99	0.021	33.0	0.95	1.56	0.98
UFA	1.0	5.0	6.04	122	0.06	0.115	6.03	0.99	0.027	25.7	0.99	6.10	0.95
Halensee	1.0	5.0	5.92	99	0.20	0.103	6.72	0.98	0.045	15.3	0.99	0.359	0.96
Effect of Ionic Strength													
DI	1.0	5.0	5.54	179	0.06	0.330	2.91	0.99	0.058	11.9	0.99	1.17	0.99
1mM $NaNO_3$	1.0	5.0	5.57	89	0.26	0.295	2.35	0.97	0.115	6.01	0.94	2.73	0.96
25 mM $NaNO_3$	1.0	5.0	6.45	61	0.19	0.338	2.05	0.92	0.122	5.68	0.99	2.32	0.99
50 mM $NaNO_3$	1.0	5.0	6.39	78	0.20	0.330	2.10	0.88	0.127	5.54	0.99	2.00	0.77
25mMNaCl	1.0	5.0	5.43	90	0.27	0.297	2.33	0.92	0.123	5.65	0.99	2.21	0.85
25 mM Na_2SO_4	1.0	5.0	6.10	81	0.21	0.358	1.94	0.85	0.087	7.96	0.99	1.43	0.65

ZVI doses of 0.5 g L^{-1} in pH_i (initial) 5.0 ± 0.1 in all experiments, *i* is initial and *f* is final
OUR was calculated based on the slope of DO vs. time profiles. R^2 based on $6<n_c<16$, n_c is the number of correlated data.
m/n is stoichiometry factor of cementation process $(\Delta Fe^{2+}/\Delta Cu^{2+})$, cf. text.

(>90%). Zn^{2+} behaved differently, as within the initial phase no detectable losses were found, however, when increasing elapsed time and pH some portions of Zn^{2+} were removed, presumably due to the adsorption and co-precipitation with iron oxide generated during cementation of copper and during anoxic corrosion processes.

A comparison of experiments in oxygen-containing solutions (DO_i 8-9 mg L^{-1}) showed that significantly greater removal rates could be achieved for Zn^{2+}, reflecting the strong involvement of DO. This is according to the fact that corrosion of iron is accelerated in presence of DO, subsequently promoting the cation adsorption. Calculation shows $t_{1/2}$ values (between controlled pH 4.0 and 7.0) of copper ion uptake decrease in a narrow range from 5.96-7.15 to 2.00-3.70 h while the values of 61.8-144.4 h and 12.6-15.2 h were obtained for Zn^{2+}, corresponding to the experiments performed under deoxygenated and oxygenated solutions, respectively. The experimental results demonstrated a modest dependency of pH on Cu^{2+} and Zn^{2+} removal in the controlled pH system. The re-dissolution of Cu^{2+} occurred at a controlled pH of 4 after a 16 h run, which can be explained by the re-oxidation of deposited copper with the accumulated Fe^{3+} (Nadkarni and Wadsworth, 1967; Bisward and Reid, 1972).

In experiments where pH was allowed to vary over the course of runs, the final pH either increased or decreased, depending on the initial pH setting (Smith, 1996). As an example for the initial pH 5.0 ± 0.1 typically employed in this study, pH rapidly drifted to the maximum value within 2-3 h. It maintained or gradually decreased to the final range between 5.26 and 5.83, in accordance with the reduction in Eh and DO owing to the corrosion of iron (e.g., in Table B9-B10, Appendix B). As a result of changes in redox chemistry, precipitation of iron (oxy)hydroxide becomes favourable. It was, therefore, observed, in general, that the depletion rates of heavy metals are higher in an uncontrolled pH system. This is especially significant in a higher ionic strength solution whereby the iron dissolution rate dramatically increases.

Effect of Temperature.

Evaluation of temperature effects on the Cu^{2+} and Zn^{2+} uptake rate was performed by changing equilibrated solution temperature between 5-35°C. Based on the results obtained, a higher temperature was observed to significantly increase the iron dissolution rate as well as metal adsorption. Comparing the results between temperatures 5 and 35°C, about a seven-fold rate increase for Zn^{2+} adsorption was evident. The varying temperature did not appear to affect copper removal rate significantly since $t_{1/2}$ values varied in a narrow range of 3.14 to 1.99 h, respectively. The temperature dependency on Cu^{2+} and Zn^{2+} uptake rates by ZVI was successfully determined by Arrhenius's equation. The calculated activation energy values of 5.23 kcal $mole^{-1}$ were obtained for Cu^{2+} and 11.4 kcal $mole^{-1}$ for Zn^{2+}, indicating that Cu^{2+} and Zn^{2+} uptakes are surface or pore diffusion controlled reactions (Annamalai and Murr, 1979).

Effect of DOC

Runoff solutions containing varying concentration and characteristics of DOC exhibit different impacts on the removal rates of Cu^{2+} and Zn^{2+} (Table 4.1., see also Figure 4.4). In the Cu^{2+} removal experiments, two distinct trends were observed. A higher rate ($t_{1/2}$~3 h) corresponded to the lower DOC content of less than 5 mg L^{-1}, in which the removal rates at 0-10 h elapsed time were identical in almost all experiments. However, in the tailing 10-24 h phases, a non-removable metal fraction (~7-9%) was found in some samples. This perhaps indicates the attribution of metal-DOC complexation effects. Higher DOC in UFA and Halensee samples decreased the process rates about twofold ($t_{1/2}$ ~ 6 h). These rates are consistent with the values obtained in the system where DO is absent, thus, may lead to the conclusion that DOC retardation is mainly associated with adsorption, i.e., complexation and competitive adsorption, but not with the cementation process.

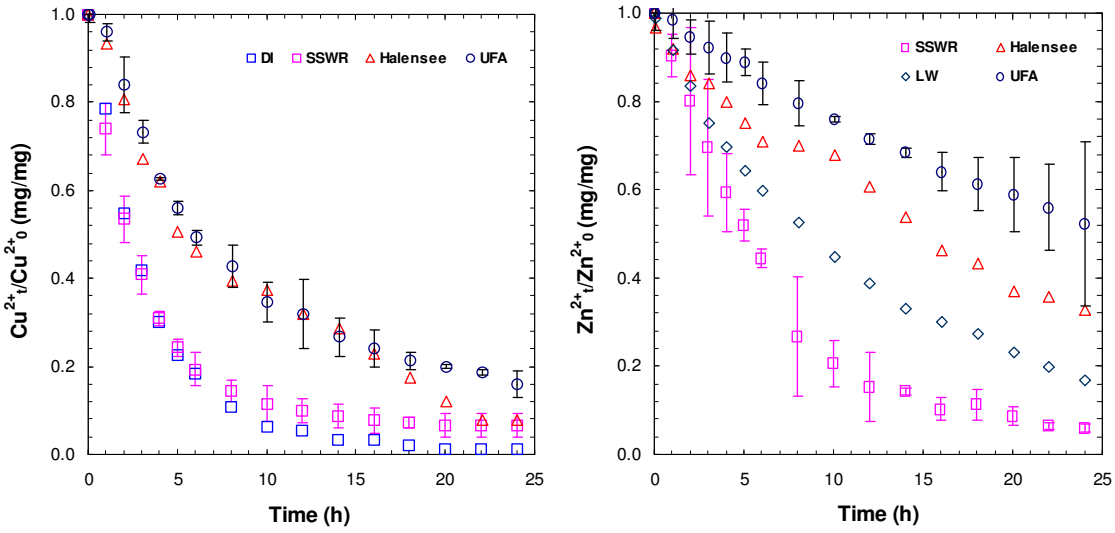

Fig.4.4 Examples of normalized concentration profiles of Cu^{2+} and Zn^{2+} vs time. Experiments were conducted with various runoff solutions (c.f., Table 3.1). Representative profiles are chosen based on the description in the text

A similar trend with much greater impact of DOC on Zn^{2+} removal rate was observed. As compared with SSRW, an increasing DOC content of up to ~ 8 mg L^{-1} in UFA hindered the removal rate of Zn^{2+} by 4.6 times. Corresponding to this, higher amounts of dissolved iron were detected remaining in solution, suggesting the complexation effects of Fe^{2+} by DOC, which may subsequently retard the oxidation of ferrous to ferric iron. The removal rate of Zn^{2+} in the Halensee sample, on the contrary, was much less impacted although it had the greatest DOC content. This could be explained by a tradeoff between DOC and a higher amount of sorption sites generated during iron corrosion in a high ionic strength solution (Furukawa *et al.* 2002; Kamolpornwijit *et al.*, 2004). Also, the behavior and interactions of DOC with iron oxides, however, could not be ruled out.

Effect of Ionic Strength.
The results in Table 4.1 indicated that IS has a minimal effect on removal rate of Cu^{2+}. Conversely, the increase in IS resulted in considerably higher Zn^{2+} uptake rates. About 75% of Zn^{2+} could be removed in the DI solution, while a higher IS leads to an over 95% Zn^{2+} achievable uptake. Types of salt background did not appear to affect the metal uptake rate, although a slightly lower rate was found when using a Na_2SO_4 background solution.

As previously discussed, the dependency of IS on the uptake of Zn^{2+} can be explained by the behaviour of iron oxide formation. Higher IS leads to iron oxide precipitation in the bulk water phases diffusing away from the iron surfaces (Farrell *et al.,* 2000). Consequently, the iron oxide production takes place continuously.

Effect of Reactant Concentration.
A set of kinetic experiments was performed with varying concentrations of Cu^{2+} and Zn^{2+}; absent, individual or in combination (0-10 mg L^{-1}). Generally, it is found that copper and zinc accelerated the iron corrosion and enhanced metal uptake capacities (equilibrium tests). However, a higher Cu^{2+} concentration was found to apparently hinder the Zn^{2+} removal rate (Table 4.1). This could possibly be attributed to the competitive adsorption effects. On the contrary, higher concentrations of Cu^{2+} and Zn^{2+} between 1-10 mg L^{-1} showed no influence on the removal of dissolved copper. The result suggests that the enhancement or inhibition effects depend individually on types and concentrations of each metal.

4.1.3 Equilibrium study

Figure 4.5 illustrates the metal and DOC uptake at equilibrium experimentally determined in the ZVI system (model runoff solutions) in comparison to the simulated data of the GFH system (DI solution) (Steiner, 2003; Ludwig, 2004). With the same initial pH setting, the literature values of metal loaded on GFH reveal a large discrepancy. Such differences might be due to the differences in experimental boundary scenarios.

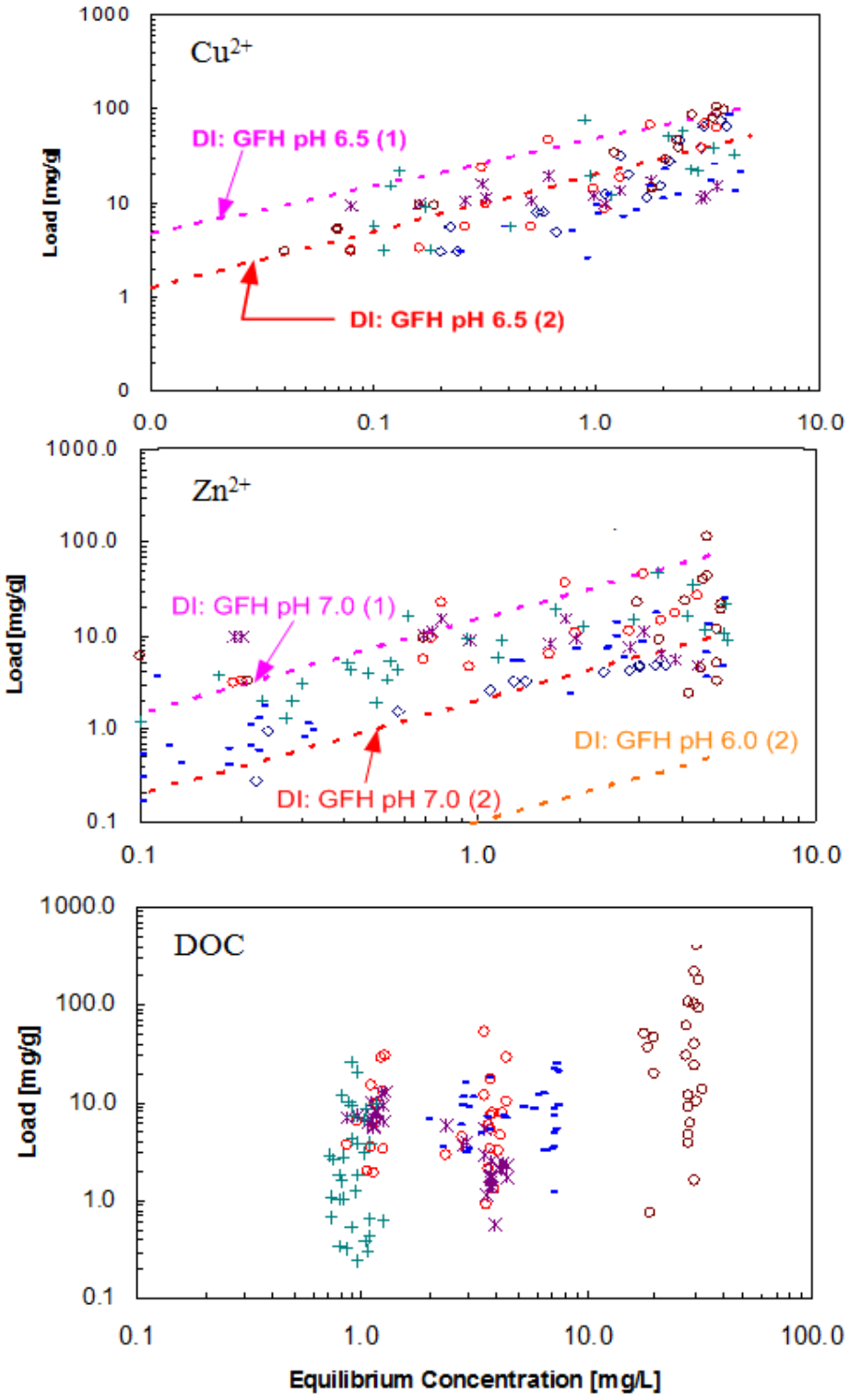

Fig. 4.5 Comparison of Cu^{2+}, Zn^{2+} and DOC equilibrium uptake load by ZVI and GFH. ZVI system contained various stormwater runoff solutions; (◇) SSWR pH_f 5.14-5.56; (+) Lankwitz pH_f 5.00-5.67; (✳) TU-SW pH_f 5.00-5.76; (□) SRFA pH_f 5.00-6.57; (■) UFA pH_f 5.33-6.51; (○) Halensee pH_f 5.59-6.70. GFH isotherms were simulated based on the results obtained from (1) Steiner (2003) and (2) Ludwig (2004) in DI solution

Cu^{2+} uptake in the ZVI system demonstrated a slightly lower performance than adsorption on GFH. This may be caused by complexation effects of Cu^{2+} caused by DOC in runoff matrixes, and the generally lower pH in the data observed in the ZVI system, i.e., 5.0-6.70. However, up to 100 mg Cu^{2+} g^{-1} ZVI could be achieved for both media at about 4 mg Cu^{2+} L^{-1} equilibrium concentration. A comparative kinetic study was carried out with pulse doses of Cu^{2+}, i.e., Cu^{2+} was re-introduced into the systems every 6 h for a total 24 h run, showing that adsorption of Cu^{2+} on GFH (controlled pH 6.0 i.e. to enhance the adsorption) takes place within 5-10 minutes. Metal uptake in the ZVI system (controlled pH 5.0, i.e., worse case for adsorption) exhibits a slower rate. However, in the overall run, a superior performance in term of its absolute metal loading capacity was observed for the latter system (Fig. B3 in Appendix B).

The equilibrium capacities of zinc, associated with ZVI corrosion products, are shown to agree well with the higher-lower boundaries of adsorption on GFH at pH 7.0, being significantly higher than adsorption at pH 6.0 (Figure 4.5). About a 10 fold lower loading of Zn^{2+} than Cu^{2+} were observed. In several data points, up to 50-100 mg Zn^{2+} g^{-1} ZVI could be obtained.

Due to the heterogeneous and complex nature of DOC as well as the interactions between DOC and metals, large variations of DOC loading were found (Figure 4.5). In the literature, Teerman and Jekel (1999) reported a load of 30-60 mg DOC g^{-1} GFH for fulvic and humic acid adsorption (Sigma Aldrich, Roth). A similar loading of Suwannee River natural organic matter (SRNOM) of up to 35 mg DOC g^{-1} GFH with a non-absorbable fraction of 0.6 mg DOC L^{-1} has also been reported (Genz *et al.* 2004). For DOC removal from roof runoff on the same media, Steiner (2003) found about 2.80 mg DOC g^{-1}, with 0.4-0.5 mg L^{-1} as a non-absorbable DOC fraction. All of these outcomes are within the range determined in this study. In most model runoff samples, about 0.8-1.0 mg DOC L^{-1} was non-absorbable DOC fraction, however, up to approximately 30 mg DOC L^{-1} was determined for the Halensee solution.

4.1.4 Characterization of DOC

According to the LC-OCD analysis, stormwater runoff solutions from different catchment areas revealed their distinct fractional characteristics. A larger molecular weight fulvic acid with strong UV absorption constitutes as the main DOC fraction of UFA (Figure 4.6a) and SRFA water samples. The signals follow similar patterns except that UFA contains a slightly higher content of polysaccharides. TU-SW and Lankwitz samples contained approximately equivalent fractions of humic substances and building blocks, either due to the low organic sources in the catchments or the waters may have been biologically degraded. On the other hand, a significant different characteristic of DOC was observed in the Halensee runoff. In comparison to other samples, LC-OCD revealed strong signatures of low molecular weight compounds in relation to a weak signal of humic substances (Figure 4.6b).

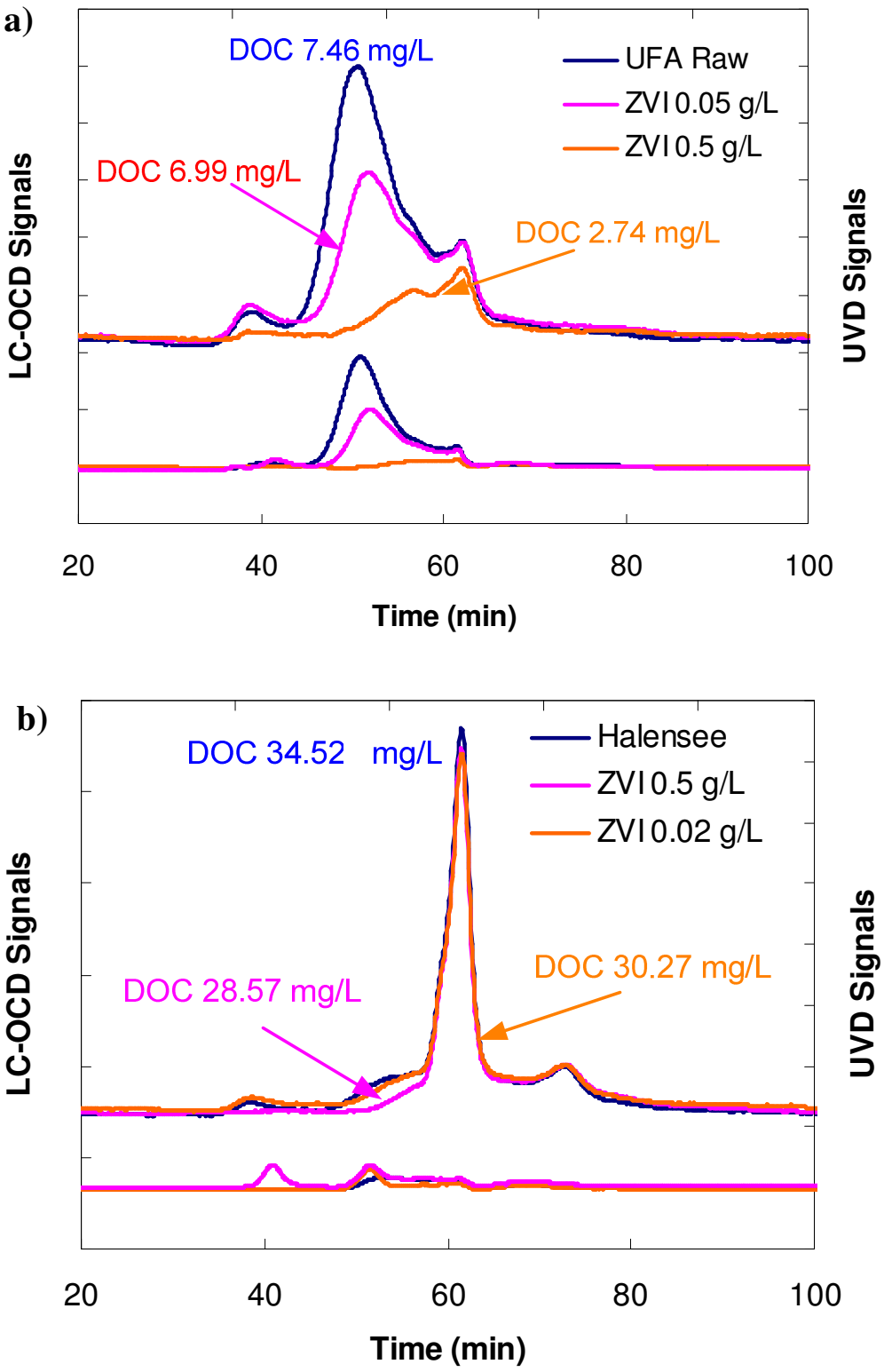

Fig. 4.6 LC-OCD and UVD signals of a) UFA and b) HS stormwater runoffs before and after equilibrium treatment with doses of 0.05 (0.02 for Halensee) and 0.5 g ZVI L^{-1}

Depicted in figures 4.6a) and 4.6b) are the comparisons of LC-OCD and UVD signals of the UFA and Halensee samples before and after treatment with doses of 0.02-0.5 g ZVI L^{-1}. In both samples, DOC and UV removal increases with higher doses of ZVI. Furthermore, larger molecular weight fulvic acids were observed to be preferentially removed. This indicates that the competitive adsorption of dissolved metals and DOC on iron oxide surfaces is impacted with a certain fraction of DOC. In accordance with a study of Gu *et al.* (1994), the adsorption of DOC on iron oxides involves a ligand exchange mechanism between carboxylic and phenolic groups of humic substances and hydroxylic iron oxide surface groups. A similar adsorption behavior has also been reported for groundwater DOC and SRNOM on GFH media (Genz *et al.* 2004). Further investigation of NOM impact is demonstrated in section 4.4.

4.1.5 Solid phase characterization

Several iron samples after ZVI treatment processes under a variety of conditions were characterized to understand the metal uptake mechanisms as well as to determine which parameters govern the long-term treatment processes.

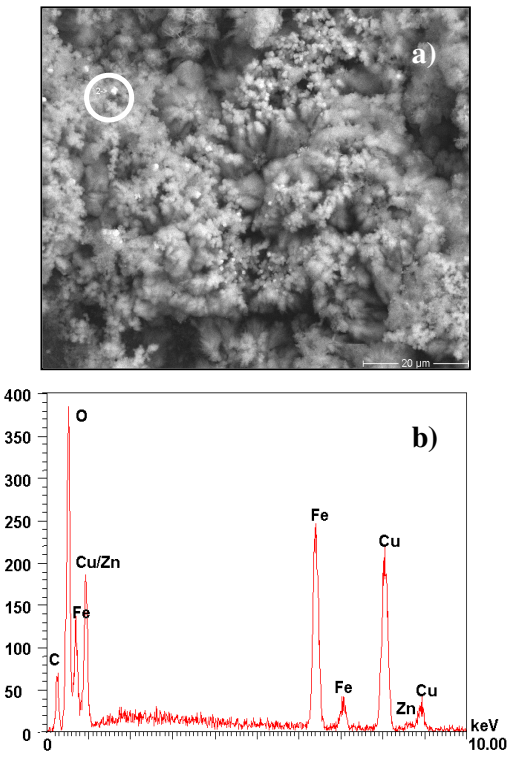

Fig. 4.7 a) SEM and b) EDX mapping of ZVI scale treated with solution [Cu_i^{2+} 10 mg L^{-1}, Zn_i^{2+} 10 mg L^{-1}, pH 7.0, DO_i 8-9 mg L^{-1}, 20°C, 150 rpm, SSWR]

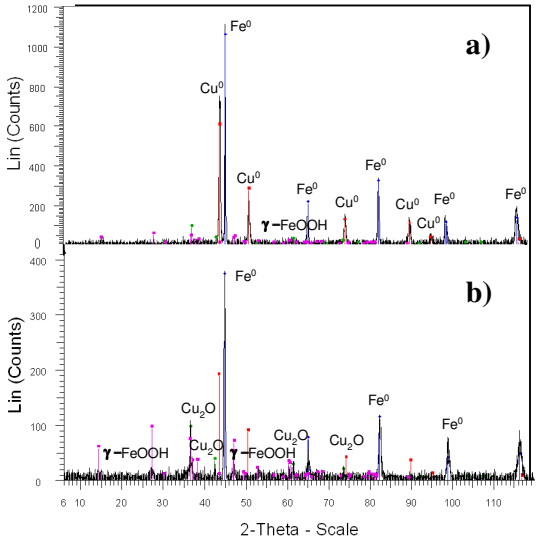

Fig. 4.8 X-Ray Diffractograms of ZVI scales treated under a) pH 4.0 DO < 0.5 mg L^{-1} and b) pH 7.0 DO_i 8-9 mg L^{-1} [Cu_0^{2+} and Zn_0^{2+} 10 mg L^{-1}, 20°C, 150 rpm, SSWR Solution]

In the case of deoxygenated acidic conditions, the iron sample was, by visual inspection, covered tightly with a black film. The strong intensive copper spectra could be detected by EDX. This corresponds to X-ray diffractograms, revealing clear, intensive and narrow reflections of two phases: metallic iron and metallic copper (Figure 4.8a). It is to be assumed that the reflections of this copper phase are a result of electro-chemical separation of the copper from the solution. The spectra indicates that copper is in a well-crystallised form.

Oxidation of copper takes place from Cu_2O (Cuprites) to CuO (Tenorite); Cu_2O has an intensive black colour. This layer is, however, probably so thin (where appropriate also X-ray amorphous) and could not be proved by XRD investigation. To verify this assumption, additional samples were analysed using AES, confirming the existence of Cu_2O (Fig. 4.9). The presence of cuprous oxide layer could probably be attributed to re-oxidation of the deposited metallic copper at the outer surface by Fe^{3+} as previously discussed. Besides, it may have been formed through a secondary pathway; a reduction of Cu^{2+} by ferrous iron bounded iron oxide surface as reported by Maithreepala and Doong (2004).

When DO was kept unlimited and pH was fixed at 7.0; iron was found predominantly covered by iron oxide (Figure 4.7a, Fig. B4 in appendix B). Using EDX, an extensive amount of copper and zinc were found to constitute at a typical iron surface and their existence of copper and zinc shows a strong association with iron oxides (Fig. 4.10). Further characterisation determined a relative strong appearance of copper precipitates at several bright spots on oxide peaks. The preferential area where copper deposition takes place as depicted in Figure 4.7a),

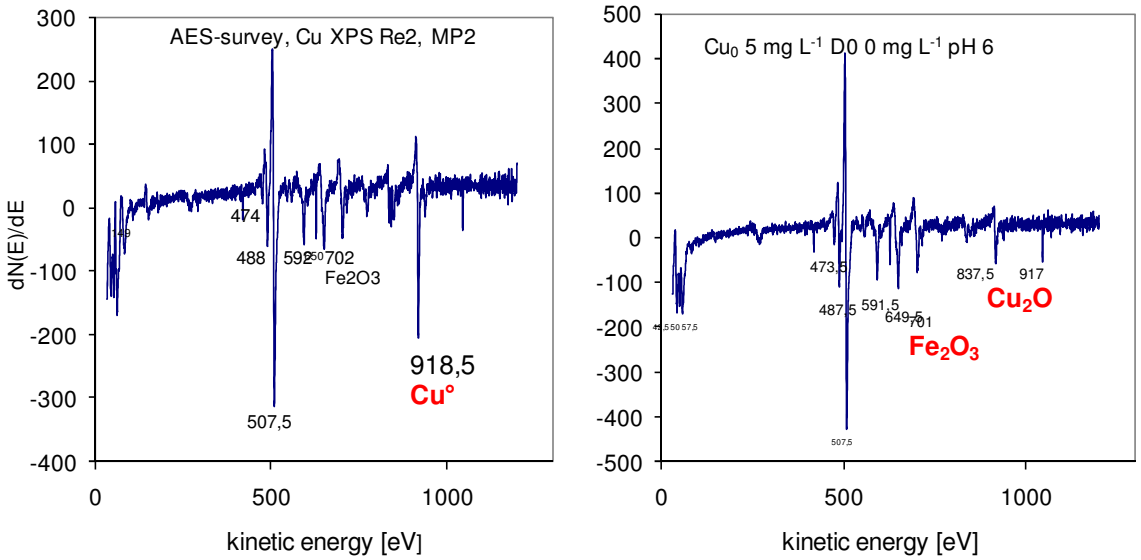

Fig. 4.9 The Auger Spectra of precipitates after cementation process [Cu_i^{2+} 5 mg L^{-1}, ZVI dimension 2.1x1.05x0.5cm^3, pH 6.0 (controlled), DO < 0.5 mg L^{-1}, T 20 ± 1.0 °C, 150 rpm in SSWR]

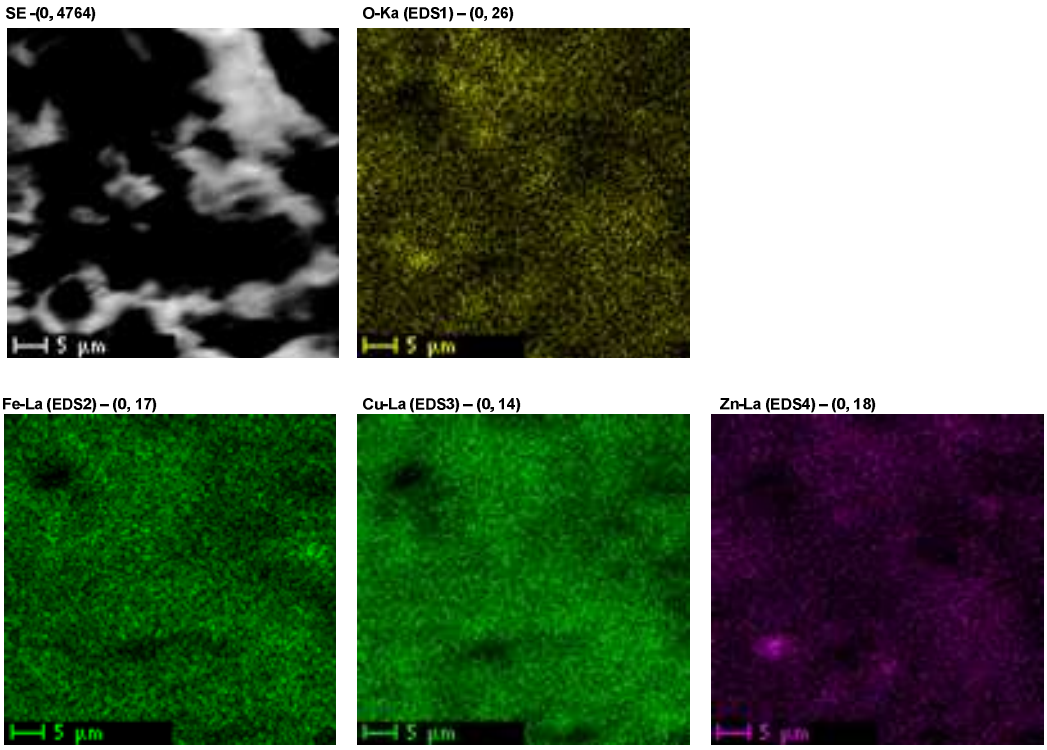

Fig. 4.10 Mapping of SEM image to EDX spectra of iron after experiment [Cu_i^{2+} 10 mg L^{-1}, Zn_i^{2+} 10 mg L^{-1}ZVI 0.192 m^2 L-1(0.5 g Fe^0 L^{-1}), pH 7.0 (controlled), T 20 ± 1.0 °C, 150 rpm in SSWR]. (c.f., supplement data in Appendix B)

reflected an electrical cell behaviour of iron, whereby iron dissolved at anodic surfaces and copper precipitated at cathodic sites (Ku and Chen, 1992).

The separate sample for phase determination was covered by a very fragile reddish-yellow layer. It was also observed that during batch experiments part of this layer had eroded out into the bulkwater solution. Diffractograms of the iron sample, Figure 4.8b) show clearly intensity-weak reflections in which four of these (in ca. 36.6°, 42.3°; 61.5° and 73.6°) could be isolated and assigned to a very low quantity of Cuprite (Cu_2O). Another reflection of the cuprites (at ca. 36.4°) is also available, superimposed, however, with two reflections of the lepidocrocites so that it has no additional supportive evidence. Two of the intensity-weak reflections (at ca. 27.0° and 46.8°) correspond to a fine crystallized form typical for the lepidocrocite (γ-FeOOH), a common phase often found as a result of iron corrosion processes in the presence of dissolved oxygen (Kamolpornwijit *et al.*, 2004). The X-ray detection of small amounts of cuprous oxides deposits may have, however, been interfered by the existing lepidocrocite on an iron surface; hence, the quantitative comparison of copper depositions between both deoxygenated and oxygenated conditions could not be established. Furthermore, the phase of lepidocrocite (γ-FeOOH) indicated that the uptake pathway of metals under this condition were, additionally, due to an adsorption process.

Regarding zinc, Figure 4.7b) illustrates some phase evident at ~1.0 and 8.6 keV. The former fell within the copper phase and is not likely to be assigned. A much weaker EDX spectra of zinc implied that uptake of zinc was less associated with ZVI corroding surface. How zinc is located could not be established by means of SEM and EDX analysis, furthermore, no attempt has been made to identify its phases. It is, nonetheless, reasonable to suggest in part that zinc ions form surface complexes with iron oxides present on corroded ZVI surfaces.

4.1.6 Conclusion

The present section demonstrated that ZVI is an efficient media for capturing of heavy metals (Cu^{2+} and Zn^{2+}) under typical runoff conditions. The mechanisms of metal uptake differ considerably, depending on the metal species and experimental conditions. ZVI interacts through reductive transformation and adsorption/co-precipitation processes. Experimentally derived parameters suggested that stormwater runoff qualities exert a significant influence on the removal of Cu^{2+} and Zn^{2+}. Compared with GFH, ZVI achieved equivalent loads while providing that it could be obtained at no-cost. A potential disadvantage of Fe^0 in regard to the immediate and long-term performance could be anticipated, as demonstrated in the following lists. The summary also includes several important aspects which must be taken into account for further implication as well as those related to the optimization approaches of ZVI processes.

(i) A pre-treatment of iron may be required to remove substances covering the iron reactive surface e.g. oil, when Fe^0 is obtained as solid waste.

(ii) The adsorption of metals on GFH takes place within 5-10 minutes. The cementation rate of Cu^{2+} by ZVI is relatively rapid, but is determined by a specific surface area and morphology of reactive surfaces (Fe^0 and probably previously deposited Cu^0) (Strickland and Lawson, 1971; Annamalai and Murr, 1979). In contrast, Zn^{2+} removal is kinetically slow with a magnitude of several hours, governed through an array of rate-limiting reactions including iron oxidation, iron (oxy)hydroxide precipitation and metal adsorption/co-precipitation. It is noteworthy that when the solution is low in DO, T, pH, IS or reactions take place under high metal and DOC concentrations, the removal rate of Zn^{2+} dramatically decreases.

(iii) Whenever favoured, precipitation of copper and iron (oxy)hydroxides has positive benefits in enhancing the cementation rate (Strickland and Lawson, 1971; Annamalai and Murr, 1979) or behaving as adsorption sites for metals in runoff solution, respectively. The precipitates may either localize on the iron surface or dissolute into the solution. This could, therefore, negatively stimulate the failure of a treatment barrier by passivation of the reactive Fe^0 surface as well as increase potential of pore blockage. The phases and morphology of precipitates on the Fe^0 reactive surfaces are the key factors determining the magnitude of rate retardation. In order to mitigate plugging of treatment barrier, Fe^0 has been typically mixed with sand. In the following section, Fe^0 mixed with pumice is tested in a flow-through configuration. The pumice possessing a high porosity might help in increasing hydraulic loading rate and lower problems of clogging of the ZVIB.

(iv) The impact of dissolved organic carbon is significant. According to the results in this study, there was sufficient evidence revealing that DOC inhibitions occurred via ligand complexation, e.g., ligate with Fe^{2+} and Cu^{2+}, and competitive adsorption. However, DOC may also directly inhibit Fe^{0} reactivity by adsorbing on the solid surface. The electrochemical modification of iron oxide surfaces by the adsorbed DOC have been extensively discussed, playing an important role in the processes of metal mobilization in a natural environment. In this regard, further investigations are required, specifically to determine the role of DOC in the long-term performance of a ZVI treatment system.

(v) Based on the results of separate experiment, it was shown that Pb^{2+} could be effectively removed by ZVI which shows that the method is also applicable for removal of other inorganic pollutants in stormwater runoff.

4.2. Column experiments with ZVI

The aim of this part was to assess the suitability of Fe^0 for the treatment of copper and zinc under both close to- and realistic-conditions employing column test. The breakthrough curves were determined using roof runoffs having varying characteristics. Furthermore, the PSD adsorption model is applied to simulate the resulting breakthrough curves.

4.2.1 Impacts of water quality

Effect of pH

It was generally noticed that there was a better metal removal of Fe^0/pumice with respect to increases of pH (Fig. 4.11). The breakthrough curve of copper at inlet pH (pH_i) 6.5 showed a steep increase at the beginning but was subsequently replaced by a declining breakthrough shape resulting in a final relative concentration (c/c_0) of copper at approximately 0.5-0.7. The columns operated at lower pHs showed a different trend; the eluted concentration constantly increases and reached c/c_0 ~ 1.0 at about 4,000 BV. As compared with the column at pH_i 5.8, the pH_i 4.2 column shows slightly better performance despite the lower inlet pH. In the treatment of zinc, an initial higher eluted concentration of c/c_0 = 0.3-0.5 was found (c/c_0 = 0.1 for copper). The breakthroughs at pH_i 6.5 show better performance compared with other pHs. A lag time which indicates the time required for the formation of iron hydroxide for adsorption sites was observed (i.e., 500-2,000 BV) for experiments at pH_i 4.2 and 5.8.

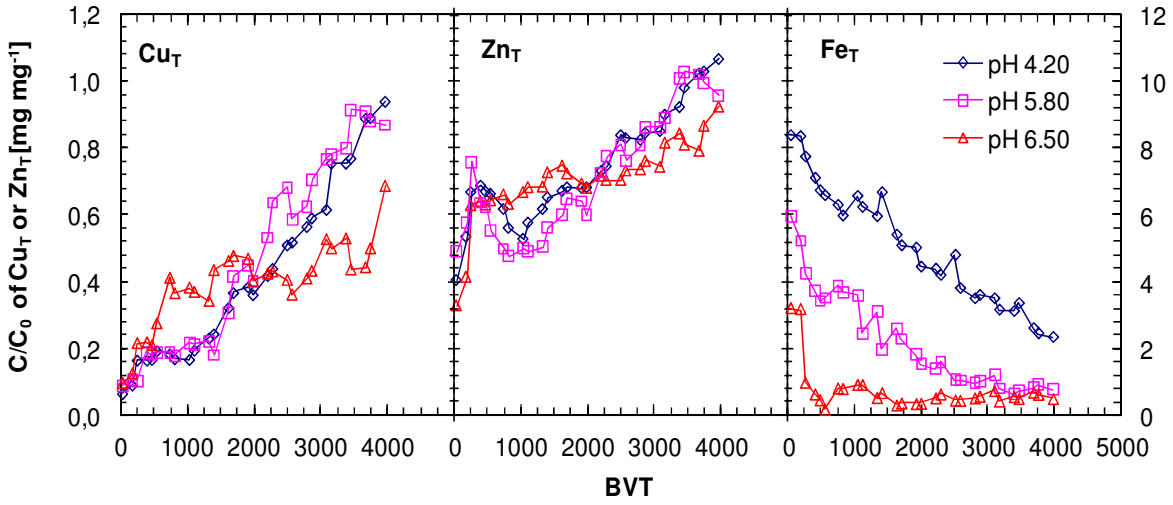

Fig. 4.11 Breakthrough behavior of copper and zinc and the corresponding iron released from column at varying pHs

The higher outlet pHs of effluents as compared with initial pH coincide with an extensive accumulation of iron hydroxides indicating the role of the adsorption/co-precipitation process. The effluent pHs from columns of initial pH_i 4.2 (4.17±0.15), 5.8 (5.85±0.63) and 6.5 (6.46±0.16) were 5.72±0.91, 6.19±0.26 and 6.31±0.23, respectively. The outlet pH (pH_f) of

column pH_i 4.2 was 6.04-6.22 at 0 – 1,406 BVT and gradually decreased to 4.84 at the end of the run. There were intensive oxides deposited for column pH_i 5.8 whereas this was only minor for pH_i 4.2, i.e., deposition of oxides occurred at the outlet end of the column and a clear water/Fe^0 mixture with a high outlet concentration of iron, was observed. This suggests that most of the metal and iron was more stabilized in the dissolved form at a lower pH_i. On the contrary, the decreased pH effluent of column pH_i 6.5 indicates the dominant process of hydroxide precipitation over the production of OH^- in the corrosion process.

The plot of Cu^{2+} removed against dissoluted Fe^{2+} shows a linear relationship with a slope of 1.38 (R^2=0.91) corresponding well with the results of Rangsivek and Jekel (2005) suggesting a dependency of the removal reaction with Fe^0 dissolution. Assuming an adsorption surface is partially formed during the run, a repulsive force between iron oxide and cations would prevent the adsorption reaction to take place at a lower pH than pH_{PZC}, i.e., ~ 7.2 (Rangsivek and Jekel, 2008). It is therefore reasonable that the observable removal of copper were partly due to the reductive transformation process. The reductive precipitation has been believed taking place through a direct reaction with Fe^0 surface; however, recently it was demonstrated that the indirect reduction with dissolved and structured Fe^{2+} in vicinity of Fe^0 surface plays a major role in this process (Noubactep, 2008a; 2008b; Ghauch et al., accepted). In this study, the pHs of the runoff fell below the range for chemical precipitation to occur (Rangsivek and Jekel, 2008).

Effect of DO and conductivity

The breakthrough results of the columns operated at different DO levels demonstrated a contrast in impact of the two metals (Fig. 4.12). The depletion rate of copper was hindered

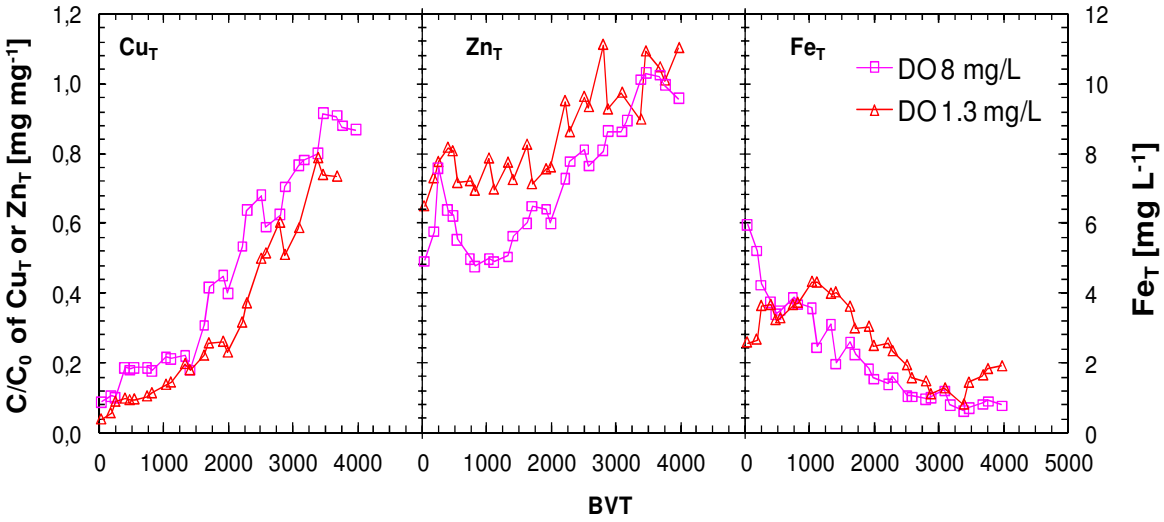

Fig. 4.12 Breakthrough curves of copper and zinc and the corresponding released concentration of iron from the columns experiment at oxygenated (6-8 mg L^{-1}) and deoxygenated (< 1.3 mg L^{-1}) conditions [Cu^{2+} 5.0 mg L^{-1}, Zn^{2+} 5.0-6.5 mg L^{-1}, pH_i 5.85±0.63 and pH_f 6.2±0.25 with 5 min EBCT,10% Fe^0 (v/v) mixed with pumice]

with increases of DO, in contrast to the removal for zinc which was enhanced. The latter was likely due to the higher availability of corrosion products in the presence of DO. A lag period for the formation of iron oxides of about 1,000 BV was observed in concomitant with decreasing iron at the outlet end, which could not be clearly seen for a low DO column. For both columns, a drift of 0.32-0.34 pH units was observed and the decreased outlet concentration of iron suggests that iron were mostly precipitated and deposited within the columns. This formation of ferric hydroxides presumably resulted in a lower Fe^{2+} concentration within the barrier which might contribute to a hindering effect for reductive transformation of Cu^{2+}.

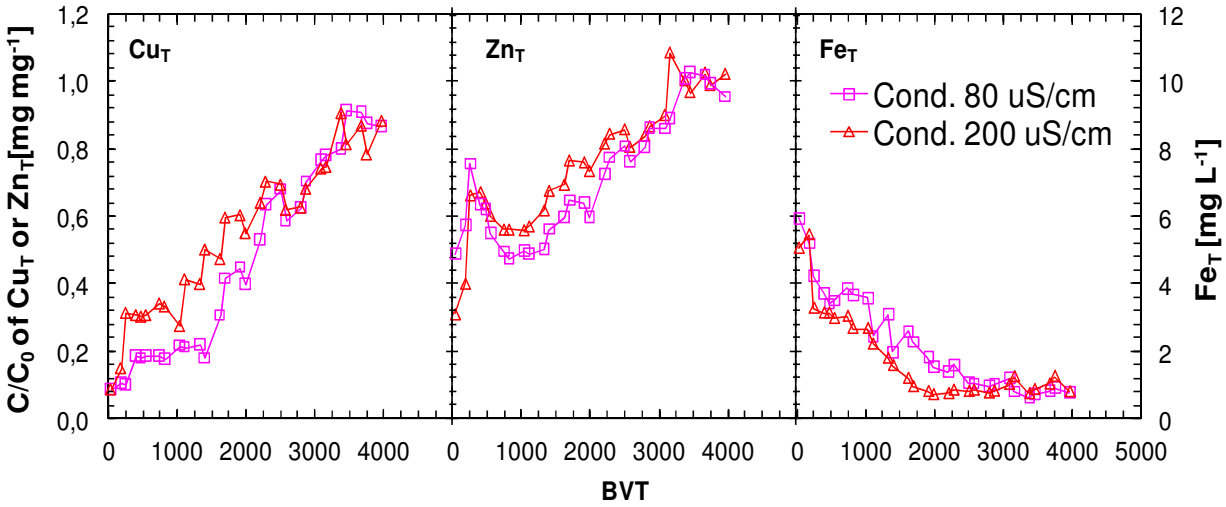

Fig. 4.13 Breakthrough curves of copper and zinc and the corresponding released concentration of iron from the columns experiments at conductivities 80 and 200 µS cm^{-1} conditions [Cu^{2+} 5.0 mg L^{-1}, Zn^{2+} 5.0-6.5 mg L^{-1}, pH_i 5.85±0.63 and pH_f 6.14±0.21, 5 min EBCT,10% Fe^0 (v/v) mixed with pumice]

A similar effect of the conductivity to DO on the breakthroughs was observed which means that the same inhibition pathways are involved. In the batch test, Rangsivek and Jekel (2005) found the removal of copper and zinc increases with higher ionic strength of water, which was attributed to a higher and spontaneous corrosion of iron. Here, the increasing removal of zinc with respect to IS was observed only in the beginning of breakthrough study (<2500 BV), but for all other periods similar removal ability for copper and zinc in both columns were generally seen (Fig. 4.13). The inconsistent results between the batch and column tests might be due to differences in system characteristics. As compared with the batch test, flow-through configurations are characterized by a significantly higher flux of metals and dissolved oxygen per unit mass of Fe^0, and as IS increases, this can yield much higher iron oxide precipitates within the columns at increasing iron dissolution rate. Thus, less iron is present in the dissolved form causing lower activities of reductive precipitation. In addition, the accumulated iron oxides in the column might hinder corrosion rate of iron though surface passivation.

Effect of temperature, NOM and EBCT

The impact of temperature on the removal of metals could not be verified when using runoff water collected in the summer period (Fig. 4.14). An immediate breakthrough occurs after only a few hundred of BVT, which was followed by a relatively stable breakthrough shape with no clear distinction of temperature impact. The most plausible reason for this result arises from the possession of a highly turbid and strong concentration of NOM in the summer water (see discussion below). For analysis of the temperature impact, DI was substituted for runoff water. The modeled water was prepared to resemble the characteristics of runoff water, with the exception of organic matter that remained zero. According to this, temperature increases from 15 to 30 °C resulted in an increase of 30% metal removal. It is also important to note that a higher elute iron concentration observed in the first period suggests that iron is more mobile in NOM solution.

Further attempts to elucidate the impact of NOM on Fe^0 system were tested using runoff of different NOM concentrations. The retention time of the runoff in the columns was set to 20 min to facilitate the examination. In addition, the effect of EBCT was to be investigated (c.f., Fig. 4.26). In the beginning of the test, runoff with ~9 mg NOM L^{-1} was fed into the columns and approximately 100% and 55% removal of copper and zinc were achieved, respectively. The iron concentration – which rationally indicates the activities of iron corrosion - was in a range of 2 mg L^{-1} and then rose to 5 mg L^{-1} indicating an extensive corrosion of iron (at 0-1,000 BV). After about 1,000 BV, the column was fed with 25 mg NOM L^{-1} runoff solution; this resulted in a substantially eluted concentration of metals occurring in concomitance with the reduced concentration of iron. The lower removal performance of metals in presence of NOM could be attributed to several reasons; i.e., a metal-ligand complex and a competitive

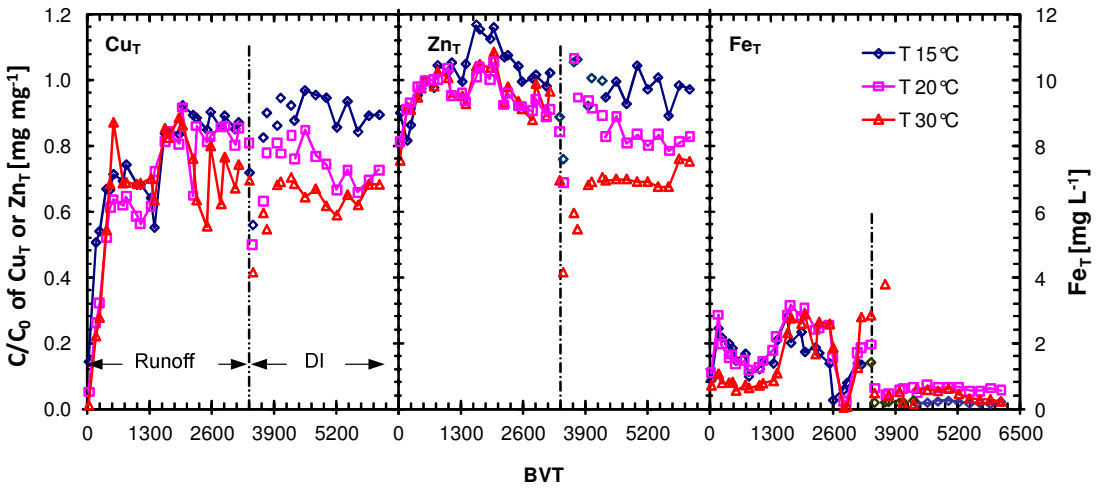

Fig. 4.14 Breakthrough behavior of copper and zinc and the corresponding iron released from column at varying temperatures (Lines divided between runoff and DI employed in the experiment, c.f., text)

adsorption, or this may also cause a modification of the chemical property of the Fe^0 by NOM coverage. A detailed investigation of NOM impacts on metal removal in Fe^0 is discussed in section 4.3. When compared with the 5 min, a 20 min contact time demonstrates a 60% and 50% better immobilization of copper and zinc, respectively.

4.2.2 Breakthrough behavior and process identification

Despite the high variability of runoff qualities, the breakthrough of copper and zinc from different columns follows a similar behavior (Fig. 4.11-4.13, exclude those at high NOM conditions of Fig. 4.14). The breakthroughs of copper were close to a sigmoidal shape. The rapid exhaustion of zinc was similar to that in a high NOM solution indicating a low metal retention capacity. In comparison to other related works, Smith (1996; 1998) reported the removal of zinc, cadmium, and lead (10 mg L^{-1} each at pH 4.0-5.5) by short-blast iron followed a sigmoidal breakthrough shape and the breakthrough occurred at less than 1,000-4,000 BV. Karschunke and Jekel (2002) reported the breakthrough of total and dissolved arsenic removal in iron corrosion system occurred at about 5,000 and 10,000 BV using simulated groundwater, respectively, but when testing with actual groundwater, immediate breakthrough was observed. In contrast, Ludwig and Jekel (2007) observed that a steady state between the uptake of contaminants (copper and zinc in roof runoff system) and the production of adsorption sites exist where exhaustion could not be observed over 6,000 BVT In their cases, a lower metal concentration of 2 mg L^{-1} with 11 min EBCT was employed. Here, probably the employed EBCT is too short to form such an equilibrium.

Another possible reason that could explain the observable high removal of metals in the studies of Karschunke and Jekel (2002) and Ludwig and Jekel (2007) is the physical characteristic of the system. In their study, spiral shaped iron without sand or pumice was employed. With higher porosity within the ZVIB, a greater hydraulic gradient at the liquid-solid interface is achieved leading to rust particles freely being removed, hence, less passivation - both as the protective film on Fe^0 surface or within the pore of the barrier. In the batch investigation with greater mixing intensity, iron oxides precipitate away from the Fe^0 surface resulting in spontaneous reactions (Rangsivek and Jekel, 2005). The important role of mixing on the iron surface passivation by iron oxides and on the removal process of contaminants by Fe^0 has been previously addressed (Ghauch et al., accepted).

To clarify whether the equilibrium of metal removal and corrosion of iron may exist and how different iron shapes influence the breakthrough curves, additional breakthrough column tests were carried out. For this, breakthroughs test using iron from Ludwig (2007)'s studies was compared with that of spiral shape and the particulate iron employed in this work. Furthermore, the typically employed Fe^0/PM column was tested using runoff water collected from other sources (UFA sample). This water has a DOC content of about 5.9 mg L^{-1} and pH of 6.2. Finally, the result from breakthrough column filled with 50%Fe^0 (v/v) were discussed.

Based on the results, it was found that the equilibrium of metal removal may exist at various conditions and this resulted in similar schematic of breakthrough developments as observed by Ludwig (2007). In comparison, the spiral of iron from Ludwig (2007) exhibited a rapid breakthrough and reached C/C_0 of approx. 0.7 for copper and 0.8 for zinc, respectively (Fig.B8). A leveling off characteristic with continual flat curves for both metals could be seen. This was also observed for spiral shape iron in this study, however, at much higher removal rate likely due to higher surface area of iron. In contrast, the breakthrough curves of the particle iron, which exhibited a similar rate to the spiral iron during 0-2,000 BVT shows a trend to much higher outlet concentrations. This phenomenon might be caused by an accumulation of iron corrosion products that may inhibit the transfer of contaminant to the metal uptake sites. However, the reduction in removal of metals could not be observed in UFA runoff (Fig. B10) and in the column filled with 50%Fe^0 (v/v) using TU runoff collected from winter period and with the same Fe^0 media (Fig. B9). The latter might be due to lower potential of precipitate formation in a rapid flow rate condition, i.e., iron concentration is diluted by the incoming metal fluxes and thus lower oxides formation at the iron-water interface. The observed leveling off schematic of the UFA breakthrough curves is likely a result of a higher pH that favors an adsorption process. The impact of NOM on the treatment efficiency should not be ruled out.

Depicted in Fig. 4.15-4.16 are the characterization results of SEM, EDX and XRD analyses of iron samples taken from the column experiments. The iron samples taken from the columns operated within a deoxygenated solution are covered tightly with a black film and resulted in little or no reddish iron oxides deposition. A nodular shape precipitate corresponding to X-ray diffractograms revealing an observed metallic copper phase (Figure 4.15(c)-4.16). The presence of copper phases can be attributed to an electro-chemical separation of the copper from the solution which agreed well with previous results of the batch studies. It is expected that the resulting copper precipitates were due to reactions with Fe^0 surface and/or Fe^{2+} (in a structured or dissipated form).

For other cases, in contrast to DO limiting conditions, extensive iron precipitates, copper, zinc and other phases such as oxygen, Al, Si, and K were found. These components distributed over the Fe^0/pumice mixtures when compared with the virgin pumice (Fig. 4.15b). The X-ray detection reveals deposition of lepidocrocite (γ-FeOOH), hemathite (α-FeOOH) and goetheit (γ-FeOOH), implying that uptake of copper and zinc were associated with the adsorption/co-precipitation processes and that aging of iron oxides had taken place.

The evidences of adsorption/co-precipitation processes were also observed by NOM removal (Fig. 4.17). The adsorption of NOM was highest in pH_i 6.5 columns followed by pH_i 4.2, which is due to an extensive accumulation of corrosion products induced by increases of pH_i and a higher affinity of NOM adsorption at low pH, respectively. The lowest NOM adsorption at pH_i 5.8 is likely due to the competitive adsorption between metal and NOM. The adsorption of NOM was also observed for the columns in deoxygenated or/and higher conductivity conditions.

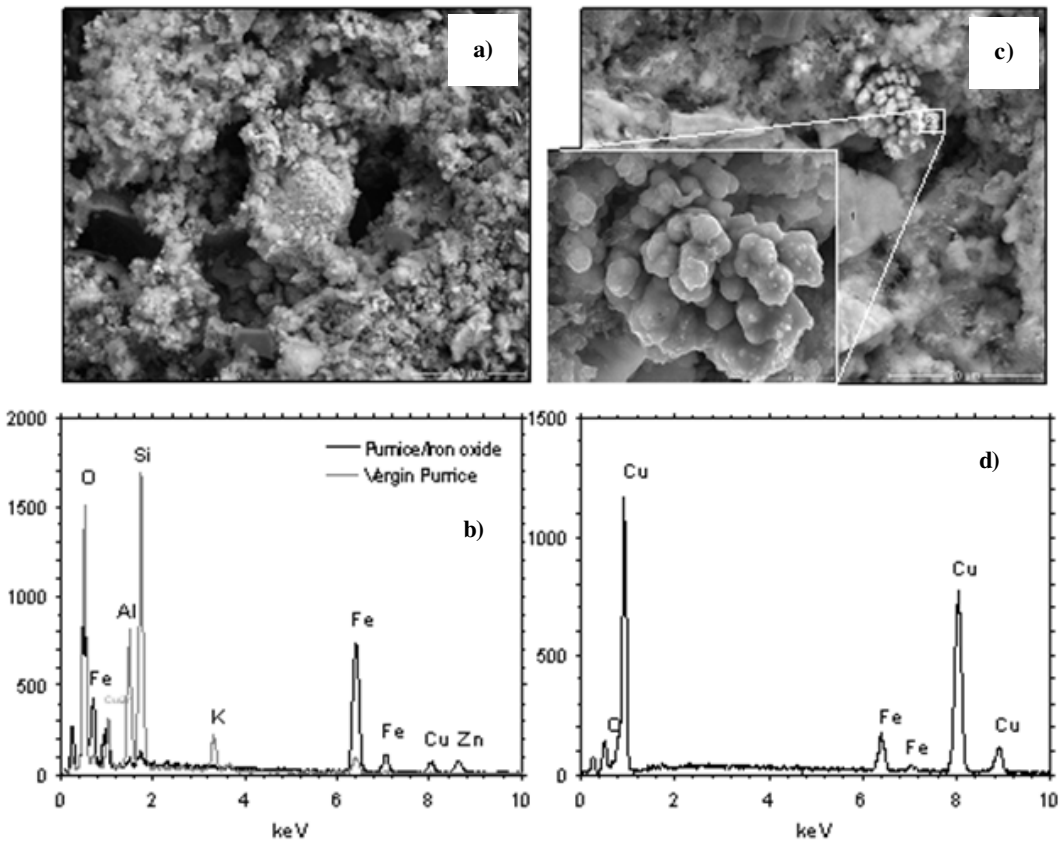

Fig. 4.15 (a) SEM and (b) EDX of of media obtained from typical column tests as compared with the original pumice, (c) The presence of nodular metallic copper on iron surface in DO-limiting solution and (d) the corresponding EDX diagram, c.f. text

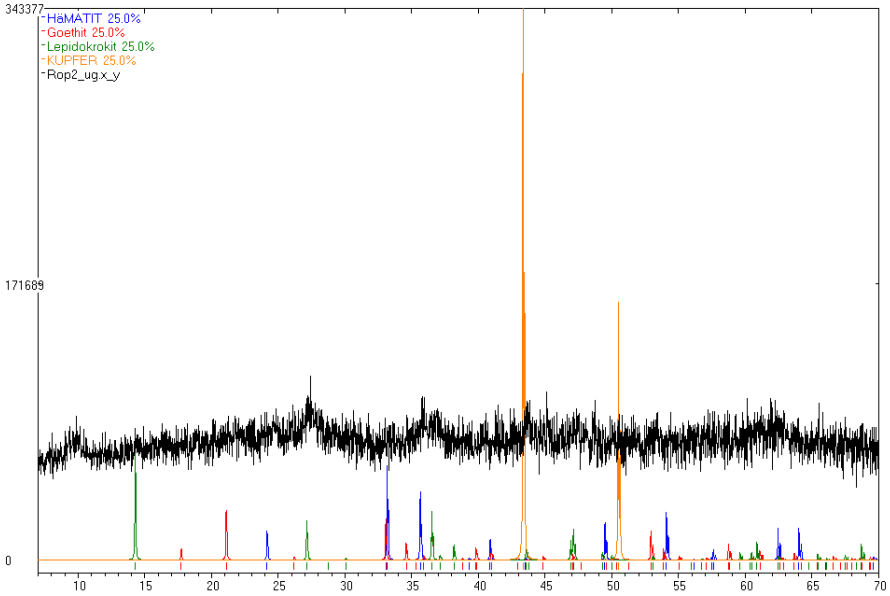

Fig. 4.16 XRD diagram of media obtained from typical column test

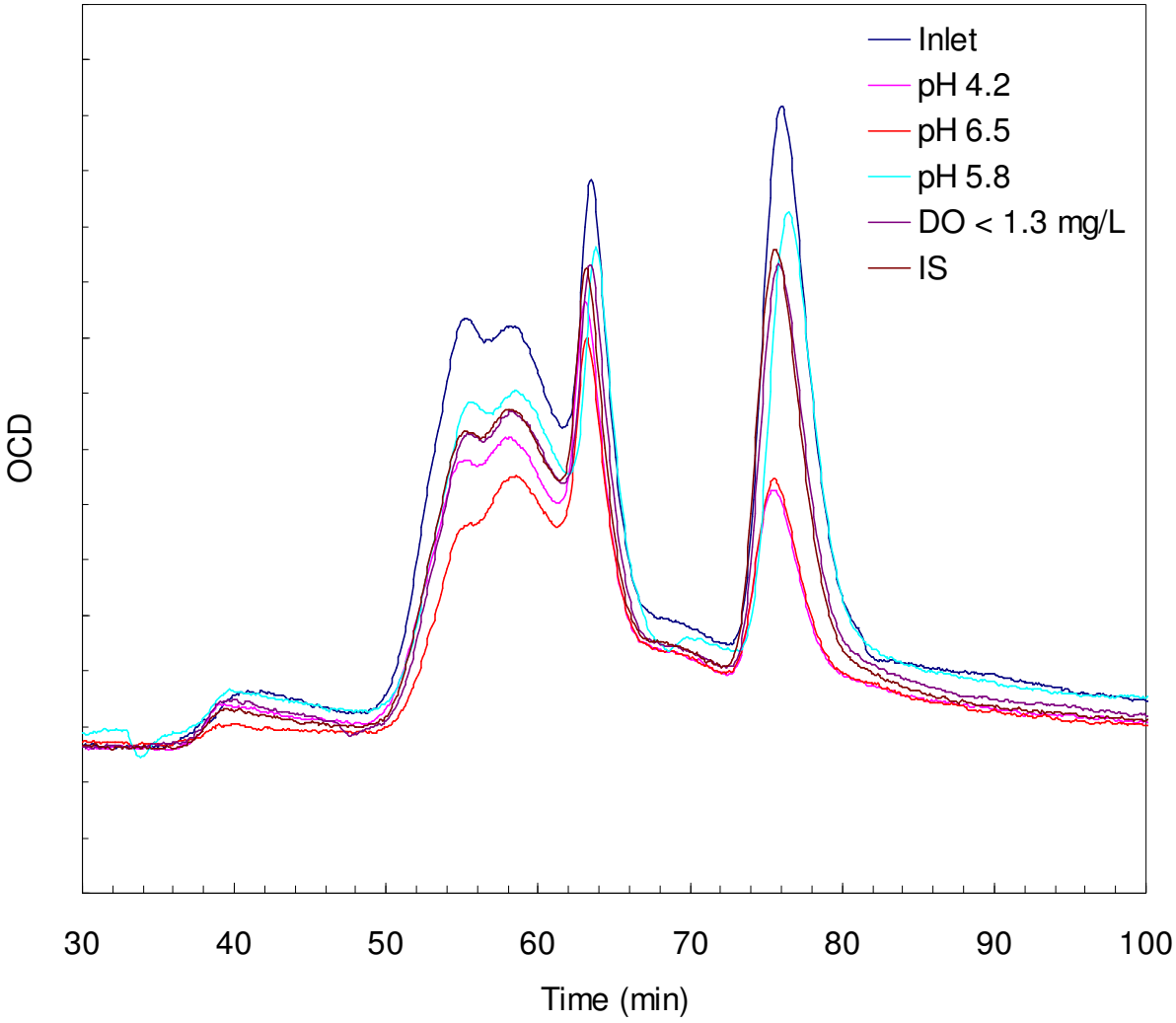

Fig. 4.17 LC-OCD diagrams of the inlet and outlet water samples obtained from different columns

4.2.3 Model prediction

Results of model calibration

Three sets of modeling parameters are required to sufficiently describe the breakthroughs of copper and zinc at different conditions (data from experiments using low NOM runoff excluded that of Fig. 4.14). The model employed K_F (and n) of 10-40 (0.6) for copper and 5-20(1.0) for zinc, respectively, and this yielded an average k_F of 0.4 x 10^{-3} cm s^{-1} for copper and k_F = 0.2 x 10^{-3} cm s^{-1} for zinc with higher and lower bound values demonstrated in Table 4.2. In the modeling of breakthroughs at increased NOM concentration, it was necessary to

Table 4.2 Operational and input parameters for modelling of the breakthrough curves

Parameters	Cu_i^{2+}	Zn_i^{2+}	*NOM*	D_i	*L*	Fe^0	*EBCT*	Cu^{2+}			Zn^{2+}		
								K_F	*1/n*	k_f	K_F	*1/n*	k_f
Conditions/Unit	[mg l^{-1}]	[mg l^{-1}]	[mg l^{-1}]	[cm]	[cm]	[g]	[min]			[x10^{-3}]			[x10^{-3}]
Varying runoffs[a]													
Lower bound	5.0	6.5	2.0	2.5	15	15	4.9	40	0.6	1.5	20	1.0	0.35
Average	5.0	6.5	2.0	2.5	15	15	4.9	20	0.6	0.4	10	1.0	0.20
Upper bound	5.0	6.5	2.0	2.5	15	15	4.9	10	0.6	0.5	5	1.0	0.09
Effect of NOM[b]													
DI	5.0	6.5	0	2.5	15	15	4.9	100	0.4	0.9	60	0.2	0.13
NOM 3-10 mg/l	5.0	6.5	4-9	2.5	15	15	4.9	20	0.6	0.4	10	1.0	0.20
NOM 5-61 mg/l	5.0	6.5	9-70	2.5	15	15	4.9	20	0.6	0.2	5	1.0	0.10
Effect of EBCT[c]													
NOM 9 mg/l	5.0	6.5	9.0	2.5	15	15	20.0	20	0.6	0.9	10	1.0	0.08
NOM 25 mg/l	5.0	6.5	25.0	2.5	15	15	20.0	20	0.6	0.07	10	0.6	0.025
Large column[d]	5.0	6.5	5.43	3.5	56	208	2.3	20	0.6	1.5	20	1.0	0.35

a) Breakthroughs from column experiment in low NOM runoff solution (Fig. 4.18)
b) Breakthroughs from column experiment at varying NOM concentration (Fig. 4.19)
c) Breakthroughs from determination of EBCT impact (Fig. 4.26 in supporting information)
d) Results from large column test (Fig. 4.20)
*For modelling of both copper and zinc, D_s = 1.0 x 10^{-10} cm^2 s^{-1} and D_p = 8.53 x 10^{-16} cm^2 s^{-1} were employed.

modify the kinetic coefficient to: k_F 0.2 x 10^{-3} cm s^{-1} for copper and k_F = 0.1 x 10^{-3} cm s^{-1} for zinc (Fig. 4.19). Furthermore, they were found to change with respect to changes of NOM concentrations. For the calibration of the breakthrough curves, K_F, n and k_F were the most influential parameters (e.g., Fig. 4.20), while varying the D_s or D_p did not significantly improve the results. This indicates that the NOM may have inhibited the removal by surface coverage leading to decreases in the mass transfer rate of metals. In all cases, the observed higher kinetic coefficient of copper over zinc was presumably due to a higher mass transfer rate reaction. The kinetic coefficients obtained from the calibration procedures in this work are comparable to values obtained in the literature, i.e., an order of magnitude difference. Smith (1998) reported k_f = 1.5-5.0 x 10^{-3} cm s^{-1} and D_s = 1.0-15 x 10^{-11} cm^2 s^{-1} for surface adsorption of Pb^{2+}, Zn^{2+} and Cd^{2+} onto short blast media. Sperlich et al. (2005) employed k_f = 1.11 x 10^{-3} cm s^{-1} and D_s = 2.64 x 10^{-9} cm^2 s^{-1} in the modeling of arsenic adsorption onto GFH.

Integrating the breakthrough curves, which describes the mass of metal removed, and divided them with mass of Fe^0 in the barrier yields a metal loading capacity of an average 76 mg g^{-1} Fe^0 for copper (with min: 55 and max: 96 mg g^{-1}, the lower line is excluded as it under predicts the curve) and 55 mg g^{-1} Fe^0 for zinc (min: 22, max: 69 mg g^{-1}). The presence of 9-61 mg L^{-1} NOM concentration results in a much lower metal uptake load of 42 and 22 mg g^{-1}, respectively. Generally, the obtained coefficients in this study agree well with previous batch works, as well as values reported in literature. In the Ludwig and Jekel (2007) studies, 50-300 mg g^{-1} of copper and zinc uptake in an iron corrosion system were found. A smaller load of metal uptake observed here as compared to Ludwig and Jekel (2007) might have been due to a shorter EBCT employed or the physical and chemical characteristics of the system, i.e., the clogging effect of the treatment barrier when pumice was filled into the columns. Smith

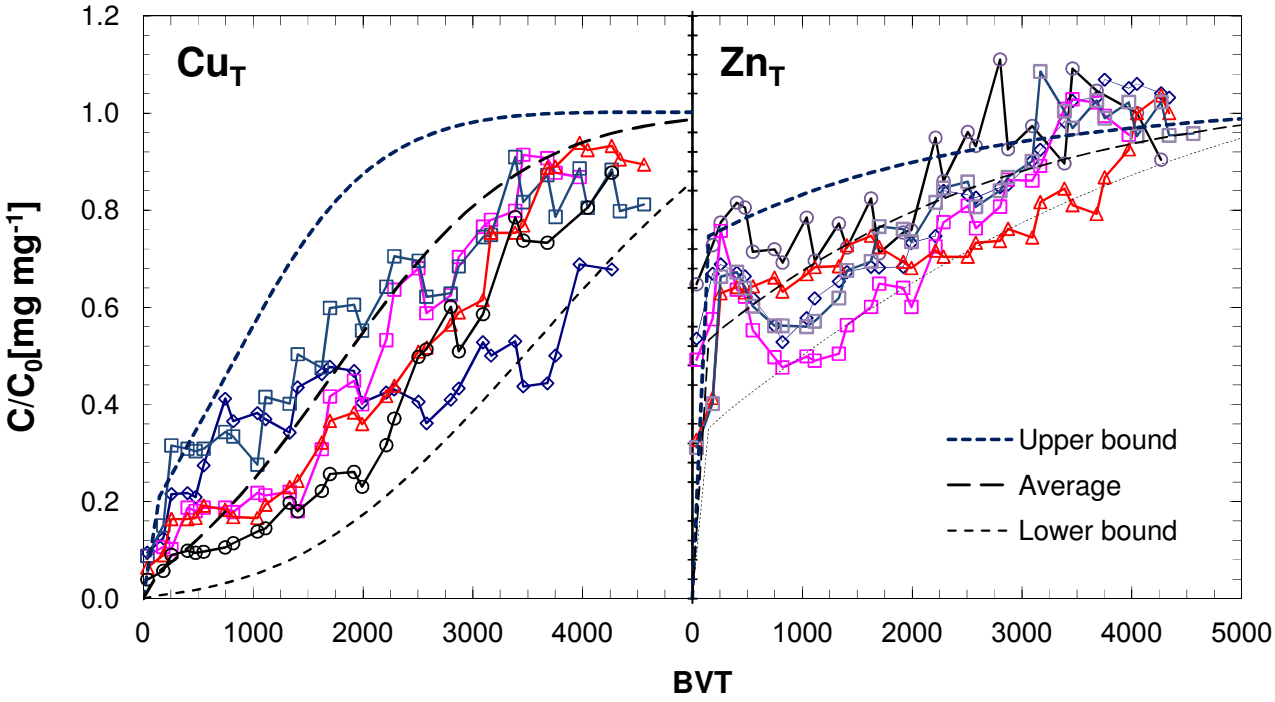

Fig. 4.18 Calibration of PSDM with breakthroughs of copper and zinc employing equilibrium and kinetic parameters demonstrated in Table 4.2

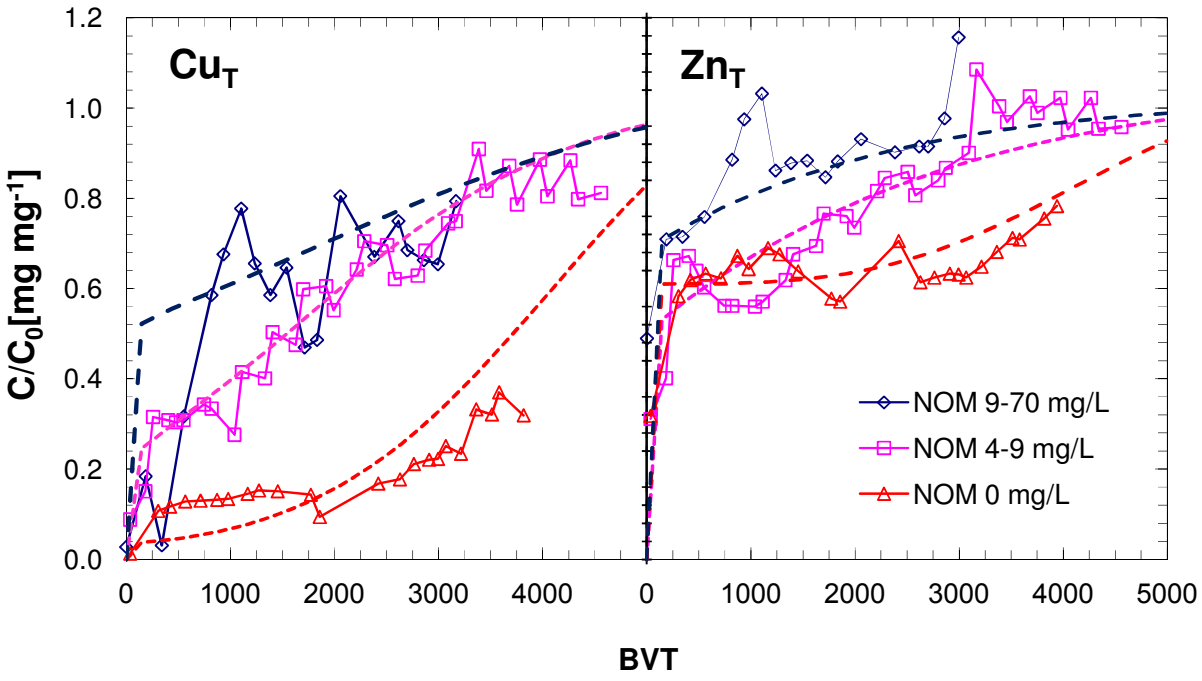

Fig. 4.19 Calibration of the PSDM with breakthroughs of copper and zinc obtained from column experiments under different NOM concentrations. The obtained kinetic parameters are demonstrated in Table 4.2

(1995; 1996) reported an individual uptake load of Pb^{2+}, Zn^{2+} and Cd^{2+} onto short blast media of 60, 40, 20 mg g^{-1}, respectively. Komnitsas et al. (2007) studied copper removal in acidic pH 2.5-4.5 range and reported a maximum removal load of 13.3 mg g^{-1} of iron. An approximate loading capacity of 40 mg g^{-1} was found in the adsorption of arsenate on GFH (Sperlich et al., 2005). It must be, however, noted that the uptake load of metals per unit mass of iron may not be representative values for comparasion with other media since iron oxides is progressively and continually generated in the Fe^0 system, and thus, sorption site is increasing over time.

Up-scaling and simulation at different scenarios

The PSDM can adequately predict the breakthrough curves in spite of differences in contact times and column size employed of the large column test (Fig. 4.21a, 4.21b). Lower bound coefficients were used in the model, whereas the average values over-predicted the results, which might be due to the low NOM of the employed winter water (Rangsivek and Jekel, 2008).

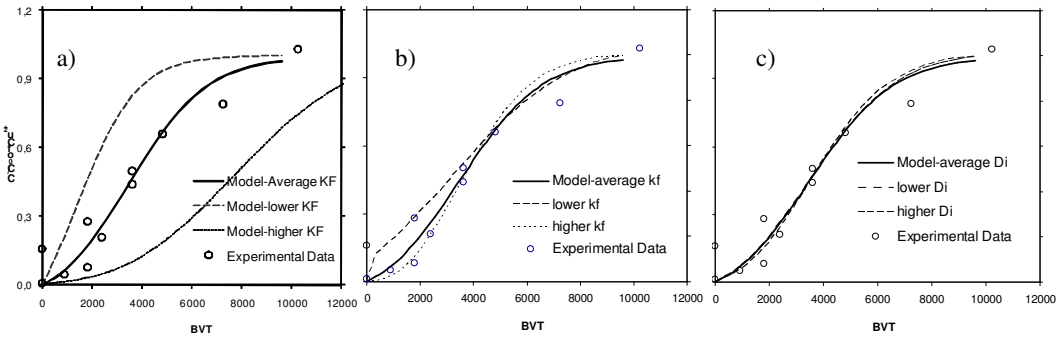

Fig.4.20 Sensitivity analysis of the breakthrough curves of copper obtained from a large column test calibrating with (a) K_F, (b) k_f and (c) D_S (modeling parameters are according to Table 4.2 for lower bound with varying of 25%)

The model simulation shows that the increase of EBCT to 30 and 40 min from the original 20 min can extend the time that copper begins to elute out of the Fe^0 columns of up to about 2,000 and 3,500 BVT, respectively, and the breakthrough follows a sigmoidal shape. To improve the treatment efficiency of zinc, at least 40 min EBCT is required. However, it must be noted that the considered system is the multi-component system where copper, zinc and NOM present and competitive adsorption can not be prevented. In a system, where zinc is the only component a better removal ability may be achieved. Fig. 4.21c and 4.21d illustrate breakthrough results of the model employing a 50%Fe^0 column. The usage of higher iron ratio shows to significantly improve the treatment performance; copper begins to elute out at about 8,000 BV while about 4,000 BV was observed for zinc. However, obviously the model fails to predict the lag period of time required for producing adsorption sites for zinc as compared with the experimental results of 50%Fe^0, illustrated in Fig. B9 (appendix B).

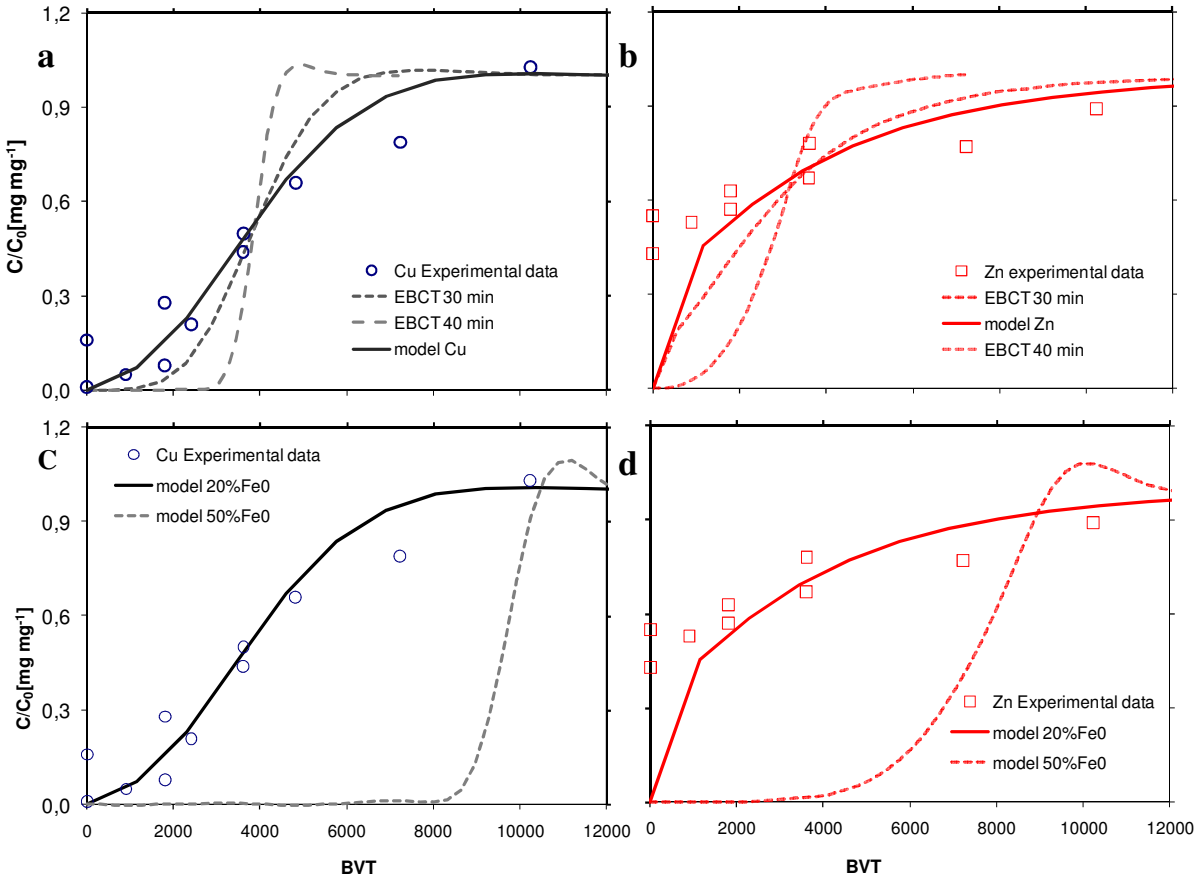

Fig. 4.21 Plots of model prediction of the breakthrough results of a large column test and the model prediction for assessment of the up-scaling and optimizing of the processes

4.2.4 Conclusion

The aim of this work was to develop a suitable system for the treatment of metal-contaminated roof runoff. The assessment of the use of Fe^0 for the treatment of copper and zinc was carried out under close to- and realistic conditions employing various column configurations. Fe^0 was firstly evaluated in the laboratory column under changing runoff characteristics. The study demonstrated that the breakthroughs of copper and zinc treated by a Fe^0 system were either accelerated or hindered under different water characteristics. Increased pH and temperature generally favor faster retention of metals whereas increased DO and IS of the solution hinders the removal of copper in the column system. The contrasting results between the batch and column tests were attributed to differences in the conditions employed and the physico-chemical characteristics of solid precipitates involved in the systems.

(i) The difference in removal pathways brings about a distinguished transport rate and breakthrough shape of copper and zinc. The uptake of zinc was mainly due to the adsorption/co-precipitation processes, whose rates are determined by an array of reactions including iron dissolution, iron precipitation and adsorption/co-precipitation. In contrast to zinc, copper is mainly reduced to metallic copper. With extensive precipitation of iron oxides, removal of copper via adsorption/co-precipitation processes could not be ruled out.

(ii) Any water qualities that tend to accelerate the rate of iron corrosion and precipitation of its oxides is beneficial to the uptake of zinc due to increasing adsorption sites. This is, however, not necessarily true in the case of copper, where accumulated products within the columns showed to hinder the reduction rate. Over time, the adsorption may be the only dominant reaction since reactive iron is fully covered. Among water quality investigated, NOM holds the most influence leading to an abrupt releasing of metals out of the barrier.

(iii) A set of kinetic and equilibrium parameters was obtained from model calibrations of the breakthroughs curves. These parameters allow the use of PSDM in designing a Fe^0 treatment system with a wide range of conditions. When the model is to be employed, accuracy of prediction depends strongly on the presence of NOM; hence, equilibrium isotherms and kinetic data should be acquired from the runoff waters in the site of installation, were K_F and n are the most prominent parameters. Increasing of Fe^0 mass will improve the performance of metal removal. It is, however, important to maintain high void area within the column, in order to sustain sufficient hydraulic conductivity. Furthermore, coefficients required for the modeling must be determined at specific site and conditions.

(iv) The model simulation suggests that sufficient iron is required to achieve a certain performance of the treatment barrier, particularly for the adsorption of zinc. On the other hand, a ratio of iron higher than 10% (v/v) can lead to failure both due to clogging or by decreasing the mass transfer rate of metals. To achieve maximum performance of metal removal by Fe^0, the incorporation of carbonatic materials into the barrier may be promising.

4.3. NOM experiments

Among water quality parameters investigated, NOM shows most significant influences on the removal rates of metals by Fe^0. In this section, the characteristic of NOM in roof runoff, mechanisms as well as the impacts of NOM on the Fe^0 treatment system are investigated.The NOM in runoff waters was characterized using XAD-4/8 adsorption resins, copper complexation, acidic capacity and liquid chromatography with online carbon detection. Batch kinetic experiments and flow-through configurations were performed and the results of metal removal were elucidated taking into account the characteristics of NOM.

4.3.1 Characterization of source water

The quality of TU runoff varied significantly over the 1 year experiment. In winter and spring, TU runoff demonstrated a generally soft characteristic, low turbidity and ionic strength with conductivity of about 30-65 µS cm^{-1}. They are mildly acidic with pH (min-max (mean value)) values of 4.80–6.26. The concentration of NOM was 2.86-10.33 (5.92) mg DOC L^{-1}, whereas the zinc concentration varied in a range of 1.76-2.30 (1.97) mg Zn^{2+} L^{-1}. Typically, the runoff samples collected in winter and spring could be considered a dilute solution.

Contrary to the winter and spring samples, the waters collected during summer and autumn are more concentrated with organic and inorganic substances. The waters are highly turbid, smelly and possess much higher conductivity than the winter sample. After a long drought in the beginning of summer, the dissolved NOM concentration was as high as 300 mg DOC L^{-1} with conductivity of 600 µS cm^{-1} (before dilution to TU-FF, Table 4.3); however, that was a small rain event. For typical runoff samples taken during summer, the concentration of NOM is 5.07-61.0 (26.3) mg L^{-1} (e.g., TU-SW, Table 4.3). The dissolved zinc concentration can range up to 6.0 mg L^{-1} in the first-flush sample but typically fell into a range of 1.46-3.54 (2.47) mg L^{-1} as an event-mean concentration, which indicates that the release of Zn^{2+} into runoff water is more or less equally distributed over the year. The concentration of copper is insignificant. Furthermore, phosphate is less than 0.1 mg L^{-1}.

Table 4.3 Characteristics of source waters for investigation of NOM impacts

Source*	pH	Condc.	DOC	UVA_{254}	SUVA	HPO	HPI	TPI
		(µS cm^{-1})	(mg L^{-1})	(m^{-1})	(m^{-1} mg^{-1} L)	%	%	%
TU-SW	6.0	134	36	104	2.9	65	17	18
TU-FF	5.0	19	9.9	16.5	1.7	8	70	22
CU-R	6.4	148	9.8	29.9	3.1	45	28	27
SR-NOM	5.0	300	4.3	24.1	5.6	93	2	5

1. TU-SW: Bitumen roof runoff with zinc gutter at TU Berlin collected during Autumn
2. TU-FF : 1 to 30 dilution of the first flush of TU-SW after long drought period in the beginning of the Summer
3. CU-R: Copper roof runoff at the university of art in Berlin (UDK)
4. SR-NOM: prepared using Suwannee River NOM in deionized water (DI)

*Prefiltrated using 0.45 µm cellulose nitrate filter; HPO hydrophobic fraction; HPI hydrophilic fraction and TPI transphilic fraction

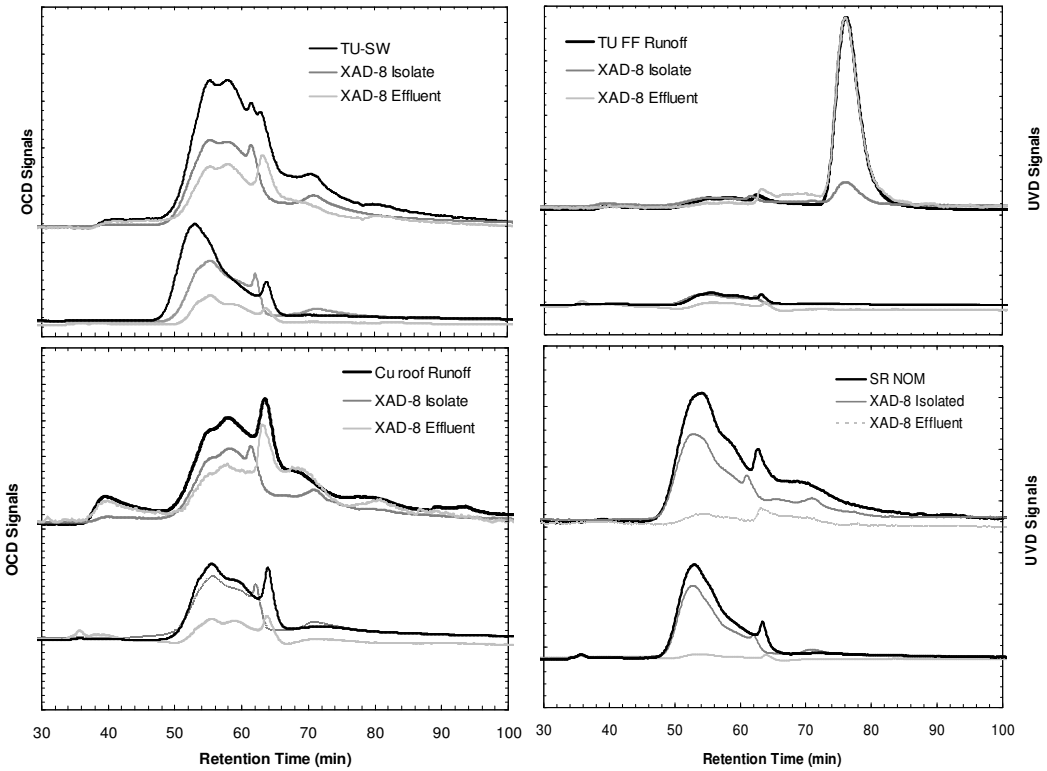

Fig. 4.22 LC-OCD of bulk water NOMs and their corresponding XAD-8 isolated and XAD-8 effluent fractions of a) TU-SW b) TU-FF c) SR-NOM and d) Cu-R runoffs, c.f., Table 4.3

There was no attempt to analyze the annual quality of runoff from the copper roof. However, a visual inspection of several samples from various periods show that the quality of runoff followed a similar tendency of annual changes as that of TU roof owning to the same catchment area. Based on a few collected samples, the concentration of copper and zinc were in the range of 4.9-9.1 (7.0) mg L^{-1} Cu^{2+}, and 0.8-1.0 (0.9) mg L^{-1} Zn^{2+}, respectively. The appearance of zinc in copper roof runoff might be because of the influence of vehicles from adjacent streets or the existing zinc components on the roof.

Hydrophobicity and molecular size

A comparison between LC-OCD chromatograms of the runoff samples shows that NOM from the same roof source, or catchment, has distinctly different characteristics (Fig.4.22). The TU-SW and Cu-R are comprised mainly of humic substances and building blocks that have a strong UV absorption, most likely derived from the decomposition of plants. In addition to that, a minor content of polysaccharides have also been detected. Fulvic acid is the main part of SR-NOM and the obtained LC-OCD diagram is similar to its corresponding fulvic fraction as determined in a previous work (Rangsivek and Jekel, 2005). In all of these runoff samples, humic substances constitute a significant proportion of the total organic carbon concentration. Similarly, the surface water NOMs are composed of approximately 60% humic substances (Ma et al., 2001).

Table 4.4 Estimated contents of carboxylic and phenolic groups

	Carboxylic (mmol g^{-1} C)	Phenolic (mmol g^{-1} C)	Total acidity (mmol g^{-1} C)	Overall acidity* (µmol L^{-1})
TU-SW	1.8	0.9	2.7	97
TU-FF	3.8	1.9	5.8	54
SR-NOM	9.1	4.5	13.6	95
Cu-R	6.4	3.2	9.7	58

* The overall acidity was calculated by taking into account the variability of DOC concentration of the raw water samples.

These waters generally exhibit hydrophobic and high aromatic characteristics as indicated by a high value for SUVA (Table 4.3). In contrast to other samples, TU-FF exhibited primarily fractions of small size range of low molecular weight acids and neutrals. The water demonstrates a hydrophilic characteristic (70%). This could be attributed to the fact that amphiphilics and neutrals possess a low content of organic functional groups (Fig. 4.22; Table 4.3). Corresponding to this, TU-FF has the lowest values of an index of aromaticity compared to other runoff samples.

Acidity of source water

The results of calculation for the acidic capacity of the NOM samples are shown in Table 4.4 (c.f., Fig. B13). The compositions of carboxylic and phenolic groups decrease in the order SR-NOM, Cu-R, TU-FF and TU-SW, respectively. TU runoff from the same source reveals similarly low organic contents (2.72 and 5.76 mmol g^{-1} C for TU-SW and TU-FF, respectively), although they have different total concentrations. The generally low ligand content in the TU-FF solution could be reasonably attributed to the composition of hydrophilic compounds. Probably, most of the hydrophobic compounds in TU-SW have low organic functional groups. However, taking into account the total concentration of dissolved organic compounds, the TU-SW sample demonstrates the highest overall acidity capacity**.** In contrast, the SR-NOM (13.61 mmol g^{-1} C) and CU-R (9.65 mmol g^{-1} C) consists of relatively high organic functional groups. The carboxylic and phenolic contents in runoff samples obtained in the present work are within the same range as the NOM samples from natural surface water (Lu and Allen, 2002).

Copper complexation capacity

According to the results of titration experiments, the copper complexed by NOM runoffs are only evident in the TU-SW (Fig. 4.23) and are minimal for others. Under experimental conditions, i.e., at total 5 mg Cu^{2+} L^{-1} about 2 mg L^{-1} is present as free copper in TU-SW. Similar results were obtained in the titration of the hydrophobic fractions of the runoff NOMs. In contrast to other studies of natural waters, however, the complexation capacity of the runoff NOMs in the present work can be considered relatively low. He et al. (2001) found that copper remained mostly in a complexed form. MacCarthy et al. (1975) employed Fourier transform infrared spectroscopy and showed that carboxyl functional groups participate in the complexation of Cu^{2+}. In this work, TU-SW NOM possesses the highest content of total acidity (Table 4.4). A low complexation capacity obtained in this study might have come about because the titration experiments were run at a low pH 5.50. In an alkaline pH solution the NOM-complexation of metals may be significantly greater (Cheng and Allen, 2006). A 10

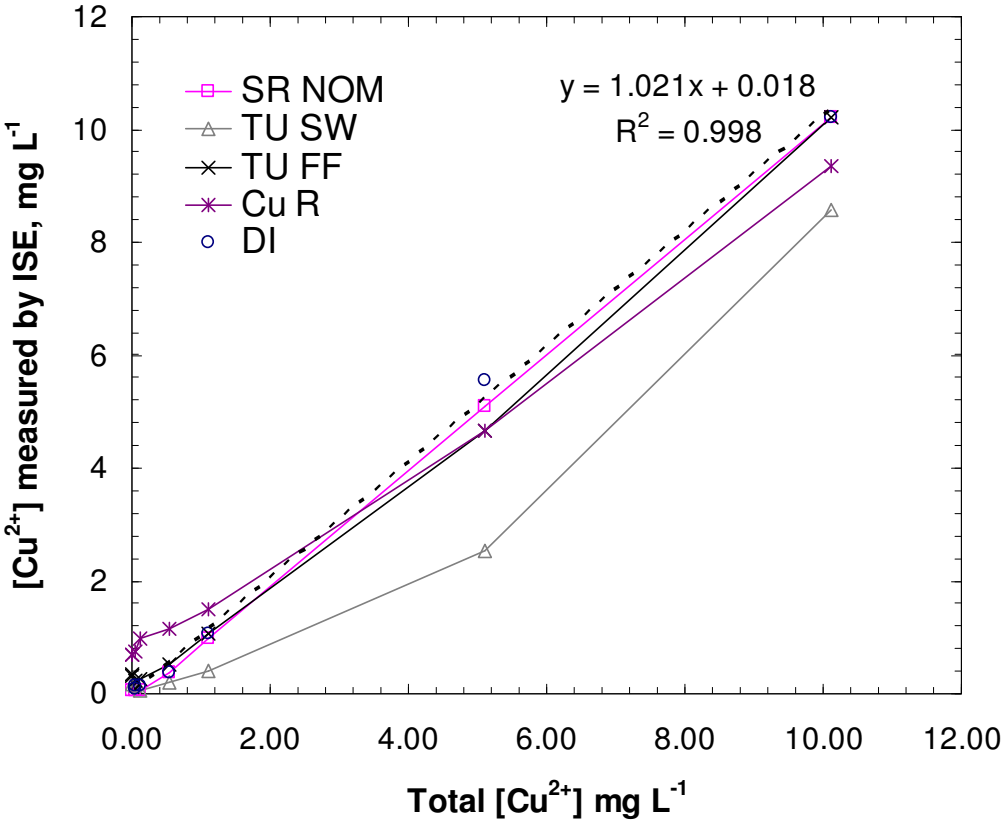

Fig. 4.23 Copper titration of runoff NOM samples from different sources

fold increase of Cu^{2+} and NOM complexation per pH unit was reported by Lu and Allen (2002).

4.3.2 Batch kinetic study with NOM

In the experiments carried out at initial pH (pH_i) 2.50 and 5.50, the Cu^{2+} depletion rate took place rapidly and a complete removal was achieved within 18 hours regardless of variation in the source of roof waters and initial pHs. The first-order rate $t_{1/2}$ of copper removal was 2.90-9.56 h. These results are comparable with that of a previous study ($t_{1/2}$ of 2.52-6.72 h at pH_i 5.0 and pH_f 5.42-6.04) using runoff from different surfaces including roof, street and highway (Rangsivek and Jekel, 2005).

Removal rate of Zn^{2+} was typically lower than that of Cu^{2+} and showed a strong dependency on pH_i. The calculated results in Fig. 4.24a and 4.24c demonstrate that removal of Zn^{2+} at pH_i 5.50 (final pH: pH_f 6.92-9.57) proceeded at higher rates than the reactions at pH_i 2.50 (pH_f

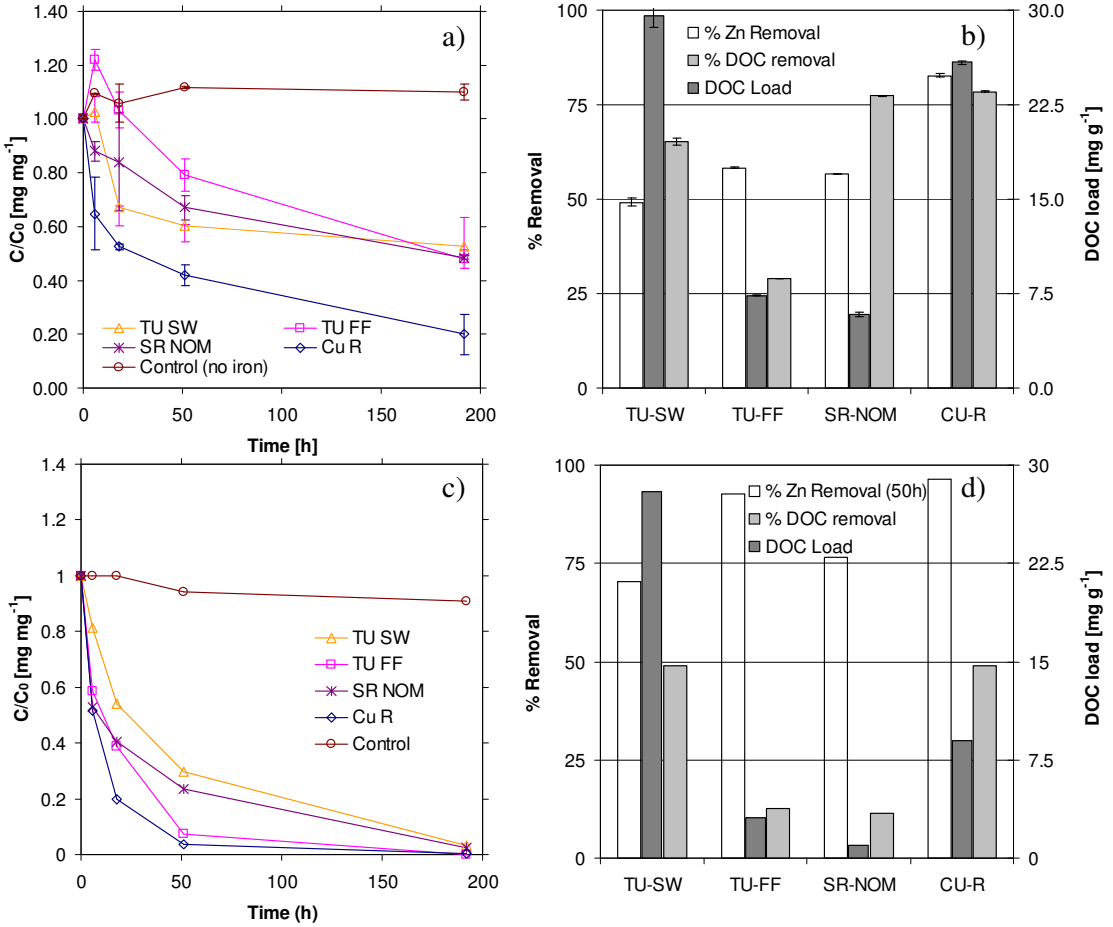

Fig. 4.24 a) and c) the kinetic removal of Zn^{2+} in TU-SW, TUFF, SR-NOM and Cu-R runoff solutions carried out in the batch test at initial pH_i 2.50 (Control: Fe^0 0 mg L^{-1}) (in order pH_f 4.54±0.13, 4.29±0.06, 4.26±0.03 and 4.61±0.04) and 5.50 (pH_f 6.92, 9.57, 9.29 and 7.95), respectively, and b) and d) a comparison of its corresponding DOC removal in correlation with removal of Zn^{2+} [Cu_i^{2+} 5.0 mg L^{-1}, Zn^{2+} 5.0 mg L^{-1}, 0.5 g Fe^0 L^{-1}, well mixed and at room temperature]

4.24-4.63) for all of the tested runoff solutions, having $t_{1/2}$ of 14.1-40.8 h and 87.7-267 h, respectively. The higher removal rates at elevated pH values could be explained by a larger number of iron oxides produced and their possession of negative surface charges that favor adsorption processes. The $t_{1/2}$ of zinc removal is comparable with the previous batch test ($t_{1/2}$ of 5.64-33.8 h). The final pH_f (pH_i 5.50) in this investigation ranged to much higher values, which can be attributed to a longer batch time and, thus, allowing rate-limiting reactions such as corrosion of iron to freely take place.

The depletion of NOM is dependent on the pH values, a higher pH is accompanied by a decreased removal of DOC for all runoff solutions (i.e., compared between pH_i 2.50 and 5.50 in Fig. 4.24 and 4.24d) indicating that adsorption is a relevant reaction. In the adsorption process of NOM, the surface-coordinated H_2O or OH^- groups on the hydroxylated iron oxide

surface (i.e., $FeOH_2^+$ and FeOH) dominate at low pH are replaced by anionic functional groups (e.g., caboxyl and hydroxyl group) of NOM (Gu et al., 1994; 1995). The hydrophobic organic acids generally possess higher affinity toward iron oxide surfaces and, due to this basis, greater amounts of NOM for TU-SW, CU-R and SR-NOM runoff solutions were removed than that of TU-FF runoff (Fig. 4.24b and 4.24d). In contrast to other runoff samples, TU-FF NOM is characterized by a hydrophilic characteristic with low aromaticity. It consists mainly of a smaller size range with low functional groups (see also in LC-OCD characterization).

4.3.3 Column study with NOM

A comparison between the breakthrough curves of copper and zinc obtained from the column experiments at varying organic content clearly shows the adverse effect of NOM on the removal processes (Fig. 4.25); a higher NOM generally results in lower metal removal efficiency. In deionised water, the outlet copper concentration gradually increases with bed volume treated and at the end of run efficiency was still at approx. 60%, whereas, a much steeper breakthrough was obtained for a solution with 5.90 mg NOM L^{-1}. An immediate breakthrough was even observed for a 26.2 mg NOM L^{-1} solution (average concentration) and yielded only 30% removal efficiency. As compared with copper, removal of zinc by the Fe^0 column appears significantly lower. This is due to the formation of adsorptive sites that are responsible for the removal of zinc (Rangsivek and Jekel, 2005). A rapid breakthrough of zinc with initial eluted concentration of c/c_0 = 0.3-0.5 followed by a much declining breakthrough shape can be attributed to a required lag time for the formation of adsorption sites by iron corrosion.

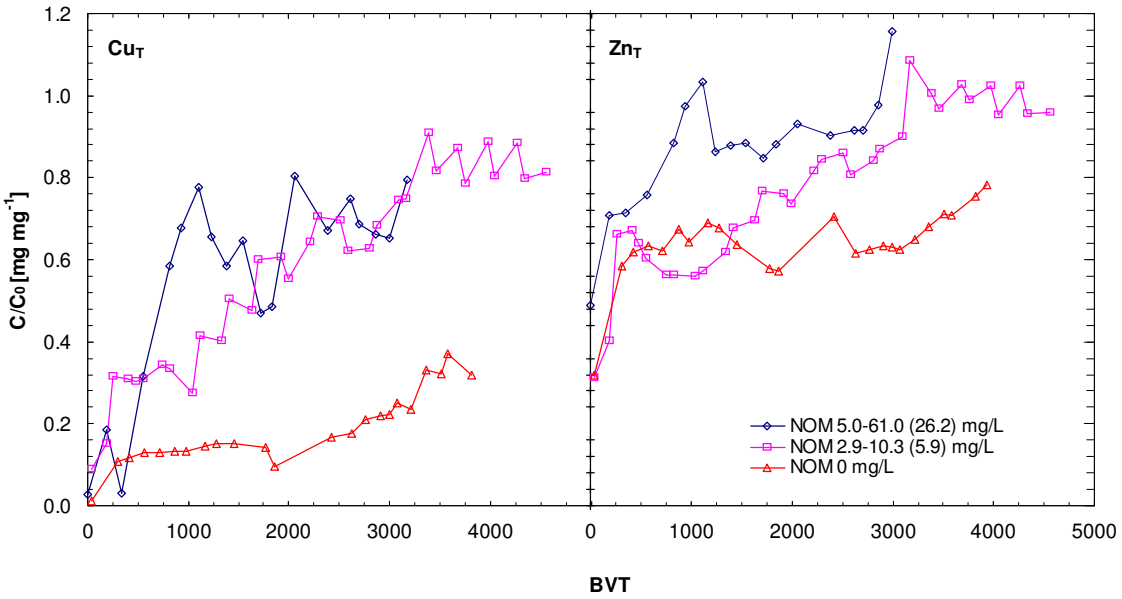

Fig. 4.25 A comparison of the breakthrough curves of copper and zinc obtained from the columns tested at varying NOM concentrations of TU Runoff [System: Cu_i^{2+} 5.0 mg L^{-1}, Zn_i^{2+} 5.0 mg L^{-1}, NOM 0 mg L^{-1} (pH_i 5.64 ± 0.38, pH_f 5.84±0.58), NOM 2.9-10.3 mg L^{-1} (pH_i 5.85 ± 0.59, pH_f 6.14±0.21) and NOM 5.0-61.0 mg L^{-1} (pH_i 5.69 ± 0.34, pH_f 6.0±0.62), 5 or 20 min EBCT, 10% particle Fe^0 (v/v) supported with pumice]

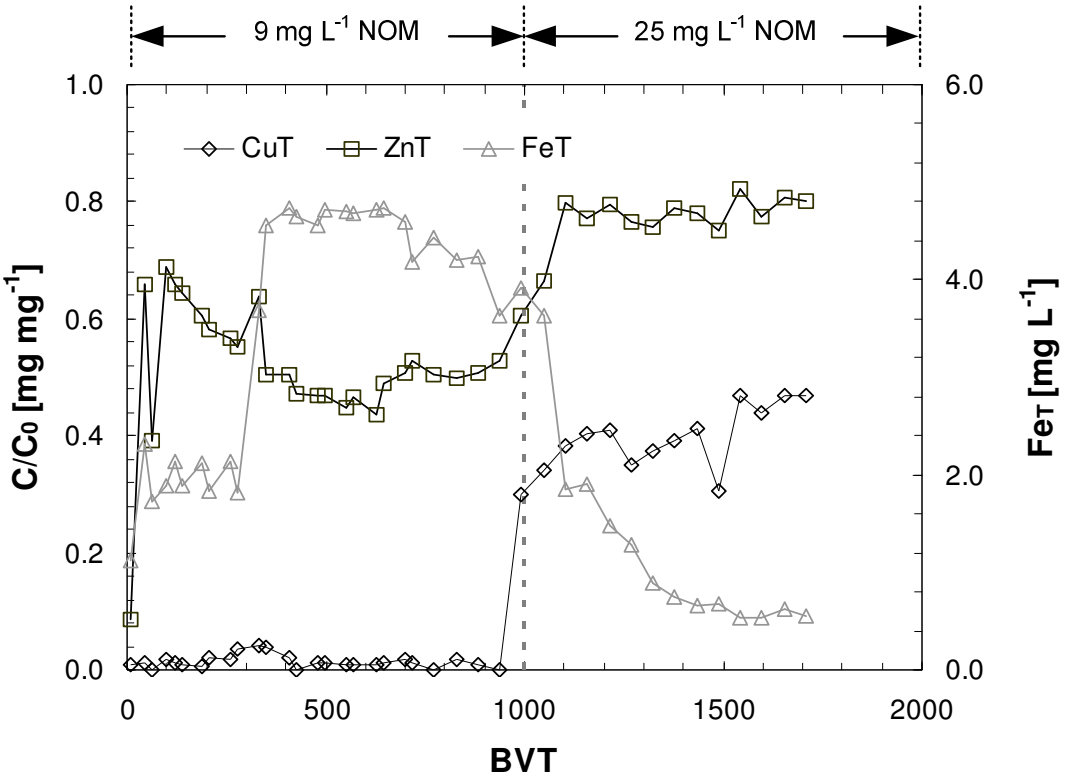

Fig.4.26 The concentration profiles of copper (c/c_0), zinc (c/c_0) and iron (total) from the breakthrough column that was continually fed with TU runoff having different NOM concentrations (~9 mg NOM L^{-1} before 1000 BV and with 25 mg NOM L^{-1} thereafter) [Cu_i^{2+} 5.0 mg L^{-1}, Zn_i^{2+} 5.0 mg L^{-1}, pH_i 5-6, 20 min EBCT, 10% particle Fe^0 (v/v) supported with pumice]

Depicted in Fig. 4.26 are the results of a flow-though column that was fed with TU runoff with different NOM concentrations during continuous operation; the first 1,000 bed volume (BV) was treated with ~9 mg NOM L^{-1} and was subsequently fed with 25 mg NOM L^{-1} runoff solution. The retention time of the runoff in the column was set to 20 min in order to facilitate the examination and also to investigate the effect of EBCT. In Fig. 4.26, approximately 100% and 55% removal of copper and zinc were achieved, respectively. The iron concentration – which rationally indicates the activities of iron corrosion - was in a range of 2 mg L^{-1} and then increased to 5 mg L^{-1} suggesting a more extensive corrosion of iron (at 0-1,000 BV). After the fed solution was substituted, both metals were substantially eluted out of the column occurring in concomitance with the reduced concentration of iron.

4.3.4 Impact of NOM on copper and zinc removal in ZVIB

The impact of NOM on metal removal in the Fe^0 system were elucidated based on the correlation of the depletion loads of DOC and the removal profile of heavy metals under different conditions. In the batch test carried out at pH_i 2.50, the removal load of NOM (Fig. 4.24b) is accompanied by the removal of zinc, ranging in order of SR-NOM (~57% Zn removal, DOC load 5.9 mg g^{-1}), TU-FF (58%, 7.4) and Cu-R (83%, 25.9), respectively. At

this low pH (pH_i 2.50 to pH_f 4.24-4.63), the adsorption affinity of metals would have been very low due to a repulsive force between positively charged iron oxide surfaces and cations (pH_{PZC} 7.2). The equilibrium calculation using MINEQL$^+$ (condition: 2-Layer model using Hydrous Ferric Oxides 300 m^2 L^{-1}, 20°C, pH 3.0–9.0) shows that no zinc could be removed at any pH below 5.0. Rodda et al. (1993) also reported that zinc removal is insignificant at pH lower than 6.0 with 0.20 g L^{-1} goethite. In addition, Crawford et al. (1993) observed that the co-precipitation and adsorption of Zn^{2+} on iron oxides followed the same lines and were insignificant at pH below 5. Therefore, one possible reason for such high removal of Zn^{2+} might have been due to the previously adsorbed runoff NOM on the iron oxides surface. Because of its permanently negative charge at all considered pH conditions, the adsorbed NOM fraction can modify the electrochemical properties of the underlying surface layer (Tombácz et al., 2004).

There is also evidence showing that metals may be complexed during batch reaction. In Fig. 4.24a, the kinetics of Zn^{2+} removal in TU-SW (pH_i 2.5) showed a decreasing rate over time (during 50-192 h) as compared with other runoffs indicating an inhibition occurs. Although, a significant removal of DOC took place in TU-SW runoff, still 21 mg DOC L^{-1} remained non-absorbable, which might form complexes with the metals preventing Zn^{2+} from being adsorbed. In support of this, Dries et al. (2005) reported the formation of metal complexes contributing to the 2.8 times reduction of Zn^{2+} removal rates in a Humic Acid (HA)-Fe^0 containing batch system (HA 20.0 mg DOC L^{-1}, 5.0 mg L^{-1} Zn and Fe^0 6 g L^{-1}.). Cheng and Allen (2006) studied the binding characteristics of NOM from three surface waters and reported that the Zinc-NOM complexes do not depend on the origin of surface waters. At pH 6, ionic strength 0.02 M and 10.0 mg L^{-1} DOC, the same authors reported a total ligand concentration of about 2.18 mmol g^{-1} carbon. If this value is used to calculate the total DOC concentration of 36 mg L^{-1} (TU-SW) assuming a stoichiometry of complexation of 1:1 (NOM:Zinc), ~2.60 mg L^{-1} Zn^{2+} would be complexed in TU-SW runoff, which is comparable to the remaining zinc concentration of ~2.18 mg L^{-1} after 192 h in the batch test. Alternatively, because complexation ability exists between different metals and Fe^{2+} has the highest affinity toward NOM as compared with Cu^{2+} and Zn^{2+}, it is more likely that a significant portion of Fe^{2+} forms complexes with NOM especially at high NOM concentration. This results in a lower Fe^{2+} oxidation rate, which subsequently hinders the overall treatment rate of the Fe^0 system, as also discussed in a previous study (Rangsivek and Jekel, 2005).

The complete removal of Zn^{2+} was obtained in pH_i 5.50 solutions (Fig. 4.24c). The results of 50 h were plotted in relation to their NOM removal profiles, which are TU-SW (~70% Zinc removal, NOM load per iron dosed 28.0 mg g^{-1} Fe^0, pH_f 6.92), SR-NOM (77%, 1.0, 9.29), TU-FF (93%, 3.1, 9.57) and Cu-R (97%, 9.0, 7.95), respectively. Zn^{2+} was removed in TU-SW less than other runoffs, possibly attributed to the pH_f, which was maintained below pH_{PZC}. At this $pH<pH_{PZC}$ condition, both ternary complex reaction and competitive adsorption are taking place. For other runoff solutions in which the pH_f values were above pH_{PZC}, both Zn^{2+} and NOMs were removed concomitantly indicating an adsorption process.

Zn^{2+} is, however, more prone to be adsorbed due to its preference toward the surface of iron corrosion products at alkaline pH. In addition, a complete removal of metals indicates an undersaturated condition exists in term of adsorption site for the adsorption of metals.

Beside other effects, the impact of NOM on the removal processes is the rise of metal solubility that prevents metals and iron from precipitating as solids, i.e., as metal and iron hydroxides, respectively. According to a calculation using MINEQL$^+$, the solubilities for copper and zinc equilibrium with hydroxide-carbonate system are about 15-50 µg L^{-1} in the pH range of 8-9 and 0.5-3.0 mg L^{-1} at pH 9-11, respectively. The lowest solubility of iron hydroxides is about 0.03 µg L^{-1} at pH 8-9 (Ludwig, 2007). At concentrations up to 0.5-2 mg L^{-1} DOC, the solubility of copper may increase up to 0.92-1 mg L^{-1} in the equilibrium with malachite (Merkel, 2002). A much more significant increase in the solubility of copper and zinc is anticipated in these high NOM containing runoffs employed in the present work. Furthermore, the removal of metals mostly takes place at the initial phase, whereas, the non-adsorbed concentrations of metals remaining in the solutions stay well below undersaturated values. For this reason, the precipitation reaction of a metal solid as a result of an increase of pH can be excluded.

The above depicted results of the column test demonstrate a lower iron concentration released in concomitance with a higher amount of metals eluting out of the Fe^0 barrier at an increasing NOM concentration of fed solution (Fig. 4.26). It was also observed that about a 20% total concentration of DOC was removed during the Fe^0 reaction at each bed volume treated. Hence, the decreased metal removal might have come about due to the fact that the adsorbed NOM had blocked the reactive surface sites of iron, which also likely competes for adsorptive sites with metals. In the study of Dries et al. (2005), a load of 4.5 mg HA g^{-1} Fe^0 was found not to interfere with the reactivity of Fe^0 toward contaminants (in deoxygenated water with much higher EBCT). Specht et al. (2000) observed an insignificant influence of 5.0 mg NOM g^{-1} for clay at pH 5.0. In contrast, Tipping and Cooke (1982) reported that adsorbed humic substances had a considerable effect on the electrophoretic mobility of goethite (40 mg g^{-1} at pH 7.0).

Another process possibly involved in the metal removal under the column experiment is metal-NOM complexation. The dominant reaction is difficult to distinguish because of the complex processes involved. However, if metal-complexation is considered to be significant, an increasing amount of iron should have been observed at the outlet as an indication of metal binding with NOM. This argument is only possible when the iron corrosion rate is noticeably high (i.e., iron concentration at the outlet is high) and the aforementioned pathway (NOM surface blockage of iron corrosion) is insignificant. For all these reasons and because of a relatively fast contact time in the column test and low operational pH_{inlet} of around ~5-6 (pH_{outlet} is about 0.2-0.3 unit higher), it can be anticipated that there is a low involvement of complexation of metals occurring in the Fe^0 system under the flow-through configuration.

4.3.5 NOM analyses by LC-OCD

The LC-OCD chromatograms of TU-SW and TU-FF bulk NOM show that larger molecular weight compounds, specifically humic substances were preferentially removed during the reaction with Fe^0. This also corresponds to the UVD diagram demonstrating a favoring of UV-absorbing fraction, e.g., aromatic moieties, being removed. The NOM of TU-FF runoff decreased only to a small extent and the NOM fraction that was removed is located in a larger size range. Gu et al. (1995) found the larger size hydrophobic fractions of NOM were preferentially adsorbed on iron oxide surfaces over smaller size hydrophilic fractions. Genz et al. (2005) reported that smaller and medium size fulvic acids are removed faster than other low molecular weight fractions because of a higher diffusion rate. A ligand-exchange mechanism between organic functional groups of humic substances and hydroxyl on iron oxides surfaces governs the reactions of NOM adsorption (Gu et al., 1995). Further elucidation of the adsorption behavior of organic compounds in the Fe^0 system was evaluated based on the hydrophobic characteristics of NOM. In the TU-SW and TU-FF samples, when the molecules are large, a non-humic fraction (XAD-8 effluent) is removed in approximately the same degree as the hydrophobic fraction (XAD-8 isolate) (Fig. 4.27). The highly hydrophobic NOM from Suwannee River exhibited almost a complete removal, whereas Cu-R showed a similar result to that of TU-SW. In contrast to these results, the TU-FF NOM was merely adsorbed. It mostly contains smaller molecular weight fractions of hydrophilic and transphilic substances. These findings in overall showed that the steric arrangement of carboxyl and hydroxyl functional groups play a greater role for the adsorption of NOM on iron oxide surfaces than by chemical interactions between adsorbent surface groups and NOM moieties. Furthermore, it was shown that the main fraction that was involved in the removal of metals in Fe^0 the system is a larger size hydrophobic fraction.

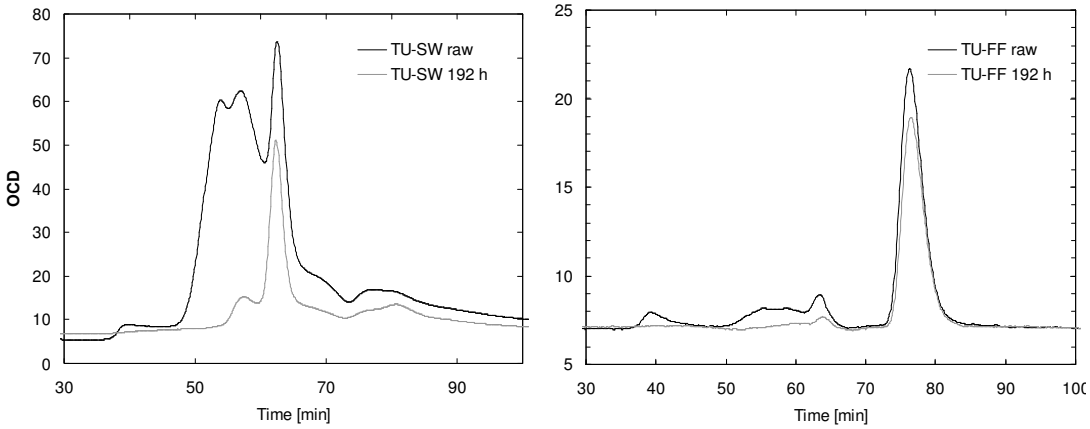

Fig. 4.27 LC-OCD diagrams of TU-SW and TU-FF measured for the raw samples and the samples at end of batch experiment

4.3.6 Conclusion

With an aim at better understanding the interaction of runoff NOM and the removal of metals in the Fe^0 system, the present section employed extensive techniques for characterizing the runoff-originated NOM samples. The results of characterization were subsequently used for describing and explaining the removal of Cu^{2+} and Zn^{2+} at varying conditions during the batch and flow-through systems. The following conclusions demonstrate the significant findings of this study;

(i) It was shown that the characteristic of roof runoff from the same roof can be significantly different. The concentration of NOM is significantly higher in the summer period as compared to the winter samples. In general, NOM in roof runoff resembles natural waters comprised mainly of humic substances with a relatively high aromaticity. This fraction of NOM is the main compound that is actively involved in the removal of metals in the Fe^0 system. In contrast to this fraction of NOM, lower molecular weight and neutral NOM fractions may only influence metal removal to a small extent.

(ii) The impact of NOM depends on the species of metal and the experimental conditions being employed. In the batch investigation, NOM caused a minimal impact on the removal of Cu^{2+}, but either enhanced or inhibited the removal of Zn^{2+} within the Fe^0 system. For the batch treatment of runoff at acidic conditions, the adsorption of metals increased by a ternary complex mechanism of NOM, metals and iron oxides. In some of the runoff solutions, it was also evident that NOM complexation prevented metals from being adsorbed on the iron oxide surface. However, under a typical runoff condition (i.e., at pH ~5.5), the main mechanism responsible for removal of Zn^{2+} and NOM is adsorption/co-precipitation, in which a competitive adsorption between these two compounds exists. Whether competitive adsorption or metal-NOM complexation is dominated at a specific condition depends largely on the experimental pH. However, there is no clear distinction of these processes observed in this study.

(iii) In the flow-through experiment, the breakthrough curves of Cu^{2+} and Zn^{2+} are significantly influenced by the NOM concentration in water. The treatment efficiency can be terminated under the presence of a relatively low NOM concentration, i.e., 5 mg NOM L^{-1}. This reduction in the removal of metal was presumably due to blockage of reactive iron surfaces by the adsorbed NOM that also compete for adsorption sites. In contrast to the batch test, the impact of metal-NOM complexes is considered insignificant under the conditions studied.

(iv) NOM concentration is extremely high during summer and low during winter-time. Nevertheless, this does not mean that the treatment of metal-contaminated runoffs by Fe^0 will be worse in the summer. In fact, the frequency and amount of rainfall has to be taken into account. A relatively small volume of the runoff in the summer makes the processes easier to manage, e.g., by increasing the EBCT of the treatment column. It is also noteworthy that the

NOM-metal complex can reduce the potential impact of bioaccumulation and, thus, the non-treatable fraction of contaminated water may not contribute to toxicity. Nevertheless, a repeated exposure of the Fe^0 system by NOM may deteriorate the performance of the barrier in the long run. During winter, the reactivity of Fe^0 and the treatment efficiency toward metals can be greatly hindered by temperature. Even though NOM concentration is relatively low, a constant releasing of metals from metal roofs generally coincides with the large volume of runoff water making the process problematic.

4.4. Column experiments with ZVI and carbonatic materials

Results from previous chapter show that the Fe^0/pumice barrier can barely cope with efficient treatment of the metal-contaminated runoff within the desirable short time frame. Furthermore, the Fe^0 barrier often failed during the long term operation due to a high potential of clogging. In this part, the optimization of the processes is investigated employing various carbonatic materials. They were tested using different configurations. It is aimed to enhance the chemical precipitation of metals and iron oxides, while still offer sufficient hydraulic loading permeability.

4.4.1 Optimization of the ZVIB using carbonatic materials

Composited carbonate/Fe^0 column (experiment. Col. 2)
A serie of experiments performed at TU and UDK roof sites clearly showed that the Fe^0/carbonate columns significantly enhance zinc removal efficiency as compared with the Fe^0 columns (Fig. 4.28 and 4.29). During the first rain events at the UDK site (less than 50 BVT), zinc was merely eluted out of the Mag/Fe^0 and DML/Fe^0 columns. The Fe^0/PM column exhibited a slower kinetic and the control pumice column achieved a total 40-50% metal removal the. The DML/Fe^0 and Mag/Fe^0 have a comparable treatment rate to zinc for the first 10-15 cm but the latter exhibited a higher performance for the rest of the column. In comparing the two sites, the removal performance of zinc was higher at the TU site, which was likely due to a higher concentration of zinc that favored the removal processes. In addition, a competitive adsorption effect of copper and zinc may be involved for the UDK runoff. In contrast to zinc, the highest removal for copper was attained in the Fe^0 column, followed by DML/Fe^0 and Mag/Fe^0, respectively. This support the previous conclusion that reductive transformation is the major removal pathway for copper rather than an adsorption and co-precipitation, or chemical precipitation processes.

In the second measurement, the carbonate incorporated column at the UDK site experienced clogging as well as preferential flow. This was found to a lesser extent for the pumice and the Fe^0 columns. Visual inspection revealed that the clogging of the infiltration layer occurred predominantly at the inlet end of the columns and was likely caused by particulates in runoff waters. In addition, the clogging may have also been caused by the accumulation of various hydroxide and carbonate precipitates within the treatment barrier. As a result of flow reduction, the removal profiles of metals in the composited columns performed onsite were only obtained at the TU site. For the second rain event at TU site (approx. at 400 BVT), the eluted concentration of 0.5 mg L^{-1} from the Fe^0 column and breakthrough of the pumice column were already observed. The observed low performance of Fe^0 likely reflected a formation state of iron oxides. It was also likely due to a pH lower than pH_{PZC} that did not favor the adsorption process. In contrast, the Mag/Fe^0 exhibited a complete removal of zinc while the DML/Fe^0 showed a slightly increasing concentration front with about 0.1 mg L^{-1} zinc is the eluted concentration (Fig. 4.29).

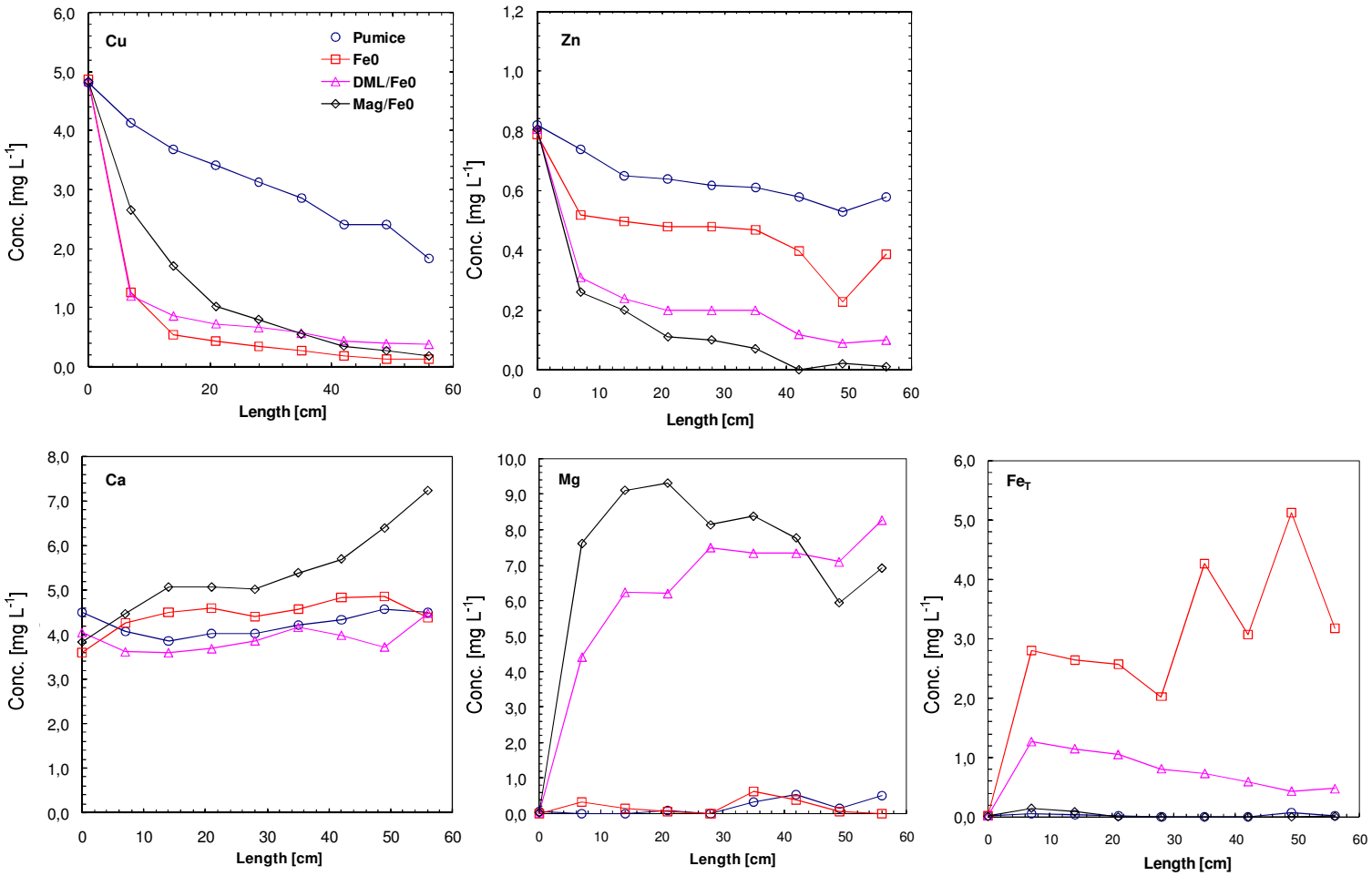

Fig. 4.28 Metal removal profiles from composited columns tested at UDK site during the first and second rain events. The columns received runoffs from a copper roof in the downflow mode (during the measurement, the average flow was 60 mL min^{-1})

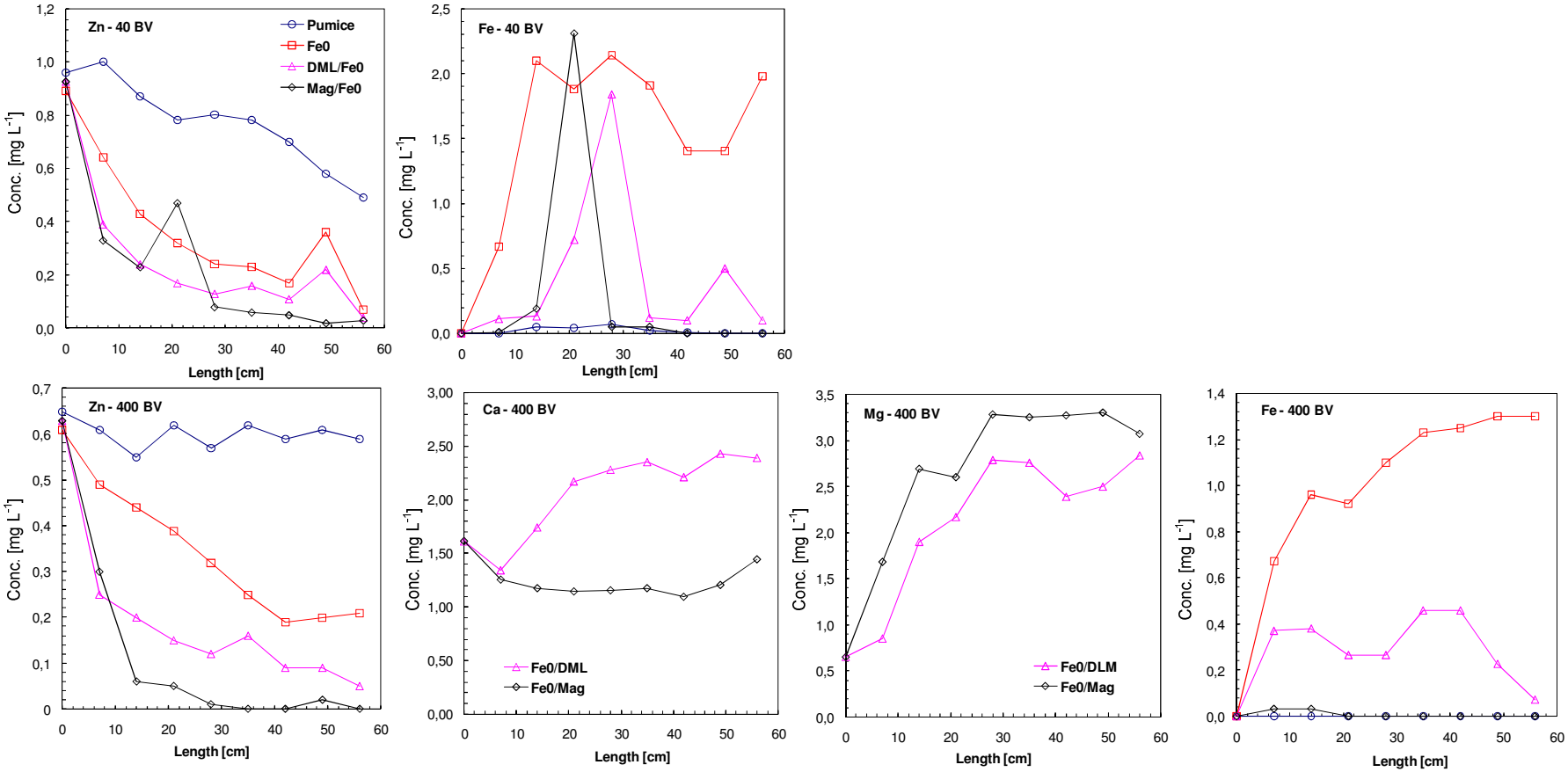

Fig. 4.29 Metal removal profiles from composited columns tested at TU site during the first and second rain events. The columns received runoffs from a bitumen roof with a zinc gutter in the downflow mode (during the measurement, the average flow was 60 mL min^{-1})

The rest of the 4 month investigation of composited columns shows a significant loss of flow permeability and finally ended at about 90% flow reduction. With the low flow rate and initial copper and zinc concentrations on average of 5.36 mg L^{-1} and 2.30 mg L^{-1} the observed total metal concentrations of the effluents were 0.035 and 0.47 mg L^{-1} for dolomite and 0.025 and 0.07 mg L^{-1} for magnesite composited columns, respectively (Fig B14). This accounts to 89-99% removal efficiency.

The incorporation of carbonate bearing materials into a Fe^0 treatment barrier is by principal to precipitate more dissolved metals into insoluble solids as well as to favor adsorption at an alkaline pH via the addition of CO_3^{2-}, HCO_3^-, OH^-, Ca^{2+} and Mg^{2+}. Based on the results of the composit columns, approximately 4-7 mg L^{-1} Ca^{2+} and 7-9 mg L^{-1} Mg^{2+} were observed for the first rain event and about two times lower for the second rain event (data from two sites were used for comparison). As a consequence, the outlet pHs were usefully maintained at 8-11 which also results in an extensive deposition of greenish precipitates, supposely Malachite, within the treatment columns of magnesite and DML. An extensive precipitation of iron oxides was apparent in the DML/Fe^0 and Fe^0 columns, whereas this was not observed in the Mag/Fe^0 column. Moreover, the concentration of iron along the Mag/Fe^0 column was minimal suggesting that Mg^{2+} may have inhibited the corrosion process of iron. It is therefore, reasonable to conclude that the removal of metals in Mag/Fe^0 was solely caused by the precipitation processes.

Sequential carbonate/Fe^0 columns (experiment. Col. 3)
A higher metal removal was generally observed for sequential carbonate/Fe^0 columns as compared with the Fe^0 column (Fig. 4.30). Nevertheless, this also brought about a high clogging potential similar to the composite configuration. In the Mag-Fe^0 columns, clogging and preferential flow was evident after a few BVT. This was observed when a greenish solid was increasingly precipitated within the column. The flow rate of the experiment was, therefore, adjusted to 30% of the initial value. Corresponding to this, the effluent pH of Mag-Fe^0 could be maintained at 8.1-11.1 and a complete removal of metals could be obtained throughout the run (Fig. 4.30e). There was also no iron precipitates within the following Fe^0 column, supporting the previous assumption that Mg^{2+} can inhibit the iron corrosion process. Nevertheless, the results showed that column containing only Mag can effectively treat metal from roof runoff. In comparison to the Mag-Fe^0 column, the effluent of the DML column was shifted to about 9.5-10.7 with complete removal of metals observed only up to 342 BV. After that DML gradually become inactive and the effluent concentration of metals increased. Due to severe clogging within the Fe^0 column, the DML-Fe^0 column was terminated at 1,500 BVT. In other columns, the calcite-Fe^0 did not seem to clog the column but it was possible to increase the pH up to 10.4 for only few BVs (Fig. 4.30b). A greenish color developed on the surface of $CaCO_3$ that might lower the effectiveness of the media in increasing pH. The DMS is considered inactive as there was no enhancement in term of pH buffering and removal of metals. After about 2,000 BVT, the DMS was replaced by DML, and a better removal of metals could be observed (Fig. 4.30c).

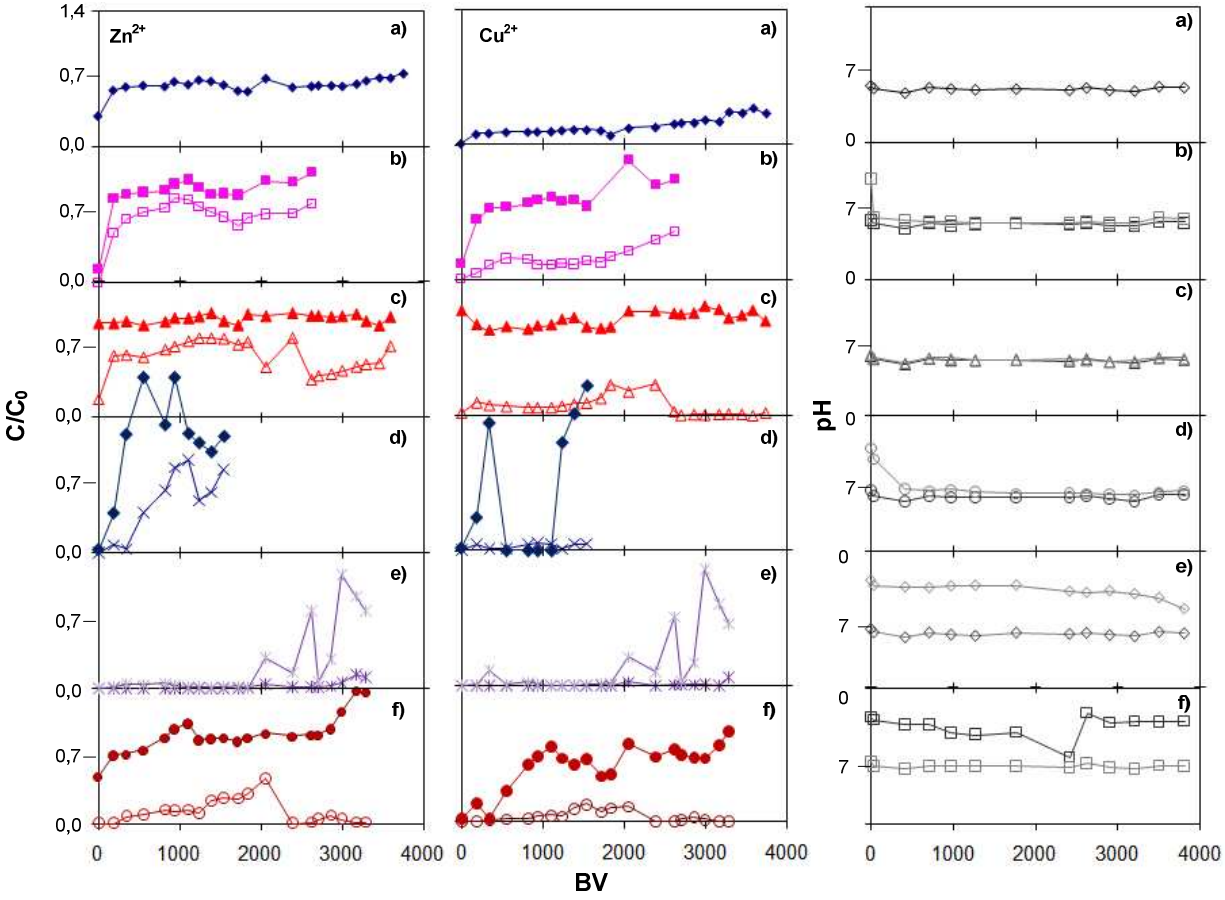

Fig. 4.30 Breakthrough curves of copper and zinc with corresponding pH measurement from sequential columns of Fe^0/carbonatic materials; (a) controlled Fe^0 column; (b) calcite-Fe^0 column; (c) DMS-Fe^0 column; (d) DML-Fe^0 column; (e) Magnesite-Fe^0 columns; and (f) Fe^0-DML column. The first line (above) represents output conc. of first column and the second line (below): output conc. of second column. pHs are in reverse order of conc. profile.

According to the results of the tested columns, it is evident that the major factor determining the life span and overall efficiency of carbonatic-Fe^0 treatment barriers is the hydraulic conductivity. Although, the increase of pH induced by the carbonate materials favor a higher treatment rate of metals, this also resulted in a high potential for plugging and preferential flow that brought about failure of the barrier. For this reason, another configuration of Fe^0 incorporated carbonatic materials, in which a sequential configuration of an Fe^0 column followed by a filter bed containing dolomite/pumice column was examined. In this setup, the system relies on the production of dissolved iron in the first Fe^0 column. The dissolved iron and metals that passed through the first column will subsequently be transformed into iron oxides in the second column of the filter bed. The incorporation of DML in the post filter bed aimed to precipitate all the metals including Fe^{2+} that may be persistent due to complexation with NOM in runoff waters (Rangsivek and Jekel, 2005; 2008). Figure 4.30f shows that the removal efficiency of copper and zinc in Fe^0-DML/PM columns were 80-100% and 50-100%, respectively. There was no significant clogging potential for up to

2,000 BV. For this configuration, the pH of the filter bed could be maintained at 9.5-11. Its buffering capacity gradually decreased when higher red oxides deposits were observed in the filter column in concomitant with the reduction in the flow rate of the filter bed. The pH at which the removal of metals become deficient was about 6.87-9.47 which occurred at BVT ~2,000, the DML/PM media were taken out and washed before reloading into the system. As a result, a complete removal of metals and a high hydraulic loading rate could be re-attained suggesting that through backwashing, the system offers maintenance of the bed.

4.4.2 Processes of metal removal in ZVI/carbonatic barrier

Based on the results of composited and sequential column tests, it could be seen that removal of metals depended strongly on the solution's pH suggesting complex processes of chemical precipitation, adsorption and co-precipitation were involved. In order to assess the role of chemical precipitation, the chemical equilibrium prediction using MINEQL$^+$ (Fig. 4.31) were employed to elucidate the composition of solid precipitates in rational to SEM and EDX analysis (Fig. 4.32).

In the composited column, the treatment media showed a visual mixture of various solid precipitates, e.g., having reddish iron oxides, greenish and brownish colors. These phases were generally fragilely deposited on the surface and pore of the pumice media. Using SEM to examine the precipitates, nodular shaped solids formed tightly and distributed uniformly over the reactive surfaces were observed (e.g., Fig. 4.32 of $CaCO_3$-Fe^0 and DML-Fe^0). Employing EDX, the reflection could be assigned to phases of copper, zinc, Mg and Ca. The metal phases usually co-exist with Ca and Mg, which are assumed to be a result of chemical precipitation at an increasing pH. Results of chemical equilibrium calculation support this assumption, in which precipitates that have a potential to precipitate were predicted as mixtures of azurite, malachite, $CuCO_3$, tenorite, $Cu(OH)_2$, ZnO, Zincite, $Zn(OH)_2$ and $ZnCO_3$ (Fig. 4.31a). Other than these phases, $Mg(OH)_2$ and Siderite ($FeCO_3$) may have also been generated. In the case of the Fe^0-DML sequential columns, the separate sample of Fe^0 columns (i.e., control column of Fe^0 with no influence of carbonate) was covered by a reddish-yellow layer. Examination of media from the Fe^0 column reveals a nodular shape growth with a strong spectrum of a copper phase. Zinc was also found to constitute at a typical iron surface.

Further examination of the role of chemical precipitation was performed by means of plotting of the effluent concentrations of Fe^0, Mag/Fe^0 and DML/Fe^0 column tests against the solubility of metal hydroxide and carbonates such as malachite and smithsonite. The equilibrium model shows that super saturation exists for all the Fe^0 integrated carbonatic columns and the observed effluent concentration of metals agree well with the solubility of metal hydroxide and carbonate (Fig. 4.31b). Based on the results, the observed effluent concentration of metals agreed well with the solubility concentrations of copper hydroxide and malachite, which are approximately 15-50 µg L^{-1} at the pH range between 8 and 9 and at 0.5-3.0 mg L^{-1} for zinc-hydroxides and smithsonite ($ZnCO_3$(s)) at pH 9-11 (Ludwig, 2007).

Hidmi and Edwards (1999) reported a solubility of copper at 0.12 -0.043 mg L^{-1}. The observed metal concentrations significantly below the solubility at pH 5-7 were likely due to the adsorption and co-precipitation processes. In this examination, the results of copper and zinc concentrations from the field experiment illustrated in Fig. 4.33 were employed.

Besides metal hydroxides and carbonates, the equilibrium model also predicted that various phases for voluminous precipitation of iron oxides would occur within the column test. The oxides phases were assigned to lepicocrocite, maghemite, goethite, hematite and ferrihydrite. Results of a model prediction correspond well with the XRD analysis performed in the batch and columns tests previously shown in section 4.1 and 4.2. On the contrary, the solubility of

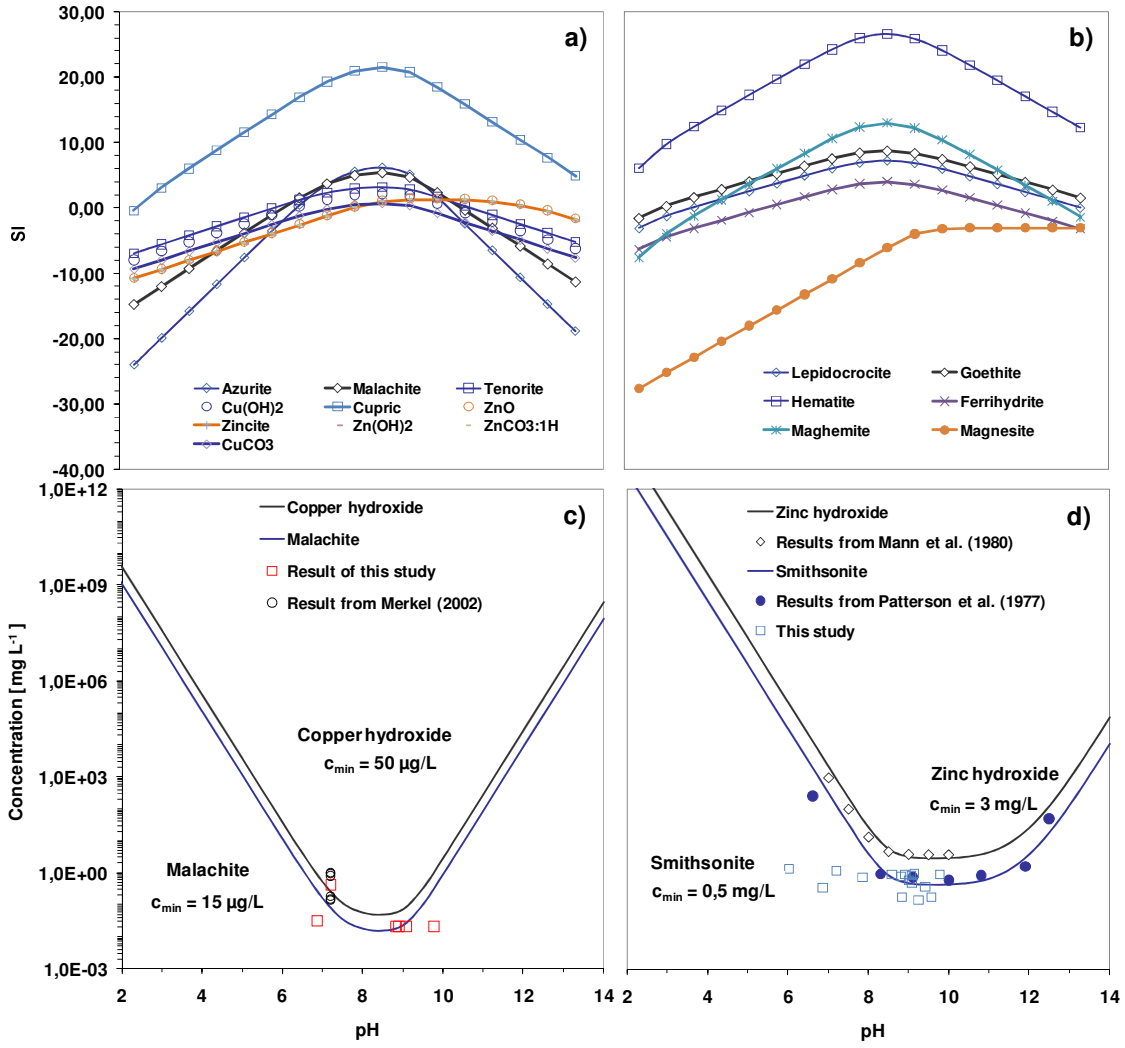

Fig. 4.31 a) and b) Illustration of saturation indexes of relevant minerals related to the Fe^0 treatment barrier of copper, zinc and iron oxides, respectively, c) and d) Plots of effluent metal concentrations obtained from this work in equilibrium with metal hydroxides (the shown data were complied by Ludwig, 2007)

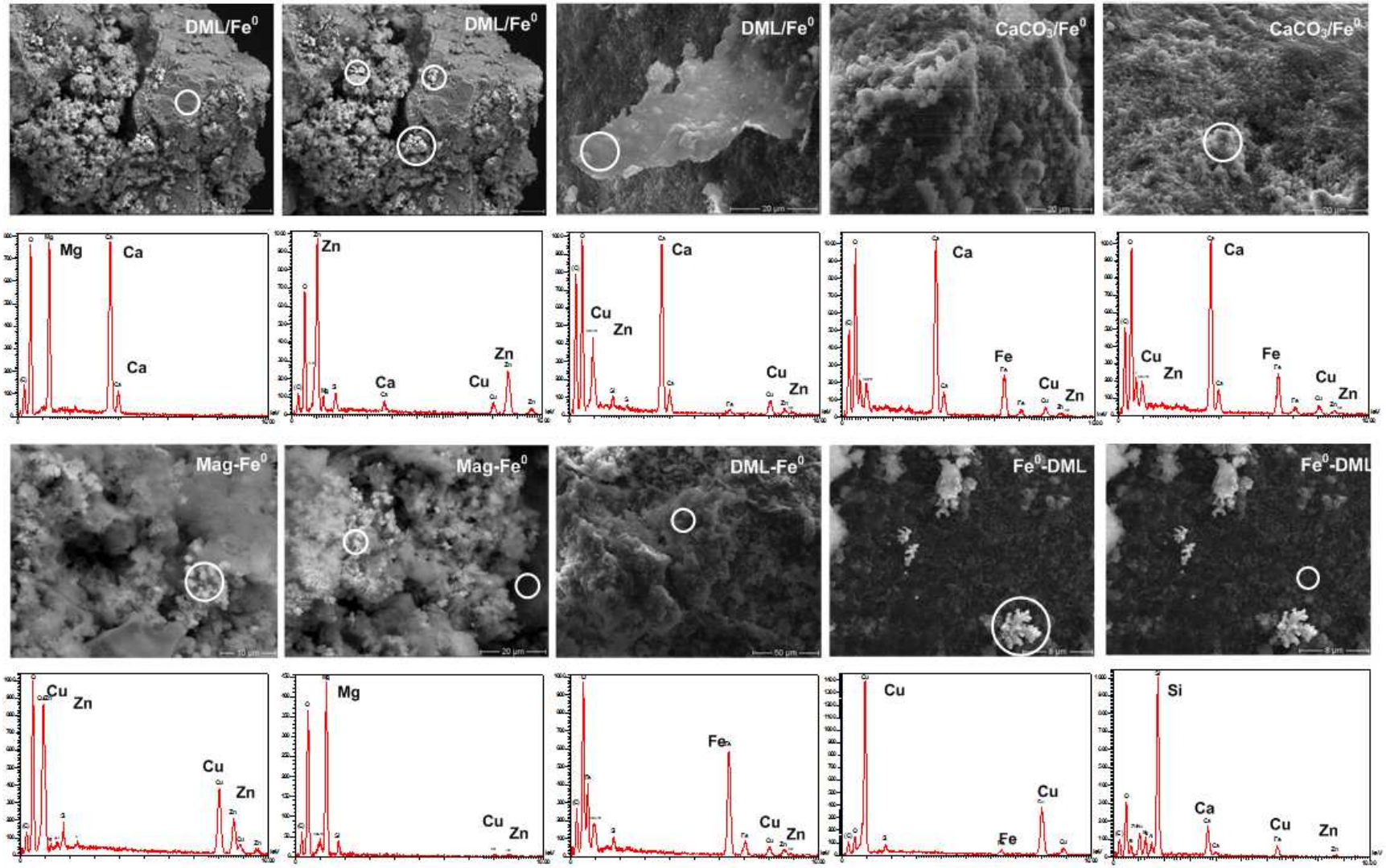

Fig. 4.32 SEM and EDX mapping of solid precipitation obtained from selected composited and sequential column tests

magnetite was well below one and, thus, not precipitated under the stromwater runoff conditions. It is well known that magnetite is only formed in deoxygenated conditions (Cornell and Schwertmann, 1996). Due to a presence of these iron phases, it is suggested that adsorption and co-precipitation process could not be ruled out and the performance of the Fe^0/carbonatic barriers was likely involved through a combined processes of adsorption/co-precipitation and chemical precipitation.

4.4.3 Implication of ZVI/carbonatic barrier

Based on the results of laboratory and field experiments, it was evident that the column with carbonatic materials exhibited a higher performance than the column filled only with Fe^0. Among media investigated, Mag possesses the highest removal rate of metals where metals

Table 4.5 Water quality of the influent to Fe^0-aeration-DML/PM system

Rainfall data	Paramter	Zn [mg L^{-1}]	Cu [mg L^{-1}]	NOM [mg L^{-1}]
1. cycle	Zn (natural runoff)	2	0-5	3
2. cycle	Zn/Cu	5	5	3
3. cycle	Zn/Cu	5	5	3
4. cycle	Zn/Cu/NOM	5	5	20

*There were some losses of metals through adsorption to particles in the storage tanks

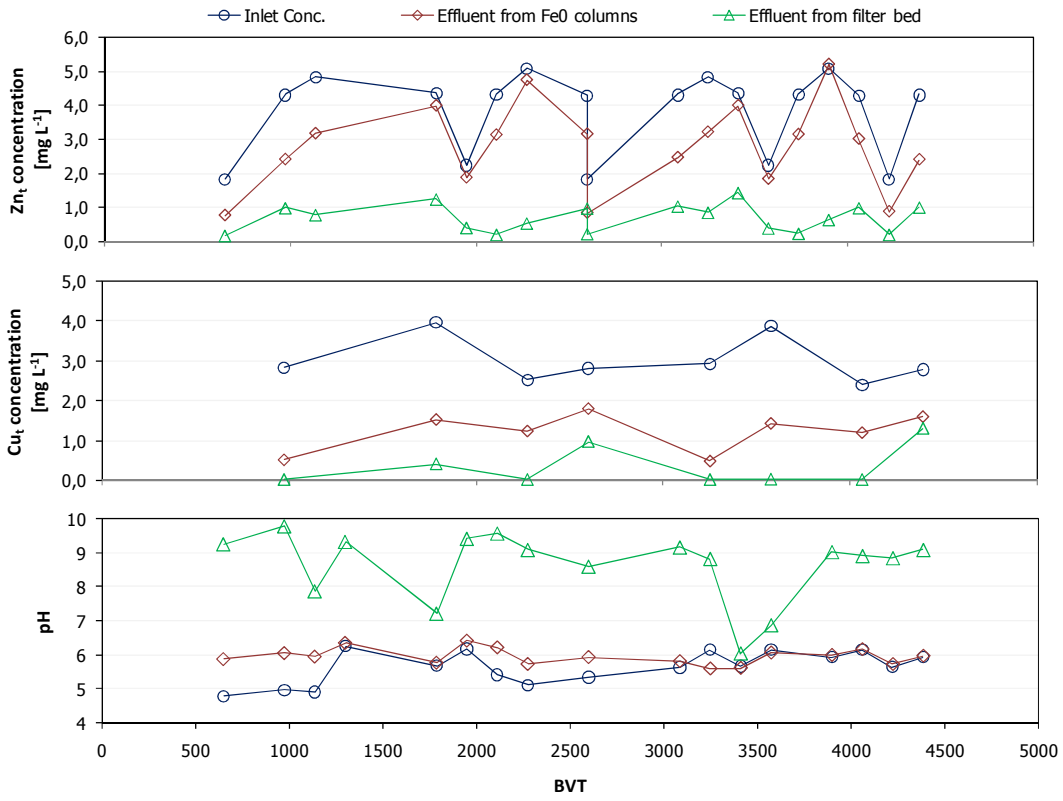

Fig. 4.33 Results of the implication of the optimized Fe^0/carbonatic barrier (Ex. Col. 4)

are immobilized purely by chemical precipitation process. Thus, when applying Mag in the field, the following ZVIB may not be necessary however post sand filtration is required to filter all metals carrying particles. The highest removal rate of Mag has a drawback due to its greatest potentials for permeability losses and preferential flow of the treatment barrier. The low hydraulic loading rate is preferentially required for actual operation. Alternative to Mag, DML may be considered more suitable for stormwater runoff treatment due to its low cost. The lower performance of the media can be justified by its ability to treat water at a higher flow rate with less difficulty.

For further assessment of the Fe^0-carbonatic barrier, a new configuration of Fe^0/carbonatic barrier was established based on the results of column tests. This treatment system consisted of spiral irons in the first column (without pumice or sand), followed by aeration and a fixed-bed system containing pumice and dolomite (or other carbonatic materials such as magnesite). The spiral iron was used in the treatment process in order to increase void area within ZVIB as it was found that building up of iron oxides inhibits the processes of metal removal. The system principally relies on the production of dissolved iron in the Fe^0 column. The iron is subsequently transformed into iron oxides within the Fe^0 column or at the later treatment steps. The aeration and post filter bed help in facilitating the oxidization rate of dissolved iron. In this case, the metals are immobilized by means of a combined process of adsorption/co-precipitation and precipitation with carbonate bearing materials while still maintaining the reactivity of the iron column. The treatment barrier was installed onsite receiving natural runoff from TU roof. Furthermore, the system was tested under natural runoff and at fluctuating runoff quality where copper, zinc and NOM were added artificially. The NOM soluion was originated from decomposition of reefs in the runoff water. The parameters investigated are demonstrated in Table 4.5.

About 60-100 % of metal concentrations could be removed at EBCT of 5 min and about 30-80% was achieved with 1 min EBCT in the ZVI/DML/PM barrier (ZVICB) (Fig. 4.33 and Table B32). For this setup, there was also less effect of source variations of waters on the treatment ability of metals. Noteworthy is that the presence of NOM in roof runoffs did not influence the reaction rate of ZVICB as was found to be significant for Fe^0 column alone. This could be due to an enhanced precipitation of metals and iron oxides by the DML filter media. When closely examining the system, a larger part of copper was found to be removed during Fe^0 passage whereby the removal of zinc mostly takes place during DML/pumice filter bed. Overall, the outlet metal concentration in the runoff after passing through a DML/pumice filter bed was kept below 1 mg L^{-1} for over 4,000 bed volumes.

Major drawbacks of the ZVICB are iron oxide-passivation of dolomite media that reduces the rate of carbonate dissolution, productivity of alkalinity as well as clogging from iron oxyhydroxides and solid precipitates. In the system of Fe^0-aeration-DML/PM filter, it was possible to recover treatment efficiency and the hydraulic loading rate by backwashing the post treatment media (Fig. 4.34). As could be observed, the efficiency of metal removal begins to decrease after about 3,500 BV accompanying with clogging of the filter bed. After

backwashing, a similar high metal removal was attained. The pH of the effluent from the filter bed and hydraulic loading rate is a good indicator of the requirement for backwashing of the media. Furthermore, the pH uplifting capacity of DML media is the main factor that determines overall effectiveness and thus the life span of the treatment barrier. If about 4 g m^{-3} of Ca and Mg are assumed to dissolve with the available 800 g of DML media, an estimated 200 m^3 of water can be treated by this system.

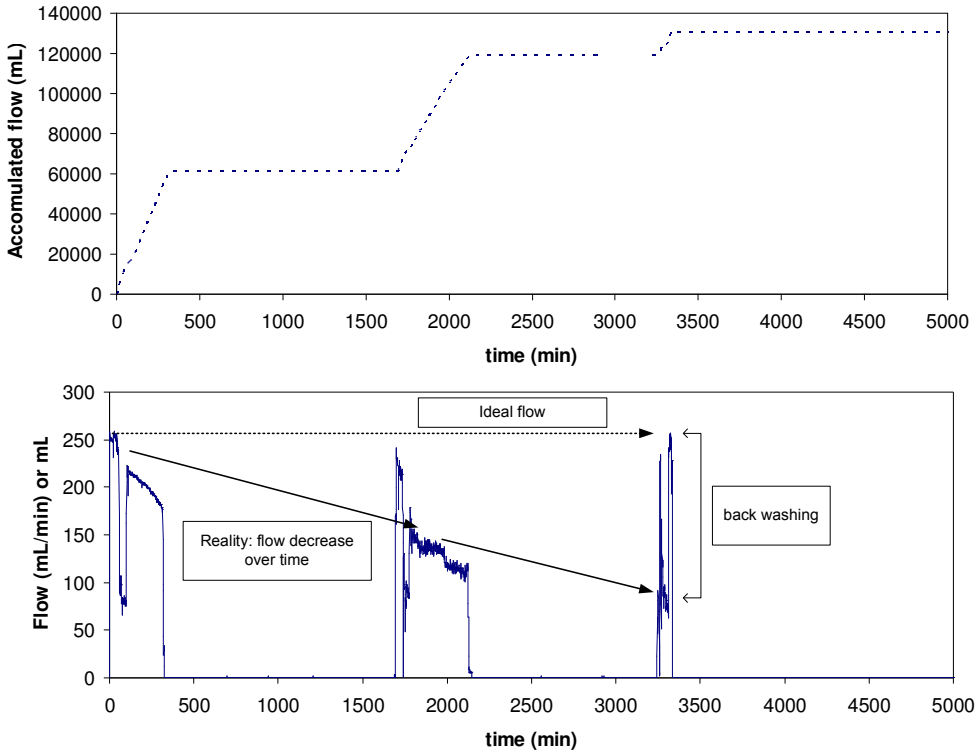

Fig.4.34 Hydraulic characteristic of the optimized Fe^0/carbonatic barrier over time. The backwashing of the media yields sustainable hydraulic performance

4.4.4 Conclusion

Based on the experimental and modeling results, Fe^0 supported with pumice column can barely cope with good requirements of water qualities. This section demonstrates the method in order to optimize the Fe^0 barrier system. The method involved a combination of various carbonatic media into the Fe^0 system both as composited and sequential columns. In this way, the performance of the barrier will be increased by means of accelerating the rate of chemical precipitation of metals. Incorporation of these materials also increases affinity of adsorption at a higher pH. The columns were both tested in the laboratory and on-site receiving realistic rain events. The results showed that Fe^0/carbonatic columns significantly enhance metals removal efficiency as compared with the Fe^0 column. By incorporating carbonate bearing materials, the rate of chemical precipitation is increased and metals are precipitated into solid and immobilized. Nevertheless, this method has its drawback due to the treatment column's

higher potential for clogging and the final configuration of the Fe^0 treatment system was therefore designed. The system consisted of columns filled with spiral shaped irons followed by an aeration unit and post filtration of pumice/dolomite. The treatment unit was installed onsite for treatment of metal-contaminated runoff under fluctuating conditions. It was found that there was little impact of water quality parameters on the treatment efficiency of metals. Nevertheless, the barrier requires a periodical backwash to retain a good removal efficiency and also to gain an optimum hydraulic loading rate.

4.5 Design of a treatment system and application of results

This section demonstrates the concepts and guidelines for the ZVICB design. The design of the treatment barrier takes into account the thorough understanding of physical-chemical removal processes of metals derived from the research results. The knowledge of kinetic removal rates of metals, conditions that suits immobilization processes, products and factors determining the life span of the treatment system will be used to quantify the amount of media required. It is important to consider the catchment and flow characteristics for the hydraulic and structural design of the system aiming to minimize the potential risks of contaminants in subsequent surface discharge or groundwater recharge. Furthermore, the chapter will illustrate how the adsorption model is used for the assessment of the system's performance over the long term period. Finally, the initial investment cost of the treatment media for ZVICB is compared with the GFH/Lime system.

4.5.1 Application of Fe^0 for highway runoff treatment

The conceptual design procedures for treatment of highway runoff are relatively well established. In general, a wet detention pond system in combination with an infiltration basin is applied (Hvitved-jacobsen et al., 1994). The immobilization processes of pollutants in the detention pond are governed by sedimentation of particulates and adsorption of dissolved compounds to sediments during the percolation period. Uptakes of soluble compounds by plants through biological processes may also take place (Barbosa, 1999). To yield efficient treatment of pollutants in the pond, physical characteristics of the treatment pond including shape, water depth, side slope, and hydraulic retention time shall be designed to allow good settling of particles and avoidance of a completely mixed condition. In general, a plug flow characteristic is preferred. Designs of wet detention ponds for highway runoff are mostly based on hydraulics and have a high return period of 10 to 100 years. Hence, during wet weather periods, the overflowing runoff volumes above the treatment capacity of the pond as well as remobilizing of the settled solids can result in lower treatment efficiency. Hence, an advanced treatment method applying a fixed bed reactor in subsequence to a pond may be integrated in order to enhance the overall treatment efficiency.

Fig. 4.35a-c illustrates the application of zero-valent iron for advanced treatment of highway runoff. These conceptual ideas, though not for Fe^0, are based on the research project initiated for treatment and re-use of urban stormwater runoff in Denmark (http://www.life-treasure.com). In the first illustrated method (Fig. 4.35a), Fe^0 may be incorporated into an existing pond for production of iron salt as flocculants, which in proportional to the flow can enhance the removal of particulates and dissolved compounds. The second method is to use Fe^0 media to increase the removal of dissolved metals during the adsorption to sediments (Fig. 4.35b). In this case, Fe^0 is filled into the bottom sediments for production of iron oxides as adsorption sites. The final method is to use ZVICB filter bed in the post treatment step of the effluent (Fig. 4.35c). This method intends to remove more dissolved compounds than the pond's capacity. Prior to filtration bed, passage through sand bed is crucial to reduce clogging

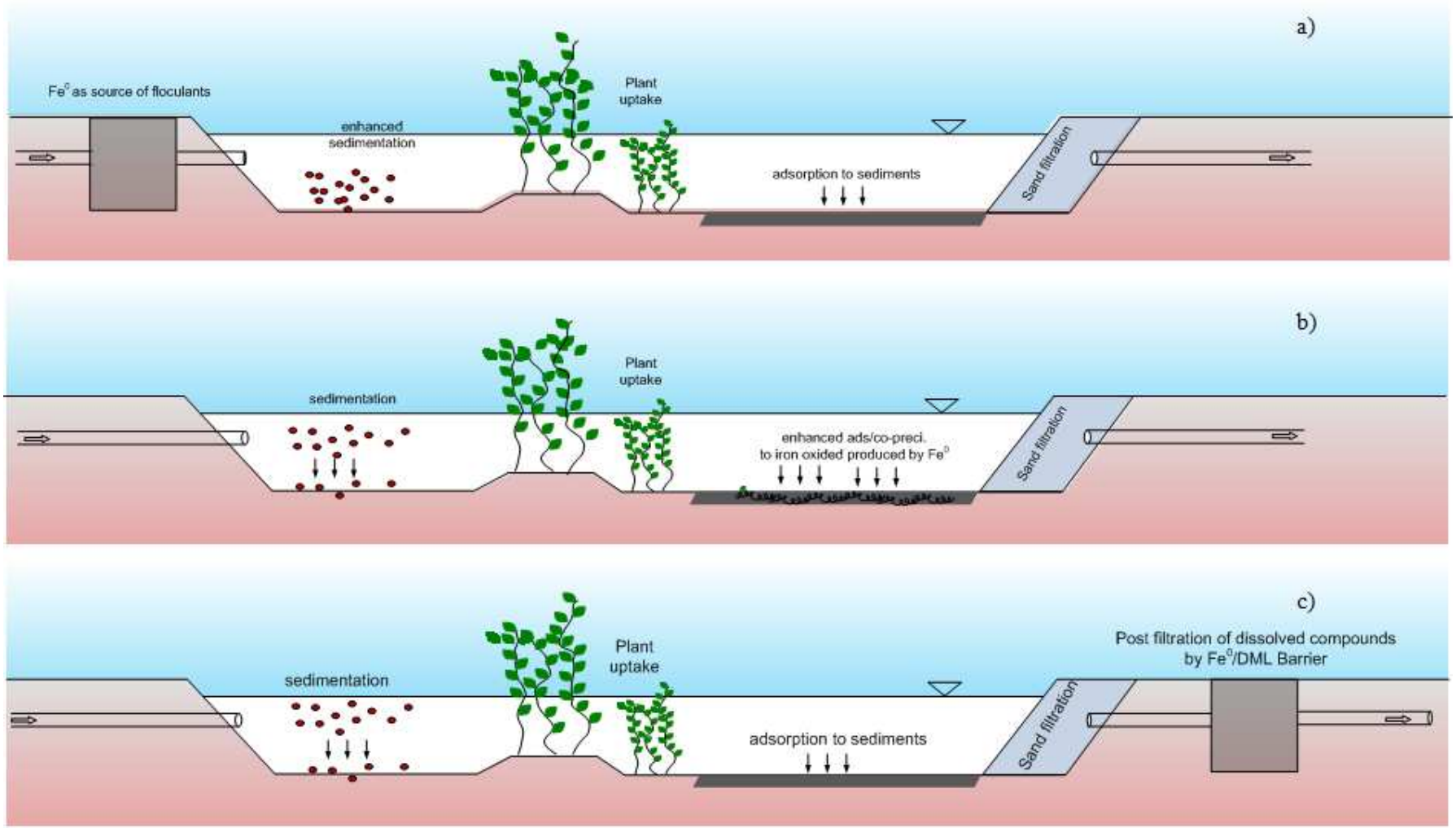

Fig. 4.35 Applications of Fe^0 for treatment of highway runoff (modified after Life-Treasure Project, http://www.life-treasure.com)

of the barrier resulting in a longer life span of the treatment barrier. These methods can be combined to achieve maximum treatment performance.

4.5.2 Application of Fe^0 for roof runoff treatment

In comparison to high way runoff, roof runoff is characterized by a higher concentration and constant flux of heavy metals. The metals in roof runoff are often present in a dissolved form due to the low content of particulates and the acidic pH of water. As compared to a pond system, a fixed-bed system is more advantageous for the design of the treatment system of roof runoffs because of the required high metal uptake rate and the shortest contact time that allows the system to use much less space and favours installation onsite. In several recent studies, the fixed bed system was successfully demonstrated. Steiner (2003) employed a GFH/$CaCO_3$ barrier for treatment of runoff from copper roof and façade for several sites in Switzerland. An ion exchange barrier using clinoptilolite media was also proven (Athanasiadis et al., 2005). Yet, a cost effective media with a high metal uptake capacity as well as the long life span of the system is further aimed for actual implication in stormwater treatment. Based on the results of this work, a novel fixed-bed system containing Fe^0/carbonatic material has been shown to possess a high removal efficiency with sufficient hydraulic stability and, hence, may be further actualized. Depending on the treatment configuration, application of ZVICB for treatment of roof runoff may be applied as illustrated in Fig. 4.35 and 4.36.

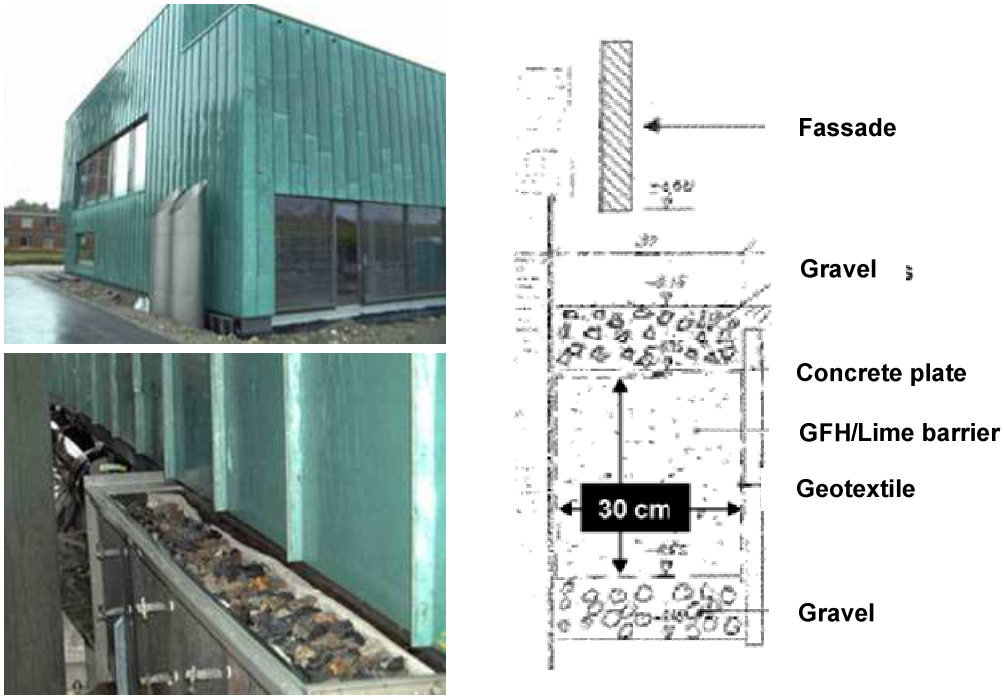

Fig. 4.36 GFH/$CaCO_3$ barrier for treatment system of copper façade (Steiner, 2003)

4.5.3 Design of ZVICB system

To illustrate how the results of the research can be utilized at actual sites, this section demonstrates the state-of-the-art design of the Fe^0/carbonatic system. The following assumptions have been drawn:

- A catchment area consists of a bitumen roof with a zinc gutter and a copper roof (Fig. 4.37). Within the catchment area and already considering losses through evaporation and adsorption to a permeable surface, it is assumed that rainfall is routed and transformed into a runoff volume with a total runoff volume of 850.6 mm (Table 4.6). The corrosion rates of metal roofs were assumed to be 3.6 g Me $m^{-2}a^{-1}$. The runoff shall be treated before infiltration into the subsurface for purposes of groundwater recharge.

- The standards of water discharge are 0.05 mg L^{-1} for copper and 0.5 mg L^{-1} for zinc. This corresponds to a required removal rate of 99 and 92%, respectively.

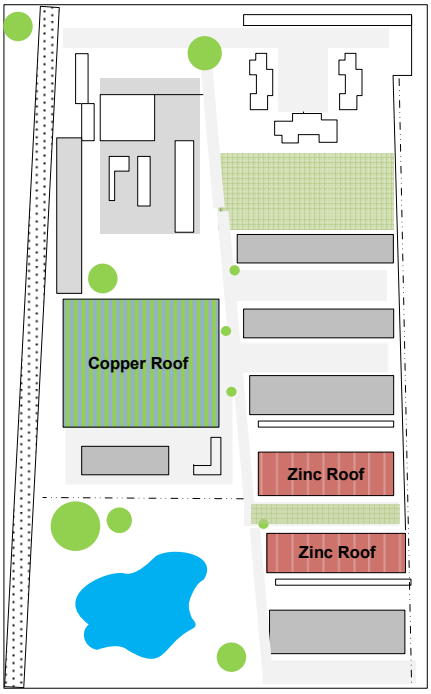

Area	**Location**	City center
	Cathment	Residential and University area
	Roof	Copper, Bitument Roofs
	Road	excluded
	Greenland	excluded
Hydrology	**Rain depth**	850.6 mm
	Summer (Jun. – Aug.)	75%
	Rest	25%
Soil	**Top Layer**	Thickness: 9 m
		Permeability: 6*10^-6 m/s

Fig. 4.37 Catchment area characteristics for illustration of the design of treatment barrier

In the design procedure, four steps are established;

(1) conceptual design of the treatment system of roof runoff
(2) determination of the media required and the treatment volume

(3) dimensioning the geometry of the treatment system, and
(4) estimation of the lifespan and the annual sludge waste

Conceptual design of the treatment system

The conceptual design of treatment system of roof runoff is illustrated in Fig. 4.38. The main components of the treatment train are a storage tank, ZVICB and the recharge well. The runoff from impervious area is transported through sewer lines and collected in the storage tank through which runoff will then be fed into the treatment system. This storage tank is designed not only to attenuate the flow but also to behave as settling step of particulates. The treatment system may be constructed underground using concrete structure or above ground as natural pond system that can be integrated into the recreation area.

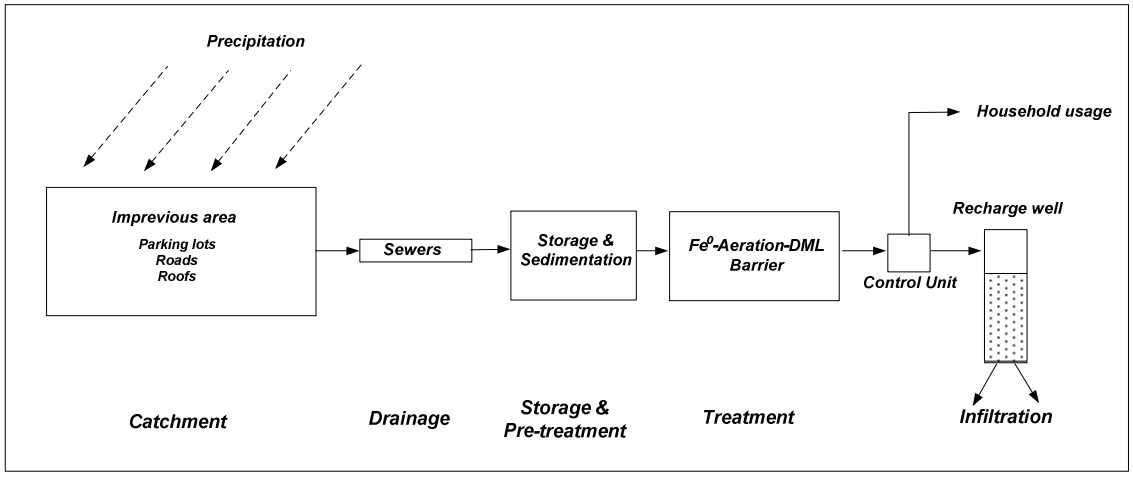

Fig. 4.38 Conceptual design of the treatment system

Design of the treatment barrier

To design of the treatment system, the metal uptake capacities of 42 and 22 g kg^{-1} Fe^0 for copper and zinc have been used, respectively. These metal uptake loads were obtained from the experiments at high NOM concentrations, which will result in a larger size of barrier for reasons of safety factor (S.F.) in case water qualities are not known. An assumption of a total 50% iron till exhaustion was assigned. The design calculation sheet has been developed (Table 4.6). The calculated results based on the work of Ludwig (2007) and Steiner (2003) are also demonstrated for comparison. These require input parameters including the physical and chemical data of iron and DO consumption rates.

Based on the calculation, it was found that about 18 and 34 kg of iron are required for the treatment of copper and zinc, respectively. The higher value will be further used in the actual

implementation. This design assumes that reactive media is to be replaced annually. An estimation of about 50% of total iron mass of 17 kg corrosion products should be classified as toxic wastes and requires special disposal.

Table 4.6 The criteria and design results of the ZVIB

Paramter	Symbol	Unit	Ludwig (2007)	Steiner (2003)	This work	
					Cu	Zn
Catchment characteristics						
Roof surface area	A	m^2	210	210	210	210
Corrosion rate	$r(Me)$	gMe $m^{-2}a^{-1}$	3.6	3.6	3.6	3.6
Precipitation intensity	r	mm a^{-1}	850.6	850.6	850.6	850.6
Runoff coefficient	ψ	-	1	1	1	1
Runoff volume	V	m^3 a^{-1}	179	179	179	179
or equal to		L h^{-1}	20	20	20	20
Design criteria of ZVIB						
Volumetric surface area of Fe^0	a_V	m^2 L^{-1}	0.8	-	-	-
Bulk density of Fe^0 media	ρ_s	kg L^{-1}	0.8	0.65[1]	0.20[2]	0.20
Bulk density of Ca media	ρ_c	kg L^{-1}		-	1.02	1.02
Oxygen uptake rate	$r(DO)$	L m^{-2} min^{-1}	0.05	-	-	-
Metal uptake load	q_M	mg Me g^{-1} Fe^0	50	30	42	22
Inlet concentration - Me	$c_{in}(Me)$	mg Me L^{-1}	6	6	6	6
Outlet concentration - Me	$c_{out}(Me)$	mg Me L^{-1}	0.5	0.05	0.05	0.5
Design of the ZVI Barrier						
Number of baffle	n	-	10.5	-	-	-
Total removal rate	η_Σ	%	92%	99%	99%	92%
Total iron mass	$m_\Sigma(Fe)$	kg	40	25	18	34
Total cabonatic matials	$m_\Sigma(Ca)$	kg	-	25	3.2	3.2
Total volume of reactor	V_Σ	L	50	38.5	95	175
Total HRT	$t_{v,\Sigma}$	h	2	-[3]	-[4]	-
Total height of bed	L_Σ	m	5	-	-	-
Life span of the system						
Time to reach 50% usage of iron	t_{50}	a	1.0	1.0	1.0	1.0
Total flow treated	Q_{50}	m^{-3}	180.6	180.6	180.6	180.6

[1]bulk density of GFH mixed with Lime; [2]filled-in density of spiral Fe^0;[3]designed to receive instant flow; [4]HRT of minimum 5 min is recommended

Design of the DML/PM barrier

Based on the results of the test, assuming 8 g m^{-3} of Ca and Mg to dissolve into the runoff water, an estimated 200 m^3 of water will require 1600 g of DML media. For a safety factor, a 50% saturation is assumed and, thus, during a one year operation of the ZVICB, about 3.2 kg of DML media is required for one year operation. The equal amount of pumice is mixed with DML to increase porosity and filterability.

Hydraulic and structural design

In term of engineering application and realization of the design in the field, about five times amount of the treatment media will be used, which prolong the life span of the system up to about five years. A larger system is preferred for installation onsite. This is also to reduce an

initial investment cost and ease of maintenance. The design was based on the assumption that a total volume of runoff (90 or 180 m^3 a^{-1}) is intercepted and collected for treatment at constant and low flow rate with up to 6 h contact time over the period of one year. This concept required sufficient storage space onsite.

An example for the hydraulic and structural design of Fe^0 treatment system for runoff has been illustrated (Fig. 4.39a). The treatment barrier was designed as a single reactor, consisted of three main components; (1) a sedimentation tank; (2) a baffle reactor tank consisting of an Fe^0 barrier, aeration and DML/PM bed; and (3) the recharge basin. Conceptually, the sedimentation tank will remove particulates as well as some metals bounded sediments from entering the barrier. The majority of metals will, however, be removed in the baffle reactor where the contaminated runoff will pass through the Fe^0 and carbonatic barriers with an up and down flow characteristic. The baffle reactor was chosen to maximize the contact between runoff and media preventing short circuit of the system. The water depth of less than 0.5-1.0 meter shall be designed to aerate water. Sufficient DO is required for complete processes of iron corrosion and for subsequently oxidized the iron bound particles during the natural aeration steps. In the last part, the baffle reactor consists of DML/PM that will fully oxidize and precipitates all persistent compounds into solids. There are units for withdrawing excess sludge from the bottom of the reactor, through gravity and a drainage pipe (Fig. 4.39b). The outlet from the reactors will then be used to recharge into the subsurface. It is anticipated that outlet water is basic so further aeration might be required before discharge. Based on the study of Karchunke (2005), it may also be possible that the post filtration bed is constructed only with sand. Nevertheless, in the case of stormwater runoff treatment at high NOM concentration, a longer contact time during sand filtration is recommended to allow full oxidation of iron into particulates. The treatment system can be constructed as a natural soil or concrete structure depending on the cost factor. It is recommended that the treatment system should be lined with HDPE in order to prevent metal diffusion into the infiltration layer. In case of constructing with natural soil, a metal-transport zone where packed soil/Fe^0 at 10-25 cm above natural soil at the bottom of adsorption zone shall be installed. After a period of time, the soil from this zone is considered toxicant wastes and must be withdrawn. It can be dried to decrease its volume for further disposal.

As an alternative to the configuration described above, the ZVICB can be constructed onsite and installed directly beneath the roof or façade surface as illustrated in Fig. 4.36 by Steiner (2003). In that case, the ZVICB shall be designed to intercept the runoff volume originating from a limited surface area and to treat the water at the shortest contact time as possible, i.e., less than 1 min in order to infiltrate the water underground immediately. The system requires no storage basin but the design volume of media must take into account a highly fluctuating flow rate, kinetic of removal, water qualities and metal influxes of the runoff at each rain event. The adsorption model can be used for dimensioning treatment barrier.

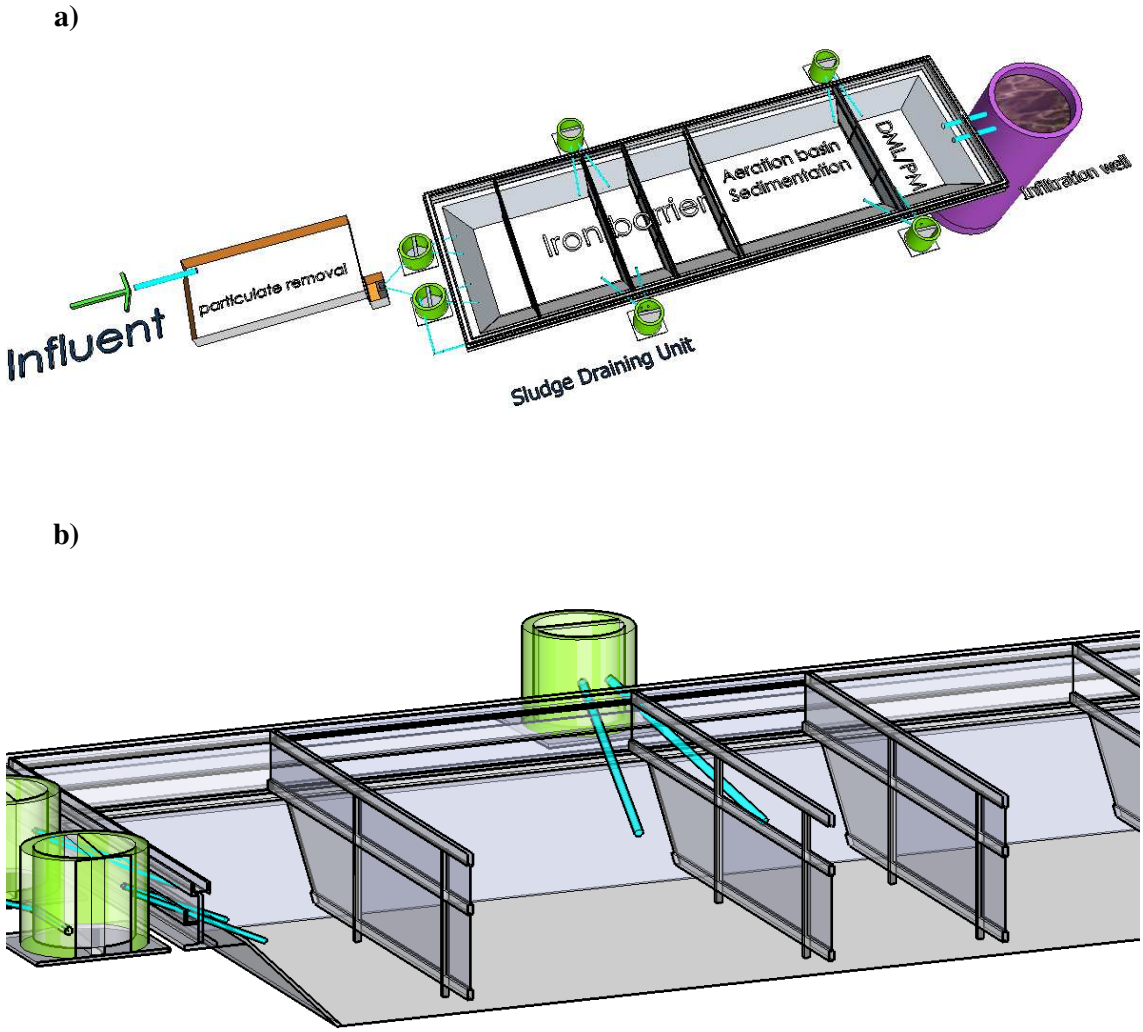

Fig. 4.39 a) 3D view of the treatment barrier b) baffle reactor and withdraw units of the excess sludge

Assessment of the treatment efficiency

The adsorption model as demonstrated in section 4.2.3 is employed for simulating the long term performance of the ZVIB (Fig.4.40). The adsorption model allows for a closer assessment of the system where the simulation of the treatment process at various scenarios, i.e., the rainfall data can be used to assess the treatment efficiency over the life span of the barrier. For modeling, the metal fluxes were simulated by multiplying the corrosion rates of metals with precipitation volumes at each rain event, where a total volume of the runoff is equal to 180 m^3 a^{-1} as used in the design criteria. The treatment contact time was assumed to be 1 h and by using an iron barrier with 180 kg Fe^0 in the barrier. It is aimed at demonstrating the application of the model to examine the treatment efficiency for further design of the barrier. In this example, it appears that the ZVIB does not capture metals sufficiently.

Nevertheless, it is expected that an incorporation of DML/PM media in the post treatment step will ensure the quality of discharge in reaching the standard of effluent.

Table 4.7 Input parameters for simulation of the long term efficiency of ZVIB

Parameters	D_i	L	Fe^0	*EBCT*	Cu^{2+}			Zn^{2+}		
					K_F	*1/n*	k_f	K_F	*1/n*	k_f
Conditions/Unit	[m]	[m]	[kg]	[min]			[x10^{-3}]			[x10^{-3}]
Final design	3	10	180	60	20	0.6	0.2	5	1.0	0.10

*For modeling of both copper and zinc, D_s = 1.0 x 10^{-10} cm^2 s^{-1} and D_p = 8.53 x 10^{-16} cm^2 s^{-1} were employed.

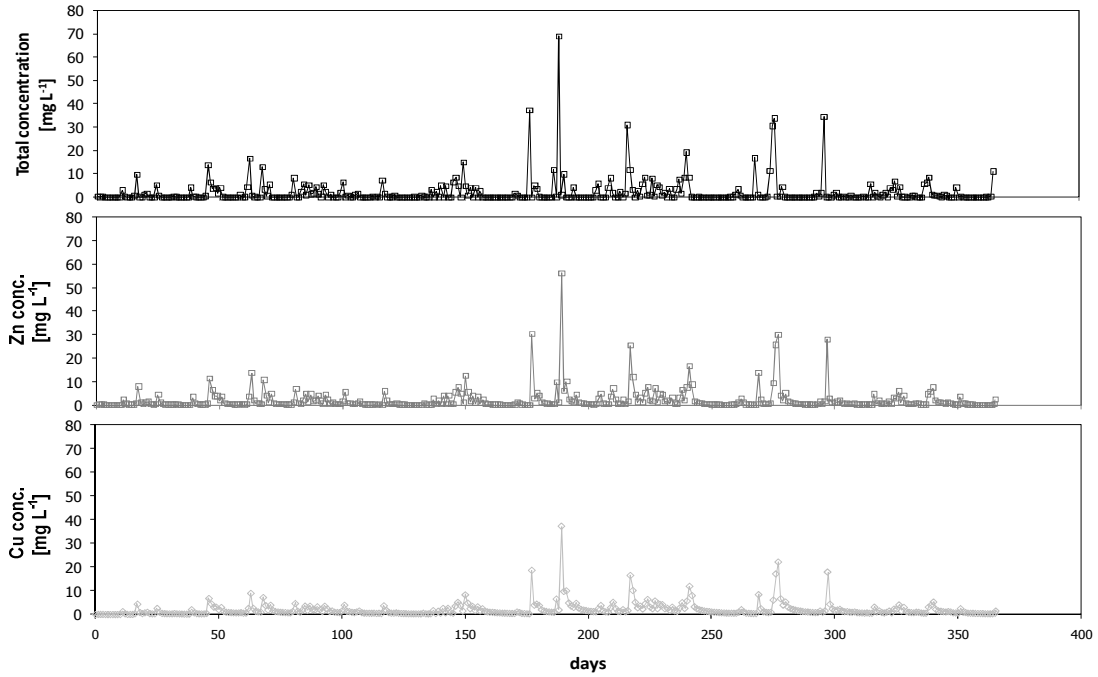

Fig. 4.40 Model simulation of outlet concentration of zinc and copper from the Fe^0 barrier. Based on the research data, with a proper design of carbonatic post treatment barrier, the effluent will meet a quality standard requirement.

Cost estimation

Table 4.8 demonstrates that the initial investment cost of treatment media for ZVICB is much lower than for the GFH/Lime system, especially when scrap iron can be utilized. The relative investment cost for the treatment media for ZVICB is likely to further decrease with an increasing scale of the system (Table B36 in Appendix B). Nevertheless, since the GFH/Lime requires a smaller foot print than the ZVICB because of a higher removal rate and the requires high void volume (>90%) of ZVICB. A complete comparison must take into account the cost of system construction. For this, total volume of reactors were estimated by dividing the required mass of treatment media by the filled-in bulk density of the media and the cost of construction can be calculated. Several factors influence the cost of treatment structure, including frequency of refilling the treatment materials, capacity, type of construction

materials, and location. Steel structures can be constructed on ground-level, while concrete structures are normally installed at or below grade. Below grade structures, e.g., lining type, require higher excavation and backfill costs. A comparison of of GFH/Lime and ZVIB system constructed with concrete, lining or bared soil (without structure) types for a range of roof surface areas are shown in Table B36. The results were used to calculate the total investment cost. The calculation shows that the investment cost of 0.39-0.66 Euro m^{-2} y^{-1} for GFH/Lime and 0.01-0.62 Euro m^{-2} y^{-1} for ZVICB system were obtained. It must be noted that the cost estimation did take only a limited requirement of factors into account and a lump-sum cost per unit workload were used for calculation. Furthermore, e.g.,the required storage tank for ZVICB was not included into the calculation, the data presented here may not be directly applicable for estimation of the actual project.

Table 4.8 Cost comparison for ZVICB and GFH/Lime treatment systems

Parameters	**ZVICB**		**GFH/Lime**
	Scrap iron	**Commercial ZVI**	
Initial cost for treatment media			
ZVI or GFH (Euro t^{-1})	45	325	3,620
Magno-dol or Lime (Euro t^{-1})	341	341	272
Mass of iron required (kg)	180	180	125
Cost of ZVI or GFH (Euro)	8.1	58.5	452.5
Mass of DML/PM or Lime (kg)	16	16	125
Cost of post treatment media (Euro)	5.5	5.5	34
Total investment of media (Euro)	13.6	64	486.2

5 Summary, conclusions and recommendations

5.1 Summary and conclusions

A comprehensive study, including batch kinetic, equilibrium and column configurations, for development of the novel treatment system of stormwater runoff has been demonstrated in this work. The batch test was carried out to understand the kinetics of metal removal under changing runoff conditions. The equilibrium tests were tested to determine the maximum uptake load of metals. Runoff waters from various sources including roof, street and highways runoff were used for examination. Following the batch test, Fe^0 was evaluated under a flow-through configuration and the behaviour of the breakthrough of the Fe^0 column was observed at actual operating conditions. Furthermore, the mechanisms involved in the removal of metals in the presence of NOM were studied. A modelling approach that allows for the prediction of the breakthrough results was validated and thus allowed for further evaluation of the up-scaling process. Finally, a method for optimizing the Fe^0 barrier and cost of the barrier were also demonstrated. The following summarizes the significant findings of this work;

Processes of copper and zinc removal
The results of batch and column tests reveal that the removal of Cu^{2+} and Zn^{2+} take place independently through different processes. The majority of Cu^{2+} is removed via a reductive transformation process and the insoluble forms of Cu^0 and Cu_2O were found as reaction products. The reduction rate of copper is closely linked to the surface area of Fe^0, where accessity of contaminant toward the Fe^0 surface plays a significant role for the process to occur. During the course of this work, the ongoing research has revealed that reduction of contaminants in the Fe^0 system under a natural pH range likely take places at the vicinity of Fe^0 surface. Unlike copper, the removal of zinc involves the adsorption and co-precipitation processes. The removal of zinc is strongly associated with the availability of freshly precipitated iron oxides as a result of an array of reactions including iron oxidation, iron (oxy)hydroxide precipitation and metal adsorption/co-precipitation. The adsorption/co-precipitation processes are also believed to play a major role in a long-term treatment of both copper and zinc, since over time, the Fe^0 surface would be passivated.

The understanding of the mechanisms involved in copper and zinc removal contributes to the process design selection of the treatment system. The treatment barrier for zinc removal should allow a spontaneous corrosion of iron whereby rust particles can be freely removed from the iron surface. On the contrary, the protective film of the Fe^0 surface might be beneficial for reductive transformation of copper at the inner layer of rust where a ferrous form of iron is available.

Impact of water quality parameters
Investigations under various water quality conditions demonstrated that the removal of copper and zinc is strongly impacted by water quality parameters. Generally, any factors that tend to

decrease iron corrosion rates, also hinder the removal rates of Zn^{2+}. Increasing pH, DO, IS and temperature generally favored faster retention rates of zinc in favor of production of sorption sites. In the batch test, it was found that increasing DO and IS of the solution increase the retention of copper but this was not the case for the flow-through column, where the removal of copper was hindered. This discrepancy between the batch and column results were due to differences in the experimental conditions employed and the physico-chemical characteristics of solid precipitates involved in the system. Among different water quality parameters investigated, NOM showed the most influence on the dramatically decrease of metal removal ability.

Equilibrium loading

The results of batch tests demonstrated that the equilibrium loadings of copper and zinc are 2-100 mg g^{-1} Fe^0 and 0.2-100 mg g^{-1} Fe^0 for copper and for zinc, respectively. These values agreed well with column investigation revealing that about 76 mg g^{-1} Fe^0 for copper (with min: 55 and max: 96 mg g^{-1}) and 55 mg g^{-1} Fe^0 for zinc (min: 22, max: 69 mg g^{-1}) could be removed. The presence of 9-61 mg L^{-1} NOM concentration resulted in a much lower metal uptake load of 42 and 22 mg g^{-1}, respectively.

NOM impact on Fe^0 treatment system

Based on the findings, it was shown that NOM influences the removal of metals in Fe^0 through several complex pathways including metal-ligand complexes, competitive adsorption and a hindrance of iron corrosion caused by NOM surface coverage of Fe^0. The NOM fraction that mainly interacts with the removal of metals is a larger size hydrophobic fraction with high aromaticity. The continuous input of NOM causes a short term effect on the treatment efficiency of the Fe^0 system, while the effectiveness over the long term cannot be concluded. Since NOM can degrade over time, the presence of NOM might contribute a smaller impact than expected. Moreover, the modification of the surface underlying the NOM might also contribute to an enhancing effect of metal removal in the long term. For the toxicology analysis and fate of the metals of runoff water, these must be assessed through the complexation capacity and biodegradation of NOM.

Modeling

The breakthrough curves of dissolved metals in the Fe^0 system are possibly predicted by the PSDM. In terms of application, a set of modeling parameters have been demonstrated for further use. The parameters were assessed in runoff solutions having different concentration ranges of NOM. The K_F (and n) of 10-40 (0.6) for copper and 5-20(1.0) for zinc and an average k_F of 0.4 x 10^{-3} cm s^{-1} for copper and k_F = 0.2 x 10^{-3} cm s^{-1} for zinc may be used for modeling of breakthrough in typical diluted solutions of roof runoff. The application of the models must be used with care, particularly, in circumstances where the runoff quality is highly polluted and their impacts on the breakthroughs seem significant, then a lower K_F may be applied. For more precise model predictions, kinetic and equilibrium parameters should be quantified from the solution collected onsite. It must be considered that the characteristic of iron and treatment configuration can tremendously affect the modeling results. As an

alternative to the modeling assessment, a small scale column test may be conducted to evaluate the performance of the treatment barrier for further up-scaling purpose.

Optimization of the barrier and final design
Optimization of the processes has been carried out using various carbonatic materials. According to these results, the recommended system for on-site treatment of metal-contaminated runoffs consisted of a spiral shaped iron barrier followed by an aeration unit and post filtration of pumice/dolomite may be applied. About 60-100 and 30-80 % of metal concentrations could be removed at EBCT of 5 and 1 min EBCT, respectively. Longer EBCT will yield a better performance. For practical operations, carbonate materials tend to be passivated by various minerals and biofilms. An occasional backwash in order to reactivate the surface of materials inside and to maintain the hydraulic conductivity of the system is required.

Investment cost
It has been shown that the investment cost of ZVICB is much lower than that of GFH/Lime system, with increasing differences at larger scale site. The simplified cost analysis shows that the total investment for GFH/Lime and ZVICB systems were about 0.39-0.66 and 0.01-0.62 Euro $m^{-2}_{\text{roof surface}}\ y^{-1}$, respectively, depending on the types of structures. A higher investment cost may be expected for actual scale sites, in which the yearly operational costs such as maintenance and replacement should be included.

5.2 Recommendations for further work

- Although, the mechanisms involving copper and zinc removal by Fe^0 system have been extensively investigated in this work, it is still not completely understood whether Cu^{2+} is reduced by Fe^0, Fe^{2+} or structured Fe^{2+}. According to the results, it is obvious that the oxide layer on the surface of iron or that is accumulated within the reactive barrier play a significant role on the treatment ability of heavy metals. The impact occurs both physically and chemically. In addition, it is also difficult to distinguish between the role of reduction, adsorption and co-precipitation processes under a wide range of conditions. Further work on these aspects may help in the engineering design and operation of the system in the long-term.

- The PSDM has been introduced in this work for prediction of breakthrough curves. Nevertheless, the parameters obtained were mostly derived using an empirical basis to determine the best fit. The model described the complex processes of metal removal in the Fe^0 system by a few “lump sum” kinetic and equilibrium parameters, which in terms of application, may not pass rigorously validation specifically when different types, shapes of iron and treatment configuration is employed. With an aim to design an up-scaled system as well as in the prediction of the long term performance of the barrier, further work on modeling is beneficial.

- In terms of applicability, the results with the carbonatic material show that an additional ZVI barrier may not necessarily be mandatory in the treatment chain. This would simplify the required treatment system. Nevertheless, as it was observed that the surfaces of carbonate materials tend to be passivated over time by various minerals and biofilms and that may reduce its effectiveness overtime. The design parameters and long term efficiency of the carbonate barrier require further investigation.

- Consider that the iron material used for the barrier may be "contaminated" itself by heavy metals such as copper, chromium and nickel. They may be released into the water during corrosion of iron, but may be caught by the corrosion products. The significance and fate of these contaminations should be evaluated in future research work. In similar regards, it is also interesting to study the remobilization of the metals that have been previously uptaken by iron oxides.

References

Abbt-Braun, G., Frimmel, F. and H. Schulten (1990) Strukturelle Charakterisierung isolierter aquatischer Huminstoffe - Anwendbarkeit, Grenzen und Vergleich ausgewählter Methoden. *Vom Wasser* ,74, 325-338.

Aiken, G.R., Mcknight, D.M., Wershaw, R.L. and P. Maccarthy (1985) Humic substances in soil, sediment, and water: geochemistry, isolation and characterization. *John Wiley & Sons*, New York, 691.

Aiken, G., McKnight, D., Thorn, K. and E. Thurman (1992) Isolation of hydrophilic organic acids from water using nonionic macroporous resins. *Org. Geochem.,* 18, 4, 567–573.

Amy, G. (2004) Fundamental insights into natural organic matter (NOM) fouling of membranes. Presentation at the department of water quality control, Technical University of Berlin, Germany.

Annamalai, V. and L.E. Murr (1979) Influence of deposit morphology on the kinetics of copper cementation on pure iron, *Hydrometallurgy*, 4, 57-82.

Athanasiadis, K., Helmreich B. and P. Wilderer (2003) Entfernung von Zink aus Dachabläufen eines Zinkdaches durch Klinoptilolith. Regenwasserversickerung - Eine Möglichkeit dezentraler Regenwasserbewirtschaftung. 31. *Abwassertechnisches Seminar*. Berichte aus Wassergüte- und Abfallwirtschaft TU München. Hrsg.: Prof. Dr. P. Wilderer.

Atkinson, R.J., Posner, A.M., and J.P. Quirk (1967) Adsorption of potential-determining ions at the ferric oxide-aqueous electrolyte interface. *J. Phys. Chem*., 71, 550-558.

Bang, S., Johnson M.D., Korfiatis G.P. and X. Meng (2005) Chemical reactions between arsenic and zero-valent iron in water. *Wat. Res.,* 39, 5, 763-770.

Barbosa, A.E. (1999) Highway runoff pollution and design of infiltration ponds for pollutant retention in semi-arid climates. *Ph.D.Thesis*, Environmental Engineering Laboratory, Aalborg University, Denmark.

Bardin, J.P., Cres, F.N., Touzo, A. and J.L. Verjat (1996) Pollution measurements in a stormwater settling and infiltration basin. *The 7th International Conference on Urban Storm Drainage*, Hanover, Germany, 3, 1611-1616.

Benjamin, M.M. (2002) Water chemistry, *McGraw-Hill*, Newyork.

Biswas, A.K. and J.G. Reid (1972) Investigation of the cementation of copper on iron. *Proc. Aust. Inst. Min. Met.*, 242, 37-45.

Blowes, D.W., Ptacek, C.J., Benner, S.G., McRae, C.W.T., Bennett, T.A. and R.W. Puls (2000) Treatment of inorganic contaminants using permeable reactive barriers, *J. Contam. Hydrol*., 45, 123-137.

Blowes, D.W. and C.J. Ptacek (1992) Geochemical remediation of groundwater by permeable reactive walls: removal of chromate by reaction with iron-bearing solids. *Subsurface restoration conference*, U.S. Environmental protection agency, Kerr Laboratory, Dallas, TX, 214-216.

Boller, M.A. (1997) Tracking heavy metals reveals sustainability deficits of urban drainage systems. *Wat. Sci. Tech.,* 35**,** 9, 77-87.

Boller, M.A. and M. Steiner (2002) Diffuse emission and control of copper in urban surface runoff. *Wat. Sci. Tech.,* 46**,** 6-7, 173-181.

Bundesbodenschutzgesetz (BBodSchG) vom 17.03.1998. BGBl. 1998, Teil 1, Nr. 16.

Dannecker, W., Au, M. and H. Stechmann (1990) Substance load in rainwater runoff from different streets in Hamburg. *Sci. Total Environ*., 93, 385-392.

Cantrell, K.J., Kaplan, D.I. and T.W. Wietsma (1995) Zero-valent iron for the in situ remediation of selected metals in groundwater. *J. Hazard. Mat.*, 42, 2, 201-212.

Cheng, T. and H.E. Allen (2006) Comparison of zinc complexation properties of dissolved natural organic matter from different surface waters. *J. Environ. Management*., 80, 222–229.

Cornell, R.M. and U. Schwertmann (1996) In: Böck, B. (Ed.), The iron oxides: structure, properties, reactions, occurrence and uses. *VCH Press*, Weinheim, Germany.

Cravotta, C.A. and G.R. Watzlaf (2002) in Handbook of groundwater remediation using permeable reactive barriers: applications to radionuclides, trace metals, and nutrients (editor: Naftz, D.L., Morrison, S.J., Fuller, C.C., Davis, J.A.), *Elsevier Science*, Amsterdam.

Crawford, R.J., Harding, I.H., and D.E. Mainwaring (1993) Adsorption and coprecipitation of single heavy metal ions onto the hydrated oxides of iron and chromium. *Langmuir*, 9, 3050-3056.

Crittenden, J.C., Luft, P. and D.W. Hand (1985) Prediction of multicomponent adsorption equilibria in background mixtures of unknown composition, *Wat. Res*. 19,12, 1537-1548.

Crittenden, J.C., Luft, P., Hand, D.W., Oravitz, J.L., Loper, S.W. and M. Ari (1985) Prediction of multicomponent adsorption equilibria using ideal adsorbed solution theory, *Environ. Sci. Technol*. 19,11,1307-1043

Croué, J. (2002) Approaches to characterizing NOM. Conference proceedings: NOM1-Characterisation and treatment of natural organic matter, School of Water Sciences, Cranfield University, U.K.

Chi, F.H. and G.L. Amy (2004) Kinetic study on the sorption of dissolved natural organic matter onto different aquifer materials: the effects of hydrophobicity and functional groups. *J. Colloid Interf. Sci*., 274, 380–391.

Davis, J.A. and J.O. Leckie (1978) Effect of adsorbed complexing ligands on trace metal uptake by hydrous oxides. *Environ. Sci. Technol*., 12, 1309-1315.

Denver, J.I. (1997) The geochemistry of natural waters. Surface and groundwater environments, 3rd edition-Prentice Hall, New Jersey.

Dries, J., Bastiaens. L., Springael, D., Kuypers, S., Agathos, S.N. and L. Diels (2005) Effect of humic acids on heavy metal removal by zero-valent iron in batch and continuous flow column systems. *Wat. Res.,* 39, 3531–3540.

Driehaus, W., Jekel, M. and U. Hildebrandt (1998) Granular ferric hydroxide – a new adsorbent for the removal of arsenic from natural water. *J. Water SRT- Aqua.*, 47 (1), 1-6.

Dzombak, D. A. and F.M. Morel (1990) Surface complexation modeling: hydrous ferric oxide, *John Wiley & Sons*, New York.

Farrell, J., Kason, M., Melitas, N. and T. Li (2000) Investigation of the long-term performance of zero-valent iron for reductive dechlorination of trichloroethylene. *Environ. Sci. Technol.*, 34, 514-521.

FHWA (1996) Federal highway administration, evaluation and management of highway runoff water quality, *Report No. FHWA-PD-96-032*, U.S. Department of Transportation.

Feitknecht, W. and P. Schindler (1963) Solubility constants of metal oxides, metal hydroxides and metal hydroxide salts in aqueous solution. *Pure and Applied Chemistry*, 6, 132-199.

Fiedor, J.N., Bostick, W.D., Jarabek, R.J. and J. Farrell (1998) Understanding the mechanism of uranium removal from groundwater by zero-valent iron using X-ray photoelectron spectroscopy. *Environ. Sci. Technol.*, 32, 1466-1473.

Förster, J. (1993) Dachflächen als Interface zwischen atmosphärischer Grenzschicht und Kanalsystem: Untersuchungen zum Transportverhalten ausgewählter organischer Umweltchemikalienan einem Experimentaldachsystem. *Dissertation an der Universität Bayreuth.*

Freundlich, H. (1906) Über die Adsorption in Lösungen. *Zeitschrift für physik.* Chemie 57, 385-470.

Friedman, G. (1984) Mathematical modelling of multicomponent adsorption in batch and fixed-bed reactors, *Mater Thesis*, Michigan Technological University.

Furukawa, Y., Kim, J.-W., Watkins, J. and R.T. Wilkin (2002) Formation of ferrihydrite and associated iron corrosion products in permeable reactive barriers of zero-valent iron. *Environ. Sci. Technol.*, 36, 5469-5475.

Genz, A., Baumgarten, B. and M. Jekel (2004) A new treatment process for removal of NOM by adsorption and regeneration of granular ferric hydroxide (GFH). *WEMS, Water Environmental Management Series* (2nd IWA Leading Edge Conference of Water and Wastewater Treatment Technolgies), 107-116.

Ghauch, A., Assi, H.A. and A. Tuqan (accepted) Investigating the mechanism of clofibric acid removal in Fe^0/H_2O systems, *J. Hazard. Mater.*

Gibert, O, de Pablo, J., Cortina, J.L. and C. Ayora (2003) Evaluation of municipal compost/limestone/iron mixtures as filling material for permeable reactive barriers for in-situ acid mine drainage treatment. *J. Chem. Technol. Biot*., 78, 489-496.

Gieska, M., Tanneberg H. and R.R. van der Ploeg (2000) Lokal erhöhte Schwermetallkonzentrationen in urbanen Böden durch Versickerung von Dachabflüssen. *Wasser und Boden,* 52, 3, 41-45.

Gillham, R.W. and S.F. O'Hannesin (1992) Metal-catalyzed abiotic degradation of halogenated organic compounds. In "Modern Trends in Hydrogeology", *IAH conference*, Hamilton, Ontario, Canada.

Gillham, R.W. and S.F. O'Hannesin (1994) Enhanced degradation of halogenated aliphatics by zero-valent iron. *Ground Water*, 32, 958-67.

Gromaire-Mertz, M.C., Garnaud S., Gonzales A. and G. Chebbo (1999) Characterisation of urban runoff pollution in Paris. *Wat. Sci. and Tech*. 39, 2, 1-8.

Gu, B., Chen, J., Vairavamurthy, M.A. and S. Choi (2000) Chemical and biological reduction of contaminant metals by natural organic matter. Extended abstract submitted to symposium on "Chemical-biological interactions in contaminant fate", the 220th American chemical society national meeting, 20-25 August, Washington, DC.

Gu, B., Liang, L., Dickey, M.J., Yin, X. and S. Dai (1998) Reductive precipitation of uranium (VI) by zero-valent iron. *Environ. Sci. Technol.*, 32, 3366-3373.

Gu, B., Schmitt, J., Chen, Z., Liang, L. and J. McCarthy (1994) Adsorption and desorption of natural organic matter on iron oxide: Mechanisms and models. *Environ. Sci. Technol.,* 28, 38-46.

Gu, B., Schmitt, J., Chen, Z., Liang, L. and J. McCarthy (1995) Adsorption and desorption of different organic matter fractions on iron oxide. *Geochim. Cosmochim. Acta*, 59, 2, 219-229.

Hamann, C.H. and W. Vielstich (1975) Elektrochemie I und II. Taschentexte Nr. 41 und 42. *Verlag Chemie*, Weinheim.

Hamilton, R.S., Revitt, D.M., Warren, R.S. and M.J. Duggan (1987) Metal mass balance studies within a small highway dominated catchment, *Sci. Total Environ*., 59, 365-368.

He, W., Wallinder, I.O. and C. Leygraf (2001) A laboratory study of copper and zinc runoff during first flush and steady-state conditions, *J. Corros. Sci*., 43, 1, 127-146.

Hedin, R.S., Watzlaf, G.R. and R.W. Nairn (1994) Passive treatment of acid mine drainage with limestone. *J. Environ. Qual*., 23, 1338-1345.

Hesse, O. (2005) Untersuchung von Regenwasser und Abläufen von Kupferdächern und Aufzeigen von Möglichkeiten zur Verminderung schädlicher Einflüsse auf die Umwelt am Beispiel einer Therme in Belzig, *Diplomarbeit an der Technische Universität Berlin*, Fakultät III Institut für Technischen Umweltschutz Fachgebiet Siedlungswasserwirtschaft.

Hewitt, C.N. and M.B. Rashed (1992) Removal rates of selected pollutants in the runoff waters from a major rural highway, *Water Res.*, 26, 3, 311-319.

Huang, Y.H. and T.C. Zhang (2005) Effects of dissolved oxygen on formation of corrosion products and concomitant oxygen and nitrate reduction in zero valent iron systems with or without aqueous Fe^{2+}. *Wat. Res*., 39, 1751-60.

Huber, S. and F. Frimmel (1996) Size-exclusion chromatography with organic carbon detection (LC-OCD): a fast and reliable method for the characterization of hydrophilic organic matter in natural waters. *Vom Wasser*, 86, 277-290.

Hvitved-Jacobsen, T. and Y.A. Yousef (1991) Highway runoff quality, environmental impacts and control in *Highway Pollution*, Studies in Environmental Science 44, R.S. Hamilton and R.M. Harrison eds., Elsevier, 166-208.

Hvitved-Jacobsen, T., Johansen, N.B. and Y.A. Yousef (1994) Treatment systems for urban and highway runoff in Denmark, *Sci. Tot. Environ*., 146/147, 499-506.

Jarrusutthirak, C. (2002) Fouling and flux decline of reverse osmosis (RO), nanofiltration (NF) and ultrafiltration (UF) membranes associated with effluent organic matter (EFOM) during wastewater reclamation/reuse. *PhD Thesis*, University of Colorado at Boulder.

Jia, Y., Aagaard P. and G.D. Breedveld (2007) Sorption of triazoles to soil and iron minerals. *Chemosphere*, 67, 250-58.

Kamolpornwijit, W., Liang, L., Westa, O.R., Molinea, G.R. and A.B. Sullivana (2003) Preferential flow path development and its influence on long-term PRB performance: column study, *J. Cont. Hydrol.,* 66, 161– 178.

Kamolpornwijit, W., Liang, L., Moline, G.R., Hart, T. and O.R. West (2004) Identification and quantification of mineral precipitation in Fe filings from a column study. *Environ. Sci. Technol.,* 38, 5757-5765.

Karschunke, K. and M. Jekel (2002) Arsenic removal by iron hydroxides, produced by enhanced corrosion of iron, *Water Supply,* 2, 2, 237–245.

Karschunke, K. (2005) Nutzung der Eisenkorrosion zur Entfernung von Arsen aus Trinkwasser. *Dissertation an der Fakultät III der TU Berlin*.

Kieber, R.J., Skrabal, S.A., Smith, B.J. and J.D. Willey (2005) Organic complexation of Fe(II) and its impact on the redox cycling of iron in rain. *Environ. Sci. Technol*. 39, 1576-1583.

Kohn, T., Livi, K.J.T., Roberts, A.L. and P.J. Vikesland (2005) Longevity of granular iron in groundwater treatment processes: corrosion product development. *Environ. Sci. Technol*., 39, 8, 2867-2879.

Korshin, G.V., Benjamin, M.M. and R.S. Sletten (1997) Adsorption of natural organic matter (NOM) on iron oxide: effects on NOM composition and formation of organo-halide compounds during chlorination. *Wat. Res*., 31, 7, 1643-1650.

Komnitsas, K., Bartzas, G., Fytas, K. and I. Paspaliaris (2007) Long-term efficiency and kinetic evaluation of ZVI barriers during clean-up of copper containing solutions, *Minerals Engineering,* 20, 200-1209.

Kouznetsova, I., Bayer, P., Ebert, M. and M. Finkel (2007) Modelling the long-term performance of zero-valent iron using a spatio-temporal approach for iron aging. *J. Cont. Hydrol*., 90, 1/2, 58-80.

Ku, Y. and C.H. Chen (1992) Kinetic study of copper deposition on iron by cementation reaction. *Sep. Sci. and Tech.*, 27, 10, 1259-1275.

Kuch, A. (1984) Untersuchungen zum Mechanismus der Aufeisenung in Trinkwasserverteilungssystemen. *Ph.D. Dissertation*, University of Karlsruhe.

Langmuir, I. (1918) The adsorption of gases on plane surfaces of glass, mica and platinum. *J. Amer. Chem. Soc.,* 40, 1361-1403.

Laxen, D.P.H. (1985) Trace metal adsorption/coprecipitation on hydrous ferric oxide under realistic conditions. *Wat. Res.*, 19, 10, 1229-1236.

Lebeth, F. (1999) Erfordernisse des Gewässerschutzes bei der Versickerung von Dachflächenwässern. *Österreichische Wasser- und Abfallwirtschaft,* 51, 1/2, 18-28.

Lee, N., Amy, G. Croué, J.-P. and H. Buisson (2004) Identification and understanding of fouling in low-pressure membrane (MF/UF) filtration by natural organic matter (NOM). *Wat. Res.*, 38, 4511-4523.

Leenheer, J. A. (2004) Comprehensive assessment of precursors, diagenesis, and reactivity towater treatment of dissolved and colloidal organic matter. *Conference proceedings: NOM research: Innovation and applications for drinking water treatment*, Victor Harbor, Australia.

Lygren, E., Gjessing, E. and L. Berglind (1984) Pollution transport from a highway, *Sci. Total Environ*., 33, 147-159.

Liang, L., Sullivan, A.B., West, O.R., Moline, G.R. and W. Kamolpornwijit (2003) Predicting the precipitation of mineral phases in permeable reactive barriers. *Environ. Eng. Sci.,* 20, 6, 635-653.

Liang, L., McNabb, J.A., Paulk, J.M., Gu, B. and J.F. McCarthy (1993) Kinetics of Fe(II) oxygenation at low partial pressure of oxygen in the presence of natural organic matter. *Environ. Sci. Technol*., 27, 1864-1870.

López, F.A., Martín, M.I., Pérez, C., López-Delgado, A. and F.J. Alguacil (2003) Removal of copper ions from aqueous solutions by a steel-making by-product. *Wat. Res.,* 37, 16, 3883-3890.

Lu, Y. and H.E. Allen (2002) Characterization of copper complexation with natural dissolved organic matter (DOM) – link to acid moieties of DOM and competition by Ca and Mg. *Wat. Res.*, 36, 5083-5101.

Ludwig, T. (2004) Adsorption isotherms of Cu^{2+} and Zn^{2+} on granular ferric hydroxide (GFH). *Unpublished data*, department of water quality control, Technical University of Berlin, Germany.

Ludwig, T. (2007) Kupfer- und Zinkentfernung aus Niederschlagsabfluss von Dächern in einem Eisen-Korrosionssystem (in English: Removal of copper and zinc from roof runoff in an iron-corrosion system). *Ph.D. Dissertation*, Institute of process engineering, Technical University of Berlin, Germany.

Lung, T.N. (1986) The history of copper cementation on iron-the world's first hydrometallurgical process from medieval china. *Hydrometallurgy*, 17, 113-129.

Ma, H., Allen, H.E and Y. Yin (2001) Characterization of isolated fractions of dissolved organic matter from natural waters and a wastewater effluent. *Wat. Res*., 35, 985-996.

MacCarthy, P., Mark, H.B., Jr., and P.R. Griffiths (1975) Direct measurement of the infrared spectra of humic substances in water by fourier transform infrared spectroscopy. *J. Agr. Food Chem.* 23, 600-602.

Maike, M. (2005) Method for fractionation of NOM, Chair Waste Management and Environmental Research, Technical Universtiy of Berlin.

Maithreepala, R.A. and R.-A. Doong (2004) Reductive dechlorination of carbon tetrachloride in aqueous solutions containing ferrous and copper ions. *Environ. Sci. Technol.*, 38, 260-268.

Mann, A.W. and D.L. Deutscher (1980) Solution geochemistry of lead and zinc in water containing carbonate, sulphate, and chloride ions. *Chem. Geol.,* 29, 293-311.

Manning, B.A., Hunt M.L., Amrhein C. and J.A. Yarmoff (2002) Arsenic(III) and arsenic(V) reactions with zerovalent iron corrosion products. *Environ. Sci. Technol., 36*, 24, 5455-5461.

Meihr, R., Tratnyek, P.G., Bandstra, J.Z., Scherer, M.M., Alowitz, M.J. and E.J. Bylaska (2004) Diversity of contaminant reduction reactions by zero-valent iron: role of reductate. *Environ. Sci. Technol*., 38, 139-147.

Merkel, T. (2002) Untersuchungen zu den chemischen Reaktionen bei der Flächenkorrosion des Kupfers in Trinkwasserinstallationen (in English: Investigation of the chemical corrosion of copper surface in drinking water installation). *Ph.D. Dissertation*, University of Karlsruhe, Germany.

Merkel, B. J. and B. Planer-Friedrich (2005) Groundwater Geochemistry: A practical guide to modeling of natural and contaminated aquatic systems, (Edited by Darrell Kirk Nordstorm), *Springer-Verlag*, Berlin Heidelberg.

Mertz, K.A., Gobin, F., Hand, D.W., Hokanson, D.R. and J.C. Crittenden (1999) Manual adsorption design software for windows (AdDesignS^{TM}), Michigan technological university.

Morel, F.M.M., and J.G. Hering (1993) Principles and applications of aquatic chemistry. *Wiley-Interscience*, New York.

Morrison, S.J. Metzler, D.R. and B.P. Dwyer (2002) Removal of As, Mn, Mo, Se, U, V and Zn from groundwater by zero-valent iron in a passive treatment cell: reaction progress modeling. *J. Contam. Hydrol.,* 56, 99-116.

Mullet, M., Fievet, P., Reggiani, J.C. and J. Pagetti (1997) Surface electrochemical properties of mixed oxide ceramic membranes: zeta-potential and surface charge density. *J. Membrane Science.,* 123, 255-265.

Mustafa, S., Dilara, B., Nargis, K., Naeem, A. and P. Shahida (2002) Surface properties of the mixed oxides of iron and silica. *Colloids. Surface., A* 205, 273-282.

Nadkarni, R.M., Jelden, C.E., Bowles, K.C., Flanders, H.E. and M.E. Wadsworth (1967) A kinetic study of copper precipitation on iron: part I. *Trans. Met. Soc. AIME.*, 239, 581-585.

Nadkarni, R.M. and M.E. Wadsworth (1967) A kinetic study of copper precipitation on iron: part II. *Trans. Met. Soc. AIME*, 239, 1066-1074.

Naftz, D.L., Morrison, S.J., Fuller, C.C. and J.A. Davis (2002) Handbook of groundwater remediation using permeable reactive barriers: applications to radionuclides, trace metals, and nutrients. Elsevier Science.

Nikolaidis, P.N., Dobbs, G.M. and J.A. Lackovic (2003) Arsenic removal by zero-valent iron: field, laboratory and modelling studies, *Wat. Res*., 37, 1417-1425.

Noubactep, C., Meinrath, G., Dietrich, P. and B. Merkel (2003) Mitigating uranium in groundwater: prospects and limitations. *Environ. Sci. Technol*., 37, 4304-4308.

Noubactep, C. (2008a) Processes of contaminant removal in "Fe^0-H_2O" systems revisited: the important of co-orecipitation, *The open Environmental Journal,* 1, 9-13.

Noubactep, C. (2008b) A critical review on the process of contaminant removal in Fe^0-H_2O systems, *Environ. Technol.,* 29, 909-920.

Oden, W. I., Amy, G.L. and M. Conklin (1993) Subsurface interactions of humic substances with Cu(II) in saturated media. *Environ. Sci. Technol*., 27, 6, 1045-1051.

Odziemkowsi, M.S., Schumacher, T.T., Gillham, R.W. and E.J. Readon (1998) Mechanism of oxide film formation on iron in simulating groundwater solutions: raman spectroscopic studies. *Corrosion Science.,* 40, 2/3, 371-389.

Perdue, E.M. (1985) Acidic functional groups of humic substances - in humic substances in soil, sediment, and water: geochemistry, isolation and characterization. *John Wiley and Sons*, New York NY.

Phillips, D.H., Gu, B., Watson, D.B., Roh, Y., Liang, L. and S.Y. Lee (2000) Performance evaluation of a zerovalent iron reactive barrier: mineralogical characteristics. *Environ. Sci. Technol*., 34, 4169-4176.

Pitt, R. (1996) Groundwater contamination from stormwater infiltration, Ann Arbor Press, Inc., Chelsea, Michigan.

Polkowska, Z., Górecki, T., and J. Namie´snik (2002) Quality of roof runoff waters from an urban region (Gda´nsk, Poland). *Chemosphere*, 49, 1275-1283.

Priggemeyer, S. and S. Priggemeyer (1999) Metallkonzentrationen in Dachablaufwässern. *Metall,* 53, 4, 204-205.

Qiu, S.R., Lai, H.-F. and M.J. Roberson (2000) Removal of contaminants from aqueous solution by reaction with iron surfaces. *Langmuir*, 16, 2230-2236.

Rangsivek, R. and M.R. Jekel (2005) Removal of dissolved metals by zero-valent iron (ZVI): Kinetics, equilibria, processes and implications for stormwater runoff treatment. *Wat. Res*., 39, 4153-4163.

Rangsivek, R. and M.R. Jekel (2007) Development of an on-site Fe^0 system for treatment of copper- and zinc- contaminated roof runoff. accepted for publication in International Journal of Environment and Waste Management (IJEWM): "Metal ions removal from liquid effluents".

Rangsivek, R. and M.R. Jekel (2008) Natural organic matter (NOM) in roof runoff and its impact on the Fe^0 treatment system of dissolved metals, *Chemosphere*, 71, 18-29.

Reardon, E.J. (1995) Anaerobic corrosion of granular iron: measurement and interpretation of hydrogen evolution rates, *Environ. Sci. Technol*., 29, 2936-2945.

Revitt, D.M., Hamilton, R.S. and R.S. Warren (1990) The transport of heavy metals within a small urban catchment. *Sci. Total Environ.*, 93, 329-337.

Robertson, W.D. and J.A. Cherry (1995) In instu denitrification of septic-system nitrate using reactive porous media barriers: Field trials. *Ground Water*, 33, 99-111.

Rodda, D.P., Johnson, B.B., and J.D. Wells (1993) The effect of temperature and pH on the adsorption of Copper(II), Lead(II) and Zinc(II) onto goethite. *J. Colloid Interf. Sci*., 161, 57-62.

Roh, Y., Lee, S.Y., and MP. Elless (2000) Characterization of corrosion products in the permeable reactive barriers, *Environ. Geol.,*40, 1-2, 184-194.

Senesi, N. (1990). Molecular and quantitative aspects of the chemistry of fulvic acid and its interactions with metal ions and organic chemicals. Part II. The fluorescence spectroscopy approach. *Analytica Chimica Acta,* 232, 77-106.

Sigg, L. and W. Stumm (1996) Aquatische Chemie. B.G. Teubner, Stuttgart.

Schecher, W.D. and D.C. McAvoy (2001) Thermodynamic data used in $MINEQL^+$ Version 4.5. Environmental Research Software. Hallowell ME 04347.

Simon, F., Meggyes, T., Tunnerrneier, T., Czurda, K., and K.E. Roehl (2001) Long-term behaviour of permeable reactive barriers used for the remediation of contaminated groundwater. *In 8th International Conference on Radioactive Waste Management and Environmental Remediation*, Sep 30–Oct 4, Bruges, Belgium: American Society of Mechanical Engineers.

Shokes, T.E. and G. Möller. (1999) Removal of dissolved heavy metals from acid rock drainage using iron metal. *Environ. Sci. Technol.,* 33, 282-287.

Smith, E.H. (1996) Uptake of heavy metals in batch systems by a recycled iron-bearing material. *Wat. Res.,* 30**,** 10, 2424-2434.

Smith, E.H. (1995) A recycled iron material for fixed-bed adsorption of heavy metals from industrial wastewaters. *Proceedings, 68th Water Environ.* Fed. Annual Conf., Water Environ. Fed., Washington, DC, 3, 559-570.

Smith, E.H. (1998) Surface complexation modelling of metal removal by recycled iron sorbent, *J. of Environ. Eng.,* 124, 10, 913-920.

Smith, S.E., Bisset, A., Colbourne, J.S., Holt, D.M. and B.J. Lloyd (1997) The occurrence and significance of particles and deposits in a drinking water distribution system. *Journal of the New England Water Works Association,* 111, 2, 135

Sontheimer, H., Crittenden, J.C. and R.S. Summers (1988) Activated carbon for water treatment. DVGW-Forschungsstelle am Engler-Bunte-Institut der Universität Karlsruhe, Karlsruhe. Second edition in english of adsorptionsverfahren zur wasserreinigung.

Specht, C.H., Kumke, M.U. and F.H. Frimmel (2000) Characterization of NOM adsorption to clay minterals by size exclusion chromatography. *Wat. Res.*, 34,16, 4063-4069.

Sperlich, A., Werner, A., Genz, A., Amy, G., Worch, E. and M. Jekel (2005) Breakthrough behavior of granular ferric hydroxide (GFH) fixed-bed adsorption filters: modeling and experimental approaches, *Wat. Res*., 39, 6, 1190-1198.

Sperlich, A., Schimmelpfenning, S., Baumgarten, B., Genz, A., Amy, G., Worch, E. and M. Jekel (2008) Predicting anion breakthrough in granular ferric hydroxide (GFH) adsorption filters. *Wat. Res.,* 42, 2073-2082.

Steiner, M. (2003) Adsorption von Kupfer aus Niederschlagsabflüssen an granuliertes Eisenhydroxid. PhD. Dissertation, Swiss Federal Institute of Technology Zurich (ETHZ), Switzerland.

Steiner, M., Pronk, W. and M.A. Boller (2006) Modeling of copper sorption on to GFH and design of full-scale GFH adsorbers, *Environ. Sci. Technol*., 40, 1629-1635.

Stevenson, F.J. (1994) Humus chemistry: genesis, composition and reactions. *John Wiley & Sons*.

Stotz, G. (1987) Investigations of the properties of the surface water run-off from federal highways in the FRG*, Sci.Total Environ.*, 59, 359-373.

Strickland, P.H. and F. Lawson (1971) The cementation of metals from dilute aqueous solutions. *Proc. Aust. Inst. Min. Met.,* 237, 71-78.

Stumm, W. (1957) Corrosion studies. *Public Works,* 88, 12, 78.

Stumm, W. (1959) Estimating corrosion rates in water. *Ind. and Eng. Chem.,* 51,12, 1487.

Su, C. and R.W. Puls (2004) Significance of iron(II,III) hydroxycarbonate green rust in arsenic remediation using zerovalent iron in laboratory column tests. *Environ. Sci. Technol.*, 38, 19, 5224 - 5231.

Teermann, I. and M. Jekel (1999) Adsorption of humic substances onto ß-FeOOH and its chemical regeneration. *Wat. Sci. Tech.,* 40**,** 9, 199-206.

Tipping, E., and D. Cooke (1982) The effects of adsrobed humic substances on the surface charge of goethite (α-FeOOH) in freshwaters. *Geochim. Cosmochim. Acta*, 46, 75-80.

Tombácz, E., Zsuzsanna, L., Illés, E., Majzik, A. and E. Klumpp (2004) The role of reactive surface sites and complexation by humic acids in the interaction of clay mineral and iron oxide particles. *Org. Geochem*. 35, 257-267.

Tombre, M.S., Thomson, B.M. and L.L. Barton (1997) Use of a permeable biological reaction barrier for groundwater remediation at a uranium mill tailings remedial action (UMTRA) site. In "*International containment technology conference prodeedings*" Febuary 9-12, St. Petersburg, FL., pp. 744-750.

Tratnyek, P.G., Scherer, M.M., Deng, B. and S. Hu (2001) Effects of natural organic matter, anthropogenic surfactants, and model quinines on the reduction of contaminants by zero-valent iron. *Wat. Res.* 35, 18, 4435-4443.

Tyrovola, K., Peroulaki, E. and N.P. Nikolaidis (2007) Modelling of arsenic immobilization by zero valent iron. *Eur. J. Soil Biol.*, 43, 356-367.

Voskamp, M., Abbt-Braun, G. and F.H. Frimmel (2005) Metallische Dachmaterialien als Quelle für die Schwermetalle Kupfer und Zink im Regenwasserablauf. Vortrag auf der 71. Jahrestagung der Wasserchemischen Gesellschaft in Bad Mergentheim.

Wang, Y. and K. Salvage (2005) Immobilization of uranium in the presence of $Fe_{0(s)}$: model development and simulation of contrasting experimental conditions. *Appl. Geochem.,* 20, 1268-1283.

Wilkin, R.T. and M.S. McNeil (2003) Laboratory evaluation of zero-valent iron to treat water impacted by acid mine drainage. *Chemosphere*, 53, 715-725.

Wong, S., Hanna, J.V., King, S., Carroll, T.J., Eldridge, R.J., Dixon, D.R., Bolto, B.A., Hesse S., Abbt-braun, G. and F.H. Frimmel (2002) Fractionation of natural organic matter in

drinking water and characterization by 13C cross-polarization magic-angle spinning NMR spectroscopy and size exclusion chromatography. *Environ. Sci. Technol.* 36, 3497-3505.

Yoon, Y., Amy, G., Cho, J. and N. Her (2005) Effect of retained natural organic matter on NOM rejection and membrane flux decline with nanofiltration and ultrafiltration. *Desalination,* 173, 209-221.

Appendix A: Relevant information

Table A1 Physical and chemical data of iron, copper and zinc.
[Ref: http://www.lenntech.com/periodic/elements; Ludwig, 2007]

Chemical properties	unit	iron	copper	Zinc
Atomic number		26	29	30
Atomic mass	g mol^{-1}	55,85	63,55	65,37
Density	kg L^{-1}	7,8	8,92	7,11
Melting point	°C	1536	1083	420
Boiling point	°C	2861	2595	907
Oxidation number		0, 2, 3	0, 1, 2	0, 2
Electronic shell		$[Ar]3d^6 4s^2$	$[Ar]\ 3d^{10}4s^1$	$[Ar]3d^{10}4s^2$
Energy of first ionization	kJ mol^{-1}	761	743,5	904,5
Vanderwaals radius	nm	0,126	0,128	0,138
Ionic radius	nm	0,076 (+2) 0,064(+3)	0,069(+3) 0,096(+1)	0,074(+2)
Standard potentials	mV	-440(Fe^{2+}/Fe^0) +770(Fe^{3+}/Fe^{2+})	+522(Cu^+/Cu^0) +345(Cu^{2+}/Cu^0)	-763(Zn^{2+}/Zn^0)

Table A2 Concentration of copper and zinc in roof, street and highway runoff samples*

Year	City	Characteristic	Copper conc. [mg L^{-1}]	Zinc conc. [mg L^{-1}]	Reference
1988	Bayreuth	Zinc roof		10-85	Förster (1993)
1991	Wien	N.A.	0.2	1.5	Lebeth (1999)
1997	Osnabrück	Copper roof	0.5-33		Piggemeyer et al. (1999)
1998	Paris	Zinc roof	0.003-0.25	0.8-38	Gromaire et al. (1999)
2000	Halle	N.A.	0.03	2.58	Gieska et al. (2000)
2001	Dübendorf	Copper roof	0.8-10		Steiner (2003)
		Copper façade	0.9-100		
2001	München	Zinc roof		5-23	Athanasiadis et al. (2003)
2004	Karlsruhe	Copper and Zinc roof	4-13	4-32	Voskamp et al. (2005)
2005	Belzig	Copper roof	1.52-7.61	0.04-0.25	Olaf (2005)
2008	Berlin	Copper and zinc roofs	4.9-9.1	0.8-6	Rangsivek and Jekel (2008)
1994	Denmark	Urban runoff	0.005-0.04	0.3-0.5	Hvitved-Jacobsen (1994)
		Highway runoff		0.125-0.4	Barbosa (1999)

* Parts of data were complied by Ludwig (2007)

Table A3 Concentration of metals in highway runoffs (data complied by Barbosa, 1999)

Country	Site characterisitcs	ADT	Lead [µg L^{-1}]	Zinc [µg L^{-1}]	Copper [µg L^{-1}]	References
Germany	A81-Pleidelsheim	41000	202	360	97	Stotz (1987)
	A6-Oberaisesheim	47000	245	620	117	
	A8/B10; Ulm/West	40600	163	320	58	
Norway	E6 Jessheim	8000	62-690	91-740	10-430	Lygren et al. (1984)
UK	Road in residential area	720	28.10	16.6	6.5	Hamiton et al. (1987)
USA	Maitland Interchange	-	30-379	13-173	10-101	Hvitved-Jacobsen and Yousef (1991)
UK	M6 motorway	37600	181		63	Revitt et al. (1990)
Germany	Street in residential area	500	122	165.6	75.9	Dannecker et al. (1990)
UK	Chilwell Gardens	150	0.6-150.5	0.7-65.3	0.1-14.3	Hewitt and Rashed (1992)
France	Urban and industrial area, Lyon	-	5.0-90.0	177-68.1	9.0-49.0	Bardin et al. (1996)

Table A4 Defined processes of contaminant removal under various experimental conditions

^{S}G - simulated groundwater; T – tabwater; S – simulated water; AMD – acid mine drainage; ^{S}AMD – simulated AMD; R – runoff water; ^{S}R – simulated R
L – laboratory; B – batch study; C – column study

Processes	Matrix	System	Components	conc.	Fe^0 conc.		T	pH_i	Condition	Uptake load	Refs.
				[mg L^{-1}]	[g L^{-1}]	[m^2 L^{-1}]	[°C]	[-]		[mg g Fe^0]	
Reduction	^{S}G	L, B	UO_2^{2+}	0-18,000	200	16-196	-	5		50	1
Co-precipitation	T	L, B	U^{6+}	20	15	-	20	7.2	-	-	2
Adsorption, Reduction	S	L, B	U^{6+}	6-8		~5/9 in dia.		6	Oxic,	-	3
						1/16 in. thick		5.7	Anoxic	-	
Adsorption, Reduction	S	SS	U^{6+}/Cr^{6+} /Se^{6+}	-	Iron foil	-	-	8-8.5	Anoxic	-	4
Adsorption, Co-precipitation	AMD	L, B	As, Ni, Cu, Hg, Mn, Zn	5-65	20-230	1-700	22	2.5-4.5	-	-	5
Adsorption, Reduction	^{S}AMD	L, C	Zn, As, Cu, Cd	2-20	-	-	23	3	-	-	6
Adsorption, Reduction	^{S}G	L, B, A	Cu	2,000	100	0.43	20	5		0.1	7
							80			40	
Reduction	S	L, B	Cu	100	1-2.5	-	15-25	2-8	Anoxic	-	8
Adsorption	S	L, B	Zn	0.1-0.4	0.05-0.8	1.3	-	4		13	9
								7		17	
Adsorption, Reduction	AMD	L, B+C	Cu	150	33	0.005	25	2.1		4.4	10
			Zn	400						0.4	
Co-precipitation	S	L, B	Clofibric acid	10	15, 40		23	4.0	Oxic, Anoxic		11
Adsorption	T	L, B, C	As			0.62 m^2 g^{-1}	20-25	7.5	Oxic,	4-60	12
Adsorption	^{s}R, R	L,C	Cu,	2	20	0.058 m^2	17-29	5.3-8	Oxic,	50-292	13
			Zn	2						35-170	
Reduction	S	L, C	Cu	5,	1050 g	0.048 m^2 g^{-1}	24	2.5-4.5	-	0.93-2.68	14
				50						6.03-13.33	
Adsorption	^{s}G	L, B	Zn, Ni, Cr(VI)	5	2-6	1.5-4.5	-	7.0	Anoxic	0.69-2.79	15
		C		5-10	102	76 m^2				2.0	

Ref: [1]Gu et al. (1998); [2]Noubactep et al. (2003); [3]Fiedor et al. (1998); [4]Qui et al. (2000); [5]Wilkin and McNeil (2003); [6]Gibert et al. (2003); [7]Lopez et al. (2003); [8]Ku and Chen (1992); [9]Smith (1996); [10]Shokes and Moller (1999); [14]Ludwig (2007); [11]Ghauch et al. (accepted); [12]Karshunke (2005); [13]Ludwig (2007);[14]Komnitsas et al (2007); [15]Dries et al (2005)

Appendix B: Supplement data for tables and figures

[The usage of ","and "." in appendix B is based on the European numerical system]

Table B1 Determination of pH_{PZC} by titration method (Fig. 3.2)

Electrolite	0.01 M		$NaNO_3$			0.051045				
Tritrants	0.2 g									
	mL 0.05M		mol/dm^{-3}		M					
	NaOH added	pH	Acid	Base mol l^{-1}	NO^{3-}	Na^+	OH^-	H^+		
0	0	2,44	0,005	0,00000	0,001	0,00000	0,00000	0,00363	0,00137	0,58716
0,12	0,07	2,45	0,005	0,00009	0,001	0,00109	0,00000	0,00355	0,00136	0,58430
0,19	0,14	2,46	0,005	0,00018	0,001	0,00118	0,00000	0,00347	0,00135	0,58063
0,26	0,21	2,46	0,005	0,00027	0,001	0,00127	0,00000	0,00347	0,00126	0,54232
0,32	0,27	2,47	0,005	0,00034	0,001	0,00134	0,00000	0,00339	0,00127	0,54333
0,38	0,33	2,48	0,005	0,00042	0,001	0,00142	0,00000	0,00331	0,00127	0,54357
0,44	0,39	2,49	0,005	0,00050	0,001	0,00150	0,00000	0,00324	0,00127	0,54306
0,51	0,46	2,5	0,005	0,00059	0,001	0,00159	0,00000	0,00316	0,00125	0,53634
0,58	0,53	2,51	0,005	0,00068	0,001	0,00168	0,00000	0,00309	0,00123	0,52890
0,64	0,59	2,52	0,005	0,00075	0,001	0,00175	0,00000	0,00302	0,00123	0,52623
0,7	0,65	2,53	0,005	0,00083	0,001	0,00183	0,00000	0,00295	0,00122	0,52288
0,77	0,72	2,54	0,005	0,00092	0,001	0,00192	0,00000	0,00288	0,00120	0,51338
0,84	0,79	2,55	0,005	0,00101	0,001	0,00201	0,00000	0,00282	0,00117	0,50322
0,9	0,85	2,57	0,005	0,00108	0,001	0,00208	0,00000	0,00269	0,00122	0,52479
0,97	0,92	2,58	0,005	0,00117	0,001	0,00217	0,00000	0,00263	0,00120	0,51275
1,04	0,99	2,59	0,005	0,00126	0,001	0,00226	0,00000	0,00257	0,00117	0,50012
1,11	1,06	2,6	0,005	0,00135	0,001	0,00235	0,00000	0,00251	0,00114	0,48690
1,18	1,13	2,61	0,005	0,00144	0,001	0,00244	0,00000	0,00245	0,00110	0,47312
1,25	1,2	2,62	0,005	0,00153	0,001	0,00253	0,00000	0,00240	0,00107	0,45877
1,32	1,27	2,64	0,005	0,00162	0,001	0,00262	0,00000	0,00229	0,00109	0,46676
1,39	1,34	2,65	0,005	0,00171	0,001	0,00271	0,00000	0,00224	0,00105	0,45082
1,46	1,41	2,66	0,005	0,00180	0,001	0,00280	0,00000	0,00219	0,00101	0,43436
1,53	1,48	2,68	0,005	0,00189	0,001	0,00289	0,00000	0,00209	0,00102	0,43828
1,6	1,55	2,69	0,005	0,00198	0,001	0,00298	0,00000	0,00204	0,00098	0,42037
1,66	1,61	2,71	0,005	0,00205	0,001	0,00305	0,00000	0,00195	0,00100	0,42694
1,76	1,71	2,72	0,005	0,00218	0,001	0,00318	0,00000	0,00191	0,00091	0,39125
1,81	1,76	2,74	0,005	0,00225	0,001	0,00325	0,00000	0,00182	0,00093	0,40067
1,88	1,83	2,76	0,005	0,00234	0,001	0,00334	0,00000	0,00174	0,00093	0,39748
1,94	1,89	2,78	0,005	0,00241	0,001	0,00341	0,00000	0,00166	0,00093	0,39819
2,01	1,96	2,79	0,005	0,00250	0,001	0,00350	0,00000	0,00162	0,00088	0,37608
2,09	2,04	2,81	0,005	0,00260	0,001	0,00360	0,00000	0,00155	0,00085	0,36360
2,16	2,11	2,83	0,005	0,00269	0,001	0,00369	0,00000	0,00148	0,00083	0,35519
2,23	2,18	2,85	0,005	0,00278	0,001	0,00378	0,00000	0,00141	0,00081	0,34543
2,3	2,25	2,87	0,005	0,00287	0,001	0,00387	0,00000	0,00135	0,00078	0,33438
2,37	2,32	2,89	0,005	0,00296	0,001	0,00396	0,00000	0,00129	0,00075	0,32211
2,45	2,4	2,92	0,005	0,00306	0,001	0,00406	0,00000	0,00120	0,00074	0,31521
2,52	2,47	2,94	0,005	0,00315	0,001	0,00415	0,00000	0,00115	0,00070	0,30010
2,59	2,54	2,97	0,005	0,00324	0,001	0,00424	0,00000	0,00107	0,00069	0,29466
2,66	2,61	3	0,005	0,00333	0,001	0,00433	0,00000	0,00100	0,00067	0,28702
2,73	2,68	3,03	0,005	0,00342	0,001	0,00442	0,00000	0,00093	0,00065	0,27734
2,8	2,75	3,06	0,005	0,00351	0,001	0,00451	0,00000	0,00087	0,00062	0,26574
2,86	2,81	3,09	0,005	0,00359	0,001	0,00459	0,00000	0,00081	0,00060	0,25784
2,92	2,87	3,13	0,005	0,00366	0,001	0,00466	0,00000	0,00074	0,00060	0,25567
2,99	2,94	3,17	0,005	0,00375	0,001	0,00475	0,00000	0,00068	0,00057	0,24534
3,07	3,02	3,21	0,005	0,00385	0,001	0,00485	0,00000	0,00062	0,00053	0,22707
3,14	3,09	3,25	0,005	0,00394	0,001	0,00494	0,00000	0,00056	0,00049	0,21203
3,22	3,17	3,3	0,005	0,00405	0,001	0,00505	0,00000	0,00050	0,00045	0,19447
3,3	3,25	3,36	0,005	0,00415	0,001	0,00515	0,00000	0,00044	0,00042	0,17843
3,37	3,32	3,42	0,005	0,00424	0,001	0,00524	0,00000	0,00038	0,00038	0,16427
3,45	3,4	3,49	0,005	0,00434	0,001	0,00534	0,00000	0,00032	0,00034	0,14477

3,52	3,47	3,58	0,005	0,00443	0,001	0,00543	0,00000	0,00026	0,00031	0,13243
3,59	3,54	3,69	0,005	0,00452	0,001	0,00552	0,00000	0,00020	0,00028	0,11936
3,67	3,62	3,83	0,005	0,00462	0,001	0,00562	0,00000	0,00015	0,00023	0,09971
3,74	3,69	4,04	0,005	0,00471	0,001	0,00571	0,00000	0,00009	0,00020	0,08572
3,81	3,76	4,4	0,005	0,00480	0,001	0,00580	0,00000	0,00004	0,00016	0,06945
3,87	3,82	5,03	0,005	0,00487	0,001	0,00587	0,00000	0,00001	0,00012	0,04969
4	3,95	7,3	0,005	0,00504	0,001	0,00604	0,00000	0,00000	-0,00004	-0,01741
4,06	4,01	8,21	0,005	0,00512	0,001	0,00612	0,00000	0,00000	-0,00012	-0,04982
4,13	4,08	9,07	0,005	0,00521	0,001	0,00621	0,00001	0,00000	-0,00020	-0,08519
4,21	4,16	9,5	0,005	0,00531	0,001	0,00631	0,00002	0,00000	-0,00029	-0,12320

Table B2 Determination of pH_{PZC} by salt addition method (Fig. 3.2)

$Salt_0$	0,001	NaNO3
$Salt_f$	0,1	NaNO3

pH_0	pH_f	pH_f-pH_0	charge
4,61	5,26	0,65	
6,77	6,89	0,12	0,0256
7,04	7,09	0,05	0,0099
7,33	7,28	-0,05	-0,0124
7,81	7,6	-0,21	-0,1102

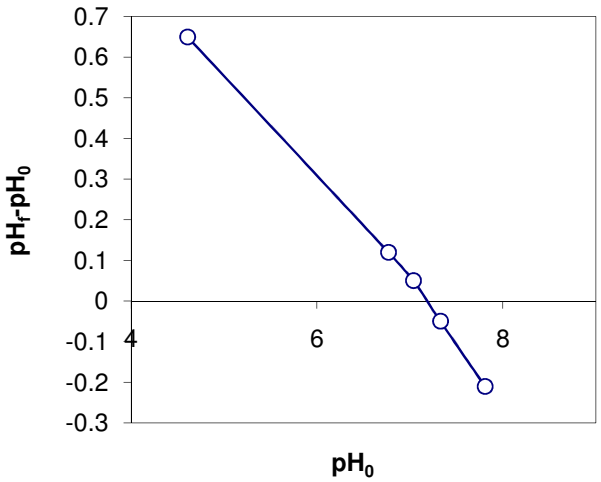

Table B3 Determination of surface area of Fe^0 (Table 3.2)

Started:	24.10.2003	10:21:53	Sat. Pressure:	762.40	mmHg
Completed:	24.10.2003	14:22:11	Meas. Freespace:	0,1983	cm^3
Report Time:	27.10.2003	10:11:35	Sample Weight:	0,1014	g
Evac. Rate:	500.0 mmHg min^{-1}		Evac. Time:	0,500000	minutes
Analysis Mode:	Equilibration		Equil. Interval:	5	secs

Summary Report

Sing point surface area at P/P_0 0,29699657:	0,3118	$m^2 g^{-1}$
BET surface area:	0,3844	$m^2 g^{-1}$
Langmuir surface area:	0,5893	$m^2 g^{-1}$
Single point total pore volume of pores less than 166,8517 nm diameter at P/P_0 0,98827072:	0,000004	$cm^3 g^{-1}$
Average pore diameter (4V/A by BET)	0,0381	nm

Langmuir Surface Area Report

Langmuir Surface Area:	0,5893	±	0,0909	$m^2 g^{-1}$
Slope:	7,387357	±	1,139686	
Y - Intercept:	0,094211	±	0,219888	
b:	0,012753			
VM:	0,135366		$cm^3 g^{-1}$ STP	
Correlation Coefficient:	8,902320E-10			
Molecular Cross-sections:	0,1620	nm^2		

Relative Pressure	Vol Adsrobed [$cm^3 g^{-1}$ STP]	1/[VA x (P_0/P)]
0,059417626	0,0672	0,883601
0,079230059	0,0877	0,903582
0,098996585	0,1027	0,96381
0,118815577	0,1338	0,887783
0,138582103	0,1487	0,931899
0,158387977	0,1472	1,076319
0,178154502	0,1510	1,179594
0,197940712	0,1494	1,32523
0,217740031	0,1530	1,422981
0,237539350	0,1512	1,571348
0,257312430	0,1384	1,858534
0,277124858	0,1147	2,415569
0,296891394	0,1019	2,914595

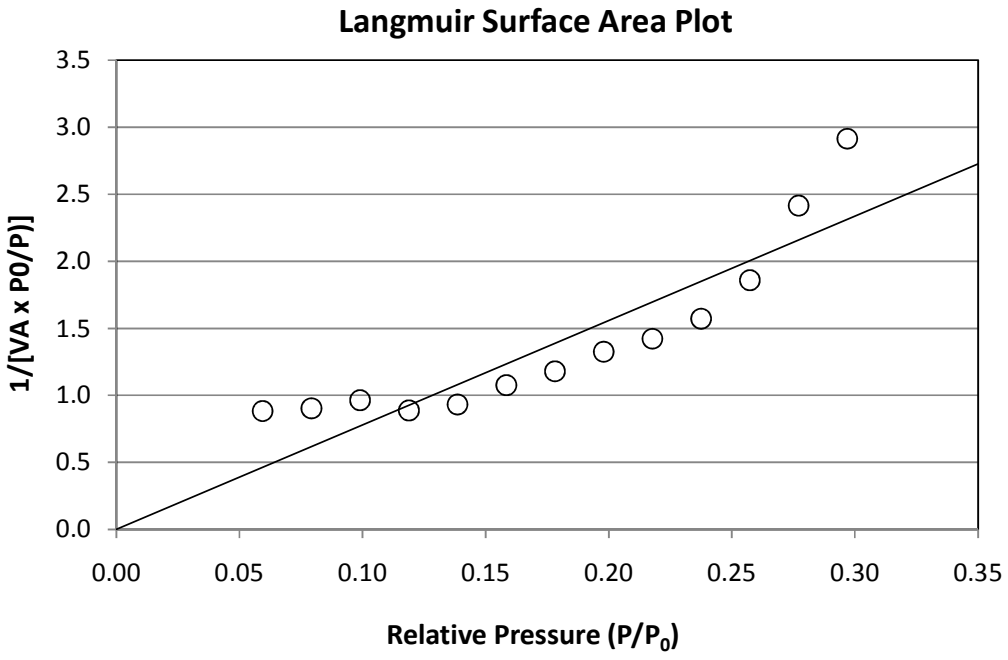

Table B4 Determination of surface area of iron oxides (rust) (Table 3.2)

Started:	03.11.2003	10:53:06	Sat. Pressure:	755,8	mmHg
Completed:	03.11.2003	15:46:20	Meas. Freespace:	0,2162	cm^3
Report Time:	04.11.2003	12:34:27	Sample Weight:	0,0176	g
Evac. Rate:	500.0 mmHg min^{-1}		Evac. Time:	0,500000	minutes
Analysis Mode:	Equilibration		Equil. Interval:	5	secs

Summary Report

Sing point surface area at P/P_0 0,29699657:	44,6559	$m^2 g^{-1}$
BET surface area:	48,7576	$m^2 g^{-1}$
Langmuir surface area:	81,0985	$m^2 g^{-1}$
Single point total pore volume of pores less than 166,8517 nm diameter at P/P_0 0,98827072:	0,187834	$cm^3 g^{-1}$
Average pore diameter (4V/A by BET)	15,4096	nm

Langmuir Surface Area Report

Langmuir Surface Area:	48,7576	±	0,9909	$m^2 g^{-1}$
Slope:	0,087195	±	0,001782	
Y - Intercept:	0,002087	±	0,000344	
b:	42,775239			
VM:	11,200416		$cm^3 g^{-1}$ STP	
Correlation Coefficient:	9,977116E-01			
Molecular Cross-sections:	0,1620	nm^2		

Relative Pressure	Vol Adsrobed [$cm^3 g^{-1}$ STP]	$1/[VA \times (P_0/P)]$
0,059427099	8,2391	0,007669
0,079233923	9,2137	0,00934
0,099001056	10,0321	0,010953
0,118821119	10,7556	0,012537
0,138614714	11,4477	0,014057
0,158288464	12,1083	0,015543
0,178168835	12,6121	0,017189
0,197955819	13,1154	0,018819
0,217775972	13,5552	0,020539
0,237549611	13,8702	0,022463
0,257389530	14,2151	0,024383
0,277176513	14,3727	0,02668
0,296996566	14,5919	0,028952

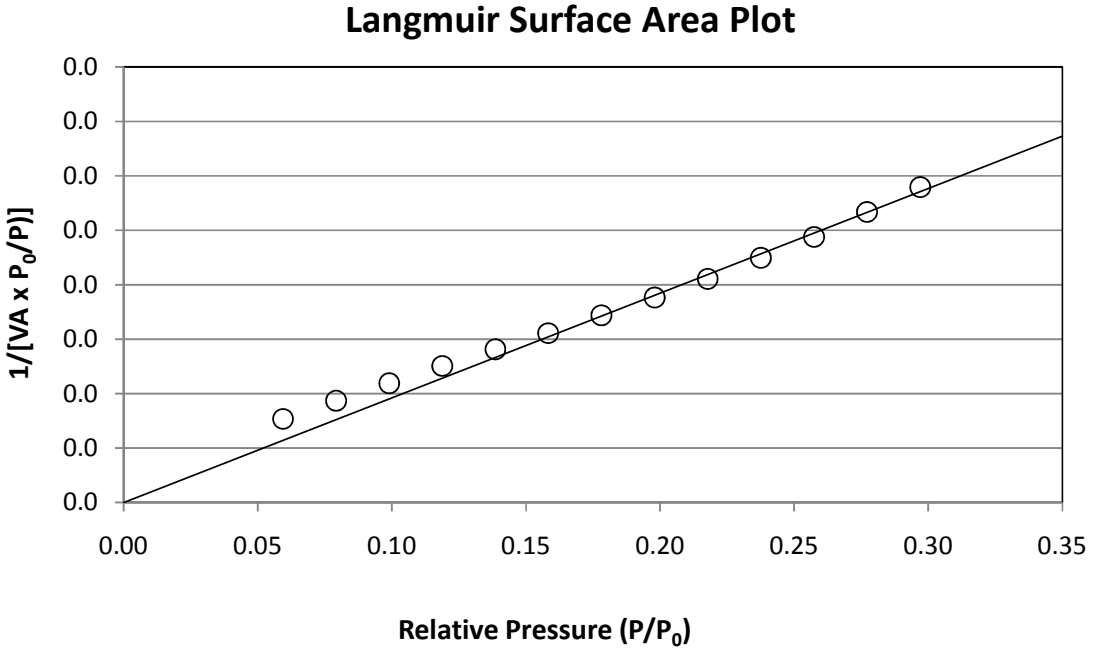

Table B5 Determination of surface area of corroded iron (Table 3.2)

Started:	29.10.2003	10:24:05	Sat. Pressure:	748,3	mmHg
Completed:	29.10.2003	14:43:23	Meas. Freespace:	0,3371	cm^3
Report Time:	30.10.2003	10:50:53	Sample Weight:	0,1515	g
Evac. Rate:	500.0 mmHg min^{-1}		Evac. Time:	0,500000	minutes
Analysis Mode:	Equilibration		Equil. Interval:	5	secs

Summary Report

Sing point surface area at P/P_0 0,29699657:	4,1863	$m^2 g^{-1}$
BET surface area:	4,3106	$m^2 g^{-1}$
Langmuir surface area:	6,7322	$m^2 g^{-1}$
Single point total pore volume of pores less than 166,8517 nm diameter at P/P_0 0,98827072:	0,012535	$cm^3 g^{-1}$
Average pore diameter (4V/A by BET)	11,6319	nm

BET surface area report:

BET surface area:	4,3106	±	0,0876	$m^2 g^{-1}$
Slope:	1,010515	±	0,020142	
Y - Intercept:	-0,000644	±	0,003888	
b:	-1569,007623			
VM:	0,990225		$cm^3 g^{-1}$ STP	
Correlation Coefficient:	9,978219E-01			
Molecular Cross-sections:	0,1620	nm^2		

Relative Pressure	Vol Adsrobed [$cm^3 g^{-1}$ STP]	$1/[VA \times (P_0/P)]$
0,05948149	0,9509	0,06651
0,07927903	1,0269	0,83848
0,099057866	1,0884	0,101018
0,118876124	1,1352	0,118847
0,13866097	1,1783	0,136618
0,158412405	1,2178	0,15456
0,178223985	1,2462	0,174025
0,198028865	1,2746	0,193735
0,217853811	1,2991	0,214399
0,237625291	1,3201	0,236111
0,257430172	1,3337	0,259943
0,277201652	1,3472	0,284674
0,296979820	1,3679	0,30882

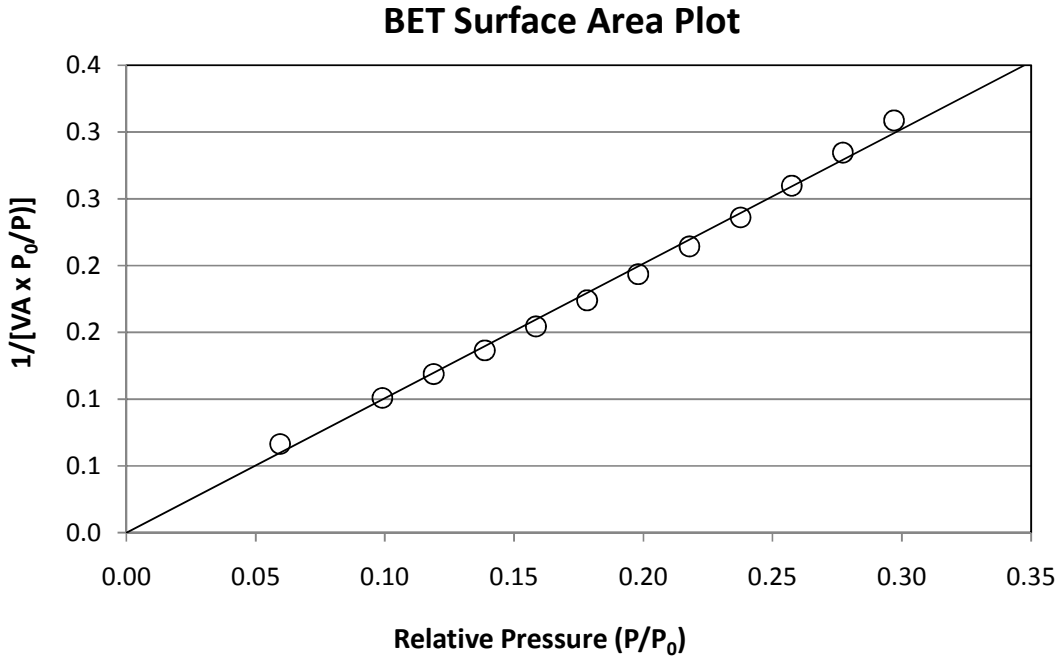

Table B6 Determination of Pb^{2+} removal in Fe^0 system with pulsed dosing (Fig. 4.2)

Metrix:	Pb^{2+} in model roof runoff
Pb^{2+}:	5 mg L^{-1}
pH:	5,0 controlled
Conductivities:	80-200 µS cm^{-1}
Temperature:	20 °C
Fe^0 bed:	0,5 g Fe^0

				C/C_0			
Time	**h**	**Pb^{2+}**	**Fe^{2+}**	**Fe conc.**	**Pb**	**ΔPb removed**	**Total ΔPb remove**
0	0,0	5,00	0,08	0	1,00	0,00	0,00
0,05	0,0	5,00	0,13	0,05	1,00	0,00	0,00
0,35	0,4	4,60	0,16	0,08	0,92	0,40	0,40
1,05	1,1	4,15	0,2	0,12	0,83	0,85	0,85
1,35	1,4	3,85	0,27	0,19	0,77	1,15	1,15
2,05	2,1	3,50	0,33	0,25	0,70	1,50	1,50
2,35	2,4	3,10	0,38	0,3	0,62	1,90	1,90
3,05	3,1	2,98	0,45	0,37	0,60	2,02	2,02
0	0,4	6,95	0,55	0,47	1,00	0,00	2,02
0,05	0,5	6,88	0,58	0,5	0,99	0,07	2,09
0,35	0,8	6,48	0,83	0,75	0,93	0,47	2,49
1,05	1,5	5,89	0,98	0,9	0,85	1,06	3,08
1,35	1,8	5,49	1,17	1,09	0,79	1,46	3,48
2,05	2,5	5,45	1,26	1,18	0,78	1,50	3,52
2,35	2,8	5,05	1,35	1,27	0,73	1,90	3,92
3,05	3,5	4,74	1,46	1,38	0,68	2,21	4,23
0	0,1	9,15	1,51	1,43	1,00	0,00	4,23
0,05	0,2	9,13	1,54	1,46	1,00	0,02	4,25
0,35	0,5	8,42	1,68	1,6	0,92	0,73	4,96
1,05	1,2	7,70	1,82	1,74	0,84	1,45	5,68
1,35	1,5	7,21	1,89	1,81	0,79	1,94	6,17
2,05	2,2	6,77	1,96	1,88	0,74	2,38	6,61
2,35	2,5	6,43	1,98	1,9	0,70	2,72	6,95
3,05	3,2	6,03	2,06	1,98	0,66	3,12	7,35
0	0,8	11,05	2,15	2,07	1,00	0,00	7,35
0,05	0,9	11,04	2,19	2,11	11,04	0,01	7,36
0,35	1,2	11,01	2,56	2,48	11,01	0,04	7,39
1,05	1,9	10,25	2,7	2,62	10,25	0,80	8,15
1,35	2,2	9,61	2,67	2,59	9,61	1,44	8,79
2,05	2,9	8,99	2,72	2,64	8,99	2,06	9,41
2,35	3,2	8,53	2,88	2,8	8,53	2,52	9,87
3,05	3,9	8,22	3	2,92	8,22	2,83	10,18

Table B7 Results of batch investigation to determine the impact of pH and DO (Fig. 4.3)

Metrix: Cu^{2+}/Zn^{2+} in DI water
Cu^{2+}: 4-5 mg L^{-1}
Zn^{2+}: 4-5 mg L^{-1}
Conductivity: 80 µS cm^{-1}
Temperature: 20 °C
DO_i: 0 and 7-8 mg L^{-1}
Fe^0: 0,5 g Fe^0

c/c_0 of copper

h	pH 4	pH 4 DO 0	pH 5	pH 5 DO 0	pH 6	pH 6 DO 0	pH 7	pH 7 DO 0
0,05	1,00	1,00	1,00	1,00	1,00	1,00	1,00	1,00
1,05	1,00	0,93	0,90	0,98	1,00	1,00	0,88	1,00
2,05	0,78	0,85	0,72	0,89	0,76	0,87	0,71	0,91
3,05	0,64	0,82	0,52	0,78	0,51	0,72	0,38	0,70
4,05	0,53	0,73	0,34	0,70	0,36	0,62	0,24	0,58
5,05	0,45	0,66	0,24	0,62	0,25	0,54	0,18	0,49
6,05	0,38	0,57	0,17	0,57	0,20	0,48	0,15	0,33
8,05	0,31	0,55	0,14	0,51	0,15	0,42	0,12	0,28
10,05	0,22	0,43	0,08	0,43	0,12	0,29	0,09	0,25
12,05	0,15	0,35	0,07	0,34	0,12	0,25	0,06	0,18
14,05	0,13	0,28	0,05	0,35	0,08	0,20	0,06	0,16
16,05	0,10	0,25	0,03	0,26	0,07	0,17	0,06	0,12
18,05	0,09	0,18	0,03	0,21	0,05	0,15	0,06	0,11
20,05	0,10	0,14	0,03	0,17	0,05	0,14	0,06	0,09
22,05	0,11	0,11	0,03	0,15	0,03	0,11	0,06	0,09
24,05	0,14	0,10	0,02	0,11	0,03	0,09	0,06	0,07

c/c_0 of zinc

h	pH 4	pH 4 DO 0	pH 5	pH 5 DO 0	pH 6	pH 6 DO 0	pH 7	pH 7 DO 0
0,05	1,00	1,01	1,00	1,01	1,00	1,00	1,00	1,00
1,05	0,95	1,05	0,94	1,03	0,96	1,00	0,98	1,00
2,05	0,94	1,01	0,89	1,03	0,90	0,99	0,92	1,00
3,05	0,89	1,03	0,78	1,00	0,83	0,97	0,88	0,99
4,05	0,84	0,99	0,77	0,99	0,77	0,95	0,82	1,00
5,05	0,82	1,01	0,70	0,99	0,71	0,94	0,78	0,98
6,05	0,77	0,99	0,66	0,97	0,66	1,00	0,74	0,94
8,05	0,68	0,99	0,59	0,95	0,58	1,00	0,68	0,94
10,05	0,60	0,96	0,51	0,92	0,50	0,96	0,62	0,91
12,05	0,52	0,95	0,45	0,95	0,45	0,91	0,57	0,88
14,05	0,47	1,01	0,40	0,96	0,40	0,89	0,52	0,82
16,05	0,43	0,99	0,36	0,91	0,36	0,85	0,48	0,86
18,05	0,40	0,97	0,34	0,89	0,32	0,81	0,44	0,85
20,05	0,40	0,95	0,30	0,86	0,29	0,79	0,40	0,82
22,05	0,39	0,92	0,27	0,81	0,26	0,78	0,37	0,79
24,05	0,43	0,90	0,26	0,75	0,23	0,75	0,34	0,79

Table B8 Impact of Suwanee river fulvic acid on the kinetic of Cu^{2+} and Zn^{2+} removal (batch system, Table 4.2)

Metrix:	Cu^{2+}/Zn^{2+} in roof runoff
Cu^{2+}:	4-5 mg L^{-1}
Zn^{2+}:	5-7 mg L^{-1}
Conductivities:	80-200 µS cm^{-1}
DOC:	5 mg L^{-1}
Temperature:	20 °C
Fe^0 bed:	0,5 g Fe^0

h	Cu	Zn	Fe	c/c_0 of Cu	c/c_0 of Zn	Cu removed
0	4,55	4,83	0,03	1,00	1,00	0,00
0,05	4,54	4,83	0,07	1,00	1,00	0,01
1,05	3,72	4,73	1,21	0,82	0,98	0,83
2,05	2,92	4,54	2,21	0,64	0,94	1,63
3,05	2,33	4,3	3,07	0,51	0,89	2,22
4,05	1,85	4,17	3,67	0,41	0,86	2,70
5,05	1,46	3,98	4,14	0,32	0,82	3,09
6,05	1,24	3,96	4,89	0,27	0,82	3,31
8,05	0,83	3,73	5,57	0,18	0,77	3,72
10,05	0,58	3,55	6,34	0,13	0,73	3,97
12,05	0,42	3,41	6,98	0,09	0,71	4,13
14,05	0,32	3,3	7,46	0,07	0,68	4,23
16,05	0,26	3,24	8,05	0,06	0,67	4,29
18,05	0,22	3,24	8,88	0,05	0,67	4,33
20,05	0,19	3,12	9,14	0,04	0,65	4,36
22,05	0,17	3,06	9,65	0,04	0,63	4,38
24,05	0,13	2,92	7,76	0,03	0,60	4,42

Table B9 Example of monitoring results of pH, ORP and DO from batch tests (example of Table 4.2)

System:	Batch investigation at pH_i = 5,0		
Metrix:	Cu^{2+}/Zn^{2+} in DI water		
Cu^{2+}:	4-5 mg L^{-1}	Conductivity:	80 µS cm^{-1}
Zn^{2+}:	4-5 mg L^{-1}	Temperature:	20 °C
DO:	7-8 mg L^{-1}	Fe^0:	0,5 g Fe^0

Time [h]	pH [-]	ORP [mV]	DO [mg L^{-1}]
0,00	5,02	308	8,50
0,43	6,16	122	7,40
0,85	6,29	78	6,54
1,27	6,25	75	6,11
1,70	6,31	65	5,79
2,12	6,31	67	5,84
2,54	6,28	71	6,11
2,96	6,31	69	6,17
3,38	6,26	67	5,47
3,80	6,24	72	6,00
4,22	6,25	74	5,36
4,64	6,34	69	5,68
5,06	6,25	69	5,26
5,48	6,30	75	5,31
5,91	6,29	76	5,68
6,75	6,28	79	4,83
7,17	6,29	78	5,26
7,59	6,26	77	4,61
8,01	6,26	78	4,40
8,42	6,29	76	4,51
8,84	6,25	79	4,29
9,27	6,22	80	4,45
9,69	6,28	79	4,56
10,11	6,26	74	4,56
10,53	6,24	77	4,35
10,95	6,20	74	3,97
11,37	6,22	78	4,40
11,79	6,17	80	3,76
12,21	6,20	77	3,54
12,63	6,26	77	3,54
13,05	6,21	74	3,81
13,48	6,17	79	3,54
14,74	6,20	84	3,70
15,16	6,25	80	3,44
15,58	6,24	82	3,76
16,00	6,13	79	3,11
16,42	6,16	83	3,11
16,84	6,16	82	3,01
17,27	6,15	77	3,11
17,69	6,11	84	3,11
18,11	6,14	86	2,90
18,53	6,16	77	3,33
18,95	6,19	86	3,11
19,37	6,14	77	3,44
19,79	6,16	79	3,33
20,21	6,15	87	3,60
20,63	6,14	82	2,85
21,06	6,11	83	2,69
21,48	6,14	79	2,69
21,90	6,11	82	2,69
22,32	6,10	91	2,47
23,16	6,10	80	3,01
24,00	6,11	80	2,95

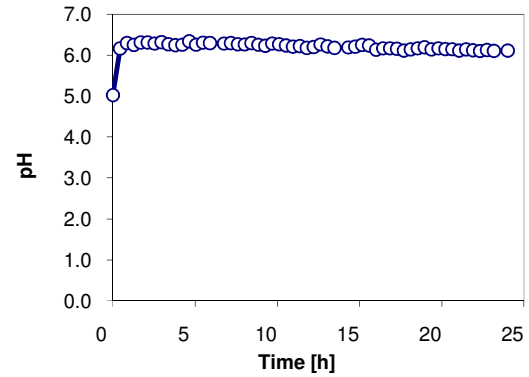

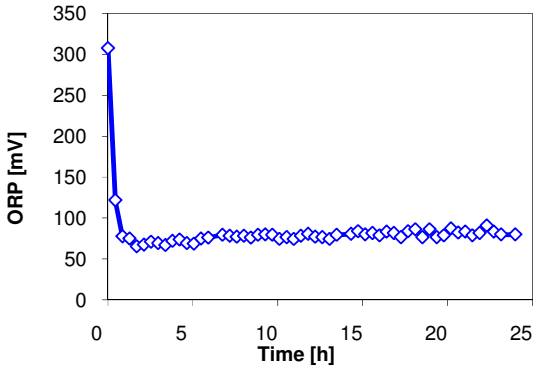

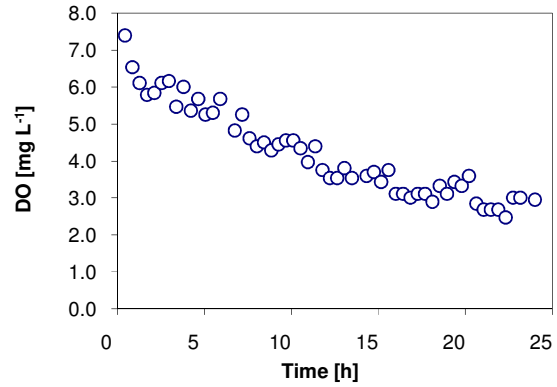

Table B10 Example of monitoring results of pH, ORP and DO from batch tests (e.g., for Table 4.2)

System:	Batch investigation at controlled pH 7,0		
Metrix:	Cu^{2+}/Zn^{2+} in DI water		
Cu^{2+}:	4-5 mg L^{-1}	Conductivity:	80 µS cm^{-1}
Zn^{2+}:	4-5 mg L^{-1}	Temperature:	20 °C
DO:	7-9 mg L^{-1}	Fe^0:	0,5 g Fe^0

Time [h]	pH [-]	ORP [mV]	DO [mg L^{-1}]
0,00	6,95	210	9,20
0,43	6,95	171	8,68
0,85	6,95	187	8,68
1,27	6,95	188	8,68
1,70	6,95	171	9,32
2,12	6,95	191	9,11
2,54	6,95	195	8,47
2,96	6,95	185	9,16
3,38	6,95	187	8,95
3,80	6,95	169	8,68
4,22	6,95	163	8,47
4,64	6,95	197	8,41
5,06	6,95	180	9,00
5,48	6,95	192	8,84
5,91	6,95	210	9,06
6,75	6,95	169	8,68
7,17	6,95	173	8,79
7,59	6,95	193	9,11
8,01	6,95	169	8,31
8,42	6,95	195	8,36
8,84	6,95	191	7,82
9,27	6,95	169	8,36
9,69	6,95	167	8,47
10,11	6,95	170	8,47
10,53	6,95	194	7,77
10,95	6,95	169	8,52
11,37	6,95	178	8,20
11,79	6,95	175	7,82
12,21	6,95	193	7,66
12,63	6,95	179	8,63
13,05	6,95	188	7,88
13,48	6,95	169	7,72
14,32	6,95	170	8,36
14,74	6,95	176	7,82
15,16	6,95	187	7,72
15,58	6,95	196	7,77
16,00	6,95	175	7,82
16,42	6,95	173	8,20
16,84	6,95	194	7,61
17,27	6,95	194	7,56
17,69	6,95	192	7,40
18,11	6,95	188	7,99
18,53	6,95	176	8,20
18,95	6,95	180	7,61
19,37	6,95	195	7,34
19,79	6,95	194	7,29
20,21	6,95	172	7,82
20,63	6,95	178	8,31
21,06	6,95	165	8,36
21,48	6,95	179	8,31
21,90	6,95	181	8,15
23,16	6,95	176	8,20
24,00	6,95	197	7,82

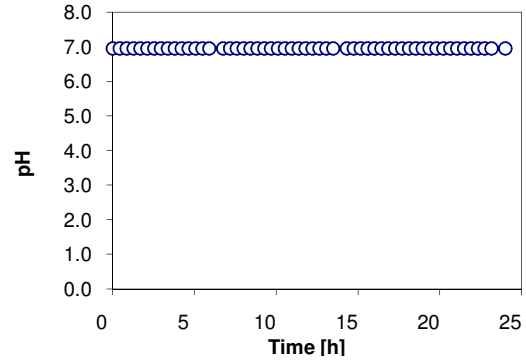

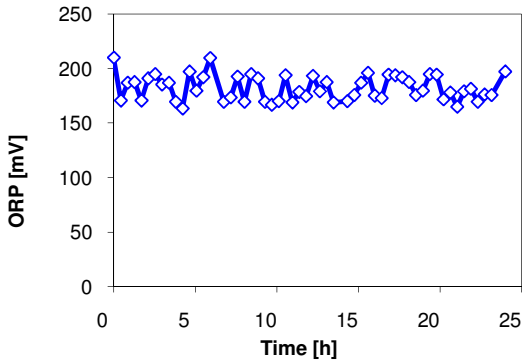

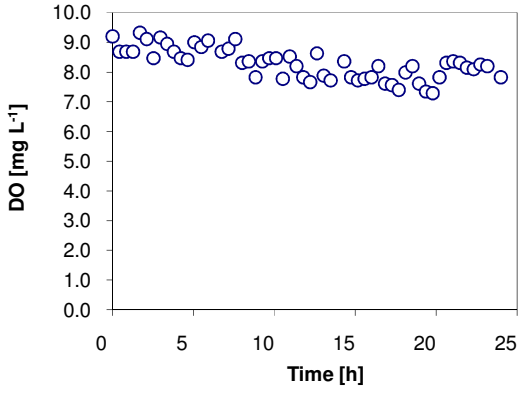

Table B11.1 Results of equilibrium batch test of Cu^{2+} and Zn^{2+} removal by Fe^0 (Fig. 4.5)

Source of water: TU-SW					DOC			Cu^{2+}			Zn^{2+}		
Samples	DOC	ZVI[g L^{-1}]	UV_{254}	UV_{436}	initial	Eq.	[mg g^{-1}]	initial	Eq.	[mg g^{-1}]	initial	Eq.	[mg g^{-1}]
S1.1	2,38	0,514	0,0462	0,004	3,94	1,12	5,49	5,12	0,16	9,65			
S1.2	2,26	0,49	0,0555	0,0032	4,03	1,04	6,10				4,92	0,19	9,65
S1.3	2,08	0,498	0,0605	0,0074	4,66	2,74							
S1.4	1,81	0,506	0,0405	0,0023	4,02	1,11	5,74	4,92	0,08	9,57	5,170	0,20	9,82
S2.1	2,02	0,442	0,0659	0,0037	3,94	0,85	7,00	5,12	0,51	10,43			
S2.2	2,42	0,44	0,1282	0,0126	4,03	1,24	6,34				4,92	0,95	9,02
S2.3	2,52	0,398	0,1644	0,0182	4,66	2,36	5,78						
S2.4	1,96	0,436	0,0489	0,0013	4,02	1,09	6,71	4,92	0,26	10,69	5,170	0,69	10,28
S3.1	1,91	0,412	0,0403	0,0016	3,94	0,94	7,29	5,12	1,09	9,78			
S3.2	2,18	0,408	0,0887	0,0125	4,03	3,57	1,13				4,92	1,63	8,06
S3.3	2,04	0,44	0,1009	0,0092	4,66	2,92	3,95						
S3.4	1,79	0,404	0,0445	0,0016	4,02	1,13	7,15	4,92	0,32	11,39	5,170	0,73	10,99
S4.1	1,66	0,348	0,0337	0,0006	3,94	1,16	7,99	5,12	0,98	11,90			
S4.2	2,31	0,34	0,1298	0,0131	4,03	2,76	3,74				4,92	1,41	
S4.3	2,21	0,358	0,1082	0,0097	4,66	3,75	2,55						
S4.4	2,67	0,352	0,0713	0,0036	4,02	1,15	8,14	4,92	1,05		5,170	1,94	9,18
S5.1	2,21	0,284	0,0657	0,0034	3,94	1,25	9,47	5,12	1,28	13,52			
S5.2	2,62	0,282	0,1379	0,0128	4,03	3,64	1,40				4,92	2,8	7,52
S5.3	2,55	0,28	0,1791	0,0155	4,66	4,04	2,20						
S5.4	1,82	0,29	0,0402	0,0004	4,02	1,10	10,07	4,92	0,31	15,90	5,170	0,78	15,14
S6.1	2,27	0,22	0,0716	0,0038	3,94	1,23	12,33	5,12	1,55				
S6.2	2,47	0,228	0,1224	0,0088	4,03	3,90	0,57				4,92	3,5	6,23
S6.3	2,33	0,25	0,1619	0,0156	4,66	4,14	2,06						
S6.4	2,29	0,218	0,0587	0,0024	4,02	1,26	12,64	4,92	0,61	19,77	5,170	1,81	15,41
S7.1	2,38	0,188	0,1024	0,01	3,94	3,62	1,72	5,12	3	11,28			
S7.2	2,55	0,192	0,1207	0,0091	4,03	3,70	1,72				4,92	3,86	5,52
S7.3	2,18	0,184	0,0751	0,0046	4,66	4,23	2,35						
S7.4	2,01	0,186	0,0534	0,0013	4,02	3,48	2,92	4,92	1,75	17,04	5,170	3,110	11,08
S8.1	2,06	0,148	0,0532	0,0013	3,94	3,71	1,59	5,12	3,15				
S8.2	2,76	0,158	0,1261	0,0084	4,03	4,23					4,92	3,95	
S8.3	2,63	0,158	0,1975	0,0187	4,66	4,39	1,72						
S8.4	2,11	0,148	0,0622	0,0026	4,02	3,82	1,35	4,92	3,12	12,16	5,170	4,470	4,73
S9.1	2,30	0,106	0,0768	0,0034	3,94	3,75	1,79	5,12	3,51	15,19			
S9.2	2,66	0,102	0,0943	0,0046	4,03	4,29					4,92	4,82	
S9.3	2,71	0,096	0,1002	0,0109	4,66	4,43	2,35						
S9.4	2,50	0,1	0,0741	0,0025	4,02	3,49	5,30	4,92	1,76		5,170	3,92	
Cu ConT1	2,82		0,1304	0,0073				5,37					
Cu ConT2	3,10		0,1271	0,0052				4,86					
Zn ConT1	3,14		0,121	0,0047							4,82		
Zn ConT2	3,13		0,1141	0,0043							5,02		
DOC ConT1	3,34		0,1136	0,004									
DOC ConT2	3,23		0,121	0,0048									
CuZnConT1	3,04		0,1233	0,0044				4,79			5,16		
CuZnConT2	3,40		0,1172	0,0041				5,05			5,18		

*ContT = controlled vials

Table B11.2 Results of equilibrium batch test of Cu^{2+} and Zn^{2+} removal by Fe^0 (Fig. 4.5)

Source of water: Lankwitz					DOC			Cu^{2+}			Zn^{2+}		
Samples	DOC	ZVI[g L^{-1}]	UV_{254}	UV_{436}	initial	Eq.	[mg g^{-1}]	initial	Eq.	[mg g^{-1}]	initial	Eq.	[mg g^{-1}]
S1.1	1,21	1,492	0,0464	0,0226	1,28	1,21	0,05	4,85	0,18	3,13	0,67	0,08	0,39
S1.2	0,85	1,512	0,0533	0,025	1,35	0,85	0,33				5,86	0,04	3,85
S1.3	0,95	1,504	0,0353	0,0153	1,31	0,94	0,24				0,64	0,04	0,40
S1.4	0,78	1,506	0,0354	0,0184	1,30	0,78	0,34	4,87	0,11	3,16	5,84	0,17	3,76
S2.1	0,73	0,81	0,0454	0,0254	1,28	0,72	0,69	4,85	0,1	5,86	0,67	0,04	0,78
S2.2	1,04	0,79	0,0567	0,0285	1,35	1,04	0,39				5,86	0,07	7,33
S2.3	0,89	0,792	0,0304	0,0118	1,31	0,88	0,54				0,64	0,02	0,78
S2.4	1,05	0,808	0,0761	0,0206	1,30	1,05	0,31	4,87	0,41	5,52	5,84	1,14	5,82
S3.1	1,08	0,492	0,0578	0,0225	1,28	1,08	0,42	4,85	0	9,85	0,67	0,10	1,16
S3.2	0,82	0,512	0,0445	0,0262	1,35	0,82	1,04				5,86	1,18	9,15
S3.3	0,79	0,498	0,0567	0,0357	1,31	0,78	1,06				0,64	0,05	1,19
S3.4	0,73	0,52	0,0537	0,0196	1,30	0,72	1,11	4,87	0,17	9,04	5,84	0,93	9,45
S4.1	1,09	0,314	0,078	0,0271	1,28	1,08	0,64	4,85	1,16	11,75	0,67	0,27	1,29
S4.2	0,79	0,306	0,0442	0,0256	1,35	0,78	1,84				5,86	2,05	12,46
S4.3	0,94	0,296	0,0353	0,0175	1,31	0,94	1,26				0,64	0,05	2,01
S4.4	0,81	0,312	0,0686	0,0178	1,30	0,80	1,59	4,87	0,12	15,24	5,84	0,62	16,74
S5.1	0,71	0,198	0,033	0,018	1,28	0,70	2,93	4,85	0,94	19,74	0,67	0,28	1,99
S5.2	0,82	0,196	0,0475	0,031	1,35	0,82	2,70				5,86	2,91	15,07
S5.3	0,94	0,204	0,0529	0,0335	1,31	0,94	1,81				0,64	0,23	2,03
S5.4	0,75	0,214	0,0764	0,0169	1,30	0,75	2,57	4,87	0,13	22,17	5,84	1,71	19,32
S6.1	1,01	0,092	0,0296	0,0114	1,28	1,00	3,04	4,85	2,85	21,73	0,67	0,50	1,90
S6.2	0,96	0,102	0,0377	0,0144	1,35	0,96	3,82				5,86	4,7	11,42
S6.3	1,24	0,112	0,0391	0,0206	1,31	1,24	0,62				0,64	0,30	3,08
S6.4	0,89	0,1	0,0473	0,0192	1,30	0,89	4,11	4,87	2,62	22,55	5,84	4,19	16,55
S7.1	1,08	0,054	0,0364	0,0124	1,28	1,07	3,89	4,85	2,1	50,92	0,67	0,47	3,79
S7.2	1,01	0,05	0,0567	0,008	1,35	1,01	6,73				5,86	5,33	10,70
S7.3	0,92	0,054	0,0408	0,0158	1,31	0,92	7,28				0,64	0,42	4,16
S7.4	0,91	0,052	0,041	0,01	1,30	0,91	7,53	4,87	0,89	76,63	5,84	3,41	46,82
S8.1	0,87	0,04	0,0353	0,0153	1,28	0,87	10,34	4,85	3,34	37,75	0,67	0,54	3,37
S8.2	1,03	0,038	0,0485	0,0032	1,35	1,03	8,33				5,86	5,52	9,07
S8.3	0,89	0,046	0,0343	0,0149	1,31	0,89	9,20				0,64	0,41	5,10
S8.4	0,80	0,042	0,0453	0,0195	1,30	0,80	11,86	4,87	2,45	57,73	5,84	4,38	34,88
S9.1	1,37	0,022	0,0602	0,0073	1,28	1,36		4,85	4,12	33,18	0,67	0,58	4,31
S9.2	1,15	0,02	0,0448	0,0022	1,35	1,15	9,83				5,86	5,43	21,75
S9.3	0,95	0,018	0,0552	0,0093	1,31	0,95	20,18				0,64	0,55	5,27
S9.4	0,89	0,016	0,0458	0,0202	1,30	0,89	25,72	4,87	2,39		5,84	4,37	
Cu ConT 1	1,14		0,0445	0,0015					4,65			0,68	
Cu ConT 2	1,23		0,0441	0,0014					5,05			0,67	
Zn ConT1	1,31		0,037	0,0015					0,07			5,67	
Zn ConT2	1,39		0,0384	0,0013					0,01			6,06	
DOC ConT1	1,22		0,0347	0,001					0			0,63	
DOC ConT2	1,41		0,0382	0,0013					0			0,66	
CuZnConT1	1,10		0,036	0,0014					4,7			5,67	
CuZnConT2	1,50		0,042	0,0013					5,05			6,02	

*ContT = controlled vials

Table B11.3 Results of equilibrium batch test of Cu^{2+} and Zn^{2+} removal by Fe^0 (Fig. 4.5)

Source of water: SRFA					DOC			Cu^{2+}			Zn^{2+}		
Samples	DOC	ZVI[g L^{-1}]	UV_{254}	UV_{436}	initial	Eq.	[mg g^{-1}]	initial	Eq.	[mg g^{-1}]	initial	Eq.	[mg g^{-1}]
S1.1	1,12	1,504	0,0182	0,0005	3,94	1,12	1,87	5,12	0,16	3,29			
S1.2	1,05	1,516	0,0342	0,0083	4,03	1,04	1,97				4,92	0,19	3,12
S1.3	2,74	1,504	0,8653	0,1326	4,66	2,74							
S1.4	1,12	1,498	0,0196	0,0008	4,02	1,11	1,94	4,92	0,08	3,23	5,17	0,20	3,31
S2.1	0,85	0,832	0,0178	0,0018	3,94	0,85	3,71	5,12	0,51	5,54			
S2.2	1,25	0,848	0,0441	0,0126	4,03	1,24	3,29				4,92	0,95	4,68
S2.3	2,36	0,8	0,5027	0,0745	4,66	2,36	2,87						
S2.4	1,10	0,828	0,0213	0,0013	4,02	1,09	3,53	4,92	0,26	5,62	5,17	0,69	5,41
S3.1	0,94	0,464	0,0142	0	3,94	0,94	6,47	5,12	1,09	8,68			
S3.2	3,58	0,522	0,4655	0,0547	4,03	3,57	0,88				4,92	1,63	6,30
S3.3	2,92	0,51	0,6672	0,0943	4,66	2,92	3,40						
S3.4	1,13	0,478	0,0188	0,0002	4,02	1,13	6,04	4,92	0,32	9,62	5,17	0,73	9,28
S4.1	1,17	0,292	0,0228	0,001	3,94	1,16	9,51	5,12	0,98	14,17			
S4.2	2,77	0,284	0,4177	0,063	4,03	2,76	4,47				4,92	1,41	
S4.3	3,75	0,28	0,8847	0,1144	4,66	3,75	3,25						
S4.4	1,16	0,298	0,0228	0,0009	4,02	1,15	9,61	4,92	1,05		5,17	1,94	10,83
S5.1	1,26	0,206	0,0298	0,0014	3,94	1,25	13,05	5,12	1,28	18,64			
S5.2	3,64	0,192	0,3762	0,0362	4,03	3,64	2,05				4,92	2,8	11,04
S5.3	4,05	0,19	0,6568	0,0775	4,66	4,04	3,23						
S5.4	1,10	0,196	0,0249	0,0007	4,02	1,10	14,89	4,92	0,31	23,52	5,17	0,78	22,39
S6.1	1,23	0,094	0,0291	0,001	3,94	1,23	28,85	5,12	1,55				
S6.2	3,91	0,098	0,3212	0,0291	4,03	3,90	1,33				4,92	3,5	14,49
S6.3	4,15	0,11	0,6351	0,0741	4,66	4,14	4,68						
S6.4	1,27	0,09	0,0324	0,002	4,02	1,26	30,62	4,92	0,61	47,88	5,17	1,81	37,33
S7.1	3,62	0,056	0,3348	0,0308	3,94	3,62	5,76	5,12	3	37,85			
S7.2	3,71	0,062	0,2666	0,0229	4,03	3,70	5,32				4,92	3,86	17,09
S7.3	4,23	0,056	0,4826	0,0519	4,66	4,23	7,71						
S7.4	3,48	0,046	0,2608	0,0228	4,02	3,48	11,80	4,92	1,75	68,91	5,17	3,11	44,78
S8.1	3,71	0,014	0,366	0,036	3,94	3,71	16,85	5,12	3,15				
S8.2	4,23	0,018	0,2632	0,0222	4,03	4,23					4,92	3,95	
S8.3	4,39	0,026	0,2028	0,0137	4,66	4,39	10,46						
S8.4	3,82	0,026	0,2205	0,0173	4,02	3,82	7,67	4,92	3,12	69,23	5,17	4,47	26,92
S9.1	3,76	0,026	0,2613	0,0217	3,94	3,75	7,28	5,12	3,51	61,92			
S9.2	4,30	0,014	0,1883	0,0118	4,03	4,29					4,92	4,82	
S9.3	4,44	0,008	0,2065	0,014	4,66	4,43	28,16						
S9.4	3,49	0,01	0,2324	0,0195	4,02	3,49	52,96	4,92	1,76		5,17	3,92	
Cu ConT 1	4,01		0,2077	0,0122				5,37					
Cu ConT 2	3,89		0,1941	0,0111				4,86					
Zn ConT1	3,72		0,1858	0,0099							4,82		
Zn ConT2	4,04		0,1859	0,0098							5,02		
DOC ConT1	4,40		0,196	0,0099									
DOC ConT2	4,93		0,1958	0,0102									
CuZnConT1	3,88		0,2022	0,012				4,79			5,16		
CuZnConT2	4,17		0,2066	0,0127				5,05			5,18		

*ContT = controlled vials

Table B11.4 Results of equilibrium batch test of Cu^{2+} and Zn^{2+} removal by Fe^0 (Fig. 4.5)

Source of water: UFA					DOC			Cu^{2+}			Zn^{2+}		
Samples	DOC	ZVI[g L^{-1}]	UV_{254}	UV_{436}	initial	Eq.	[mg g^{-1}]	initial	Eq.	[mg g^{-1}]	initial	Eq.	[mg g^{-1}]
S1.1	2,24	1,528	0,0642	0,0	3,94	1,12	1,84	5,12	0,16	3,24			
S1.2	2,91	1,474	0,1832	0,1	4,03	1,04	2,02				4,92	0,19	3,2
S1.3	2,87	1,468	0,1153	0,0	4,66	2,74							
S1.4	2,79	1,52	0,0823	0,0	4,02	1,11	1,91	4,92	0,08	3,18	5,17	0,20	3,3
S2.1	2,67	0,82	0,071	0,0	3,94	0,85	3,77	5,12	0,51	5,62			
S2.2	3,56	0,794	0,2331	0,1	4,03	1,24	3,51				4,92	0,95	5,0
S2.3	3,29	0,794	0,0873	0,0	4,66	2,36	2,89						
S2.4	1,91	0,804	0,0765	0,0	4,02	1,09	3,63	4,92	0,26	5,79	5,17	0,69	5,6
S3.1	2,74	0,504	0,0684	0,0	3,94	0,94	5,95	5,12	1,09	7,99			
S3.2	4,22	0,492	0,5916	0,1	4,03	3,57	0,93				4,92	1,63	6,7
S3.3	3,54	0,512	0,1588	0,0	4,66	2,92	3,39						
S3.4	2,93	0,5	0,0701	0,0	4,02	1,13	5,77	4,92	0,32	9,20	5,17	0,73	8,9
S4.1	3,01	0,402	0,0771	0,0	3,94	1,16	6,91	5,12	0,98	10,29			
S4.2	6,35	0,422	0,4987	0,0	4,03	2,76	3,01				4,92	1,41	
S4.3	4,14	0,422	0,6396	0,1	4,66	3,75	2,16						
S4.4	2,73	0,418	0,0667	0,0	4,02	1,15	6,85	4,92	1,05		5,17	1,94	7,7
S5.1	5,12	0,268	0,3964	0,0	3,94	1,25	10,0	5,12	1,28	14,32			
S5.2	6,77	0,288	0,5181	0,0	4,03	3,64	1,36				4,92	2,80	7,4
S5.3	6,23	0,316	0,6893	0,1	4,66	4,04	1,94						
S5.4	2,77	0,304	0,0668	0,0	4,02	1,10	9,60	4,92	0,31	15,16	5,17	0,78	14,4
S6.1	5,68	0,21	0,4315	0,0	3,94	1,23	12,91	5,12	1,55				
S6.2	6,98	0,214	0,3417	0,0	4,03	3,90	0,60				4,92	3,50	6,6
S6.3	7,01	0,182	0,4862	0,0	4,66	4,14	2,83						
S6.4	3,60	0,212	0,1056	0,0	4,02	1,26	13,00	4,92	0,61	20,33	5,17	1,81	15,8
S7.1	6,28	0,096	0,3682	0,0	3,94	3,62	3,361	5,12	3,00	22,08			
S7.2	7,07	0,118	0,3497	0,0	4,03	3,70	2,79				4,92	3,86	9,0
S7.3	7,39	0,11	0,543	0,0	4,66	4,23	3,92						
S7.4	5,92	0,126	0,3862	0,0	4,02	3,48	4,30	4,92	1,75	25,15	5,17	3,11	16,3
S8.1	6,99	0,056	0,3278	0,0	3,94	3,71	4,21	5,12	3,15				
S8.2	7,29	0,046	0,3107	0,0	4,03	4,23					4,92	3,95	
S8.3	6,95	0,056	0,4146	0,0	4,66	4,39	4,85						
S8.4	6,96	0,062	0,3352	0,0	4,02	3,82	3,22	4,92	3,12	29,03	5,17	4,47	11,3
S9.1	6,90	0,026	0,3205	0,0	3,94	3,75	7,28	5,12	3,51	61,92			
S9.2	7,31	0,02	0,3	0,0	4,03	4,29					4,92	4,82	
S9.3	7,26	0,018	0,3305	0,0	4,66	4,43	12,51						
S9.4	7,11	0,012	0,302	0,0	4,02	3,49	44,13	4,92	1,76		5,17	3,92	
Cu ConT 1	6,62		0,319	0,0				5,37					
Cu ConT 2	7,41		0,315	0,017				4,86					
Zn ConT1	7,55		0,296	0,0							4,82		
Zn ConT2	7,88		0,295	0,016							5,02		
DOC ConT1	7,30		0,292	0,0									
DOC ConT2	7,15		0,292	0,016									
CuZnConT1	7,52		0,312	0,0				4,79			5,16		
CuZnConT2	6,24		0,313	0,017				5,05			5,18		

*ContT = controlled vials

Table B11.5 Results of equilibrium batch test of Cu^{2+} and Zn^{2+} removal by Fe^0 (Fig. 4.5)

Source of water: SSWR		Cu^{2+}			Zn^{2+}		
Samples	ZVI[g L^{-1}]	initial	Eq.	[mg g^{-1}]	initial	Eq.	[mg g^{-1}]
S1.1	1,522	4,78	0,20	3,01	0,04	0,07	
S1.2	1,498	4,82	0,24	3,06	5,08	0,96	2,8
S1.3	1,502				5,13	0,21	3,3
S1.4							
S2.1	0,828	4,78	0,66	4,98	0,04	0,01	
S2.2	0,834	4,82	0,22	5,52	5,08	0,27	
S2.3	0,792				5,13	0,92	5,3
S2.4							
S3.1	0,524	4,78	0,54	8,09	0,04	0,00	
S3.2	0,526	4,82	0,58	8,06	5,08	1,57	6,7
S3.3	0,464				5,13	1,72	7,3
S3.4							
S4.1	0,266	4,78	1,67	11,69	0,04	0,03	
S4.2	0,298	4,82	1,09	12,52	5,08	2,63	8,2
S4.3	0,292				5,13	1,51	12,4
S4.4							
S5.1	0,186	4,78	1,94	15,27	0,04	0,01	
S5.2	0,17	4,82	1,39	20,18	5,08	3,23	10,9
S5.3	0,206				5,13	2,02	15,1
S5.4							
S6.1	0,096	4,78	2,15	27,40	0,04	0,03	
S6.2	0,112	4,82	1,28	31,61	5,08	3,32	15,7
S6.3	0,096				5,13	2,67	25,6
S6.4							
S7.1	0,046	4,78	3,00	38,70	0,04	0,05	
S7.2	0,056	4,82	2,83		5,08	4,29	14,1
S7.3	0,048				5,13	4,32	16,9
S7.4	0,052	4,82	2,37	47,12	5,08	4,06	19,6
S8.1	0,016	4,78	3,58		0,04	0,05	
S8.2	0,026	4,82	3,01	69,62	5,08	4,55	20,4
S8.3	0,02				5,13	4,47	33,0
S8.4	0,014	4,82	3,36	104,29	5,08	4,83	17,9
S9.1	0,014	4,78	3,87		0,04	0,06	
S9.2	0,01	4,82	3,62	120	5,08	4,86	22,0
S9.3	0,012		0,05		5,13	5,07	5,0
S9.4	0,028	4,82	3,02		5,08	4,82	9,3
Cu ConT 1		4,78			0,05		
Cu ConT 2		4,78			0,04		
Zn ConT1					5,13		
Zn ConT2							
DOC ConT1		4,82			5,08		
DOC ConT2							
CuZnConT1							
CuZnConT2							

*ContT = controlled vials

Table B11.6 Results of equilibrium batch test of Cu^{2+} and Zn^{2+} removal by Fe^0 (Fig. 4.5)

Source of water: Halensee					DOC			Cu^{2+}			Zn^{2+}		
Samples	DOC	ZVI [g L^{-1}]	UV_{254}	UV_{436}	initial	Eq.	[mg g^{-1}]	initial	Eq.	[mg g^{-1}]	initial	Eq.	[mg g^{-1}]
S1.1	30,11	1,6	0,0182	0,0005	32,66	30,11	1,59	4,95	0,08	3,04			
S1.2	25,50	1,576	0,0342	0,0083	21,12	25,50					5,43	0,62	
S1.3	23,44	1,604	0,8653	0,1326	19,00	23,44							
S1.4	28,29	1,612	0,0196	0,0008	34,53	28,29	3,89	4,96	0,04	3,05	5,46	0,21	3,25
S2.1	28,19	0,964	0,0178	0,0018	32,66	28,19	4,64	4,95	0,07	5,06			
S2.2	27,43	0,964	0,0441	0,0126	21,12	27,43					5,43	2,18	
S2.3	20,03	0,922	0,5027	0,0745	19,00	20,03							
S2.4	28,87	0,906	0,0213	0,0013	34,53	28,87	6,25	4,96	0,07	5,39	5,46	0,10	5,91
S3.1	28,09	0,51	0,0142	0	32,66	28,09	8,95	4,95	0,16	9,39			
S3.2	27,96	0,504	0,4655	0,0547	21,12	27,96					5,43	4,21	2,42
S3.3	23,48	0,492	0,6672	0,0943	19,00	23,48							
S3.4	28,57	0,504	0,0188	0,0002	34,53	28,57	11,82	4,96	0,19	9,46	5,46	0,69	9,46
S4.1	30,49	0,216	0,0228	0,001	32,66	30,49	10,04	4,95	1,79	14,63			
S4.2	24,08	0,194	0,4177	0,063	21,12	24,08					5,43	4,59	4,33
S4.3	25,66	0,208	0,8847	0,1144	19,00	25,66							
S4.4	27,66	0,228	0,0228	0,0009	34,53	27,66	30,10	4,96	1,8	13,86	5,46	3,46	8,77
S5.1	30,24	0,1	0,0298	0,0014	32,66	30,24	24,18	4,95	2,06	28,90			
S5.2	22,47	0,096	0,3762	0,0362	21,12	22,47					5,43	5,12	3,22
S5.3	20,65	0,104	0,6568	0,0775	19,00	20,65							
S5.4	27,93	0,11	0,0249	0,0007	34,53	27,93	59,92	4,96	1,22	34,00	5,46	2,97	22,63
S6.1	29,97	0,066	0,0291	0,001	32,66	29,97	40,63	4,95	2,37	39,09			
S6.2	19,83	0,064	0,3212	0,0291	21,12	19,83	20,08				5,43	5,11	5,00
S6.3	20,05	0,056	0,6351	0,0741	19,00	20,05							
S6.4	28,58	0,056	0,0324	0,002	34,53	28,58	106,22	4,96	2,31	47,32	5,46	4,11	24,10
S7.1	29,98	0,026	0,3348	0,0308	32,66	29,98	103,01	4,95	2,68	87,30			
S7.2	20,03	0,024	0,2666	0,0229	21,12	20,03	45,35				5,43	5,15	11,66
S7.3	18,99	0,022	0,4826	0,0519	19,00	18,99	0,76						
S7.4	30,27	0,02	0,2608	0,0228	34,53	30,27	212,75	4,96	3,37	79,50	5,46	4,67	39,50
S8.1	31,36	0,014	0,366	0,036	32,66	31,36	92,50	4,95	3,49	104,28			
S8.2	21,34	0,008	0,2632	0,0222	21,12	21,34					5,43	5,28	18,75
S8.3	18,54	0,013	0,2028	0,0137	19,00	18,54	35,39						
S8.4	31,68	0,016	0,2205	0,0173	34,53	31,68	178,02	4,96	3,5	91,25	5,46	4,76	43,75
S9.1	32,49	0,012	0,2613	0,0217	32,66	32,49	13,47	4,95	3,78	97,50			
S9.2	20,80	0,008	0,1883	0,0118	21,12	20,80					5,43	5,26	21,25
S9.3	18,10	0,018	0,2065	0,014	19,00	18,10	50,19						
S9.4	31,93	0,006	0,2324	0,0195	34,53	31,93	431,9	4,96	3,66	216,66	5,46	4,78	113,33
Cu ConT 1	31,58		0,2077	0,0122				4,95					
Cu ConT 2	33,73		0,1941	0,0111									
Zn ConT1	20,38		0,1858	0,0099							5,51		
Zn ConT2	21,86		0,1859	0,0098							5,34		
DOC ConT1	18,10		0,196	0,0099									
DOC ConT2	19,91		0,1958	0,0102									
CuZnConT1	33,58		0,2022	0,012				4,89			5,32		
CuZnConT2	35,47		0,2066	0,0127				5,03			5,6		

*ContT = controlled vials

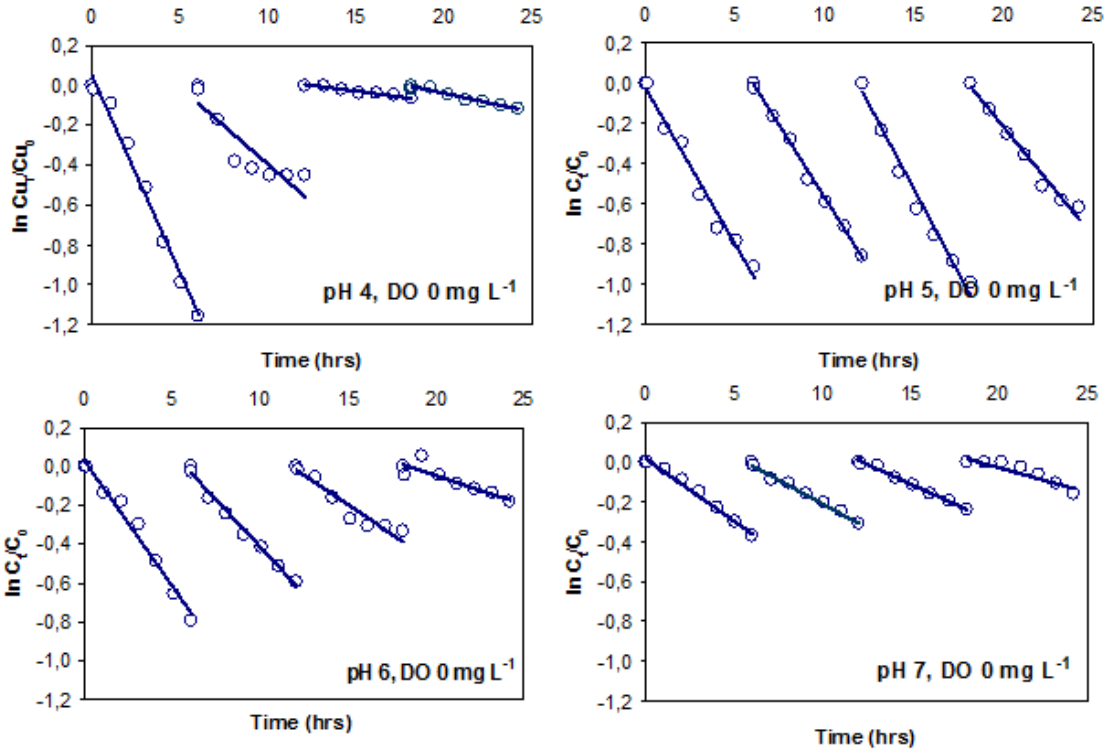

Fig. B1 Results of batch test with pulse doses of Cu^{2+} [Cu^{2+} 5.0 mg L^{-1} with total doses of 20 mg L^{-1}, Fe^0 0.5 g L^{-1}, DO 0 mg L^{-1}, T 20°C at pH 4.0-7.0 (controlled) at 150 rpm].

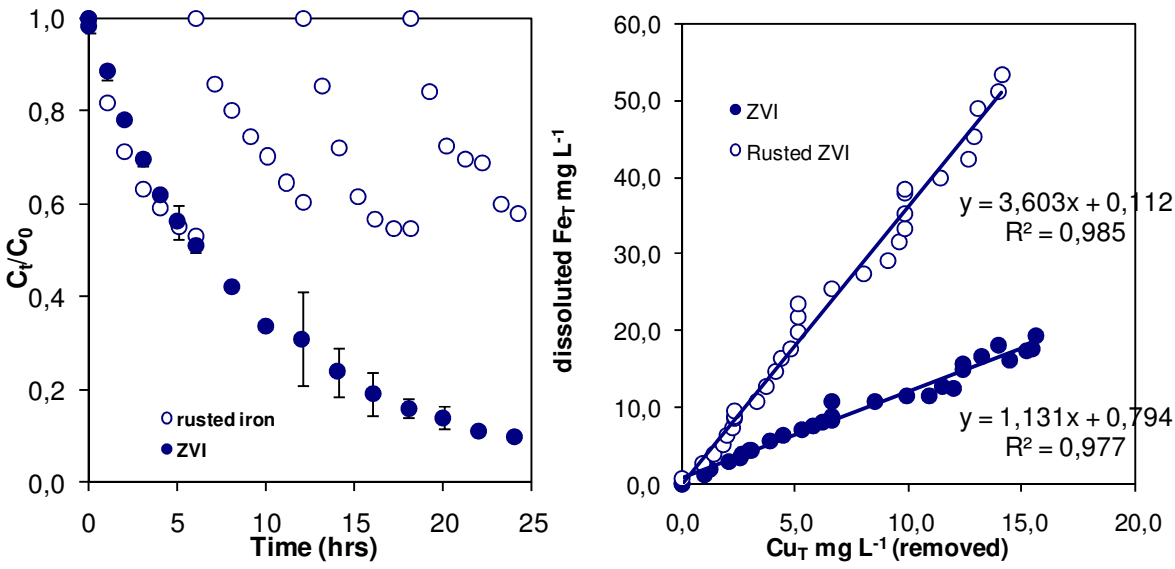

Fig. B2 A comparison of batch results with pulse doses of Cu^{2+} using Fe^0 and rusted (corroded) Fe^0 at 0.5 g L^{-1} each [Cu^{2+} 5.0 mg L^{-1} with total doses of 20 mg L^{-1}, T 20°C at pH 5.0 (controlled) at 150 rpm].

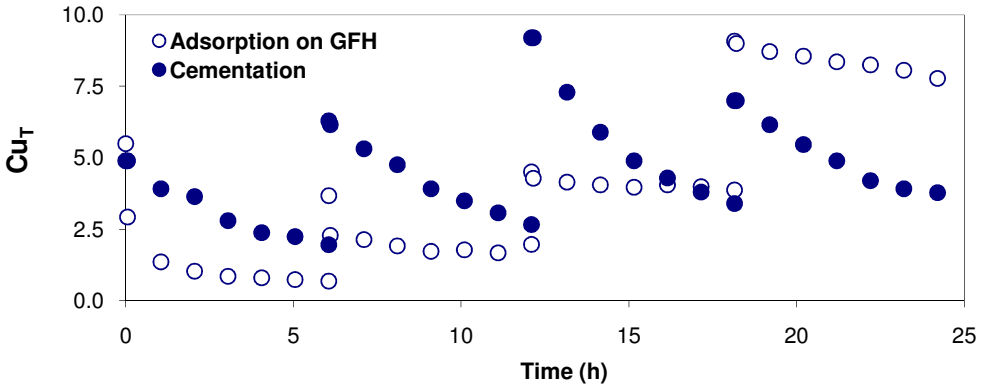

Fig. B3 A comparison of batch results with pulse doses of Cu^{2+} using Fe^0 and GFH at 0.5 g L^{-1} each [Cu^{2+} 5.0 mg L^{-1} with total doses of 20 mg L^{-1}, DO 0 mg L^{-1}, T 20°C at pH 5.0 (controlled) (pH 6.0 for GFH) at 150 rpm].

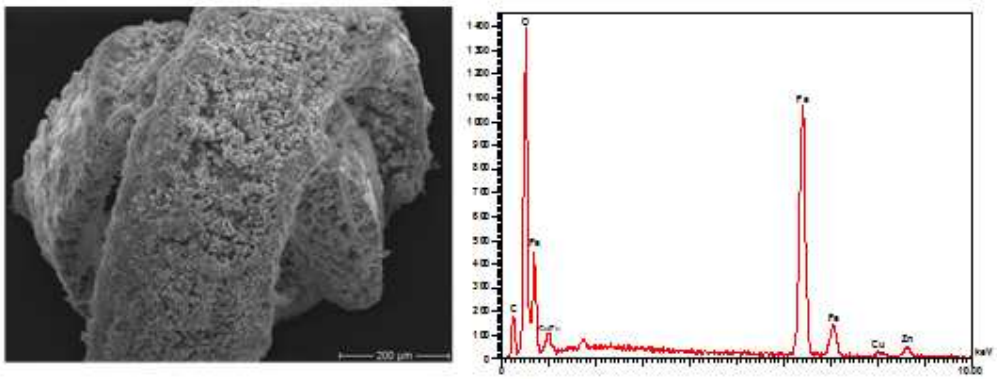

Fig. B4 Mapping of SEM and EDX spectra of iron from typical batch experiment in oxygenate solution

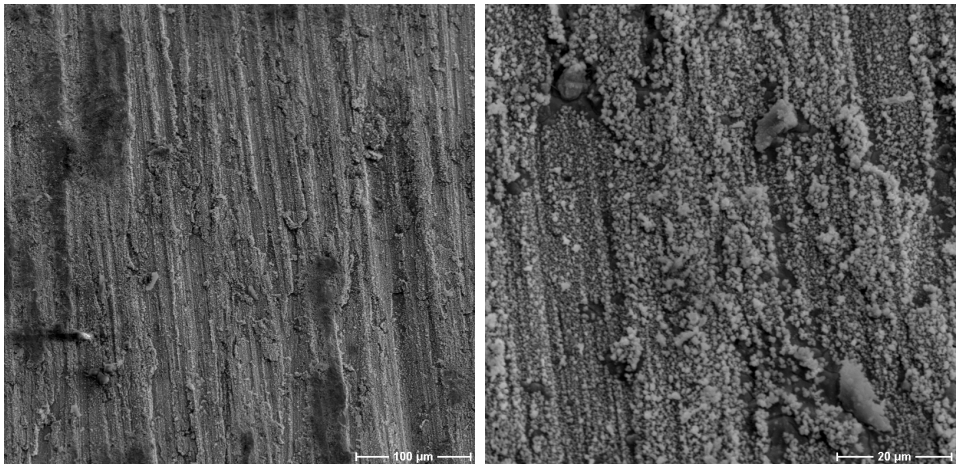

Fig. B5 SEM spectra of iron from batch experiment containg Pb^{2+} [Pb^{2+} 5.0 mg L^{-1}, Fe^0 0.5 g L^{-1}, T 20°C, DO 0 mg L^{-1}, pH 5.0 (controlled) at 150 rpm] (in supplement to Fig. 4.2)

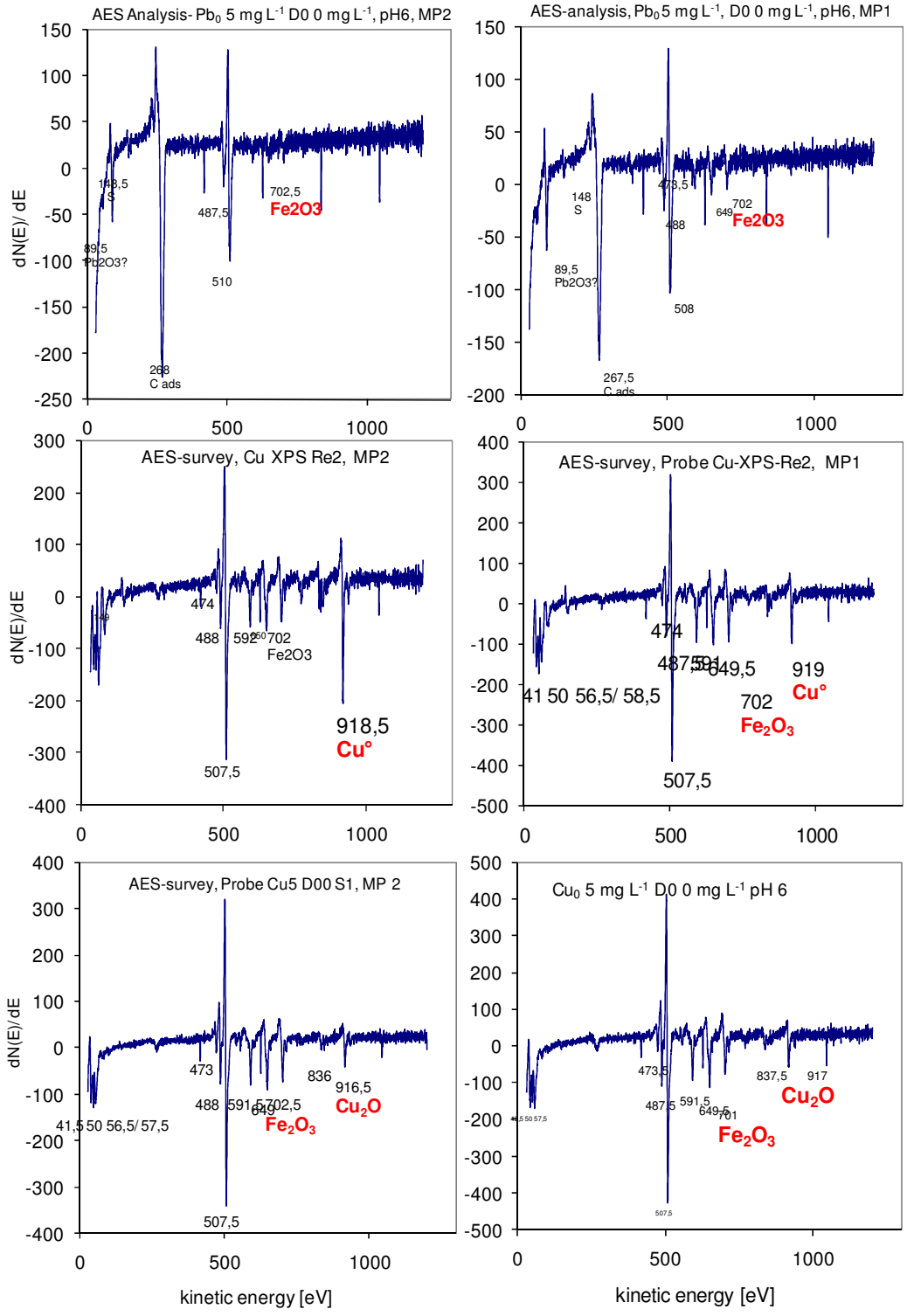

Fig. B6 Auger spectra of precipitates after experiments [Cu_i^{2+} or Pb_i^{2+} 5.0 mg L^{-1}, Fe^0 dimension 2.1x1.05x0.5cm^3, pH 6.0 (controlled), DO < 0.5 mg L^{-1}, T 20 ± 1.0 °C, 150 rpm in SSWR] (supplement data for Fig. 4.9 and B4).

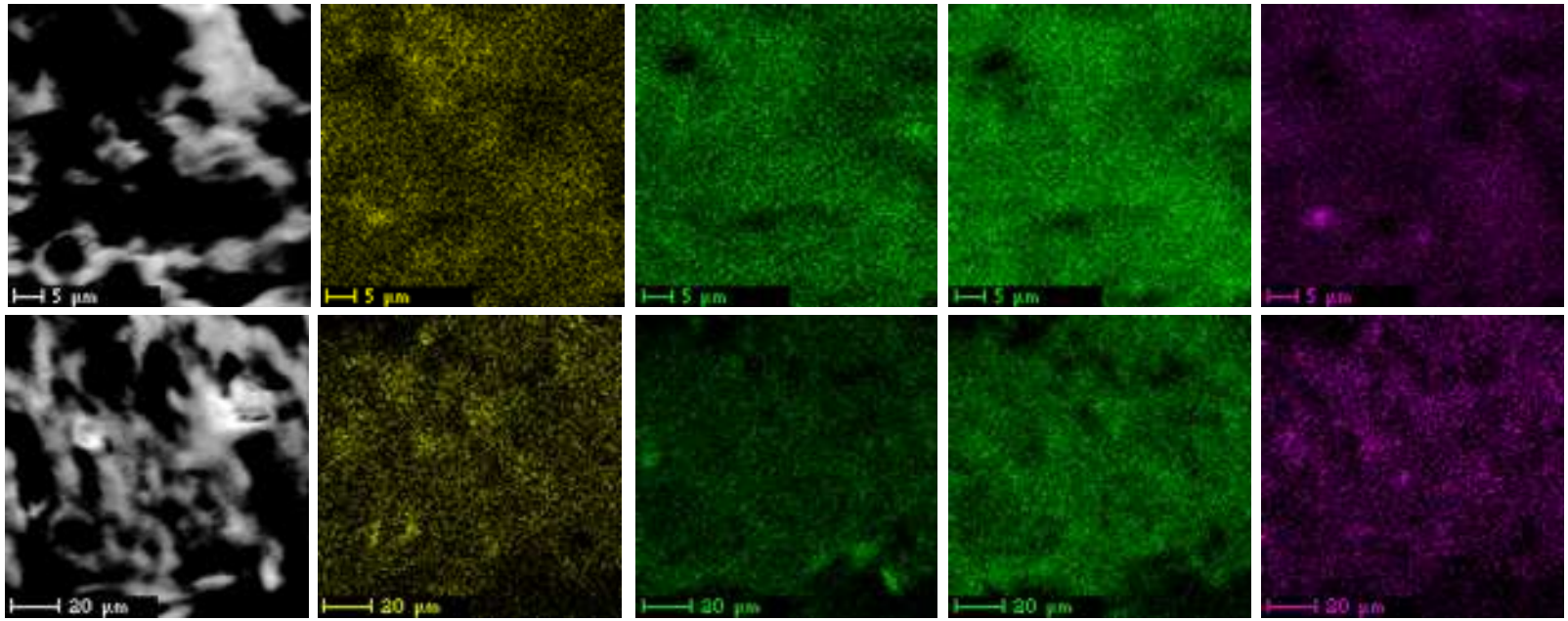

Fig. B7 SEM and EDX spectra of precipitates after experiments [Cu_i^{2+} 10 mg L^{-1}, Zn_i^{2+} 10 mg L^{-1}, 0.5 g Fe^0 L^{-1}, pH 7.0 (controlled), , T 20 ± 1.0 °C, 150 rpm in SSWR] (supplement data for Fig. 4.10).

Table B12 Determination of pH impacts on breakthrough curves (Fig. 4.11 and Fig. 4.18)

Metrix: Cu^{2+}/Zn^{2+} in roof runoff

Cu^{2+}: 4-5 mg L^{-1}

Zn^{2+}: 5-7 mg L^{-1}

Conductivity: 80 µS cm^{-1}

Temperature: 20 °C

DO: 7-8 mg L^{-1}

Fe^0 bed: 15 g Fe^0 with pumice, 5 min EBCT

	c/c_0 for Cu^{2+}			c/c_0 for Zn^{2+}			Fe^{2+}		
BV	pH 4.2	pH 5.8	pH 6.5	pH 4.2	pH 5.8	pH 6.5	pH 4.2	pH 5.8	pH 6.5
37	0,06	0,09	0,10	0,41	0,49	0,33	0,84	0,60	0,32
183	0,09	0,11	0,12	0,54	0,58	0,41	0,84	0,52	0,32
257	0,16	0,10	0,22	0,67	0,76	0,63	0,77	0,42	0,10
403	0,16	0,19	0,22	0,69	0,64	0,64	0,71	0,37	0,06
477	0,17	0,18	0,21	0,67	0,62	0,63	0,67	0,34	0,05
550	0,19	0,19	0,27	0,66	0,55	0,64	0,66	0,35	0,02
746	0,18	0,19	0,41	0,62	0,50	0,66	0,63	0,39	0,08
819	0,17	0,18	0,37	0,56	0,48	0,63	0,60	0,37	0,08
1039	0,17	0,22	0,38	0,53	0,50	0,67	0,66	0,36	0,09
1112	0,19	0,21	0,37	0,58	0,49	0,68	0,62	0,24	0,09
1332	0,23	0,22	0,34	0,62	0,50	0,68	0,60	0,31	0,05
1406	0,24	0,18	0,44	0,65	0,56	0,73	0,67	0,20	0,07
1626	0,32	0,31	0,46	0,67	0,60	0,75	0,54	0,26	0,03
1699	0,37	0,42	0,48	0,68	0,65	0,72	0,51	0,23	0,04
1919	0,38	0,45	0,47	0,68	0,64	0,69	0,50	0,18	0,03
1992	0,36	0,40	0,40	0,68	0,60	0,68	0,44	0,15	0,04
2212	0,42	0,53	0,42	0,73	0,73	0,72	0,44	0,14	0,05
2286	0,44	0,64	0,43	0,75	0,78	0,70	0,42	0,16	0,06
2506	0,51	0,68	0,41	0,84	0,81	0,70	0,48	0,11	0,05
2579	0,52	0,59	0,36	0,83	0,76	0,73	0,38	0,10	0,04
2799	0,56	0,62	0,41	0,83	0,81	0,74	0,35	0,10	0,05
2872	0,59	0,70	0,43	0,85	0,86	0,76	0,36	0,10	0,06
3092	0,62	0,77	0,53	0,85	0,86	0,74	0,35	0,12	0,07
3166	0,75	0,78	0,50	0,90	0,89	0,82	0,32	0,08	0,04
3386	0,75	0,80	0,53	0,92	1,01	0,84	0,31	0,06	0,06
3459	0,77	0,91	0,44	0,98	1,03	0,81	0,34	0,07	0,05
3679	0,89	0,91	0,44	1,03	1,02	0,79	0,26	0,08	0,07
3753	0,89	0,88	0,50	1,03	0,99	0,87	0,24	0,09	0,06
3973	0,94	0,87	0,69	1,07	0,96	0,93	0,23	0,08	0,05

Table B13 Determination of DO impacts on breakthrough curves (Fig. 4.12 and Fig. 4.18)

Metrix: Cu^{2+}/Zn^{2+} in roof runoff

Cu^{2+}: 4-5 mg L^{-1}

Zn^{2+}: 5-7 mg L^{-1}

Conductivity: 80 µS cm^{-1}

Temperature: 20 °C

DO: ~1,3 and 7-8 mg L^{-1}

Fe^0 bed: 15 g Fe^0 with pumice, 5 min EBCT

	c/c_0 for Cu^{2+}		c/c_0 for Zn^{2+}		Fe^{2+}	
BV	DO 8	DO 1,3	DO 8	DO 1,3	DO 8	DO 1,3
37	0,09	0,04	0,49	0,65	5,96	2,59
183	0,11	0,06	0,58	0,73	5,21	2,67
257	0,10	0,09	0,76	0,77	4,23	3,63
403	0,19	0,10	0,64	0,82	3,73	3,66
477	0,18	0,09	0,62	0,81	3,41	3,23
550	0,19	0,10	0,55	0,71	3,50	3,28
746	0,19	0,11	0,50	0,72	3,87	3,66
819	0,18	0,11	0,48	0,69	3,68	3,72
1039	0,22	0,14	0,50	0,78	3,58	4,32
1112	0,21	0,14	0,49	0,70	2,44	4,30
1332	0,22	0,20	0,50	0,77	3,09	3,98
1406	0,18	0,18	0,56	0,72	1,97	4,02
1626	0,31	0,22	0,60	0,82	2,59	3,61
1699	0,42	0,26	0,65	0,71	2,26	2,99
1919	0,45	0,26	0,64	0,75	1,82	3,04
1992	0,40	0,23	0,60	0,76	1,54	2,49
2212	0,53	0,32	0,73	0,95	1,39	2,57
2286	0,64	0,37	0,78	0,86	1,59	2,34
2506	0,68	0,50	0,81	0,96	1,06	1,94
2579	0,59	0,51	0,76	0,93	1,03	1,57
2799	0,62	0,60	0,81	1,11	0,97	1,48
2872	0,70	0,51	0,86	0,93	1,00	1,11
3092	0,77	0,59	0,86	0,97	1,20	1,28
3166	0,78		0,89		0,80	0,95
3386	0,80	0,79	1,01	0,90	0,62	0,82
3459	0,91	0,74	1,03	1,09	0,71	1,44
3679	0,91	0,73	1,02	1,05	0,82	1,65
3753	0,88		0,99	1,01	0,90	1,83
3973	0,87		0,96	1,10	0,77	1,91

Table B14 Determination of conductivity impacts on breakthrough curves (Fig. 4.13 and Fig. 4.18)

Metrix:	Cu^{2+}/Zn^{2+} in roof runoff
Cu^{2+}:	4-5 mg L^{-1}
Zn^{2+}:	5-7 mg L^{-1}
Conductivity:	80 and 200µS cm^{-1}
Temperature:	20 °C
DO:	7-8 mg L^{-1}
Fe^0 bed:	15 g Fe^0 with pumice, 5 min EBCT

	c/c_0 for Cu^{2+}		c/c_0 for Zn^{2+}		Fe^{2+}	
BV	80	200	80	200	80	200
37	0,09	0,09	0,49	0,31	5,96	5,06
183	0,11	0,15	0,58	0,40	5,21	5,46
257	0,10	0,32	0,76	0,66	4,23	3,29
403	0,19	0,31	0,64	0,67	3,73	3,15
477	0,18	0,30	0,62	0,64	3,41	3,15
550	0,19	0,31	0,55	0,60	3,50	2,99
746	0,19	0,34	0,50	0,56	3,87	3,05
819	0,18	0,33	0,48	0,56	3,68	2,69
1039	0,22	0,28	0,50	0,56	3,58	2,69
1112	0,21	0,42	0,49	0,57	2,44	2,23
1332	0,22	0,40	0,50	0,62	3,09	1,81
1406	0,18	0,50	0,56	0,68	1,97	1,60
1626	0,31	0,48	0,60	0,69	2,59	1,22
1699	0,42	0,60	0,65	0,77	2,26	0,97
1919	0,45	0,61	0,64	0,76	1,82	0,83
1992	0,40	0,55	0,60	0,74	1,54	0,74
2212	0,53	0,64	0,73	0,82	1,39	0,77
2286	0,64	0,71	0,78	0,85	1,59	0,87
2506	0,68	0,70	0,81	0,86	1,06	0,83
2579	0,59	0,62	0,76	0,81	1,03	0,87
2799	0,62	0,63	0,81	0,84	0,97	0,78
2872	0,70	0,68	0,86	0,87	1,00	0,84
3092	0,77	0,74	0,86	0,90	1,20	1,04
3166	0,78	0,75	0,89	1,09	0,80	1,27
3386	0,80	0,91	1,01	1,00	0,62	0,77
3459	0,91	0,82	1,03	0,97	0,71	0,89
3679	0,91	0,87	1,02	1,03	0,82	1,05
3753	0,88	0,79	0,99	0,99	0,90	1,28
3973	0,87	0,89	0,96	1,02	0,77	0,82

Table B15 Determination of temperature impacts on breakthrough curves (Fig. 4.14)

Metrix:	Cu^{2+}/Zn^{2+} in roof runoff (high NOM) and DI
Cu^{2+}:	4-5 mg L^{-1}
Zn^{2+}:	5-7 mg L^{-1}
Conductivity:	80 µS cm^{-1}
Temperature:	20 °C
DO:	7-8 mg L^{-1}
Fe^0 bed:	15 g Fe^0 with pumice, 5 min EBCT

	c/c_0 for Cu^{2+}			c/c_0 for Zn^{2+}			Fe^{2+}		
BV	15	20	35	15	20	35	15	20	35
37	0,14	0,05	0,01	0,90	0,81	0,76	0,89	1,09	0,71
183	0,51	0,26	0,22	0,81	0,91	0,92	2,45	2,86	1,06
257	0,54	0,32	0,28	0,86	0,93	0,91	2,17	1,96	0,78
403	0,67	0,52	0,54	0,95	0,98	0,95	1,99	1,56	0,79
477	0,67	0,61	0,68	0,97	0,98	0,98	1,85	1,64	0,81
550	0,71	0,64	0,87	1,00	1,00	1,00	1,47	1,36	0,55
746	0,69	0,62	0,69	0,97	1,00	0,98	1,68	1,47	0,72
819	0,74	0,65	0,69	1,04	1,00	1,03	1,00	1,17	0,63
1039	0,68	0,59	0,68	1,02	1,04	1,01	1,22	1,25	0,71
1112	0,68	0,56	0,69	1,05	0,95	0,95	1,43	1,46	0,77
1332	0,64	0,62	0,70	0,99	0,96	0,95	1,39	1,78	0,84
1406	0,55	0,72	0,63	1,05	0,94	0,93	2,09	2,19	1,08
1626	0,84	0,81	0,85	1,17	1,01	1,04	2,81	2,84	2,30
1699	0,84	0,84	0,82	1,15	1,04	1,05	2,01	3,15	2,75
1919	0,83	0,81	0,88	1,12	1,00	1,04	2,34	2,82	2,59
1992	0,92	0,92	0,86	1,16	1,05	1,08	1,74	3,05	2,88
2212	0,89	0,65	0,76	1,07	0,92	0,93	1,87	2,40	1,66
2286	0,88	0,86	0,63	1,07	0,96	0,98	1,70	2,44	2,64
2506	0,85	0,81	0,56	1,04	0,92	0,94	1,39	2,55	2,58
2579	0,90	0,83	0,80	0,99	0,92	0,91	0,28	1,54	1,86
2799	0,86	0,86	0,62	1,00	0,91	0,88	0,59	0,24	0,03
2872	0,89	0,86	0,77	1,01	0,94	0,99	0,80	0,22	0,06
3092	0,85	0,80	0,67	0,98	0,89	0,89	1,39	1,71	1,24
3166	0,87	0,85	0,74	1,02	0,91	0,97	1,35	1,85	2,79
3386	0,72	0,81	0,70	0,89	0,84	0,89	1,40	1,95	2,85
3459	0,56	0,50	0,42	0,76	0,69	0,84	0,18	0,63	0,49
3679	0,82	0,63	0,60	1,05	1,07		0,19	0,43	3,79
3753	0,90	0,78	0,55	1,06	0,95	0,43	0,20	0,47	0,42
3973	0,86	0,81	0,68	0,92	0,94	0,85	0,18	0,59	0,53
4046	0,94	0,78	0,69	1,00	0,91	0,79	0,20	0,62	0,20
4266	0,92	0,83	0,70	1,00	0,89	0,80	0,24	0,65	0,16
4339	0,88	0,76	0,68	0,95	0,83	0,69	0,16	0,48	0,62
4559	0,97	0,85	0,64	1,00	0,89	0,70	0,19	0,71	0,58
4779	0,95	0,77	0,67	0,93	0,81	0,70	0,23	0,64	0,55
4999	0,95	0,74	0,62	1,04	0,83	0,69	0,25	0,65	0,62
5219	0,86	0,67	0,59	0,97	0,80	0,69	0,20	0,67	0,45
5439	0,94	0,73	0,65	1,01	0,83	0,67	0,16	0,54	0,31
5659	0,84	0,66	0,62	0,89	0,78	0,67	0,18	0,54	0,28
5879	0,89	0,69	0,68	0,98	0,81	0,76	0,15	0,63	0,29
6099	0,89	0,73	0,68	0,97	0,83	0,75	0,22	0,56	0,22

Table B16 Determination of NOM impacts on breakthrough curves (Table 4.2 and Fig. 4.25)

Metrix:	Cu^{2+}/Zn^{2+} in roof runoff
Cu^{2+}:	4-5 mg L^{-1}
Zn^{2+}:	5-7 mg L^{-1}
Conductivities:	80-200
Temperature:	20 °C
Fe^0 bed:	15 g Fe^0 with pumice, 5 min EBCT

BV	DI water		BV	NOM 2,9-10,3		BV	NOM 5,0-61,0	
C/C_0	Cu	Zn		Cu	Zn		Cu	Zn
37	0,013	0,318	37	0,088	0,311	0	0,028	0,489
306	0,108	0,583	183	0,151	0,402	186	0,184	0,709
419	0,117	0,620	257	0,315	0,663	342	0,031	0,715
566	0,128	0,633	403	0,309	0,672	553	0,317	0,759
713	0,130	0,623	477	0,304	0,639	818	0,586	0,885
872	0,132	0,673	550	0,309	0,602	935	0,676	0,975
978	0,134	0,644	746	0,343	0,562	1104	0,777	1,032
1165	0,145	0,690	819	0,334	0,562	1235	0,656	0,862
1274	0,153	0,676	1039	0,276	0,560	1384	0,586	0,878
1455	0,151	0,639	1112	0,415	0,571	1539	0,647	0,884
1772	0,144	0,578	1332	0,401	0,619	1714	0,470	0,847
1858	0,094	0,571	1406	0,503	0,676	1833	0,486	0,882
2420	0,168	0,706	1626	0,476	0,695	2057	0,805	0,931
2628	0,178	0,614	1699	0,598	0,766	2383	0,671	0,902
2762	0,212	0,625	1919	0,605	0,761	2615	0,750	0,915
2909	0,221	0,633	1992	0,552	0,735	2701	0,685	0,915
2995	0,223	0,632	2212	0,643	0,816	2860	0,663	0,977
3068	0,251	0,625	2286	0,705	0,846	2994	0,654	1,157
3215	0,234	0,649	2506	0,696	0,858	3169	0,794	1,366
3361	0,332	0,682	2579	0,622	0,807		0,936	1,357
3512	0,321	0,713	2799	0,629	0,840			1,452
3581	0,370	0,709	2872	0,684	0,868			1,545
3817	0,319	0,756	3092	0,745	0,901			
3940		0,783	3166	0,749	1,086			
3386			3386	0,909	1,004			
3459			3459	0,817	0,969			
3679			3679	0,872	1,026			
3753			3753	0,786	0,989			
3973			3973	0,886	1,022			
			4046	0,805	0,952			
			4266	0,884	1,022			
			4339	0,798	0,954			
			4559	0,812	0,958			

Table B17 Determination of NOM impacts on breakthrough curves (Table 4.2 and Fig. 4.26)

Metrix: Cu^{2+}/Zn^{2+} in roof runoff

Cu^{2+}: 4-5 mg L^{-1}

Zn^{2+}: 5-7 mg L^{-1}

Conductivity: 80 µS cm^{-1}

Temperature: 20 °C

DO: 7-8 mg L^{-1}

Fe^0 bed: 15 g Fe^0 with pumice, 5 min EBCT

BV	Cu_T	Zn_T	Fe_T
37	0,052	0,811	1,09
183	0,262	0,910	2,86
257	0,320	0,931	1,96
403	0,519	0,978	1,560
477	0,612	0,978	1,640
550	0,636	0,998	1,360
746	0,618	1,000	1,470
819	0,645	1,002	1,170
1039	0,587	1,037	1,250
1112	0,562	0,953	1,460
1332	0,616	0,959	1,780
1406	0,722	0,935	2,190
1626	0,812	1,008	2,840
1699	0,842	1,039	3,150
1919	0,806	1,002	2,820
1992	0,916	1,053	3,050
2212	0,648	0,923	2,400
2286	0,860	0,959	2,440
2506	0,810	0,919	2,550
2579	0,828	0,919	1,540
2799	0,855	0,906	0,240
2872	0,860	0,941	0,220
3092	0,801	0,888	1,710
3166	0,853	0,911	1,850
3386	0,808	0,843	1,950
3459	0,499	0,688	0,630
3679	0,632	1,066	0,430
3753	0,779	0,947	0,470
3973	0,808	0,939	0,590
4046	0,776	0,912	0,620
4266	0,830	0,893	0,650
4339	0,761	0,827	0,48
4559	0,849	0,889	0,71
4779	0,768	0,808	0,64
4999	0,744	0,835	0,65
5219	0,666	0,800	0,67
5439	0,726	0,835	0,54
5659	0,658	0,784	0,54
5879	0,695	0,811	0,63
6099	0,726	0,827	0,56

Table B18 pH before and after the breakthrough column experiments (Fig. 4.11-4.14)

Metrix: Cu^{2+}/Zn^{2+} in roof runoff

Cu^{2+}: 4-5 mg L^{-1}

Zn^{2+}: 5-7 mg L^{-1}

Conductivity: 80 µS cm^{-1}

Temperature: 20 °C

Fe^0 bed: 15 g Fe^0 with pumice, 5 min EBCT

pH data	Inlet					Outlet				
BVT	pHi 4	pHi 6,5	pHi 5,8	DO 0	Cond. 200	pHi 4	pHi 6,5	pHi 5,8	DO 0	Cond. 200
37						6,06	6,23	6,18	6,24	6,14
183	4,3	6,44	5,59	5,62	5,6	6,22	6,5	6,21	6,26	6,17
257						6,07	6,3	6,2	6,24	6,12
403						6,16	6,42	6,26	6,34	6,18
477						6,08	6,26	6,2	6,22	6,13
550	4,24	6,58	5,85	5,85	5,85	6,18	6,21	6,27	6,19	6,16
746						6,17	6,19	6,21	6,21	6,1
819	4,33	6,35	5,05	5,05	5,05	6,04	6,2	5,98	6,17	5,98
1039						5,91	5,97	5,93	5,79	5,89
1112	4,11	6,36	5,71	5,78	5,63	6,09	6,45	6,09	6,08	6,03
1332						6,05	6,15	6,13	6,12	6,02
1406	4,14	6,35	5,65	5,65	5,65	6,09	6,3	6,13	6,15	6,12
1699	4,16	6,47	5,67	5,93	5,86	5,99	6,33	6,2	6,29	6,26
1992	4,15	6,41	5,98	6,03	6,2	5,89	6,24	6,17	6,18	6,1
2212						5,92	6,3	6,1	6,26	6,07
2286	4,14	6,43	5,83	6	6,12	5,84	6,29	6,02	6,2	6,11
2506						5,65	6,24	6,11	6,16	5,98
2579	4,11	6,46	6,19	6,25	6,17	5,54	6,45	6,16	6,13	6,28
2799						5,51	6,32	6,25	6,3	6,27
2872						5,42	6,5	6,35	6,43	6,28
3092	4,13	6,51	6,11	5,96	5,77	5,32	6,38	6,38	6,2	6,2
3166	4,12	6,46	6,16	6,08	6,08	5,31	6,22	6,17	6,2	6,11
3386		6,6	5,86		5,84	5,27	6,6	6,36	6,37	6,29
3459	4,11	6,45	6,02	6,05	6,03	4,89	6,32	6,14	6,1	6,11
3679						4,95	6,31	6,35	6,32	6,23
3753	4,16	6,56	6,26	6,09	6,09	4,88	6,38	6,32	6,37	6,23
3973						4,84	6,28	6,34	6,08	6,28
average	4,17	6,46	5,85	5,87	5,85	5,72	6,31	6,19	6,21	6,14

conductivity	Inlet					Outlet				
BVT	1	2	3	4	5	1	2	3	4	5
37						107,4	107	95,5	90,6	239
183						99,5	105,3	82,3	87	213
477						96,5	106,5	79,6	80,6	200
746						81,3	75,4	66,1	70	181,1
1112	121,7	93,1	68,9	69,9	197,6	87	89	68,1	69,5	198
1406	105,9	90,1	71,5	76,3	192,8	85,9	87,8	71,8	76	183,4
1699	104,2	90,9	77,6	76,6	193,3	88,1	88,2	77,2	77,8	186,9
1992	108	94	82	85	203	86,2	89,6	81,7	84,3	203
2286	120,3	94,3	82,9	85,7	202	95,6	91,3	82,8	85,7	202
2579	122,4	94,4	83,7	90,1	192,5	96,3	91,8	83,2	84,1	193,2
3092	127,6	97,8	87,1	88,4	225	104,3	94,1	86,5	90,4	216
3166	123,2	98,6	96,7	88,8	224	99,1	94,1	95,4	90,1	218
3459	124,4	100,9	90,2	90,6	236	110,5	97,8	89,8	92,7	237
average	117,52	94,90	82,29	83,49	207,36	95,21	93,68	81,54	82,98	205,43

Table B19 pH before and after the breakthrough column experiments (Cont.)

Metrix: Cu^{2+}/Zn^{2+} in roof runoff

Cu^{2+}: 4-5 mg L^{-1}

Zn^{2+}: 5-7 mg L^{-1}

Conductivity: 80 µS cm^{-1}

Temperature: 20 °C

Fe^0 bed: 15 g Fe^0 with pumice, 5 min EBCT

	Inlet							Outlet					
BV	BV	30°C	15°C	high NOM	20°C	DI	Int. NOM	30°C	15°C	high NOM	20°C	DI	Int. NOM
37	9	6,26	6,36	6,34	6,45	6,66	6,48	6,42	6,52	7,03	6,5	6,79	6,78
183	46							6	6,22	6,39	6,2	6,51	6,34
257	64							6,1	6,35	6,39	6,3	6,63	6,43
403	101	6,14	6,18	6,16	6,12	6,54	6,25	6,14	6,43	6,41	6,3	6,65	6,43
550	138	6,06	6,15	6,18	6,09	6,55	6,28	6,1	6,33	6,37	6,21	6,56	6,3
819	205	6,05	6,12	6,27	6,24	6,63	6,31	6,14	6,32	6,34	6,17	6,51	6,29
1112	278	6	5,94	6,12	5,91	6,24	5,93	6	6,22	6,35	6,06	6,3	6,07
1406	351	6,02	5,99	5,99	6,02	6,26	6,15	6,02	6,33	6,09	6,08	6,35	6,19
1699	425	5,15	5,08	5,85	5,14	5,26	5,1	5,55	5,61	5,76	5,5	5,9	5,53
1992	498	4,98	5,02	5,65	4,98	5,08	4,98	5,37	5,38	5,34	5,27	5,4	5,24
2286	571	5,11	5,07	5,19	5,11	5,79	5,15	5,54	5,38	5,76	5,54	5,46	5,5
2579	645	5,28	5,06	5,73	5,26	5,17	5,34	5,57	5,41	5,73	5,5	5,44	5,52
2872	718	4,75	4,83	5,68	4,9	5,01	4,55	5,32	5,2	5,58	5,25	4,97	4,79
3166	791	4,91	4,93	5,77	4,98	5,07	5	5,4	5,16	5,53	5,32	5,13	5,23
3679	920	5,42	5,54	5,83	5,38	5,04	5,04	5,85	5,79	6,05	5,76	5,24	5,44
3973	993	5,59	5,6	5,71	5,69	5,12	5,07	5,71	6,01	5,95	5,52	5,37	5,32
4413	1103							5,37	5,65	5,65	5,41	5,18	5,21
4853	1213	5,48	5,5	5,79	5,34	5,12	5,08	5,38	5,61	5,98	5,63	5,26	5,33
5293	1323	5,67	5,59	5,87	5,69	5,03	5,01	5,61	6	6,15	5,21	5,4	5,27
5733	1433	5,83	5,89	6,01	5,76	5,09	5,08	5,78	6,18	5,87	5,43	5,35	5,34
6173	1543	5,81	5,79	6,01	5,95	5,08	5,1	5,79	6,16	5,9	5,47	5,36	5,29
average		5,55	5,56	5,89	5,59	5,74	5,55	5,83	5,92	6,07	5,84	5,95	5,84

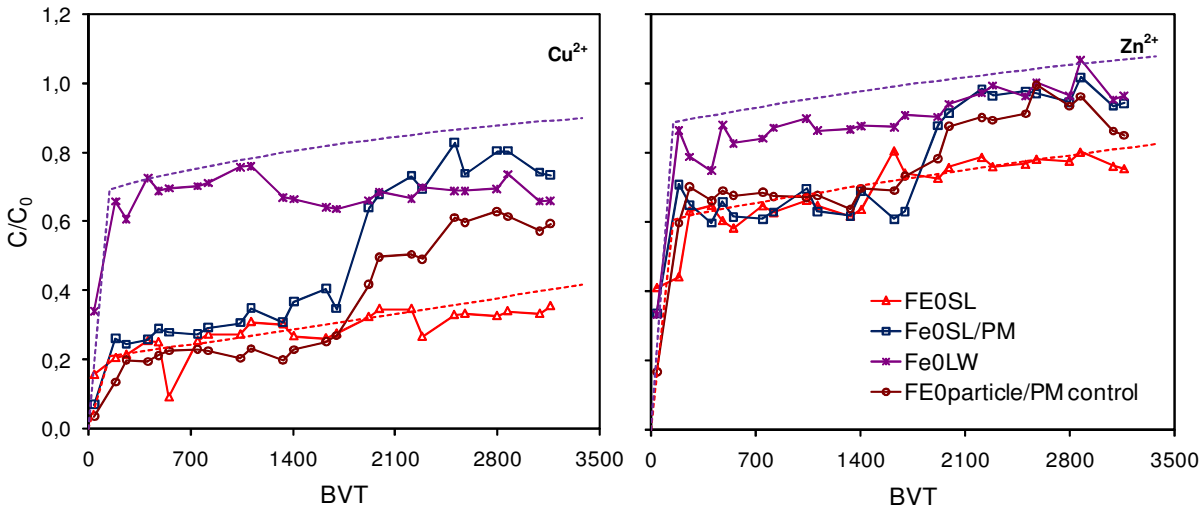

Fig. B8 Breakthrough behaviors of copper and zinc from columns containing iron from various sources. The Fe^0-SL represent a spiral iron shape illustrated in Table 3.2 and the Fe^0-LW is the iron used in the study of Ludwig (2007).

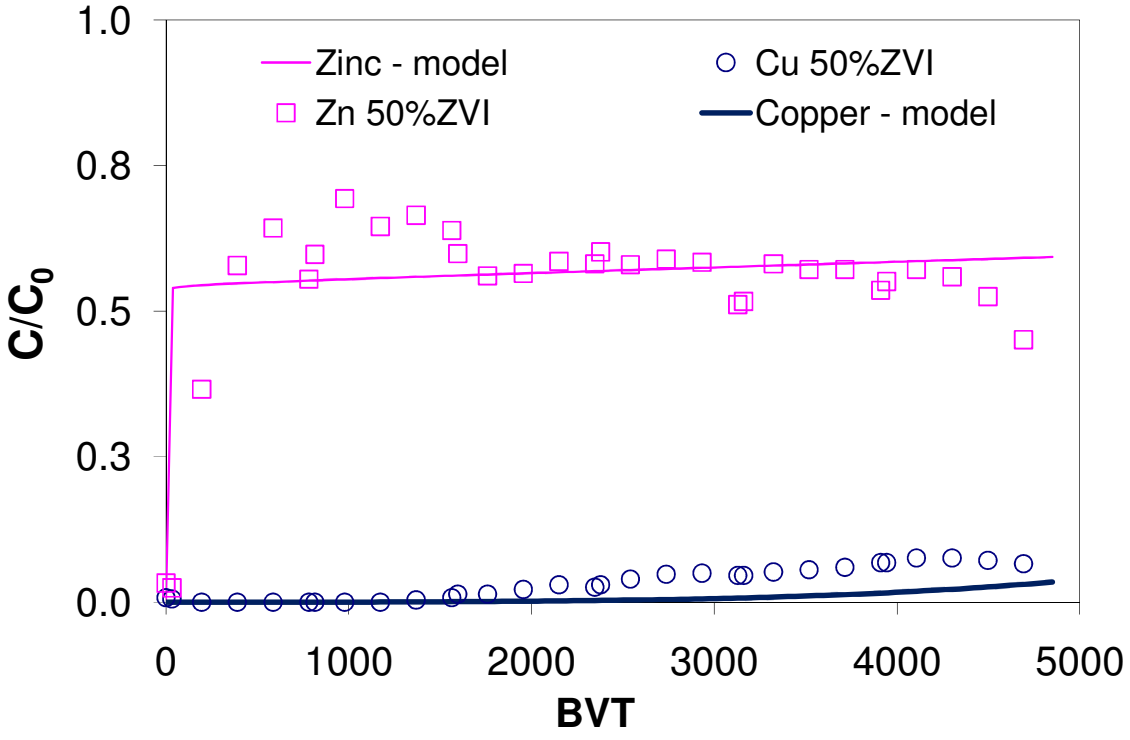

Fig. B9 Breakthrough behaviors of copper and zinc in a Fe^0/PM column (50% v/v – 47 g). The column was operated as following; Cu^{2+} 6.5 mg L^{-1}, Zn 7.3 mg L^{-1} using winter TU-runoff, 9.6 cm bed high, diameter 2.5 cm, EBCT 1.8 min. The test was terminated due to clogging. Lines represent simulation.

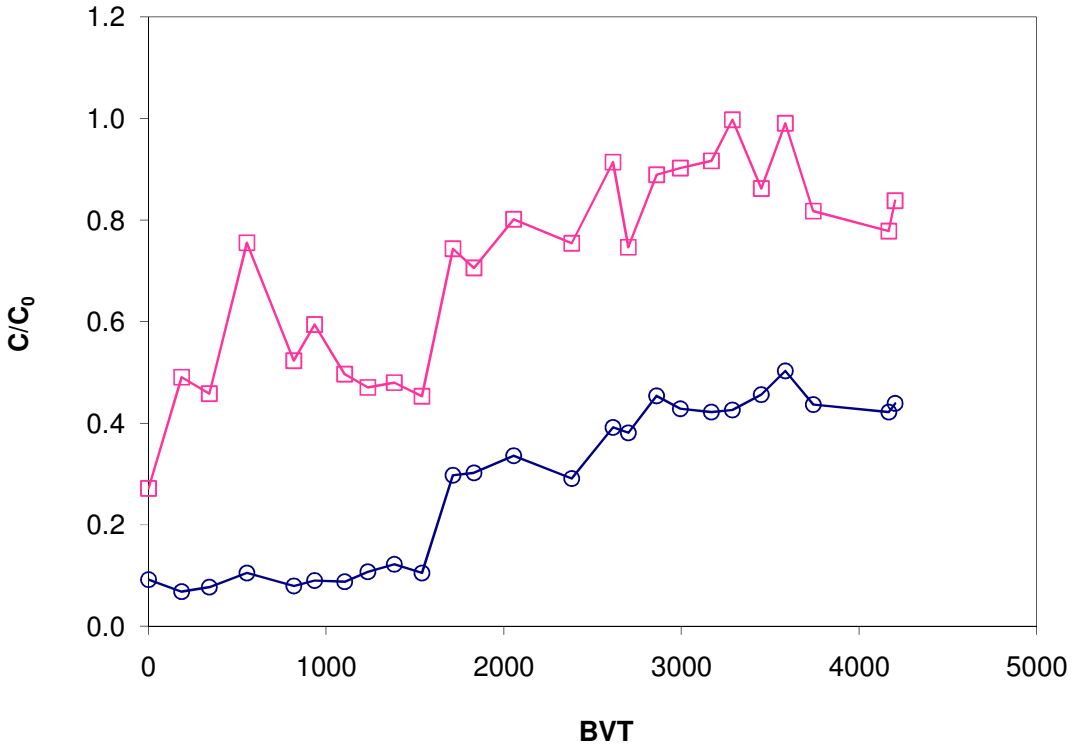

Fig. B10 Breakthrough behaviors of copper and zinc in Fe^0/PM column (10% v/v) in UFA runoff. The column was operated as following; [Cu^{2+} 5 mg L^{-1}, Zn 5-7 mg L^{-1}, the UFA water was collected in the summer period, pH~6.2, DOC_{in} 5.9 and DOC_{out} 5.1 mg L^{-1}, EBCT 5 min].

Table B20 Model prediction of breakthrough curves at EBCT 40 min (example of Fig. 4.21)

PSDM Results -- Filename = "c:\etdot10\ads\examples\trial big bed.dat"

Time	BVT	Usage Rate	Copper-Middel	Zinc-middel	DOC
Minutes	-	$m^3\ kg^{-1}$	C, mg L^{-1}	C, mg L^{-1}	C, mg L^{-1}
0,00	0,00	0,00	0,00	0,00	0,00
2880,00	576,00	1,49	0,00	1,29	0,86
5760,00	1152,00	2,98	0,03	2,03	2,35
8640,00	1728,00	4,48	0,14	2,79	2,41
11520,00	2304,00	5,97	0,44	3,53	2,22
14400,00	2880,00	7,46	1,03	4,20	2,12
17280,00	3456,00	8,95	1,90	4,77	2,06
20160,00	4032,00	10,44	2,85	5,23	2,03
23040,00	4608,00	11,94	3,71	5,60	2,02
25920,00	5184,00	13,43	4,35	5,88	2,01
28800,00	5760,00	14,92	4,75	6,10	2,00
31680,00	6336,00	16,41	4,97	6,28	2,00
34560,00	6912,00	17,90	5,07	6,42	2,00
37440,00	7488,00	19,40	5,09	6,53	2,00
40320,00	8064,00	20,89	5,09	6,63	2,00
46080,00	9216,00	23,87	5,05	6,75	2,00
48960,00	9792,00	25,36	5,04	6,79	2,00
51840,00	10368,00	26,86	5,03	6,83	2,00
54720,00	10944,00	28,35	5,03	6,86	2,00
57600,00	11520,00	29,84	5,02	6,87	2,00
60480,00	12096,00	31,33	5,02	6,89	2,00
63360,00	12672,00	32,82	5,02	6,91	2,00
66240,00	13248,00	34,32	5,01	6,92	2,00
69120,00	13824,00	35,81	5,01	6,94	2,00
72000,00	14400,00	37,30	5,01	6,94	2,00
74880,00	14976,00	38,79	5,01	6,95	2,00
77760,00	15552,00	40,28	5,01	6,96	2,00
80640,00	16128,00	41,78	5,01	6,97	2,00
83520,00	16704,00	43,27	5,00	6,97	2,00
86400,00	17280,00	44,76	5,00	6,98	2,00
89280,00	17856,00	46,25	5,00	6,98	2,00
92160,00	18432,00	47,74	5,00	6,98	2,00
95040,00	19008,00	49,24	5,00	6,98	2,00
97920,00	19584,00	50,73	5,00	6,99	2,00
100800,00	20160,00	52,22	5,00	6,99	2,00
103680,00	20736,00	53,71	5,00	6,99	2,00
106560,00	21312,00	55,20	5,00	6,99	2,00
109440,00	21888,00	56,70	5,00	6,99	2,00
115200,00	23040,00	59,68	5,00	6,99	2,00
118080,00	23616,00	61,17	5,00	6,99	2,00
120960,00	24192,00	62,66	5,00	7,00	2,00
123840,00	24768,00	64,16	5,00	7,00	2,00
126720,00	25344,00	65,65	5,00	7,00	2,00
129600,00	25920,00	67,14	5,00	7,00	2,00
132480,00	26496,00	68,63	5,00	7,00	2,00
135360,00	27072,00	70,12	5,00	7,00	2,00
138240,00	27648,00	71,62	5,00	7,00	2,00
141120,00	28224,00	73,11	5,00	7,00	2,00
144000,00	28800,00	74,60	5,00	7,00	2,00

Table B21 Model prediction of breakthrough curves at Fe^0 50% (example of Fig. 4.21)

Time	BVT	Usage Rate	Copper-Middel	Zinc-middel	DOC
Minutes	-	$m^3\ kg^{-1}$	C, mg L^{-1}	C, mg L^{-1}	C, mg L^{-1}
0	0	0,00	0,00	0,00	0,00
5760	320	0,33	0,00	0,00	-0,01
11520	640	0,67	0,00	0,00	0,01
17280	960	1,00	-0,01	0,01	0,00
23040	1280	1,33	-0,01	0,00	0,00
28800	1600	1,67	0,00	0,00	0,01
34560	1920	2,00	0,00	0,00	0,02
40320	2240	2,33	0,01	0,01	0,46
46080	2560	2,67	0,01	0,01	3,06
51840	2880	3,00	0,02	0,04	3,28
57600	3200	3,33	0,02	0,06	2,70
63360	3520	3,66	0,01	0,09	2,35
69120	3840	4,00	0,01	0,12	2,36
74880	4160	4,33	0,00	0,17	2,62
80640	4480	4,66	-0,01	0,26	2,84
86400	4800	5,00	-0,01	0,37	2,85
92160	5120	5,33	-0,01	0,51	2,68
97920	5440	5,66	0,00	0,70	2,49
103680	5760	6,00	0,01	0,93	2,37
115200	6400	6,66	0,05	1,59	2,34
120960	6720	7,00	0,06	2,01	2,35
126720	7040	7,33	0,06	2,49	2,30
132480	7360	7,66	0,05	3,03	2,24
138240	7680	8,00	0,04	3,63	2,20
144000	8000	8,33	0,04	4,31	2,17
149760	8320	8,66	0,07	5,04	2,16
155520	8640	9,00	0,24	5,78	2,13
161280	8960	9,33	0,64	6,46	2,09
167040	9280	9,66	1,37	7,01	2,07
172800	9600	9,99	2,40	7,36	2,03
178560	9920	10,33	3,57	7,52	2,01
184320	10240	10,66	4,55	7,53	2,00
190080	10560	10,99	5,17	7,43	2,00
195840	10880	11,33	5,43	7,30	2,00
201600	11200	11,66	5,47	7,16	1,99
207360	11520	11,99	5,33	7,05	2,00
213120	11840	12,33	5,16	6,97	2,00
218880	12160	12,66	5,02	6,90	2,00
224640	12480	12,99	4,94	6,89	2,00
230400	12800	13,33	4,92	6,90	2,00
236160	13120	13,66	4,91	6,91	2,00
241920	13440	13,99	4,93	6,92	2,00
247680	13760	14,33	4,95	6,94	2,00
253440	14080	14,66	4,96	6,95	2,00
259200	14400	14,99	4,97	6,95	2,00
264960	14720	15,33	4,98	6,96	2,00
270720	15040	15,66	4,99	6,97	2,00
276480	15360	15,99	5,00	6,97	2,00
282240	15680	16,32	5,00	6,98	2,00
288000	16000	16,66	5,00	6,98	2,00

Table B22 Characterization of runoff NOM in term of hydrophobicity (Table 4.3)

					Hydrophilic		Hydrophobic		
Column	Blind 1	HPI	TPI	Blind 2	(HPI x 1)-B1	TPI-B2	HIX + HOS	Total DOC	Total DOC
TUSW	0,52	6,76	7,71	1,77	6,24	5,94	12,18	12,975	12,975
CUR	0,57	3,25	3,14	1,37	2,68	1,77	4,45	5,7	5,7
TUFF	0,55	7,73	3,07	0,62	7,18	2,45	9,63	9,5	9,5
SSWR	0,76	0,97	2,01	1,75	0,21	0,26	0,47	0,39	0,39

	TUSW	CUR	TUFF	SSWR
DOC total [mg C]	1,04	0,46	0,76	0,03
HIX [mg C]	0,50	0,21	0,57	0,02
HIS [hydrophilic acid]				
HIN [hydrophilic neutral]				
HIB [hydrophilic base]				
HOS [hydrophobic acid]	0,30	0,09	0,12	0,01
HIX [hydrophilic fraction]	48,09	47,02	75,58	53,85
HIS [hydrophilic acid]				
HIN [hydrophilic neutral]				
HIB [hydrophilic base]				
HOX [hydrophobic Fraction]	51,91	52,98	24,42	46,15
HOS [hydrophobic acid]	28,61	19,41	16,12	41,67
HON [hydrophobic neutral]	23,29	33,57	8,30	4,49
	6,74	3,02	2,32	0,18
	6,24	2,68	7,18	0,21
	36,41	9,74	10,25	4,27
	18,50	31,01	22,63	4,22
	17,14	27,52	70,05	4,92
	64,80	45,30	7,60	93,40
	100,44	103,82	100,28	102,53
	100,00	100,00	100,00	100,00
	18,06	27,18	22,35	1,68

*The method of calculation was described in Appendix C

Table B23 Determination of NOM impacts using batch test at initial acidic pH_i 2.5 (Fig. 4.24)

Metrix:	Cu^{2+}/Zn^{2+} in roof runoff
Cu^{2+}:	4-5 mg L^{-1}
Zn^{2+}:	5-7 mg L^{-1}
Conductivity:	80-200
Temperature:	20 °C
Fe^0 bed:	0,5 g Fe^0

Zn removal at low pH

source/h	0	6	18	51	192
TU FF 1	1,00	1,20	1,07	0,82	0,49
TU FF 2	1,00	1,24	1,00	0,76	0,46
average	1,00	1,22	1,03	0,79	0,48
SD	0,00	0,02	0,03	0,03	0,02
Error	0,00	0,04	0,07	0,06	0,03
TU SW 1	1,00	1,06	0,67	0,61	0,58
TU SW 2	1,00	1,00	0,67	0,60	0,47
average	1,00	1,03	0,67	0,60	0,53
SD	0,00	0,03	0,00	0,00	0,05
Error	0,00	0,06	0,01	0,00	0,11
Cu R 1	1,00	0,58	0,52	0,40	0,16
Cu R 2	1,00	0,71	0,53	0,44	0,24
average	1,00	0,65	0,53	0,42	0,20
SD	0,00	0,07	0,01	0,02	0,04
Error	0,00	0,13	0,01	0,04	0,08
SSWR 1	1,00	0,86	0,75	0,65	0,48
SSWR 2	1,00	0,90	0,93	0,69	0,49
average	1,00	0,88	0,84	0,67	0,48
SD	0,00	0,02	0,09	0,02	0,00
Error	0,00	0,04	0,18	0,05	0,01
Control 1	1,00	1,10	1,10	1,12	1,12
Control 2	1,00	1,09	1,02	1,12	1,09
average	1,00	1,09	1,06	1,12	1,10
SD	0,00	0,00	0,04	0,00	0,02
Error	0,00	0,00	0,07	0,00	0,03

Cu removal

source	Conc. Initial	B1	B2	Average	Error	% Removal
TU-SW	4,68	0,16	0,01	0,09	0,15	98
TUFF	5,27	1,30	1,13	1,22	0,17	77
SSWR	5,14	0,33	0,23	0,28	0,10	95
CUR	6,30	0,03	0,02	0,03	0,01	100

Zn removal

source	Conc. Initial	B1	B2	Average	Error	% Removal
TU-SW	10,22	5,75	4,65	5,20	1,10	49
TU-FF	5,74	2,45	2,33	2,39	0,12	58
SR-NOM	5,41	2,33	2,36	2,35	0,03	57
CU-R	6,29	0,89	1,28	1,09	0,39	83

DOC removal

source	Conc. Initial	B1	B2	Average	Error	% Removal	Load [mg L^{-1}]
TU-SW	22,69	7,40	8,39	7,89	1,00	65	29,6
TUFF	12,66	8,97	8,99	8,98	0,02	29	7,4
SR NOM	3,80	0,77	0,95	0,86	0,18	77	5,9
CUR	16,48	3,62	3,48	3,55	0,14	78	25,9

Table B24 Determination of NOM impacts using batch test at initial runoff pH_i 5.0 (Fig. 4.23)

Metrix:	Cu^{2+}/Zn^{2+} in roof runoff
Cu^{2+}:	4-5 mg L^{-1}
Zn^{2+}:	5-7 mg L^{-1}
Conductivity:	80-200
Temperature:	20 °C
Fe^0 bed:	0,5 g Fe^0

Cu removal

source/h	0	6	18	51	192	% Removal
TU-SW	1,00	0,37	0,08	0,02	-	98
TUFF	1,00	0,19	0,02	0,02	-	98
SSWR	1,00	0,08	0,00	0,00	-	100
CuR	1,00	0,38	0,00	0,02	-	98

Zn removal

vials/h	0	6	18	51	192	% Removal
TU SW	1,00	0,81	0,54	0,30	0,03	70
TU FF	1,00	0,59	0,39	0,07	0,00	93
SR NOM	1,00	0,53	0,41	0,24	0,02	76
Cu R	1,00	0,52	0,20	0,04	0,00	96

DOC removal

vials/h	0	50	c/c_0	% Removal	Load [mg g^{-1}]
TU SW	28,60	14,62	0,51	49	28,0
TU FF	12,20	10,67	0,87	13	3,1
SR NOM	5,82	4,31	0,74	26	3,0
Cu R	9,74	4,98	0,51	49	9,5

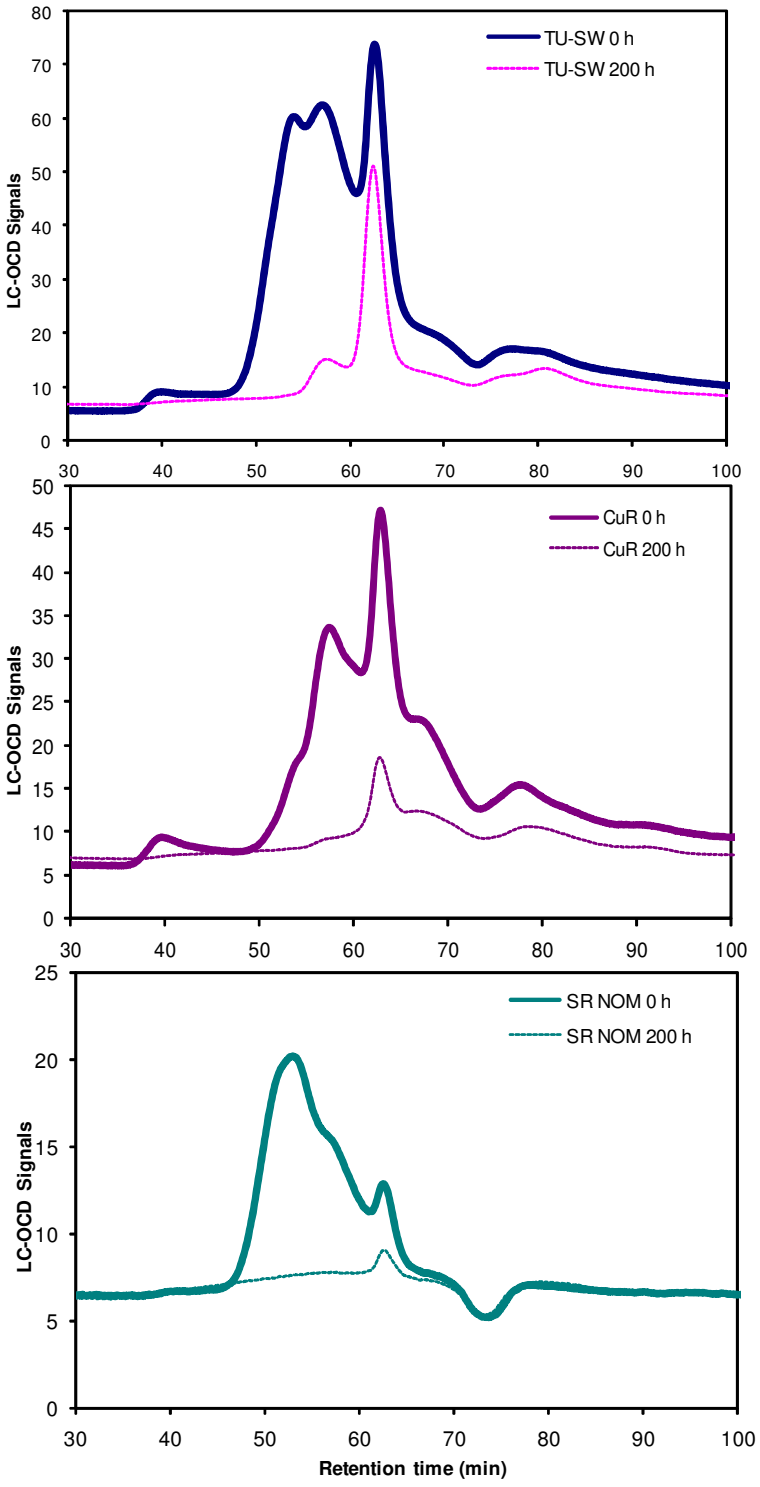

Fig. B11 LC-OCD diagrams of NOM runoff from various sources before and after Fe^0 treatment (in supplement to Fig. 4.22 and 4.27)

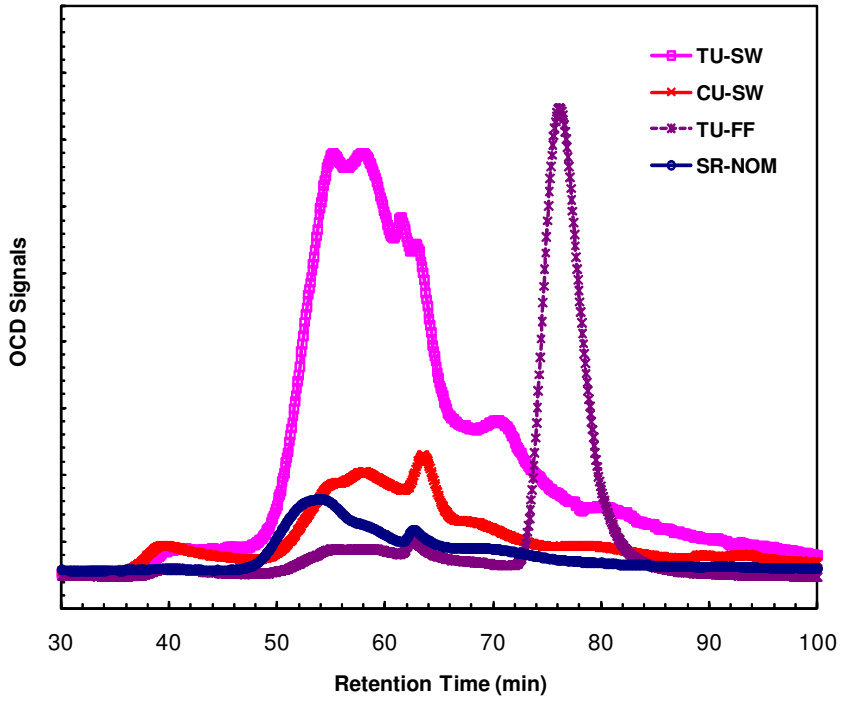

Fig. B12 A comparison of LC-OCD diagrams of NOM runoff from various sources (in supplement to Fig. 4.22)

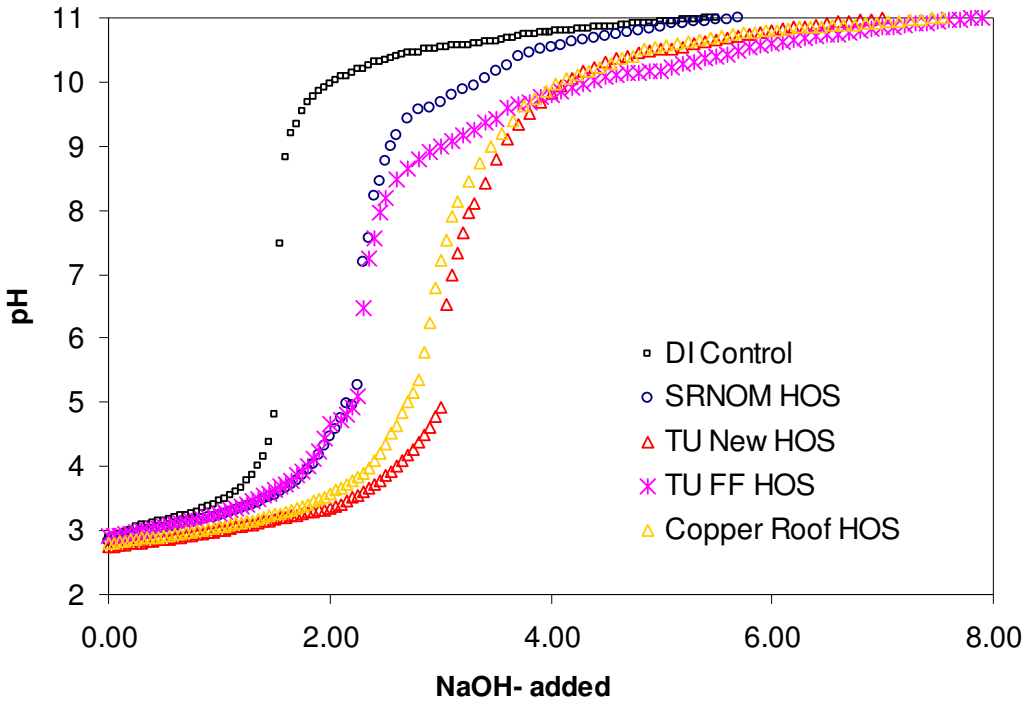

Fig. B13 Example of acidity determination of HOS fraction of runoffs (in supplement to Table 4.4)

Table B25 Results of field study of composited column (Fig. 4.28-4.29)

Metrix:	Cu^{2+}/Zn^{2+} from roof runoffs								
Fe^0 bed:	100 g Fe^0 with pumice, 5 min EBCT								
Site:	copper roof runoff at UDK				Site:	zinc roof runoff at TU			
Date:	26.07.2005				Date:	25.07.2005			
Day of exp.	1				Day of exp.	1			
Copper concentration					Zn concentration				
Length/Column	1	2	3	4	Column	1	2	3	4
0	4,82	4,87	4,845	4,845	0	0,96	0,89	0,925	0,925
7	4,13	1,26	1,2	2,66	7	1	0,64	0,39	0,33
14	3,68	0,55	0,86	1,71	14	0,87	0,43	0,24	0,23
21	3,42	0,44	0,73	1,02	21	0,78	0,32	0,17	0,47
28	3,13	0,34	0,66	0,8	28	0,8	0,24	0,13	0,08
35	2,85	0,28	0,57	0,55	35	0,78	0,23	0,16	0,06
42	2,41	0,19	0,44	0,35	42	0,7	0,17	0,11	0,05
49	2,4	0,13	0,39	0,27	49	0,58	0,36	0,22	0,02
56	1,83	0,13	0,38	0,18	56	0,49	0,07	0,04	0,03
Site:	copper roof runoff at UDK				Site:	zinc roof runoff at TU			
Date:	26.07.2005				Date:	28.07.2005			
Day of exp.	1				Day of exp.	4			
Zinc concentration					Zinc concentration				
Column	1	2	3	4	Column	1	2	3	4
0	0,82	0,79	0,805	0,805	0	0,65	0,61	0,63	0,63
7	0,74	0,52	0,31	0,26	7	0,61	0,49	0,25	0,3
14	0,65	0,5	0,24	0,2	14	0,55	0,44	0,2	0,06
21	0,64	0,48	0,2	0,11	21	0,62	0,39	0,15	0,05
28	0,62	0,48	0,2	0,1	28	0,57	0,32	0,12	0,01
35	0,61	0,47	0,2	0,07	35	0,62	0,25	0,16	0
42	0,58	0,4	0,12	0	42	0,59	0,19	0,09	0
49	0,53	0,23	0,09	0,02	49	0,61	0,2	0,09	0,02
56	0,58	0,39	0,1	0,01	56	0,59	0,21	0,05	0
Site:	copper roof runoff at UDK				Site:	zinc roof runoff at TU			
Date:	26.07.2005				Date:	28.07.2005			
Day of exp.	1				Day of exp.	4			
Ca concentration					Ca concentration				
Column	1	2	3	4	Column	1	2	3	4
0	4,51	3,59	4,05	3,85	0	1,61	1,61	1,61	1,61
7	4,08	4,25	3,61	4,48	7			1,34	1,25
14	3,87	4,49	3,59	5,08	14			1,74	1,17
21	4,03	4,6	3,68	5,08	21			2,17	1,14
28	4,04	4,4	3,86	5,03	28			2,28	1,15
35	4,22	4,58	4,17	5,4	35			2,35	1,17
42	4,33	4,83	3,99	5,71	42			2,21	1,09
49	4,57	4,86	3,72	6,4	49			2,43	1,2
56	4,5	4,37	4,49	7,24	56			2,39	1,44
Site:	copper roof runoff at UDK				Site:	zinc roof runoff at TU			
Date:	26.07.2005				Date:	26.07.2005			
Day of exp.	1				Day of exp.	1			
Iron concentration					Iron concentration				
Column	1	2	3	4	Column	1	2	3	4
0	0,01	0,01	0,01	0,01	0	0	0	0	0
7	0,05	2,8	1,27	0,15	7	0	0,67	0,11	0,01
14	0,03	2,64	1,15	0,09	14	0,05	2,1	0,13	0,19
21	0,01	2,56	1,05	0	21	0,04	1,88	0,72	2,31
28	0	2,02	0,81	0	28	0,07	2,14	1,84	0,05
35	0	4,27	0,73	0	35	0,02	1,91	0,12	0,05
42	0	3,06	0,59	0	42	0,01	1,4	0,1	0
49	0,07	5,12	0,43	0	49	0	1,4	0,5	0
56	0,02	3,17	0,47	0,01	56	0	1,98	0,1	0

Table B26 Long term monitoring of field study of composited columns (Fig. 4.28-4.29)*

System:	Field composited column test	System:	Field composited column test
Metrix:	UDK	Metrix:	TU roof
Cu^{2+}:	5,4 mg L^{-1}	Cu^{2+}:	0,0 mg L^{-1}
Zn^{2+}:	0,0 mg L^{-1}	Zn^{2+}:	2,3 mg L^{-1}
columns:	Fe^0 with carbonate bearing materials	columns:	Fe^0 with carbonate bearing materials

column	Cu [mg L^{-1}]	average	error	column	Zn [mg L^{-1}]	average	error
PM	3,75	5,355	3,21	PM	2,35	2,295	0,11
	6,96				2,24		
Fe^0/PM	0,6	0,5	0,20	Fe^0/PM	0,46	0,495	0,07
	0,4				0,53		
Fe^0/PM/DML	0,01	0,035	0,05	Fe^0/PM/DML	0,6	0,47	0,26
	0,06				0,34		
Fe^0/PM/Mag	0,02	0,025	0,01	Fe^0/PM/Mag	0,08	0,07	0,02
	0,03				0,06		

* The long term monitoring of metal concentration. 100 mL each were collected for 12 rain events to total samples and they were measured.

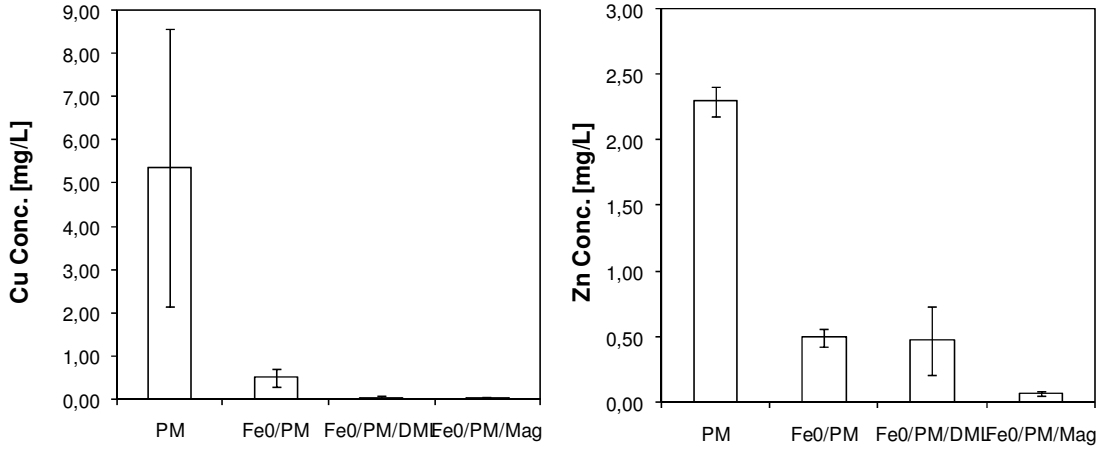

Fig. B14 Results of longterm performance of carbonatic/Fe^0 composited columns

Table B27 Breakthrough of copper in sequential column tests (Fig. 4.30)

Metrix: Cu^{2+}/Zn^{2+} in roof runoff

Cu^{2+}: 4-5 mg L^{-1}

Zn^{2+}: 5-7 mg L^{-1}

Conductivity: 80 µS cm^{-1}

Temperature: 20 °C

DO: 7-8 mg L^{-1}

Fe^0 bed: 15 g Fe^0 with pumice and carbonate materials, 5 min EBCT (see describtion in chapter 3)

BVT	Fe^0 Cu	Af $CaCO_3$Cu	Af DMSCu	Af DMLCu	Af MagCu	Af DMLCu
0	0,01	0,01	0,03	0,01	0,00	0,00
186	0,11	0,06	0,14	0,06	0,00	0,00
342	0,12	0,15	0,11	0,03	0,00	0,01
553	0,13	0,22	0,10	0,02	0,00	0,03
818	0,13	0,21	0,08	0,06	0,00	0,03
935	0,13	0,16	0,08	0,08	0,00	0,05
1104	0,13	0,15	0,08	0,07	0,00	0,06
1235	0,15	0,16	0,10	0,02	0,00	0,06
1384	0,15	0,16	0,12	0,07	0,00	0,14
1539	0,15	0,20	0,13	0,07	**0,00**	0,18
1714	0,14	0,18	0,18		0,01	0,10
1833	0,09	0,24	0,32		0,01	0,14
2057	0,17	0,30	0,25		0,04	0,15
2383	0,18	0,42	0,32		0,01	0,00
2615	0,21	0,49	0,04		0,01	0,00
2701	0,22		0,01		0,01	0,02
2860	0,22		0,01		0,01	0,04
2994	0,25		0,01		0,02	0,02
3169	0,23		0,02		0,00	0,00
3287	0,33		0,02		0,09	0,00
3450	0,32		0,02			
3584	0,37		0,00			
3742	0,32		0,03			
4167			0,02			

BVT		Af ZVI Cu	Af ZVI Cu	Af ZVI Cu	Af ZVI Cu	Af ZVI Cu
0		0,17	1,08	0,03	0,00	0,03
186		0,62	0,94	0,34	0,01	0,18
342		0,74	0,88	1,32	0,17	0,03
553		0,75	0,91	0,00	0,01	0,32
818		0,79	0,89	0,00	0,04	0,59
935		0,83	0,92	0,00	0,02	0,68
1104		0,86	0,93	0,00	0,00	0,78
1235		0,81	0,99	1,12	0,00	0,66
1384		0,82	1,01	1,42	0,00	0,59
1539		0,76	0,91	1,71	0,01	0,65
1714			0,90	1,39	**0,02**	0,47
1833			0,91	0,00	0,03	0,49
2057		1,24	1,08	0,76	0,30	0,81
2383		0,98	1,08	1,12	0,15	0,67
2615		1,04	1,05	2,66	0,72	0,75
2701		1,29	1,04	1,76	0,05	0,69
2860		1,00	1,05	1,87	0,24	0,66
2994		0,79	1,13	1,47	1,21	0,65
3169		0,82	1,09	5,95	0,86	0,79
3287		0,81	1,00	0,93	0,64	0,94
3450			1,03	0,00		
3584			1,08	0,00		
3742			0,97	0,00		
4167				0,00		

Table B28 Breakthrough of zinc in sequential column tests (Fig. 4.30)

Metrix: Cu^{2+}/Zn^{2+} in roof runoff

Cu^{2+}: 4-5 mg L^{-1}

Zn^{2+}: 5-7 mg L^{-1}

Conductivity: 80 µS cm^{-1}

Temperature: 20 °C

DO: 7-8 mg L^{-1}

Fe^0 bed: 15 g Fe^0 with pumice and carbonate materials, 5 min EBCT

BVT	ZVI Zn	Af CaCO3Zn	Af DMSZn	Af DMLZn	Af MagZn	Af DMLZn
0	0,32	0,00	0,20	0,00	0,00	0,49
186	0,58	0,51	0,64	0,08	0,00	0,71
342	0,62	0,66	0,65	0,04	0,00	0,71
553	0,63	0,73	0,63	0,42	0,00	0,76
818	0,62	0,77	0,70	0,65	0,00	0,89
935	0,67	0,87	0,74	0,88	0,00	0,98
1104	0,64	0,86	0,79	0,96	0,00	1,03
1235	0,69	0,78	0,82	0,54	0,00	0,86
1384	0,68	0,74	0,82	0,63	0,00	0,88
1539	0,64	0,68	0,82	0,86	0,00	0,88
1714	0,58	0,59	0,76	0,87	0,00	0,85
1833	0,57	0,67	0,78	0,71	0,01	0,88
2057	0,71	0,71	0,53	0,49	0,04	0,93
2383	0,61	0,71	0,83	0,67	0,01	0,90
2615	0,62	0,82	0,40	0,84	0,02	0,91
2701	0,63	0,75	0,43	0,92	0,02	0,91
2860	0,63	0,56	0,45	0,99	0,02	0,98
2994	0,62		0,49	1,11	0,06	1,16
3169	0,65		0,53	0,85	0,14	1,37
3287	0,68	0,10	0,55	1,00	0,11	1,36
3450	0,71	0,82	0,56	0,00	0,02	1,45
3584	0,71		0,74	0,00	0,01	1,55
3742	0,76		1,01	0,00		
4167	0,78			0,00		
BVT		Af ZVI Zn	Af ZVI Zn	Af ZVI Zn	Af ZVI Zn	Af ZVI Zn
0,00		0,13	0,98	0,03	0,00	0,00
186		0,86	0,98	0,41	0,01	0,00
342		0,91	1,00	1,22	0,05	0,08
553		0,93	0,96	1,82	0,04	0,09
818		0,94	0,99	1,32	0,05	0,14
935		1,01	1,03	1,82	0,03	0,13
1104		1,05	1,03	1,23	0,02	0,14
1235		0,98	1,05	1,14	0,01	0,11
1384		0,90	1,08	1,04	0,01	0,24
1539		0,91	1,00	1,20	0,02	0,27
1714		0,90	0,96	1,18	0,02	0,26
1833			1,07		0,00	0,31
2057		1,05	1,05	0,85	0,31	0,47
2383		1,03	1,08	1,03	0,16	0,00
2615		1,13	1,05	1,35	0,80	0,01
2701		1,21	1,05	1,36	0,07	0,05
2860		1,18	1,04	1,39	0,30	0,09
2994		0,91	1,05	1,52	1,17	0,05
3169		0,92	1,07	1,82	0,95	0,01
3287		0,92	1,00	0,90	0,80	0,01
3450		0,89	0,95	0,85	0,40	0,01
3584		0,88	1,04	0,79	0,59	0,01
3742		0,87		0,86	0,40	0,01
4167		0,88		0,84	0,42	

Table B29 pH of the sequential column tests (Fig. 4.30)

BVT	CaCO3/ZVI	DML/ZVI	DMS/ZVI	Mag/ZVI	ZVI/DML	ZVI
pH of the influent						
0	6,16	6,31	6,1	6,08	6,03	5,96
37	5,77	5,77	5,80	5,75	5,81	5,70
419	5,23	5,21	5,26	5,25	5,32	5,22
713	5,82	5,76	5,82	5,73	5,81	5,76
978	5,57	5,63	5,66	5,52	5,73	5,64
1274	5,71	5,67	5,67	5,40	5,70	5,56
1772	5,78	5,62	5,74	5,71	5,72	5,62
2420	5,63	5,62	5,60	5,58	5,65	5,50
2628	5,82	5,79	5,79	5,68	5,84	5,74
2909	5,53	5,48	5,52	5,47	5,60	5,48
3215	5,46	5,22	5,42	5,35	5,43	5,43
3512	5,88	5,86	5,88	5,78	5,76	5,86
3817	5,85	5,85	5,73	5,65	5,67	5,77
pH of the effluents of carbonate columns						
0	10,35	10,67	6,35	11,12	6,36	
37	6,38	9,53	5,92	10,58	5,93	
419	6,17	6,42	5,41	10,42	5,63	
713	5,94	6,21	5,93	10,34	5,91	
978	6,00	6,33	5,90	10,52	5,93	
1274	5,84	6,14	5,65	10,58	5,88	
1772	5,84	5,96	5,71	10,62	5,93	
2420	5,82	5,98	5,78	9,96	5,83	
2628	5,98	5,92	5,68	9,82	6,16	
2909	5,82	5,85	5,53	10,01	5,76	
3215	5,83	5,83	5,64	9,68	5,66	
3512	6,38	6,11	5,99	9,28	5,98	
3817	6,26	6,24	5,90	8,13	5,94	
pH of the effluents of Fe^0 columns (except that of ZVI- DML/PM column)						
0	10,77	10,85	6,9	11,33	11,05	6,3
37	6,23	10,09	5,96	10,67	10,74	5,82
419	6,09	6,36	5,81	10,54	10,26	5,74
713	6,22	6,38	6,19	10,29	10,23	6,04
978	6,05	6,27	5,97	10,03	9,4	5,57
1274	6,27	6,49	5,91		9,2	6,04
1772	5,95	6,22	5,98	10,57	9,47	5,56
2420	5,94	6,01	5,95	10,11	6,87	5,93
2628	5,96	5,86	5,92	9,78	11,44	5,6
2909	5,8	5,8	5,98	10,05	10,48	5,76
3215		5,78	5,9	9,82	10,58	5,46
3512			6,23	9,39	10,52	6,24
3817			6,15	8,8	10,58	6,24

Table B30 Field study of sequential columns (Fig. 4.33)

Metrix: Cu^{2+}/Zn^{2+} from roof runoffs
Cu^{2+}: - mg L^{-1}
Zn^{2+}: - mg L^{-1}
Fe^0 bed: 100 g Fe^0 with pumice, 1(MF) -5(SF) min EBCT

			Inlet		Outlet		Filter bed	
date	L water	BVT	Cu	Zn	Cu	Zn	Cu	Zn
1	350	650		1,83		0,76		0,15
2	525	974	2,83	4,305	0,52	2,405	0,02	0,97
3	613	1137		4,83		3,165		0,765
6	963	1786	3,95	4,36	1,53	3,985	0,41	1,23
7	1050	1949		2,24		1,87		0,385
8	1137	2110		4,32		3,125		0,18
9	1225	2274	2,53	5,08	1,24	4,74	0,02	0,515
15	1400	2598		4,28		3,15		0,96
27	1400	2598	2,82	1,83	1,8	0,83	0,97	0,2
41	1663	3086		4,305		2,46		1,02
42	1750	3248	2,92	4,83	0,49	3,21	0,02	0,835
43	1838	3410		4,36		3,99		1,42
44	1925	3573	3,87	2,24	1,43	1,83	0,03	0,37
47	2013	3735		4,32		3,14		0,21
49	2100	3898		5,08		5,2		0,62
50	2188	4060	2,41	4,28	1,2	3,01	0,02	0,97
51	2275	4222		1,83		0,87		0,18
55	2363	4385	2,78	4,305	1,6	2,4	1,3	0,99

Table B31 pH of field study of sequential column (Fig. 4.33)

BVT	pH_{inlet}	pH_{outlet}	$pH_{after\ filtration}$
650	4,79	5,87	9,25
974	4,96	6,05	9,78
1137	4,90	5,95	7,86
1299	6,24	6,36	9,32
1786	5,68	5,76	7,21
1949	6,16	6,43	9,41
2111	5,41	6,22	9,56
2274	5,10	5,73	9,08
2598	5,33	5,93	8,59
3086	5,63	5,81	9,15
3248	6,13	5,59	8,82
3410	5,65	5,61	6,04
3573	6,14	6,07	6,87
3898	5,93	6,00	9,02
4060	6,13	6,17	8,90
4222	5,64	5,72	8,84
4385	5,92	5,97	9,08

Table B32 Field study of Fe^0-DML/PM system (Slow Flow rate) (in supplement to Fig. 4.33)

Inlet concentration

Date	Length	Column1	Column 2	Average	SD	Error	C/C_0
1	0	1,76	1,9	1,83	0,07	0,14	1,00
2	0	4,31	4,3	4,305	0,005	0,01	1,00
3	0	4,73	4,93	4,83	0,1	0,2	1,00
6	0	4,26	4,45	4,355	0,095	0,19	1,00
7	0	2,18	2,3	2,24	0,06	0,12	1,00
8	0	4,3	4,34	4,32	0,02	0,04	1,00
9	0	5,06	5,1	5,08	0,02	0,04	1,00
15	0	4,36	4,2	4,28	0,08	0,16	1,00

Outlet concentration

Length	Column1	Column 2	Average	SD	Error	C/C_0
56	0,7	0,82	0,76	0,06	0,12	0,415
56	2,73	2,08	2,405	0,325	0,65	0,559
56	2,86	3,47	3,165	0,305	0,61	0,655
56	3,69	4,28	3,985	0,295	0,59	0,915
56	1,85	1,89	1,87	0,02	0,04	0,835
56	3,33	2,92	3,125	0,205	0,41	0,723
56	4,61	4,87	4,74	0,13	0,26	0,933
56	3,37	2,93	3,15	0,22	0,44	0,736

Filtrate concentration

Filter column	Column1	Column 2	Average	SD	Error	C/C_0
out.fil	0,16	0,14	0,15	0,01	0,02	0,08
out.fil	0,49	1,45	0,97	0,48	0,96	0,23
out.fil	0,91	0,62	0,765	0,145	0,29	0,16
out.fil	1,24	1,22	1,23	0,01	0,02	0,28
out.fil	0,36	0,41	0,385	0,025	0,05	0,17
out.fil	0,09	0,27	0,18	0,09	0,18	0,04
out.fil	0,71	0,32	0,515	0,195	0,39	0,10
out.fil	0,9	1,02	0,96	0,06	0,12	0,22

Table B33 Field study of Fe^0-DML/PM system (Max flow rate) (in supplement to Fig. 4.33)

Inlet concentration

Date	Length	Column1	Column 2	Average	SD	Error	C/C_0
1	0	1,82	1,86	1,84	0,02	0,04	1,00
2	0	4,39	4,5	4,445	0,055	0,11	1,00
9	0	4,95	5,04	4,995	0,045	0,09	1,00
15	0	4,55	4,47	4,51	0,04	0,08	1,00

Outlet concentration

Length	Column1	Column 2	Average	SD	Error	C/C_0
56	1,44	1,35	1,395	0,045	0,09	0,758152
56	3,66	2,96	3,31	0,35	0,7	0,744657
56	5,09	5,14	5,115	0,025	0,05	1,024024
56	4,22	4,24	4,23	0,01	0,02	0,937916

Filtrate concentration

Filter column	Column1	Column 2	Average	SD	Error	C/C_0
out.fil	0,44	0,44	0,44	0	0	0,24
out.fil	2,58	2,25	2,415	0,165	0,33	0,54
out.fil	1,31	0,94	1,125	0,185	0,37	0,23
out.fil	1,51	2,62	2,065	0,555	1,11	0,46

Table B34 Parameter used for cost estimation

					Estimated cost*	
Corrosion rate	3.6	mg Me m^{-2} y^{-1}	(i) Structure cost per unit volume		500	Euro m^{-3}
Runoff	850.6	mm	(ii) Lining cost per unit volume		70	Euro m^{-3}
GFH loading	30	mg g^{-1}	(iii) Excavation cost per unit volume		10	Euro m^{-3}
ZVI loading	42	mg g^{-1}	(iv) media cost per unit volume	GFH/Lime	3.62	Euro kg^{-1}
Period of changing media	20	years	(vi)	ZVICB	0.045	Euro kg^{-1}
year of operation	20	years				

* Estimation of construction and media cost take into account the decrease of cost for larger project based on the data in Table B35

Table B35 Data for calculation of cost factor (cost in Euro)

Volume (m^3)	(i)	(ii)	(iii)	(iv)	(vi)	Volume (m^3)	(i)	(ii)	(iii)	(iv)	(vi)
25	500	70	19.2	3.62	0.045	5000	150	45	5.8	3.2	0.04
2500	200	60	7.7	3.5	0.043	10000	130	40	5.5	3	0.04

Table B36 Estimated investment cost for GFH/Lime and ZVICB treatment barrier (cost is simplied for comparison)

GFH/Lime

Roof surface	**Media**	**Vol. of Reactor**	**Total construction cost [Euro]**			**Total construction cost [Euro $m^{-2}_{roof\ surface}$ y^{-1}]***		
[m^2]	**[kg]**	**[m^3]**	**Concrete type**	**Lining type**	**Soil type**	**Concrete type**	**Lining type**	**Soil type**
100	240	0.36	1327	887	849	0.66	0.44	0.42
300	720	1.10	3590	2570	2466	0.60	0.43	0.41
700	1680	2.58	5721	4215	4049	0.56	0.42	0.40
1100	2640	4.06	7786	5840	5613	0.54	0.41	0.40
1500	3600	5.5	9807	7450	7165	0.52	0.41	0.39
1900	4560	7.01	11795	9050	8707	0.51	0.40	0.39
2300	5520	8.49	13758	10641	10241	0.51	0.40	0.39

ZVICB

100	171	1.17	1230	163	53	0.62	0.08	0.03
300	514	3.52	2897	429	128	0.48	0.07	0.02
700	1200	8.23	4313	675	193	0.40	0.07	0.02
1100	1886	12.94	5607	911	254	0.36	0.06	0.02
1500	2571	17.64	6821	1139	312	0.34	0.06	0.02
1900	3257	22.35	7976	1362	368	0.32	0.06	0.02
2300	3943	27.05	9086	1581	421	0.31	0.06	0.01

*Concrete type = structure + excavation + media; Lining type = lining + excavation + media; Soil type = excavation + media and the cost take into account the decreasing cost at larger volume

Appendix C Fractionation method – in German

Fraktionierung von DOC über XAD-8 (Adsorberharz), AG-MP 50 (Kationenaustau-scherharz), und Duolite A-7 (Anionenaustauscherharz) (Mai, 2005)

Allgemeine Hinweise zur Apparatur

Grundsätzlich dürfen die Harze nie trockenlaufen, und für eine optimale Fraktionierung dürfen keine Luftblasen im System enthalten sein.

Deshalb müssen beim Anschluß einer neuen Vorratsflasche an die Schlauchpumpe immer erst die Schläuche entlüftet werden, ehe der Weg auf die Säulen freigegeben wird. Das heißt, es wird zuerst der obere Hahn so eingestellt, daß nur der Weg zur Abfallflasche frei ist, dann wird solange Flüssigkeit gepumpt, bis keine Luftblasen mehr auf dem Weg bis zum Hahn enthalten sind; anschließend kann der Hahn so eingestellt werden, daß die Flüssigkeit in die Säulen gelangt

Die Vorratsflaschen sollten immer gut gefüllt sein, damit das Einsaugrohr immer in die Flüssigkeit hineinragt und somit keine Luftblasen angesaugt werden.

Beim Spülen mit Methanol treten am XAD-8 durch die Änderung der Oberflächenspannung Luftblasen auf. Diese müssen anschließend wieder entfernt werden. Hierzu muß man das System öffnen, wobei darauf zu achten ist, daß der Auslauf der jeweiligen Säule gesperrt ist, sonst läuft die Flüssigkeit beim Öffnen des Systems aus. Am Schliff zwischen Säule und Hahn wird das System geöffnet. Dann können die Luftblasen mit einen gedrehten Draht entfernt werden. Beim Schließen des Systems muß wiederum darauf geachtet werden, daß beim Zusammenstecken der Schliffverbindung keine Luftblasen zurückbleiben.

Generell ist immer darauf zu achten, daß die Schlauchpumpe nur eingeschaltet wird, wenn ein Weg für die Flüssigkeit geöffnet ist, damit nirgends ein Schlauch abplatzt.

Die Flußraten der Schlauchpumpe von 1 bzw. 4 ml/min müssen ab und zu überprüft und neu eingestellt werden, da sich die Eigenschaften der Pumpenschläuche mit zunehmender Einsatzzeit ändern.

Durchführung der Fraktionierung

Vor und nach jeder Fraktionierung muß das gesamte System mit verschiedenen Flüssigkeiten zur Reinigung gespült werden (s. 1.-5.). Hierbei ist zu beachten, daß alle Lösungen nur mit bidest. H_2O anzusetzen sind.

Nach der Reinigung der Harze werden die Blindwerte für die Fraktionen 1-3 gewonnen (s. 6.-8.), deren DOC-Gehalt möglichst vor der Fraktionierung der Probe bestimmt werden sollte. Die Differenz zwischen DOC der zugeführten Lösung (= bidest. H_2O) und DOC des Blindwertes sollte möglichst klein sein. (In der Literatur wird von <0,4 ppm gesprochen; dies

konnte an dieser Apparatur jedoch bisher nicht eingehalten werden.) Sollten die Blindwerte 2 ppm übersteigen, muß nochmals die Reinigung duchgeführt werden.

(Die Glasgefäße, in denen die Lösungen aufgefangen und der DOC-Gehalt bestimmt wird, sollten mit 0,1M HCl und bidest. H_2O imUltraschallbad gereinigt und anschließend mehrfach gespült werden.)

Sind die Blindwerte niedrig genug, kann mit der Fraktionierung der Probe begonnen werden (s. 9.-13.). Die Probe muß membranfiltriert sein, ihr DOC-Gehalt ca. 15 ppm und der pH-Wert 2,0 betragen. Die zur Elution der hydrophoben Säuren verwendete 0,1 M NaOH (s. 13.) sollte frisch angesetzt sein, damit der Anteil an absorbiertem CO_2 möglichst gering ist.

Ist die Fraktion 4 der Probe abgenommen, wird weiterhin 0,1 M NaOH durch das XAD-8-Harz gepumpt, um den Blindwert der 4. Fraktion zu gewinnen (s. 14.). Alle hydrophoben Säuren wurden vorher mit 50 ml NaOH desorbiert und somit kann der zugehörige Blindwert auch nach der Probenfraktionierung abgenommen werden; das erspart das Eluieren mit NaOH und anschließendes Spülen mit bidest. H_2O vor der Probenfraktionierung.

Danach folgt wieder die Reinigungsprozedur (s. 15./16. u. 1.-5.)

Alle gesammelten Lösungen werden angesäuert und bis zur DOC-Bestimmung, die innerhalb von 24 Stunden erfolgen sollte, dunkel und kühl gelagert. Für die Fraktionen 1-3 ist es günstig, den NPOC zu ermitteln, bei der NaOH-Fraktion kann auch die TC-IC-Differenz günstiger sein.

Berechnung der Anteile der einzelnen Fraktionen am Gesamt-DOC

Angabe in mg C (in 80 ml Probenlösung):

DOC_{gesamt} [mg C] = DOC_{Probe} [mg/l] * 80/1000
HIX [mg C] = (Frakt. 3 - $Blw_{Frakt.\ 3}$) [mg/l] * 80/1000
HIS [mg C] = ((Frakt. 2 - $Blw_{Frakt.\ 2}$) - (Frakt. 1 - $Blw_{Frakt.\ 1}$)) [mg/l] * 80/1000
HIN [mg C] = (Frakt. 1 - $Blw_{Frakt.\ 1}$) [mg/l] * 80/1000
HIB [mg C] = ((Frakt. 3 - $Blw_{Frakt.\ 3}$) - (Frakt. 2 - $Blw_{Frakt.\ 2}$)) [mg/l] * 80/1000
HOS [mg C] = (Frakt. 4 - $Blw_{Frakt.\ 4}$) [mg/l] * 50/1000

Angabe in %

HIX [%] = HIX [mg C] * 100% / DOC_{gesamt} [mg C]
HIS [%] = HIS [mg C] * 100% / DOC_{gesamt} [mg C]
HIN [%] = HIN [mg C] * 100% / DOC_{gesamt} [mg C]
HIB [%] = HIB [mg C] * 100% / DOC_{gesamt} [mg C]

HOX [%] = 100% - HIX [%]
HOS [%] = HOS [mg C] * 100% / DOC_{gesamt} [mg C]
HON [%] = HOX [%] - HOS [%]
(HOB = vernachlässigbar = <1% von DOC_{gesamt})

Abkürzungen

HIX = hydrophile Fraktion (= HIS + HIN + HIB)
HIS = hydrophile Säuren
HIN = hydrophile Neutralstoffe
HIB = hydrophile Basen
HOX = hydrophobe Fraktion (= HOS + HON + HOB)
HOS = hydrophobe Säuren
HON = hydrophobe Neutralstoffe
HOB = hydrophobe Basen

80/1000 und 50/1000 = Faktor zur Umrechnung von mg/l auf mg/80ml

Appendix D The pore and surface diffusion model (PSDM) – Mertz et al. (1999)

The PSDM is a dynamic fixed bed model that incorporates the following assumption

- Constant flow rate
- Plug-flow conditions exist in the bed
- Linear driving force describes the local bulk phase mass flux at the exterior surface of the adsorbent particle
- Local adsorption equilibrium exists between the solute adsorbed onto the GAC particle and the solute in the intraaggregate stagnant fluid
- Intraparticle mass flux is described by surface and pore diffusion
- Adsorption equilibrium of individual compounds can be represented by the Freundlich isotherm equation and IAST describes the competition between the compounds
- There are no interactions between adsorbing compounds during the diffusion process.

From the mass balance on the bulk phase and adsorbent phase, two partial differential equations are obtained for each adsorbing component. A coupling equation between the bulk phase and the adsorbent pahse is obtained from assuming local equilibrium at the exterior of the adsorbent particle. In cases where pore and surface diffusion are present, local equilibrium is assumed along the pore walls. These equations are non-dimensionalized and solved numerical methods. The orthogonal collocation method is used to convert the partial differential equation into a set of ordinary differential equations. The set of ordinary differential equations is solved using the backward differentiation method formular, also known as Gear's stiff method. The partial differential equations describing the adsorber dynamics in a fixed-bed adsorber is given below. Crittenden et al. (1986) and Friedman (1984) have presented the derivation of the equations and the computer algorithms that were used to solve the model equations.

The liquid phase mass balance for component *i* is given by:

$$\frac{\partial C_i}{\partial t}(z,t) + V\frac{\partial C_i}{\partial z}(z,t) + 3\frac{k_{f,i}(1-\varepsilon)}{\varepsilon R}\left[C_i(z,t) - C_{p,i}(r=R,z,t)\right] = 0 \qquad \text{(D-1)}$$

The initial condition for equation D-1 is

$$C_i(z,t) = 0 \text{ at } 0 \le z \le L, t = 0$$

The boundary condition for equation D-1 is

$$C_i(z,t) = C_{0,i} \text{ at } z = 0, t > 0$$

The intraparticle phase mass balance for component *i* is given by:

$$\frac{1}{r^2}\frac{\partial}{\partial r}\left[r^2 D_{s,i}\frac{\partial q_i}{\partial r}(r,z,t) + \frac{r^2 D_{p,i}\varepsilon_p}{\rho_a}\frac{\partial}{\partial}C_{p,i}(r,z,t)\right] = \frac{\partial}{\partial t}\left[q_i(r,z,t) + \frac{\varepsilon_p}{\rho_a}C_{p,i}(r,z,t)\right] \qquad \text{(D-2)}$$

The initial condition for equation D-2 is

$$q_i(r,z,t) + \frac{\varepsilon_p}{\rho_a} C_{p,i}(r,z,t) = 0 \text{ at } 0 \le r \le R, t = 0$$

The first boundary condition for equation D-2 is:

$$\frac{\partial}{\partial r}\left[q_i(r,z,t) + \frac{\varepsilon_p}{\rho_a} C_{p,i}(r,z,t)\right] = 0 \; at \; r = 0, t \ge 0$$

The second boundary condition for equation D-2 is:

$$D_{s,i}\rho_a \frac{\partial q_i}{\partial r}(r = R,z,t) + D_{p,i}\varepsilon_p \frac{\partial C_{p,i}}{\partial r}(r = R,z,t) = k_{f,i}\left[C_i(t) - C_{p,i}(r = R,z,t)\right]$$

The equation coupling the aqueous phase concentration of component *i* within the adsorbent pores to the adsorbent phase concentration of component *i* is given by:

$$C_{p,i}(r,z,t) = \frac{q_i(r,z,t)}{\sum_{k=l}^{m} q_k(r,z,t)}\left[\frac{\sum_{k=l}^{m} q_{k(r,z,t)}}{n_i K_i}\right]^{n_i}$$

The above equation is derived assuming that the adsorption reaction rate is much faster than the mass transfer rate (assumption of local equilibrium).

Nomenclature:

$C_{0,i}i$	initial concentration
$C_i(z,t)$	adsorbent concentration in bulk phase
$C_{p,i}(r,z,t)$	adsorbate concentration in adsorbent pores
$D_{p,i}$	pore diffusivity
$D_{s,i}$	surface diffusivity
$k_{f,i}$	film transfer coefficient
L	bed length
m	number of components
$q_i(r,z,t)$	adsorbent phase concentration
R	average adsorbent particle radius
V	loading rate

Greek letters

ε_P	particle void fraction (porosity)
ρ_A	apparent adsorbent density

index *i* refers to component number *i*